ANNUAL **REPORT** 2016

NEUTRONS FOR SOCIETY

INSTITUT LAUE-LANGEVIN

The world's leading facility in neutron science and technology.

ANNUAL REPORT

INSTITUT LAUE-LANGEVIN

2016

PUBLISHING INFORMATION

Editors:
Giovanna Cicognani and Mark Johnson

Production team:
Giovanna Cicognani, Virginie Guerard, Robert Corner and Susan Tinniswood

Design:
Morton Ward Limited

Photography:
Serge Claisse – ILL (unless otherwise specified)

Further copies can be obtained from:
Institut Laue-Langevin
Communication Unit
CS 20156, F-38042 Grenoble Cedex 9

communication@ill.eu
www.ill.eu

CONTENTS

FOREWORD 4

WHAT IS THE ILL
- About the Institut Laue-Langevin 6
- Why neutron scattering is useful 7

HAPPY BIRTHDAY TO THE ILL 8

THE ILL IN THE PRESS 10

SCIENTIFIC HIGHLIGHTS 12
- College introductions 14
- Materials science 16
- Magnetism 28
- Liquids and glasses 42
- Soft matter 48
- Biology and health 58
- Nuclear and particle physics 68
- Theory 72

MODERNISATION PROGRAMME AND TECHNICAL DEVELOPMENTS 76
- Modernisation programme 78
- Instruments and technical developments 80
- New experimental techniques 84

INDUSTRIAL ACTIVITIES 86

EXPERIMENTAL AND USER PROGRAMME
- Introduction 91
- User programme 92
- User and beamtime statistics 94
- Instrument list 98

REACTOR OPERATION 100

MORE THAN SIMPLY NEUTRONS 104
- Partnerships 106
- Training and outreach 108

WORKSHOPS AND EVENTS 110
- Chronicle 111
- Scientific events 112
- A year in photos 114

FACTS AND FIGURES
- Facts and figures 118
- Publications 121
- Organisation chart 122

FOREWORD

May this spirit of excellence, service and trust endure! It is the ILL's own hallmark.

It has been an honour, and a real pleasure for me to chair the ILL Steering Committee during 2016. What a remarkable research infrastructure, and what remarkable staff.

This year has been quite intense in many aspects.

On the management side, we said farewell to Prof. Bill Stirling who has retired. On behalf of the Associates, I would like to thank him for the strong leadership he has shown during his directorship. We then welcomed the new senior management team – Prof. Helmut Schober as the new ILL Director, Prof. Mark Johnson as the new UK Associate Director and Head of Science, and Dr. Charles Simon continuing as the French Associate Director and Head of Projects and Techniques – with the strong feeling that we were handing a unique and magnificent institute into very safe hands.

On the scientific side, we felt blessed with the nomination for the Nobel Prize for Physics of Duncan Haldane, who worked as a post-doctoral researcher in the ILL's Theory group from 1977 to 1981. The reactor operated safely throughout the year, allowing us to welcome more than 800 scientific visitors eager to carry out excellent science thanks to this outstanding neutron research centre.

The ILL is constantly looking to the future, upgrading its instruments in order to provide a state-of-the-art service to its visitors. The Millennium Project (representing an investment by the Associates of 49 M€ between 2007 and 2017) is coming close to completion, with WASP and the IN5 magnet becoming operational this year.

I would like to thank the Associates and Scientific Members for their rich, open and respectful discussions, and the ILL staff for its involvement, enthusiasm and excellent work.

The ILL is unique and very special to many of us. I am sure that those who attended the 50th anniversary felt a deep sense of friendship and pride. May this spirit of excellence, service and trust endure! It is the ILL's identity; the ILL's own hallmark.

Maria Faury
Chair of the ILL Steering Committee

From the ILL's perspective, 2016 was the year in which the Nobel Prize in Physics was awarded to Thouless, Kosterlitz and Haldane for their studies into exotic quantum states in hard condensed matter. Duncan Haldane was a post-doctoral researcher in the ILL's Theory group. It was here that he laid the foundations for his seminal work on one-dimensional quantum liquids and spin chains. Since these theoretical predictions, neutron scientists have played a major role in investigating these phenomena experimentally, and many of their experiments have been conducted at the ILL.

The work of this year's Nobel laureates is just one of many examples of how fundamental research can enrich our understanding of the workings of Nature, creating new avenues for technological development. The ILL is conscious of the intricate entanglement of scientific knowledge and technological know-how. We have therefore recently published a topical brochure highlighting some of our recent successes in unravelling the hidden, more fundamental aspects of Nature. You will find other examples of exciting science in this our latest Annual Report.

The ILL's science programme continued with vigour in 2016, thanks to the successful operation of three full reactor cycles. We were, of course, committed in parallel to the modernisation of our instruments and services, and in this context the launch of the Endurance Programme has to be considered a resounding success. Given the official go-ahead at the end of 2015, Endurance added capacity almost instantaneously to the ILL's user programme. Let me just highlight "FIPPS", a new instrument designed for the study of nuclear fission products using prompt gamma-ray spectroscopy. FIPPS was up and running, producing experimental data before the end of 2016.

The ILL is a nuclear operator at the service of science, and we take this role extremely seriously. We continue to invest strongly in nuclear safety, and we place particular emphasis on continuous compliance with the latest regulations. For this, and to ensure dependable operations and continuous modernisation, we rely on a network of industrial partners capable of providing sophisticated quality-assured services. We paid a lot of attention in 2016 to securing these services. We also, with the Associates' assistance, made good progress in consolidating our fuel cycle for the decade to come.

Had 2016 been a normal year I could stop at this point. However, 2016 was not a normal year. It was a year that shattered convictions so deeply rooted in our collective consciousness that many of us had taken them for granted. Every year the Oxford Dictionaries editorial team chooses a word that "captures the ethos, mood, or preoccupations of that particular year". Their 2016 word of the year is "*post-truth*". The prefix *post-*, when employed to describe a historical epoch, implies (again according to Oxford Dictionaries) – "belonging to a time in which the specified concept, i.e. truth, has become unimportant or irrelevant".

As members of one of the world's leading scientific institutions, we at the ILL completely refute the very idea of a *post-truth* society. All our efforts combine to produce factual knowledge. History has shown that the generation of knowledge verified by experiment, a process initiated in Europe centuries ago, has been the force driving society across the world. It is the ILL's mission, as the European Neutron Source, to defend and perpetuate this process. As the ILL's new logo proclaims, we will do so by performing neutron science in the spirit of truth and excellence for the good of our societies.

Helmut Schober
ILL Director

About the Institut Laue-Langevin

The Institut Laue-Langevin (the ILL) is an international research centre at the leading edge of neutron science and technology, where neutrons are used to probe the microscopic structure and dynamics of a broad range of materials at molecular, atomic and nuclear level.

The ILL is owned by the three founding countries – France, Germany and the United Kingdom. These three Associate countries contributed a total of about 66 M€ to the institute in 2016, a sum enhanced by significant contributions from the ILL's Scientific Member countries of Austria, Belgium, the Czech Republic, Denmark, Italy, Poland, Spain, Slovakia, Sweden and Switzerland. The ILL's overall budget in 2016 amounted to approximately 98 M€.

The institute operates the most intense neutron source in the world, based on a single-element, 58.3 MW nuclear reactor designed for high brightness. The reactor normally functions round-the-clock for four 50-day cycles per year, supplying neutrons to a suite of 40 high-performance instruments constantly maintained at the highest state of the art.

As a service institute, the ILL makes its facilities and expertise available to visiting scientists. It has a global user community – around 2 000 researchers from almost 40 countries come to work at the ILL every year. The 800 experiments they perform annually are pre-selected by a scientific review committee. Over 600 scientific papers are published annually, following the treatment and interpretation of data obtained from the use of our facilities. About 127 of these articles are published in high-impact journals. This is a factor of two higher than the next most productive neutron source in the world.

The ILL's Director and two Associate Directors are appointed for a period of five years. They each represent one of the three Associate countries. The ILL Scientific Council, comprising external scientists from the Scientific Members countries, advises the directors on the scientific priorities for the institute as well as the development of the instrument suite and technical infrastructure. It also assesses the scientific output of the institute. The ILL's main governing body is the Steering Committee, composed of representatives of the Associates; it meets twice yearly. Scientific Member observers participate in the Steering Committee meetings, as do ILL senior management, the Chair of the Scientific Council and staff representatives. The Steering Committee lays down the general directives for management, and the Associates have ultimate responsibility for determining the operational and investment strategies employed by the institute.

NEUTRONS FOR SOCIETY

The scope of the research carried out at the ILL is very broad, embracing condensed matter physics, chemistry, biology, materials and earth sciences, engineering, and nuclear and particle physics. Much of it impacts on many of the challenges facing society today, from generating sustainable sources of energy, better healthcare and a cleaner environment, to new materials for information and computer technology. Neutron scattering experiments have, for example, given us new insights into the structure and behaviour of biological and soft condensed matter; this is important in designing better drug delivery systems and in improving the processing of polymers. They also provide a unique probe into phenomena such as high-temperature superconductivity and the molecular magnetism liable to provide the technology for computers of the future.

PREPARING FOR THE FUTURE

In 2001 the ILL launched an ambitious programme to modernise its instruments and infrastructure. The aim of the Millennium Programme was to optimise the ILL's instrument suite over and beyond the first decade of the new millennium. The Millennium Programme achieved its goals, but the need for ever more sensitive and powerful instrumentation is constant. The ILL is therefore perpetuating progress with its new Endurance Programme, which will continue to develop instrumentation and support services with a view to maintaining the institute's world-leading position for another decade at least.

Why neutron scattering is useful

When used to probe small samples of materials, neutron beams have the power to reveal what is invisible using other forms of radiation. Neutrons can appear to behave as particles, waves, or microscopic magnetic dipoles; with these very specific properties they can provide information that is often impossible to obtain using other techniques. Below are a few of the special characteristics of neutrons.

WAVELENGTHS OF TENTHS OF NANOMETERS

Neutrons have wavelengths varying from 0.01 to 100 nanometers. This makes them an ideal probe into atomic and molecular structures, whether composed of single atomic species or complex biopolymers.

ENERGIES OF MILLI-ELECTRONVOLTS

The milli-electronvolt energies associated with neutrons are of the same magnitude as the diffusive motions of atoms and molecules in solids and liquids, the coherent waves in single crystals (phonons and magnons) and the vibrational modes in molecules. Any energy exchange, therefore, of between 1 μeV (or even 1 neV with neutron spin-echo techniques) and 1 eV between the incoming neutron and the sample is easy to detect.

MICROSCOPICALLY MAGNETIC

Neutrons possess a magnetic dipole moment which makes them sensitive to the magnetic fields generated by unpaired electrons in materials. They therefore play an important role in the investigation of the magnetic behaviour of materials at the atomic level. In addition, as the neutron scattering effect of the atomic nuclei in a sample depends on the orientation of the spin of both the neutron and the atomic nuclei, neutron scattering techniques are ideal for detecting nuclear spin order.

ELECTRICALLY NEUTRAL

As neutrons are electrically neutral they can penetrate far into matter without doing damage. They are therefore precious allies for research into biological samples or engineering components under extreme conditions of pressure, temperature or magnetic field, or within chemical-reaction vessels.

HIGH SENSITIVITY AND SELECTIVITY

The scattering from nucleus to nucleus in a sample varies in a quasi-random manner, even for different isotopes of the same atom. This means that light atoms remain visible in the presence of heavy atoms, and atoms close to each other in the periodic table can be clearly distinguished. This makes it possible to use **isotopic substitution** (substituting deuterium for hydrogen, for example, or one nickel isotope for another), in order to vary the contrast in certain samples and thus highlight specific structural features.

Neutrons are also particularly sensitive to hydrogen atoms and are therefore essential for research into hydrogen storage materials, organic molecular materials, and biomolecular samples or polymers.

HAPPY BIRTHDAY TO THE ILL!

NEUTRONS FOR SOCIETY

The ILL has firmly established itself as a pioneer in neutron science. In 2017, it celebrates its 50th anniversary and yet remains in the prime of youth!

The celebration of the ILL's 50th birthday was carried out in the presence of Mr Thierry Mandon, French Secretary of State for Higher Education and Research, Mr Nikolaus Meyer-Landrut, German Ambassador to France, and the Rt Hon Lord Llewellyn, British Ambassador to France. The event was attended by close to 600 ILL staff members and external guests, including many prominent personalities from the world of European research. Judging by the positive feedback we received from many external guests, the event could be considered a great success.

The ILL was founded 50 years ago, on 19 January 1967, with the signing of an agreement between the governments of the French Republic and the Federal Republic of Germany. The aim of this ambitious project was to create an intense, continuous source of neutrons devoted exclusively to civil fundamental research.

In 1971 the first neutron beams were produced and, two years later, the UK joined the partnership as the institute's third Associate member country. Since then, the ILL has taken on a truly international dimension, with the signing of Scientific Membership agreements with many other countries. What began under the impetus of Franco-German reconciliation is now a shining example of international co-operation: an institute that both reflects and drives European integration.

The ILL was one of the first research facilities in the world to be given the innovative status of "service institute", a model that has since been copied by countless laboratories around the globe. It owes much of its long-lasting success to its ability to adapt quickly in an ever-changing research environment. By constantly upgrading and developing its facilities, the ILL has ensured that its instrumentation defines the state-of-the-art. Consequently, the demand for beam time at the ILL is as high as ever, as is the quality of the science performed at the institute. "For me there is absolutely no doubt that science in Europe will continue to need the unrivalled services provided by the ILL, and its reliable and safely operated neutron source, far into the 2020s," stated Helmut Schober, Director of the ILL. And indeed, despite the increasing complexity of operating a nuclear facility and the ever more stringent demands of the safety authorities, the ILL is setting, and will continue to set, the standard for other, future, neutron sources.

L–R: Helmut Schober, Director of the ILL, during his address speech.
The legendary Bill Stirling, former Director of the ILL, acting as Master of the Ceremony.
A total of 33 directors have led the ILL over its 50 years, 16 of whom were able to join us during the ceremony.
Musical interlude during the programme.
The World Trade Center in Grenoble, which hosted the event.

THE ILL IN THE PRESS

1. Published in *Physics* on 17 October 2016
2. Published in *Belfast Telegraph* on 9 September 2016
3. Published in *R&D magazine* on 7 September 2016
4. Published in *News Medical* on 21 July 2016
5. Published in *Spektrum der Wissenschaft* on 22 June 2016

1.

Physics ABOUT BROWSE PRESS

Meetings: Physics Gets in Touch with Its "Softer" Side

2.

Belfast Telegraph

HOME NEWS SPORT BUSINESS ENTERTAINMENT TECH LIFE OPINION ARCHIVE

Titanic wreck 'will dissolve in 14 years'

By Claire McNeilly

If visiting the wreck of the Titanic is on your to-do list, you'd better get your diving equipment on.

3.

'Extremophile Bacteria' Will Eat Away Wreck of the Titanic by 2030

4.

NEWS MEDICAL LIFE SCIENCES

Neutrons key to discovering new HIV drugs? An interview with Dr Matthew Blakeley

Dr. Matthew Blakeley

THOUGHT LEADERS ...insight from the world's leading experts

What is neutron crystallography and how does it differ from X-ray crystallography?

5.

Das Neutronenrätsel

Zwei hochpräzise Experimente liefern unterschiedliche Ergebnisse für die Lebensdauer des Neutrons. Liegt die Differenz schlicht an Messfehlern, oder deutet sie auf ein bislang unbekanntes Phänomen?

Geoffrey L. Greene und Peter Geltenbort

SIGNIFIKANTE SEKUNDEN

6.

Neutron reflectivity gives insight to the role of the N-terminal sequence in Alzheimer's beta-amyloid peptide assembly

7.

ScienceDaily

Drug Discovery & Dev.

Science News

Neutrons probe structure of enzyme critical to development of next-generation HIV drugs

8.

A Puzzle Lies at the Heart of the Atom

Two precision experiments disagree on how long neutrons live before decaying. Does the discrepancy reflect measurement errors or point to some deeper mystery?

9.

Smart nanogels at the air/water interface: structural studies by neutron reflectivity

10.

Succès d'une approche innovante contre un cancer de l'intestin

6. Published in *Phys.org* on 30 May 2016
7. Published in *Science Daily* on 21 May 2016
8. Published in *Scientific American* on 1 April 2016
9. Published in *Phys.org* on 2 February 2016
10. Published in *Le Figaro* on 4 February 2016

More articles on:
http://www.ill.eu/press-and-news/press-room/ill-in-the-media/

SCIENTIFIC HIGHLIGHTS

The scientific highlights presented in this year's annual report demonstrate how research with neutrons continues to push back the frontiers of science.

14 COLLEGE INTRODUCTIONS
16 MATERIALS SCIENCE
28 MAGNETISM
42 LIQUIDS AND GLASSES
48 SOFT MATTER
58 BIOLOGY AND HEALTH
68 NUCLEAR AND PARTICLE PHYSICS
72 THEORY

As Head of the Science Division since last October, a period spanning the 50th anniversary of the founding of the ILL, I am acutely aware of the vibrant, scientific ecosystem centred around the ILL. In 1967, the ILL was the first neutron facility to be designed to serve a broad user community, the European neutron community. As a result of continuous evolution and improvement, the ILL and its users have now produced more than 21 000 scientific publications. Underpinning this world-leading scientific output, there is a team of almost 500 dedicated staff in administration, reactor, technical and science divisions who enable us to operate the highest flux reactor in the world and a comprehensive suite of state-of-the-art instruments. The Science Division, with its scientists and technicians at the interface with the user community, provides a scientific service which in most cases is a strong scientific collaboration. In-house science and these collaborations with users are key to pushing back the limits of neutron techniques, opening the door to tackling ever more complex problems in science and innovation.

The scientific highlights that follow are a small selection of the 500-plus articles that the ILL has produced in 2016, of which about 130 are considered 'high impact'. In the next two pages, the secretaries of the scientific colleges at the ILL give an indication of more general trends in neutron science. The articles reflect the unique characteristics of the neutron as a particle and a probe – it is ideally suited to studying the structure and dynamics of light atoms, for example in energy and biological materials, and, with its nuclear spin, the neutron is the best probe of magnetism. These are scientific fields that have been recognised recently with Nobel prizes in chemistry and physics, in particular in 2016! The set of articles also reflects the need to bring together technical infrastructure and instrumentation with support labs that allow the best samples to be produced and characterised for beamtime, and simulations and theory to gain deeper insight into the way that Nature works. Taken together, the support activities allow maximum benefit to be obtained from our invaluable beamtime.

The scientific and technical success of the ILL, its European partners and the scientific community underpin the construction of the European Spallation Source, which will become the most powerful spallation source of neutrons, with a user programme starting in 2023. Looking back at the ramp-up of the ILL in the '70s, ISIS (UK) in the '80s and SNS (USA) at the start of this millennium shows that, every time, ten years is required for a new facility to reach a level of scientific output commensurate with its funding and ambition. It is therefore essential that the ILL continues to invest and evolve, responding to new challenges in research and innovation and new opportunities that come with new technology, for many years to come. The ILL is a cornerstone of the European scientific community that will ensure the long-term, scientific and financial return on investment in the ESS.

The ILL is a cornerstone of the European scientific community that will ensure the long-term, scientific and financial return on investment in the ESS.

Mark R. Johnson
Associate Director,
Head of Science Division

COLLEGE INTRODUCTIONS

COLLEGE 1 – APPLIED METALLURGY, INSTRUMENTATION AND TECHNIQUES

E. Farhi (College 1 Secretary)

College 1 is dedicated to applied science and industrial applications, which mostly includes metallurgy, cultural heritage, imaging and instrumentation.

More than half of our proposals focus on residual stress, welds and industrial process, using the SALSA strain scanning instruments and other diffractometers. Subjects range from automotive, marine and aeronautical components, civil engineering, surface processing and coatings, as well as fatigue measurements, and stresses in nano-material, metals, super-alloys and ceramics.

Other College 1 activities deal with experiments that border the work of other Colleges (especially crystallography with College 5A and soft matter with College 9). This is especially true for polymers, thin-films, materials for energy, and nano-material studies using, e.g. small-angle neutron scattering. Around 15 % of the proposals involve inelastic neutron scattering spectrometers to study the fast motions in applied science materials (nuclear industry, catalysis and so on).

Finally, developments in neutron instrumentation and techniques represent about 15 % of our proposed experiments. These include the design and testing of polarised neutron beam options, to separate hydrogenated contribution to a signal for example, as well as cells for high pressure and biology.

COLLEGE 2 – THEORY

M.B. LePetit (College 2 Secretary)

In 2016 the ILL Theory Group was proud to see one of its former members, F. Duncan Haldane, receive a Nobel prize in physics. During his time with the ILL (1977-1981), Duncan Haldane collaborated with Ph. Nozières and J. Vilain, both of whom remain active emeritus members of our group.

This year we were glad to see two new collaborators join the group, namely S. Gautier working on electronic structure, and B. Tomasello working on spin ice. In addition to our regular visitors, over several months we hosted both senior collaborators – Pavel Grigoriev (Landau Institute), Mariya Gvozdikova and Avinash Singh (Indian Institute of Technology, Kanpur) – and young scientists – Ghassen Yahia (University Paris-Sud) and Begüm Koçak (CNRS). While at the ILL they worked on subjects as diverse as the interaction of ultra-cold neutrons with a He surface, spin dynamics, multiferroics physics and thin-films, collaborating with the Nuclear and Particle Physics, Spectroscopy and Diffraction groups at the ILL as well as with external users.

Finally, we would like to single out Airidas Korolkovas, and his successful defense in December of his thesis. A student working with both the Large Scale Structures and Theory groups, Korolkovas conducted both experimental and theoretical studies on the shear responsive friction at solid-liquid interfaces.

COLLEGE 3 – NUCLEAR AND PARTICLE PHYSICS

T. Jenke (College 3 Secretary)

Last year was a very exciting and promising one for College 3, as three new instruments went on line.

In spring, the instrument PN3 celebrated the commissioning of the new GAMS-6 spectrometer with its first users. As the first experiment, the refractive indices of ten different materials in an energy range between 0.1 to 2 MeV were measured with unprecedented precision and accuracy.

In November, the installation of the STEREO detector was completed successfully and data-taking began. STEREO re-establishes neutrino-physics at the ILL: the 90-ton experiment at the entrance of Level C is equipped with 68 photomultipliers and will be used to search for sterile neutrinos. Their discovery would explain the reactor anti-neutrino anomaly, and point to physics beyond the Standard Model of particle physics.

Finally, at the end of the year, FIPPS – the new fission product prompt gamma-ray spectrometer for studying exotic nuclei – came on line and produced its first results. FIPPS is the first operational instrument of the Endurance Programme. The first user experiment was dedicated to low-spin spectroscopy of 206-Tl, two nucleons away from the doubly magic 208-Pb nucleus, providing a fundamental test for nuclear models.

COLLEGE 4 – MAGNETIC EXCITATIONS

J. Ollivier (College 4 Secretary)

College 4 deals with magnetic excitations, with this year's highlights focusing on superconductors and on frustrated magnetism. Exotic magnetic excitations related to the magnetic coupling between electrons in high-Tc superconductors have been actively studied. Three-axis spectrometers with full polarisation analysis, greatly helped by the ILL high flux, are unbeatable in this game at the current time. The so-called "hour-glass"-shaped dispersion, long thought to be a universal characteristic of high-Tc superconductors and now also found in insulating parent compounds, resurfaced this year. An alternative explanation that contrasts with the one published last year in this report has been proposed, although not for the same family of materials. The origin of this type of dispersion is still openly debated.

In frustrated magnetism, the widely studied, corner-sharing, tetrahedral, magnetic pyrochlore family, is still a source of surprises. It led to the discovery of a new state of matter, where the magnetic moment splits into a fluctuating and an ordered part. This fragmentation of the magnetic degree of freedom, observed in diffraction and inelastic data, goes beyond what is observed for excitations such as the spinons in low-dimensional systems.

COLLEGE 5A – CRYSTALLOGRAPHY

E. Mossou (College 5A Secretary)

College 5A focuses on studies of single crystals and polycrystalline powder materials allowing detailed, atomic-level, structural information to be obtained from these well-ordered, solid-state materials. These studies deal with the nuclear, non-magnetic part of the structure, making use of the large suite of the ILL and CRG instruments that cover a broad length-scale from wide-angle to small-angle scattering, as well as diffuse-scattering and PDF analysis.

College 5A covers a wide range of scientific topics. Functional material and large structure proposals are amongst the most prevalent. Solid electrolyte, zeolite, hydride and catalyst materials are very popular. There has been a steady increase in lithium-ion

battery-work and more generally *in situ, in operando* studies, encouraged by recent high-profile publications. Organometallic and metal-organic frameworks represent about 20 % of our proposals.

In view of the trends in College 5A, the majority of the work is of clear relevance to innovation and industry. Direct implications for companies, identified through co-proposer affiliations and funding, however, represent a small proportion of the proposals (5 % of proposals submitted last round).

COLLEGE 5B – MAGNETIC STRUCTURES

N. Qureshi (College 5B Secretary) and **T. Saerbeck** (vice-Secretary)

As in the past, College 5B proposals were handled by the main group (diffraction) and the focus group (small-angle scattering and reflectivity), which ensured an appropriate scientific discussion for each proposal during evaluation meetings.

Among the diffraction proposals a strong interest in frustrated compounds persists, especially in pyrochlore structures for which extremely good proposals have been submitted. Multiferroic systems are still popular, including new experiments using an applied electric field in special setups. Spin-orbit coupling systems with Ir, Ru are also popular, leading to challenging experiments because of the rather weak magnetic signal and emphasising the need for the ILL's high flux.

Within the focus group, despite a reduction in the number of vortex lattice experiments the field is still active with the study of the effects of pressure and vortex depinning. There is also sustained interest in skyrmion lattices and the exploration of diverse material systems. We have seen too an increased interest in nano-magnetic systems studied using polarised SANS techniques and polarised reflectometry, such demands being ably met by the recent upgrade to full time-of-flight polarisation analysis.

COLLEGE 6 – STRUCTURE AND DYNAMICS OF LIQUIDS AND GLASSES

G. Cuello (College 6 Secretary)

The activities of College 6 are moving strongly to the field of confined and porous systems. The number of proposals has continuously increased since this new keyword has been ascribed to College 6, accounting for almost one third of submitted proposals.

The other field steadily increasing is structure determination using pair distribution function (PDF) analysis, representing around 20 % of submitted proposals. In this context, we organised the ADD2016 conference in March, bringing together more than 100 scientists.

A couple of years ago a new trend appeared in our College: the study of the structure of hydrogenated molecular liquids using polarised neutrons. This technique enables coherent and (spin) incoherent contributions to the total structure factor to be separated, which is particularly useful for those systems for which deuteration is too expensive, too difficult or simply impossible. The application of this method is not restricted to liquids, but is relevant to disordered materials in general. The best instrument for this kind of study is D3, a hot neutron diffractometer traditionally devoted to single crystals, but used in powder diffraction mode.

COLLEGE 7 – SPECTROSCOPY IN SOLID STATE PHYSICS AND CHEMISTRY

A. Piovano (College 7 Secretary)

Spectroscopy and modelling attracts a broad variety of topics in solid-state physics and chemistry fields, ranging from fundamental aspects of physics to more applied studies tackling societal challenges in environment, energy and life sciences.

Proposals are spread evenly across a range of instruments including the inelastic spectrometer LAGRANGE, the TOF machines IN4, IN5 and IN6, the three-axis instrument IN8 as well as the high-resolution instruments IN11 and IN16B. This suite of state-of-the-art instruments gives a very flexible choice of Q and energy ranges on both powders and single crystal samples.

Almost all studies are now coupled with simulations, often DFT-based, to rationalise and understand the output of experimental results. Lattice dynamics and phase transitions of complex systems, as well as the spectroscopy of molecules absorbed on surfaces, are now too complex to be explained by simple empirical models.

COLLEGE 8 – STRUCTURE AND DYNAMICS OF BIOLOGICAL SYSTEMS

A. Martel (College 8 Secretary)

College 8 deals with biological samples, using different techniques to study macromolecular structure in solution (SANS) and in crystals (LADI, D19), bio-mimicking surfaces (reflectometers, D16) and macromolecular dynamics (IN15, IN13, IN11). The systems studied are generally of health relevance but fundamental science and material science are also represented.

The information provided by these techniques is unique, thanks to their ability to distinguish macromolecules by their type (DNA versus protein), often taking advantage of deuteration to underline a particular component of the system or to focus on hydrogen bonds which are so often critical in enzymatic processes. The D-lab is available to support users wanting to deuterate biological molecules. The PSB platforms and the PSCM offer many techniques for complementary characterisation, while the biology laboratories of the EMBL are available for specific sample preparation.

COLLEGE 9 – STRUCTURE AND DYNAMICS OF SOFT CONDENSED MATTER

O. Czakkel (College 9 Secretary) and **Y. Gerelli** (vice-Secretary)

In 2016, soft matter studies remained in second place, but only by a fraction, in terms of proposals submitted to the College. Both fundamental and applied science are represented, their distribution by topic being fairly balanced. As far as proposals examining societal challenges are concerned, we have seen numerous health and environment studies. In recent years a significant increase in energy-related studies has been observed as well, looking mainly at components for future solar cells or batteries. The continuous improvement in instrumentation at the ILL has resulted in a notable increase in the complexity of the experiments in recent years. The majority of soft matter studies represent purely academic research, although approximately 10 % of proposals indicate industrial links.

The Partnership for Soft Condensed Matter (PSCM) offers a wide range of complementary techniques for soft matter studies including light scattering, ellipsometry, film balances, calorimetry and many others. In 2016 the laboratories hosted more than 100 users, with an average of 60 neutron proposals requesting access to PSCM facilities.

Multiferroic nano-clusters might help to enable the next generation of processor and memory devices

High intensity diffractometer D20

Multiferroics are materials that display both ferroelectricity and magnetism. They are promising, mainly for applications in sensor and processor technology. One of the main goals of research on multiferroics is switching magnetic bits for storing and processing data, using an electric field. Now this magnetoelectric switching has been observed for the first time, in a single-phase material at room temperature.

AUTHORS

L. Henrichs (Karlsruhe Institute for Technology, Germany)
T. Hansen (ILL)

REFERENCES

[1] M. Fiebig, J. Phys. D: Appl. Phys. 38 (2005) R123
[2] L.F. Henrichs *et al.*, Adv. Funct. Mater. 26 (2016) 2111

Magnetoelectric multiferroics are materials that are both ferroelectric and display magnetic order. The coupling that exists between these two order parameters allows for manipulation of both magnetisation by an electric field and, *vice versa*, of electric polarisation with a magnetic field. Despite the fact that extensive research has been carried out on multiferroic materials, no single-phase multiferroic with unambiguous ferroelectric and ferro- or ferrimagnetic order at room temperature has been reported to date. Single-phase multiferroics usually only display weak ferromagnetic (WFM) behaviour at room temperature, which arises from antiferromagnetic order with spin canting that causes low magnetic susceptibility and in turn limits magnetoelectric coupling [1]. This situation has now been substantially improved by a recent discovery [2]. The authors found novel nano-sized regions called multiferroic clusters in perovskite ceramics of the composition $(BiFe_{0.9}Co_{0.1}O_3)_{0.4}$-$(Bi_{1/2}K_{1/2}TiO_3)_{0.6}$, using piezoresponse force microscopy (PFM) and magnetic force microscopy (MFM).

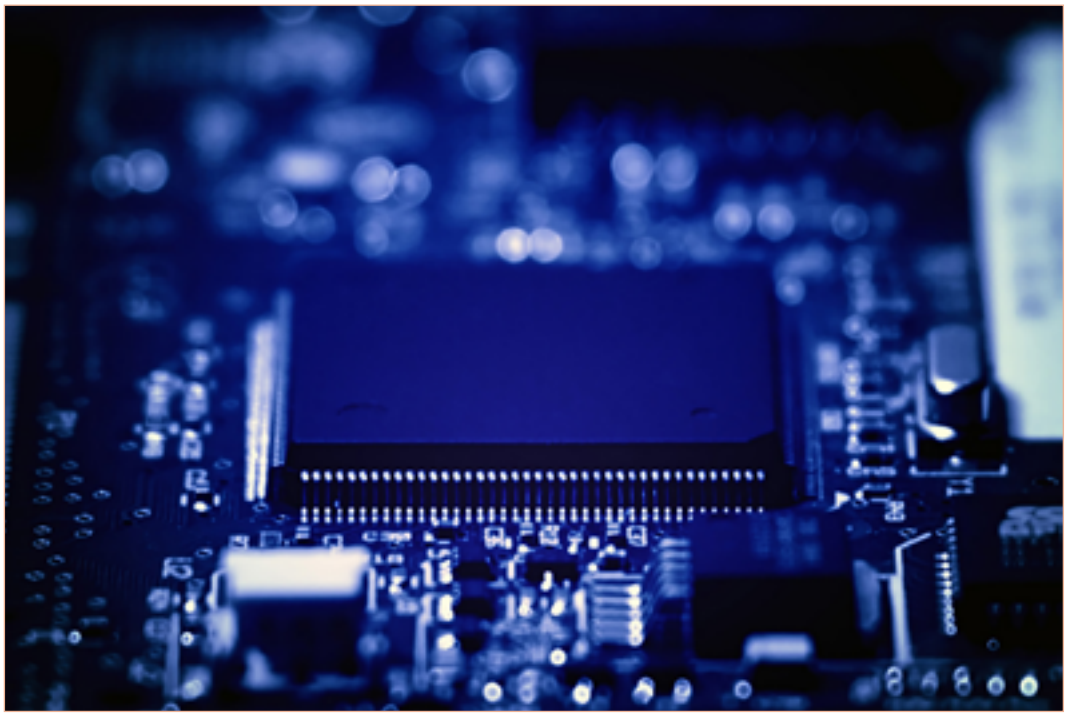

Figure 1

MFM and PFM images of a multiferroic cluster in combination with electric field poling, showing magnetoelectric switching. After local poling of the polarisation of a multiferroic cluster by applying a voltage to the AFM tip (see **d** and **e**), the magnetisation of the multiferroic cluster is switched (see **a**, **b** and **c**).

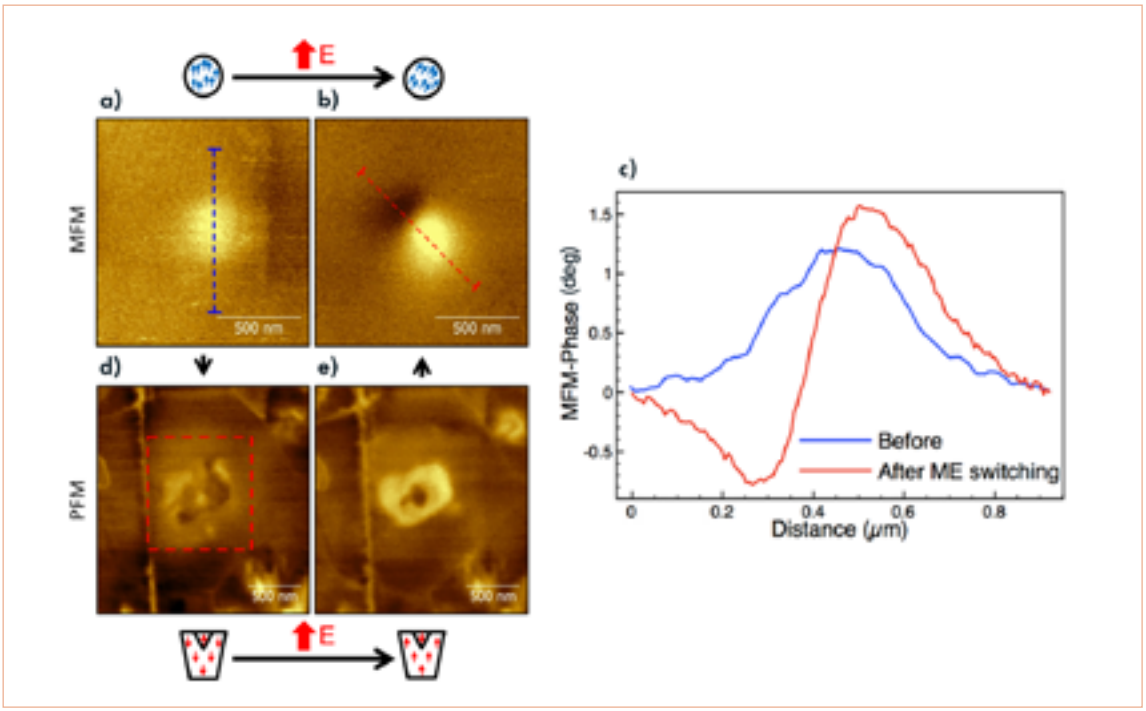

The material belongs to the class of core-shell type relaxor ferroelectrics where $BiFe_{1-x}Co_xO_3$-rich cores are surrounded by a $Bi_{1/2}K_{1/2}TiO_3$-rich shell within one grain, as was confirmed by secondary ion mass spectrometry (SIMS). The multiferroic clusters exhibit exceptionally strong magnetoelectric coupling, as found using PFM and MFM in combination with tip-induced poling (**figure 1**).

The observed electric field-induced switching of magnetisation is especially interesting in terms of applications, since in principle it enables electrically driven magnetic memory – one of the "holy grails" in information technology research. Using an electric field rather than a magnetic field to manipulate magnetic bits would drastically reduce energy consumption, which is one of the main obstacles for current technologies since it limits the frequency of processors due to waste heat.

But the multiferroic clusters exhibit not only the converse but also the direct magnetoelectric coupling effect, as found by PFM under *in situ* magnetic field. From PFM signal variation as a function of magnetic field, the local magnetoelectric coupling coefficient could be estimated to be $\alpha \approx 1.0 \times 10^{-5}$ s/m ($dE/dH \approx 1.3$ kV/(cm Oe)), which is one of the largest magnetoelectric coupling coefficients reported in the literature so far. This represents another promising perspective for the material, namely as a potential magnetic field sensor. Such multiferroic magnetic field sensors might one day compete with the extremely expensive and elaborate superconducting quantum interference devices (SQUID), for example, in biomedical diagnostics and imaging.

It is assumed that the strong magnetism stems from ferrimagnetic order of Fe and Co in the multiferroic clusters, which requires a superstructure of Fe and Co on the B site of the perovskite lattice. At the powder diffractometer D20 at the ILL, the authors were able to determine the Néel temperature $T_N = 670 \pm 10$ K using neutron diffraction. Due to magnetic impurity phases present in the samples, this was not possible with other techniques. This finding is very important, since the Néel temperature is remarkably high, being even higher than that for pure $BiFeO_3$. This is completely unexpected given the fact that the material contains a large amount of diamagnetic titanium ions. The high Néel temperature is proposed to be a consequence of the ferrimagnetic order and thus underpins the extraordinary magnetic properties of the material.

However, there are still many challenges. One of them is that the multiferroic clusters have far too low a concentration in the ceramic material to be meaningful for any application. This will be addressed in future research. But it is also anticipated that deeper understanding of the multiferroic clusters might give valuable insights for the design of, e.g. a thin-film material with similar multiferroic properties to the multiferroic clusters. That is where the true value of this discovery might unfold.

Dynamically slow solid-to-solid phase transition induced by thermal treatment of DimimFeCl$_4$ magnetic ionic liquid

High-resolution powder diffractometer D2B, high-resolution two-axis powder diffractometer D1B and diffuse scattering spectrometer D7

The field of ionic liquids (ILs) is growing at a very fast rate, as the many useful features of these liquids are recognised and applied. A subset of ILs are magnetic ionic liquids (MILs), which are produced through the incorporation of a paramagnetic component in either the cation or anion of the IL structure [1]. Often comprising transition metal or lanthanide metal ions, MILs can combine IL characteristics with additional intrinsic, thermochromic, magneto-electrochromic or luminescent [2] properties depending on the enclosed paramagnetic ion used. Moreover these molten salts, with a melting point below 100 °C, have properties which in a liquid state can be tuned by means of external magnetic fields [3].

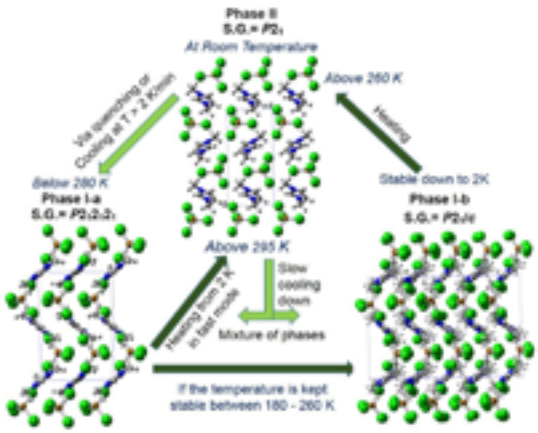

AUTHORS

I. de Pedro, **J. Junquera** and **J. Rodríguez Fernández** (CITIMAC, University of Cantabria, Santander, Spain)
O. Fabelo, **A. Wildes** and **M.T. Fernández-Díaz** (ILL)

REFERENCES

[1] R. Hayes, G.W. Gregory and R. Atkin, Chem. Rev. 115 (2015) 6357
[2] **(a)** P. Brown, C.P. Butts, J. Eastoe, E.P. Hernández, F.L. de Araujo Machado and R. de Oliveira, Chem. Eng. Commun. 49 (2013) 2765; **(b)** B. Mallick, B. Balke, C. Felser and A.-V. Mudring, Angew. Chem. Int. Ed. 47 (2008) 7635
[3] T. Torimoto, T. Tsuda, K.I. Okazaki and S. Kuwabata, Adv. Mater. 22 (2010) 1196
[4] I. de Pedro, O. Fabelo, A. García-Saiz, O. Vallcorba, J. Junquera, J.A. Blanco, J.C. Waerenborgh, D. Andreica, A. Wildes, M.T. Fernández-Díaz and J. Rodríguez Fernández. Phys. Chem. Chem. Phys. 18 (2016) 21881
[5] **(a)** A. Garcia-Saiz, I. de Pedro, P. Migowski, O. Vallcorba, J. Junquera, J.A. Blanco, O. Fabelo, D. Sheptyakov, J.C. Waerenborgh, M.T. Fernández-Díaz, J. Rius, J. Dupont, J.A. González and J. Rodríguez Fernández, Inorg. Chem. 53 (2014) 8384; **(b)** A. García-Saiz, P. Migowski, O. Vallcorba, J. Junquera, J.A. Blanco, J.A. González, M.T. Fernández-Díaz, J. Rius, J. Dupont, J. Rodríguez Fernández and I. de Pedro, Chem. Eur. J. 20 (2014) 72

We have observed that cooling rate could be a very important variable for the dynamical process, structural transformations and magnetic behaviour of MILs [4]. In previous studies, we have synthesised one family of MILs based on tetrahaloferrate(III) anions and imidazolium cation, and have established an accurate relationship between their crystal structure and magnetic properties [5]. One of these compounds, DimimFeCl$_4$, shows a sequence of structural phase transition as a function of the cooling and heating protocol. The RT form (hereafter **II**) transforms into **I-a** phase if a "fast" cooling is used, either by thermal quenching of the sample in a N_2 flux (down to about 100 K) or by placing the sample in a standard orange cryostat, pre-cooled to increase the cooling rate (**figure 1**).

The application of a thermal treatment to the **I-a** phase can induce an unprecedented solid-to-solid phase transition in this MIL. We have determined its crystal structure by combining synchrotron and high resolution neutron powder diffraction on the D2B diffractometer. The new **I-b** phase (**figure 1**) was not observed by differential scanning calorimetry or specific heat upon either cooling or warming the sample. Only after keeping the **I-a** under a critical temperature for several minutes was the transformation to **I-b** phase observed. This solid-to-solid phase transition involves a translational and reorientational process of the $[Dimim]^+$ counterions and $[FeCl_4]^-$ anions. The main goal of this work is to relate this transformation, obtained by simple thermal treatment, to the changes in the physical properties and macroscopic magnetic interactions of MILs. This observation could pave the way for novel stimuli-responsive materials using temperature effects [4]. Similar trends are expected in ILs in which bulky cations exhibit a strong electrostatic coupling with small anions such as halides.

Figure 1

Phase transitions of Dimim[FeCl$_4$] observed as a function of temperature – brown (iron), green (chloride), grey (carbon), blue (nitrogen) and white (hydrogen). The blue dashed square represents the unit cell.

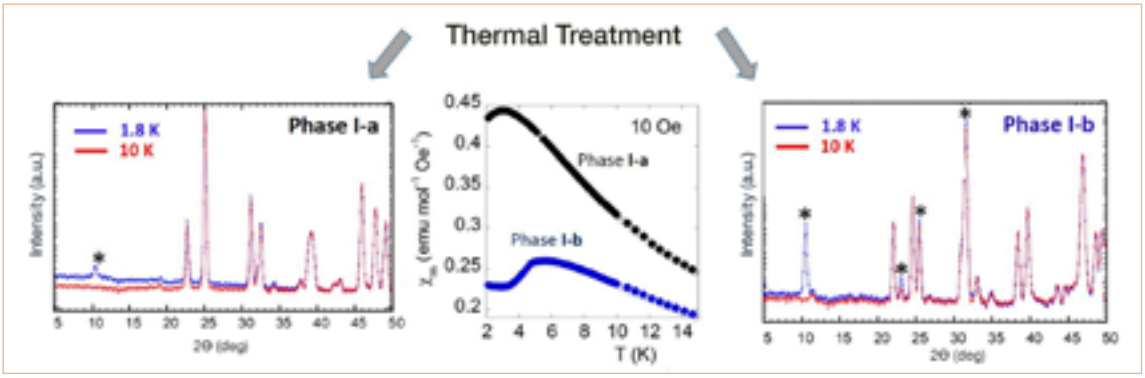

Figure 2 (above)

Centre) Low temperature ZFC-FC magnetic susceptibility at 10 Oe for phases **I-a** and **I-b**.

Right and **left)** The neutron diffraction profiles of **I-a** and **I-b** phases at 10 K (red) and 1.8 K (blue) obtained in D1B. The (*) dots show the magnetic contributions.

The magnetic behaviour of these phases is closely associated with the structural features. The molar magnetic susceptibilities of both phases increase with decreasing temperature, presenting a broad maximum and suggesting the existence of a long-range antiferromagnetic ordering (**figure 2**). The long-range magnetic order has been confirmed by neutron diffraction. The comparative view of the neutron diffraction data collected at D1B, above and below order temperature (10 K and 1.8 K) on **I-a** phase, reveals a small, sharp, Bragg peak (indicated by * in **figure 2**). This additional elastic intensity is weak but sufficient to prove the long-range antiferromagnetic order. However, the same comparison carried out after the structural transformation into the **I-b** phase displays the occurrence of several well defined magnetic peaks, which is the signature of a long-range magnetic order. An interesting feature observed in this compound is the increase of the background at low temperature (below T_N). The effect is more significant in the **I-a** phase, and this, together with its occurrence in the same temperature range as that of the long-range magnetic order, suggests that it can be related to the magnetic interactions on these compounds.

Polarised neutron diffraction studies through XYZ-analysis on D7 have been used to study the origin of these signals. The results unambiguously show that the increase of background in the neutron diffraction data is not of magnetic origin. From the polarisation analysis the increase of background is compatible only with a significant increase of the signal on the nuclear-spin incoherent channel. Therefore, it should be associated with structural features probably due to the hydrogen atoms of the methyl groups.

The magnetic scattering observed on D7 is very similar for both compounds: both are compatible with a propagation vector **k** = (0, 0, 0), although the intensity of the magnetic reflections are notably lower for the **I-a** phase. The magnetic structure was refined using the **I-b** data, giving rise to ferromagnetic layers extended into the *ac*-plane which are antiferromagnetically coupled along the *b*-axis. This model is compatible with the splittings observed in the

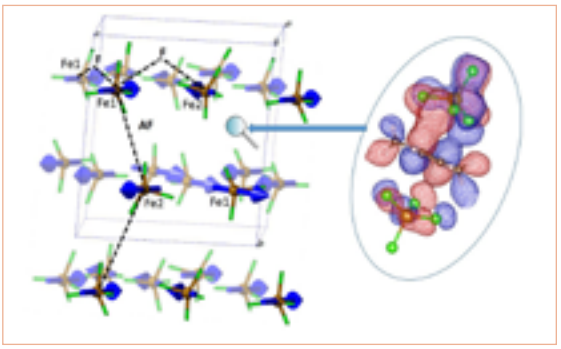

Figure 3

Left) Magnetic structure of phase **I-b** at 1.8 K. The Dimim counterions have been omitted for the sake of clarity.

Right) Shorter π–d interaction distances between the metal complex and imidazolium centroid. Representation of the wave function for the state with energy of –2.34 eV below the Fermi energy, where there is orbital overlapping (red and blue colours represent the positive and negative parts respectively).

Mössbauer data below T_N, suggesting that the magnetic structure of **I-b** should have two Fe^{3+} magnetic sub-lattices with different magnetisation directions relative to the crystallographic axes (**figure 3**).

The magneto-structural correlations involving mainly the interatomic distances and angles reveal the reason why the strength of these super-exchange anion–anion interactions (Fe–Cl···Cl–Fe) can be stronger within phase **I-b**. The main factor should be attributed to the shorter Cl···Cl distances, which are correlated with stronger magnetic exchange constants. Moreover, the possibility that **I-b** could also have indirect super-exchange antiferromagnetic interactions through anion-π pathways (Fe–Cl···Im···Cl– Fe) between adjacent planes should also be considered. These results were confirmed by density functional theory calculations using the projected density of states (PDOS) of the imidazolium with the chloride of the metal complex anion.

ACKNOWLEDGMENT

The authors also gratefully acknowledge the computer resources, technical expertise and assistance provided by the Red Española de Supercomputación. The paper is (partly) based on the results of experiments carried out at the Paul Scherrer Institut, Villigen, Switzerland, the ALBA synchrotron light source in Barcelona and the Institute Laue-Langevin (ILL) in Grenoble.

Influence of Li^+ and H^+ distribution on the crystal structure of highly stable garnets

High-resolution two-axis diffractometer D2B

AUTHORS

A. Orera, **G. Larraz**, **J. Campo** and **M.L. Sanjuán** (Instituto de Ciencia de Materiales de Aragón, CSIC-University of Zaragoza, Spain)
J.A. Rodríguez-Velamazán (ILL)

REFERENCES

[1] V. Thangadurai, S. Narayanan and D. Pinzaru, Chem. Soc. Rev. 43 (2014) 4714
[2] C. Ma, E. Rangasamy, C. Liang, J. Sakamoto, K.L. More and M. Chi, Angew. Chem. Int. Ed. 54 (2015) 129

Lithium-containing compounds with garnet-type structure have attracted significant interest in the last decade for their potential applications as electrolytes in all-solid-state Li batteries [1]. However, an important issue for their application is the known reactivity of these materials with water, either from the air or in aqueous media, which results in important losses of Li and the appearance of secondary phases that may be detrimental for conductivity.

One of the processes that takes place in these materials in the presence of water is hydration through H for Li exchange. On principle it was assumed that hydration was harmful and to be avoided, but it has recently been proposed that for a particular family of this class of materials, $Li_{7-x}H_xLa_3Zr_2O_{12}$ (LLZO), the stability of the most hydrated compound can be advantageous for its possible use as a separator between the Li anode and the electrolyte in aqueous Li batteries [2]. LLZO is one of the compounds of its class with the highest Li content; it presents the particularity of being tetragonal in its most stable form at room temperature, instead of showing the usual cubic structure of the garnets. The high Li content of LLZO results in an especially high sensitivity of this compound to moisture. In this context, whether for use as a solid electrolyte or as a separator between the Li anode and a liquid electrolyte, it is clear that the reactivity and/or stability of these materials in contact with water is a matter of interest.

Figure 1

Schematic representation of the Li and H sites in the crystal structure of the parent LLZO compound **(left)**, and in the two hydrated phases: non-centrosymmetric **(top right)** and centrosymmetric **(bottom right)**.

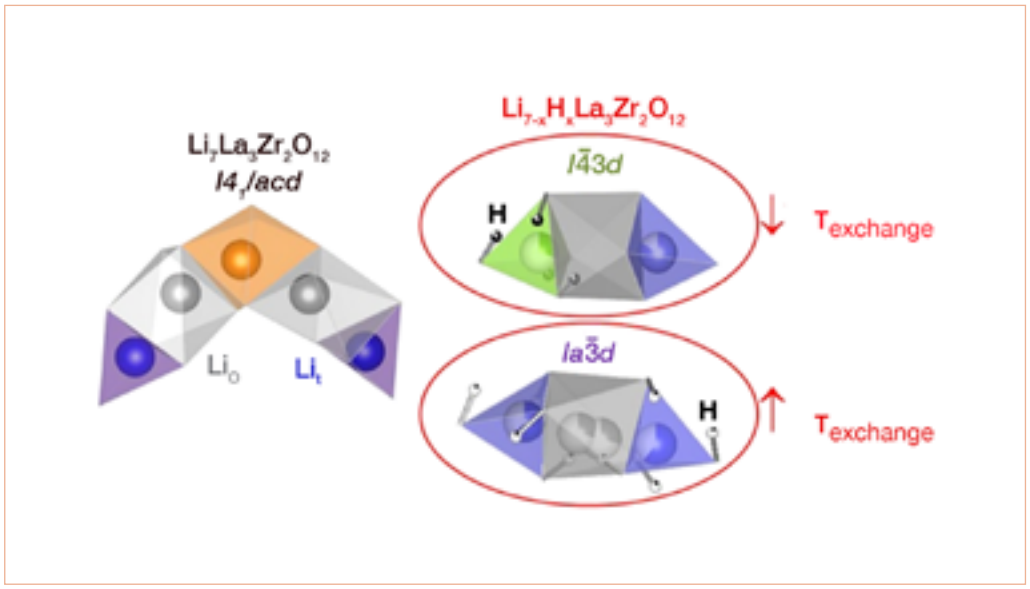

Figure 2

Neutron powder diffraction patterns of the two phases of hydrated LLZO recorded at 77 K. The points are the experimental data and the continuous curve the result of the refinements. The bottom curve represents the difference between the experimental data and the calculated pattern. **Left)** Non-centrosymmetric $I\bar{4}3d$ form. **Right)** Centrosymmetric $Ia\bar{3}d$ form. Li_2CO_3 was included in the refinement as second phase in this last case.

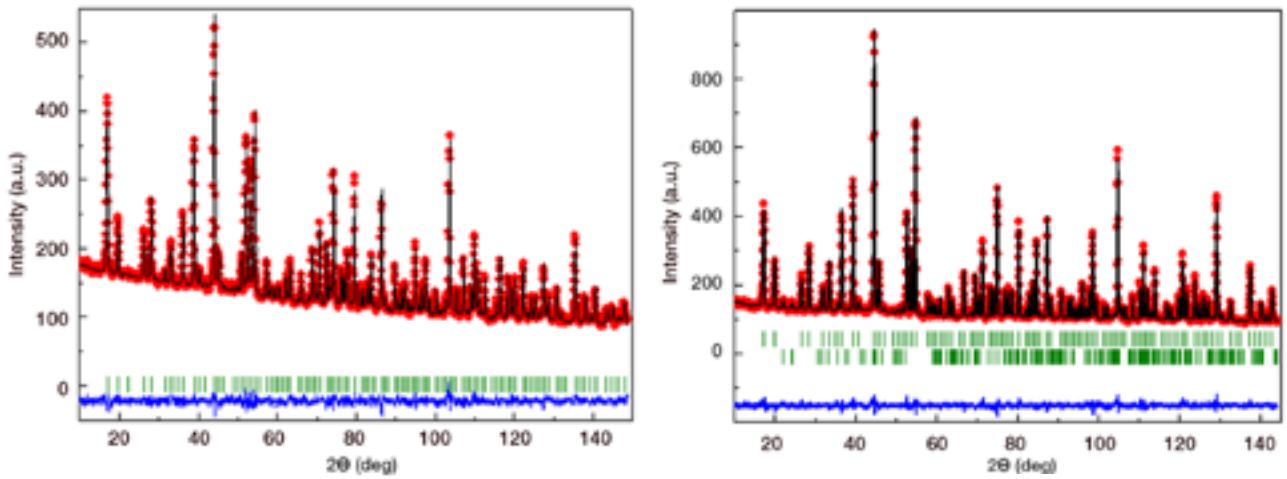

By performing H for Li exchange of tetragonal LLZO in a wide range of experimental conditions, we have been able to propose a landscape of phases formed as a function of the exchange temperature and H content (**figure 1**). Using neutron diffraction, which provides unique insights to elucidate Li and H location, we have addressed the structural changes undergone by LLZO as a result of H^+/Li^+ exchange and related them to the amount of H content and atomic distribution. Two different cubic phases with quite different Li distribution derive from LLZO through H^+/Li^+ exchange:

- The first one is a non-centrosymmetric $I\bar{4}3d$ phase (**figure 1 and figure 2, left**), which is reached by deep hydration at low temperature (up to 150 °C). In this phase octahedral Li ions are exchanged by H ions, tetrahedral Li ions split into two sites with very different occupancies, and H ions form O_4H_4 entities around the less occupied tetrahedral site.
- The second phase, with lower H content, is centrosymmetric $Ia\bar{3}d$ (**figure 1 and figure 2, right**), and stabilising it requires annealing above 300 °C. In this phase, Li occupies the usual sites (octahedral and tetrahedral) of the Li conducting cubic garnets and H ions occupy a split pseudo-octahedral site.

The centrosymmetric or non-centrosymmetric character is determined by the temperature at which exchange is performed (linked to Li dynamics) and the H content. Neither factor is independent: at low temperature, the high H content favours H ordering around the vacant tetrahedra, while low H content and higher mobility at 350 °C lead to a disordered configuration of both Li and H ions. The deeply hydrated garnets show an excellent stability, up to at least 300 °C and also upon ageing at room temperature.

Lithiation of crystalline silicon: an *in situ* neutron reflectivity study

Reflectometer D17

Lithium-ion batteries are widely developed and used as rechargeable power sources for several portable devices and will be essential in the field of automotive transportation. Crystalline silicon is a promising anode material with a very high specific capacity of 3579 mAh/g. We studied the processes occurring during electrochemical cycling directly at the electrode/electrolyte interface, with *in situ* neutron reflectivity, and gained information on the concentration distribution of lithium inside the electrode and on the mechanisms and kinetics.

AUTHORS

B.-K. Seidlhofer, **M. Trapp**, **S. Risse**, **R. Steitz** and **M. Ballauff** (HZB, Germany)
B. Jerliu, **E. Hüger** and **H. Schmidt** (TU Clausthal, Germany)
R. Cubitt (ILL)

REFERENCES

[1] M. McDowell *et al.*, Adv. Mater. 25 (2013) 4966
[2] J. Zhao *et al.*, Nat. Commun. 5 (2014) 5088
[3] B. Jerliu *et al.*, Phys. Chem. Chem. Phys. 15 (2013) 7777
[4] B. Seidlhofer *et al.*, ACS Nano 10 (2016) 7458

The major drawback of silicon anodes is the enormous volumetric expansion, of up to more than 300 %, at full lithiation. This is followed by fragmentation of the electrode, which leads to capacity loss and poor cycling stability. Decreasing the particle size to the nanoscale leads to materials that are better able to accommodate the stress and strain occurring during cycling without fracture [1]. At the present time, several systems containing nanoscopic silicon particles show promising cycling rates and may be used in future battery technologies [2]. Nevertheless, for future applications it is important, if not necessary, to gain a microscopic understanding of the mechanisms and kinetics going on during cycling.

To obtain a deeper insight into the processes occurring during cycling, a quantitative and time-resolved study of the lithiation/delithiation of crystalline silicon was performed at the neutron reflectometer D17 under *operando* conditions (**figure 1**; see [3] and [4] for more information on the electrochemical cell used). A very low current density (2 µA / cm²) and short data acquisition time (5 minutes) were used to allow a precise determination of all intermediate stages arising during battery operation. Due to the strong scattering contrast between silicon and lithium, a precise depth profile of Li within the silicon anode can be gained as a function of time (**figure 2**, [4]).

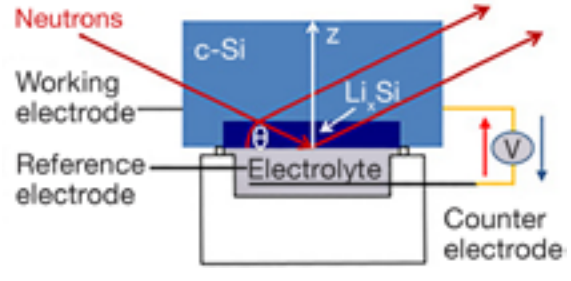

Figure 1

Sketch of the electrochemical cell used for the neutron reflectometry studies. The cell is composed of a crystalline silicon working electrode, a lithium counter and reference electrode, and 1 M $LiClO_4$ in propylene carbonate as the electrolyte. The Li_xSi layer formation is indicated in dark blue.

Figure 2

SLD profiles of the first **(a)** and second **(b)** cycle as a function of time and distance from the interface: c-Si (green), deep lithiation (red-yellow), surface lithiation (red/dark-red), native SiO_2 (violet), surface layer (light-green), surface enrichment (orange) and electrolyte (yellow).

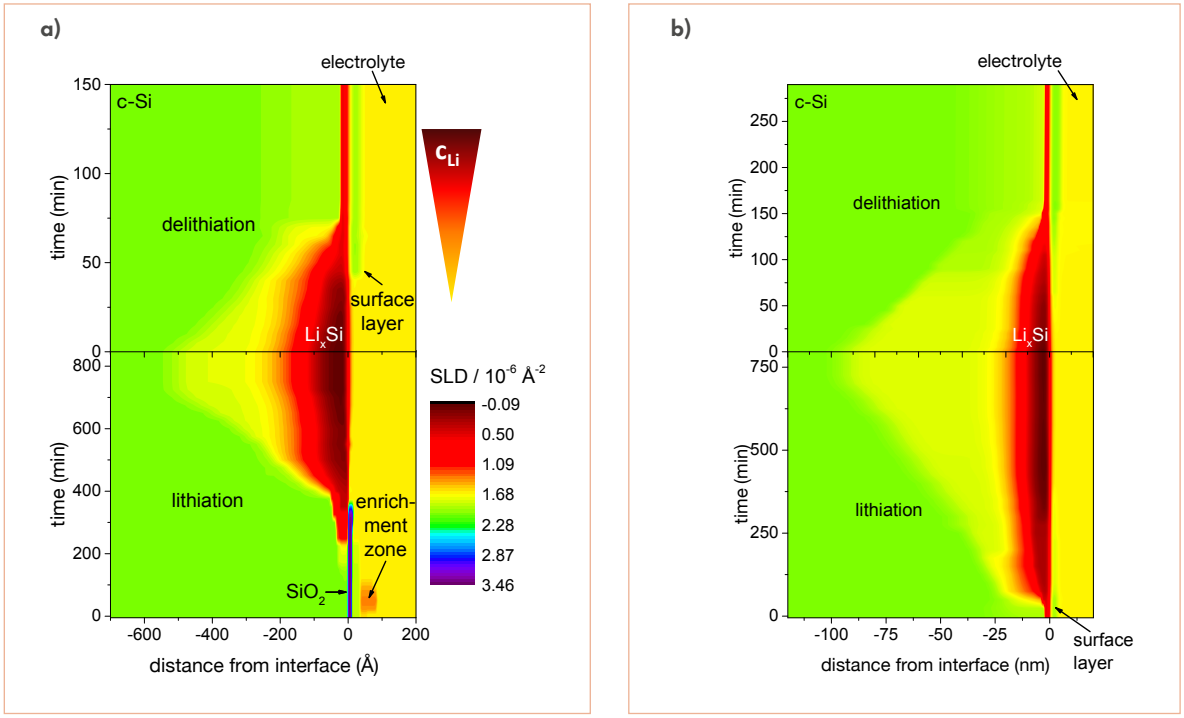

Figure 2 shows a colour map of the scattering length density (SLD) profiles – which are related to the lithium concentration inside the silicon electrode – plotted against the reaction time and distance from the electrode/electrolyte interface of the first (**a**) and second (**b**) cycle. Four regions are observable before the first lithiation starts: crystalline silicon c-Si (green), native silicon oxide SiO_2 (violet), a surface layer composed of decomposition products from the electrolyte (light-green) and the electrolyte (yellow) (**figure 2a**).

The first lithiation occurs via two different stages. At the beginning, reactions occur at the electrode surface followed by the lithiation of the electrode. The first stage starts with the formation of a lithium enrichment zone adjacent to the electrode surface (**figure 2a**, orange). After some time the lithium enrichment zone, the surface layer and the native SiO_2 successively decompose. Now the lithiation of silicon starts (dark-red to yellow). The lithiated zone is subdivided into two distinct parts: a highly lithiated zone in the skin region of the electrode, composed of $Li_{x\sim2.5}Si$ with a thickness of ~ 20 nm; and a lowly lithiated zone in an adjacent growth region towards c-Si, composed of $Li_{x\sim0.1}Si$ with a thickness of ~ 32 nm. During delithiation a solid electrolyte interface is formed at the electrode/electrolyte interface and a well-defined amount of lithium remains present in the skin region of the electrode with the composition $Li_{x\sim1.1}Si$ (**figure 2a**).

During the second lithiation no enrichment zone is visible at the electrolyte/electrode interface. Growth and skin region are formed containing the same lithium concentration in Li_xSi as in the first cycle, while the thickness of the growth region increases from ~ 32 to ~ 76 nm. Additionally, the solid electrolyte interface is decomposed during the second lithiation and formed again during the delithiation (**figure 2b**).

The *operando* analysis performed on D17 demonstrates that neutron reflectivity is able to track the kinetics of lithiation and delithiation with high temporal and spatial resolution. We conclude that the thickness and the composition of the highly lithiated skin layer is independent of the cycle number. Rather, the thickness of the growth region increases from the first to the second lithiation while its composition remains the same, independent of cycle number. The experiments show that crystalline silicon slabs can be effectively used as an anode material, if the lithiation is limited to ~ 20 nm by, for example, decreasing the particle size [2] or an appropriate charge/discharge programme.

Quasi-elastic neutron spectroscopy sheds light on the molecular dynamics of organic photovoltaic solar cells

Time-of-flight spectrometer IN6

Today, primary energy consumption is about 18 TW worldwide and is projected to reach 30 TW by 2050. Our current energy mix is dominated by fossil fuels, at about 80 %, while renewable energies account only for about 10 %, the difference being made up of nuclear energy [1]. The continued use of fossil fuels on a massive scale is associated with tremendous hidden costs. The National Research Council has estimated the aggregate damages of electricity production unrelated to climate change in 2005 at about 30 % of the levelised price of electricity per kWh produced from coal for instance [2]. The costs associated with climate change were 5 to 25 % of the levelised price of electricity per kWh produced from fossil fuels. This poses the following societal question: Are we prepared to assume the costs linked to the utilisation of these energy sources at those scales?

AUTHORS

A.A.Y. Guilbert, **M.V.C Jenart** and **J. Nelson** (Imperial College London, UK)
C.B. Nielsen (Imperial College London and Queen Mary University of London, UK)
M. Zbiri (ILL)

REFERENCES

[1] S.B. Darling and F. You, RSC Adv. 3 (2013) 17633
[2] Global Wind Energy Council, Global Wind Energy Outlook 2014.
[3] http://www.solarserver.com/news/news-e-1275.html
[4] http://cen.acs.org/articles/94/i18/future-low-cost-solar-cells.html
[5] A.A.Y. Guilbert, M. Zbiri, M.V.C. Jenart, C.B. Nielsen and J. Nelson, J. Phys. Chem. Lett. 7 (2016) 2252
[6] A.A.Y. Guilbert, M. Zbiri and J. Nelson, J. Phys. Chem. Lett. (submitted).

Renewable energies are possible alternatives to energy from fossil fuel. Solar energy is especially promising, with the potential to deliver up to 67 TW assuming 2 % of land coverage with an average power conversion efficiency of 12 % [1].

Secure and widespread access to energy sources requires new functionalised materials that combine high availability, low environmental impact, high throughput processing, high efficiency and low cost. The search for such solar conversion technologies has led to growing interest in solution-processable semiconductors, among them molecular electronic materials. Molecular electronic materials offer facile synthesis combined with low energy production, tuneability of their optical and electronic properties through chemical design and thus versatility of applications and, finally, compatibility with high throughput fabrication routes such as roll-to-roll processing. They can also be semi-transparent, aesthetic, and thus easily integrated into architecture design.

The best organic photovoltaic devices have an efficiency of over 10 % and a lifetime of just a few years, which has hindered their commercialisation. It has been shown that efficiency is directly linked to the microstructure of the organic active layer, and that the operational lifetime is affected by the stability – under illumination and thermal cycling – of the active layer. The active layer is a blend of a donor material, typically a conjugated polymer, and an acceptor molecule, typically a fullerene derivative. Few characterisation techniques allow the dynamics of this blend to be probed; quasi-elastic neutron scattering (QENS) is one of them. QENS is a very powerful technique, especially when combined with selective deuteration which allows different components of the blend to be probed independently. QENS time scales are directly relevant to electronic processes within the blend. A better understanding of these dynamics at the atomistic level will help to guide the chemical design of new donor and acceptor materials to achieve better efficiencies and longer lifetimes.

In this context, we investigated the active layer blend of poly(3-hexylthiophene-2,5-diyl) (P3HT) and phenyl-C61-butyric acid methyl ester (PCBM) (**figure 1**) [5]. This presented some challenges: (i) resolving the signal from P3HT (donor) and PCBM (acceptor) in the blend; and (ii) resolving

Figure 1

a) Integrated organic solar modules [3];
b) Flexible organic solar modules from roll-to-roll process [4];
c) Organic solar cell structure;
d) Molecular dynamic simulation snapshot of the active layer blend;
e) Chemical structure of poly(3-hexylthiophene);
f) Chemical structure of fullerene derivative phenyl-C61-butyric acid methyl ester.

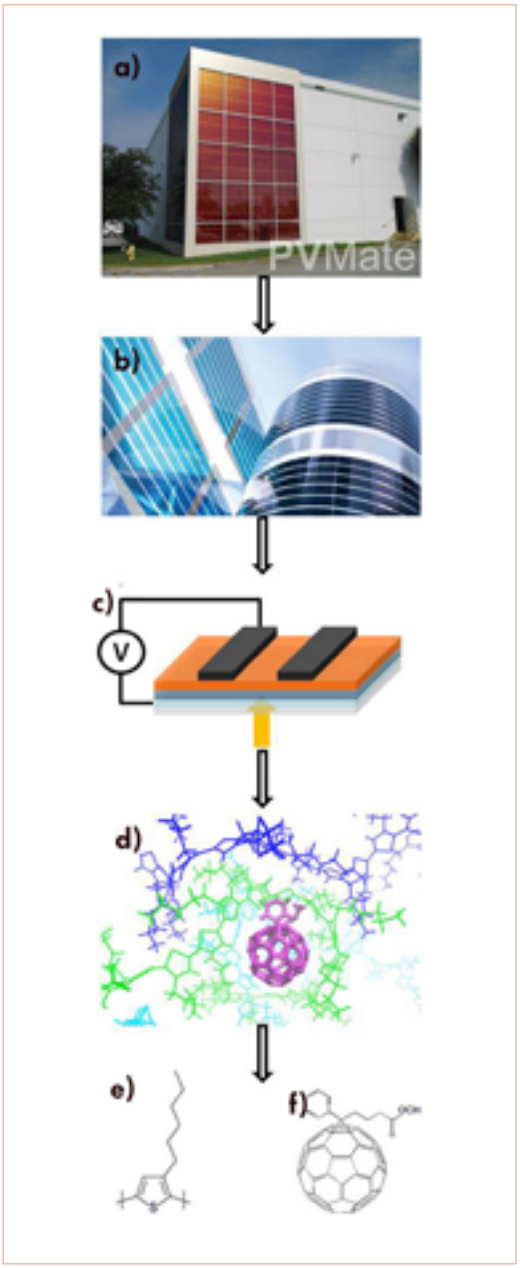

Figure 2

QENS spectra measured on IN6 showing: **a)** the frustration of P3HT, and **b)** the plasticisation of PCBM upon blending; **c)** scheme of the complex microstructure of the blend with P3HT crystals, PCBM crystalline needles and an amorphous mixture of P3HT and PCBM; and, MD simulation snapshots of **d)** PCBM crystals, **e)** P3HT crystals and **f)** P3HT-PCBM amorphous mixture.

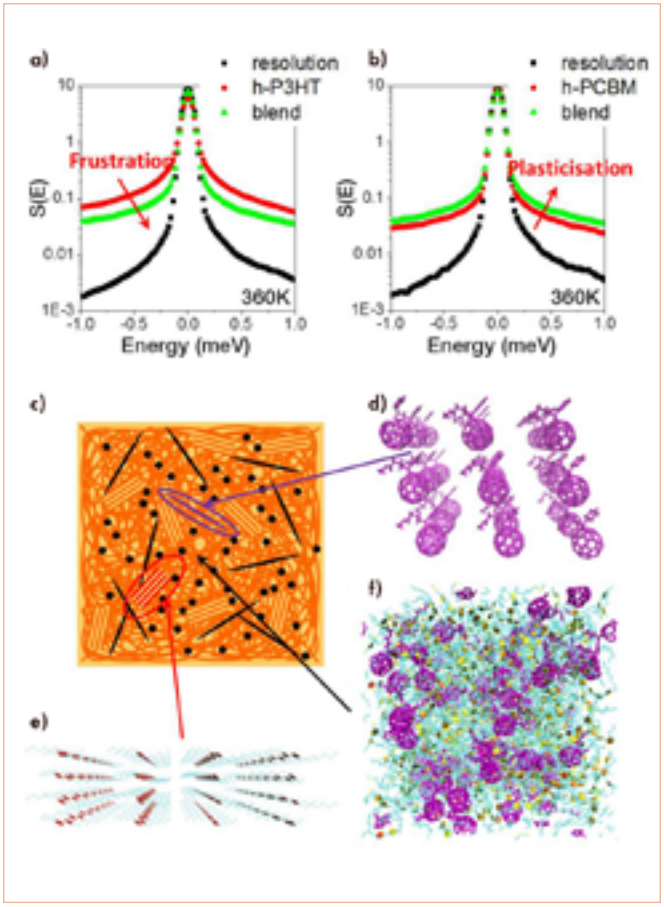

the different phases of the blend microstructure (neat crystalline phase or amorphous mixture). We successfully used the deuteration technique to enhance the signal of one component of the active layer with respect to the other [5]. Using the time-of-flight spectrometer IN6, we showed that P3HT dynamics becomes frustrated when mixed with PCBM, while PCBM becomes more mobile in the blend above the glass transition of P3HT (**figure 2**). This enhanced mobility is likely to lead to further phase segregation and is one of the degradation mechanisms of organic solar cells. This work also highlighted rich, temperature-dependent dynamics of the side chain of both components. In combination with QENS, we used molecular dynamics simulations [6] to study separately the different phases of the microstructure and to unravel the observed complex dynamical behaviour [5].

As far as the electronic aspect is concerned side chains are mainly insulators, and thus the appearance of heterogeneous dynamics of these side chains on a time scale relevant for charge generation is likely to modulate the intermolecular electronic coupling between polymer and fullerene due to screening effects. On the time-of-flight time scale we found that side chains dynamics are strongly impacted by temperature, especially for a low glass transition polymer such as P3HT, and are likely to play an important role in the solar cell degradation. These are very promising results, which call for a continuation in order to probe longer time scales. We are therefore in the process of extending our study to cover further dynamical aspects using the backscattering technique.

Neutrons reveal 'quantum tunnelling' on graphene

Three-axis spectrometer
IN1-LAGRANGE

AUTHORS

C. Cavallari, **S. Rols**, **M. Jiménez-Ruiz**, **M.R. Johnson**, **H. Fischer**, **O. Meulien** and **A. Bertoni** (ILL)
D. Pontiroli and **M. Riccò** (University of Parma, Italy)
S.F. Parker (ISIS, UK)

REFERENCES

[1] P.A. Denis and F. Iribarne, J. Phys. Chem. C 117 (2013) 19048 [doi: 10.1021/jp4061945]
[2] C. Cavallari *et al.*, Phys. Chem. Chem. Phys. 18 (2016) 24820 [doi: 10.1039/C6CP04727K]

Graphene is known as the world's thinnest material due to its stable 2D structure, where each sheet is only one carbon atom thick, allowing each atom to engage in a chemical reaction from two sides. Graphene flakes can have a very large proportion of edge atoms, with a specific chemical reactivity. In addition, chemically active voids created by missing atoms are surface defects of graphene sheets. These structural defects and edges play a vital role in carbon chemistry and physics, as they alter the chemical reactivity of graphene. In fact, chemical reactions have repeatedly been shown to be favoured at these defect sites [1].

Interstellar molecular clouds are predominantly composed of hydrogen in molecular form (H_2), but also contain a small percentage of dust particles mostly in the form of carbon nanostructures, called polyaromatic hydrocarbons (PAH). The abundance of H_2 in inhospitable regions of space, despite the intense cosmic radiation that constantly cracks the hydrogen molecules into single atoms, raises the controversial question of the origin of its stability. Astrochemists have suggested that carbon flakes in interstellar clouds catalyse the chemical mechanism responsible for the recombination of atomic H into molecular H_2. This theory is challenged by the need for a very efficient surface chemistry scenario to explain the observed equilibrium between dissociation and recombination. In this context, the presence of highly reactive sites for the capture of atomic H nearby appears crucial for the sustainability of the overall process, known as Eley-Rideal reaction, which recombines two H atoms into one H_2 molecule.

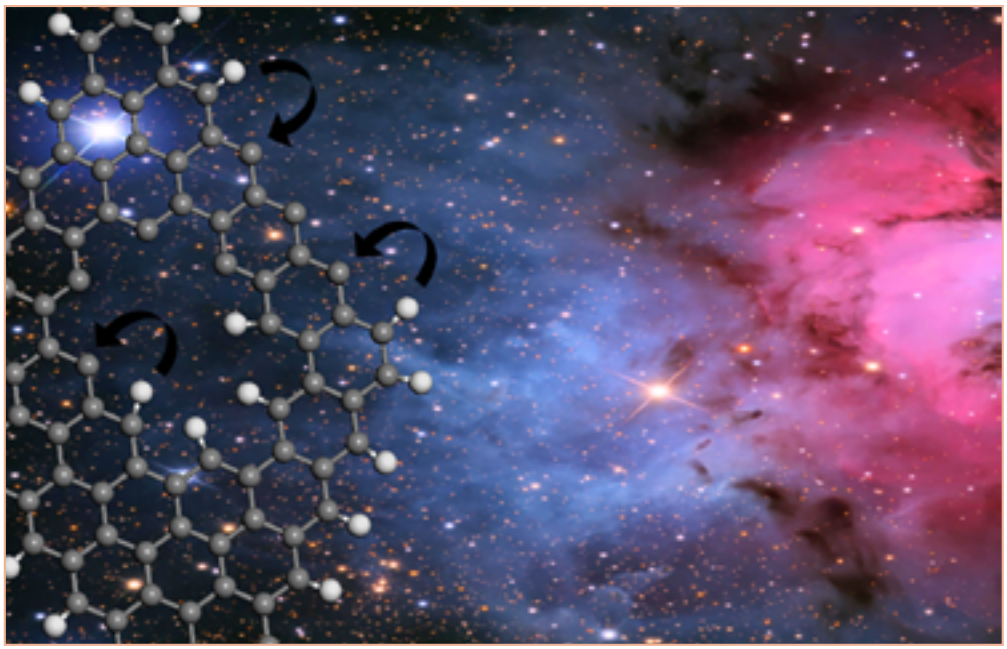

Figure 1

Atomic model of the graphene flake used to simulate the data. Carbon atoms are in grey and H atoms in white. The latter populate either the edges or the in-plane vacant defects. Arrows schematically depict the quantum jump of the H atoms.

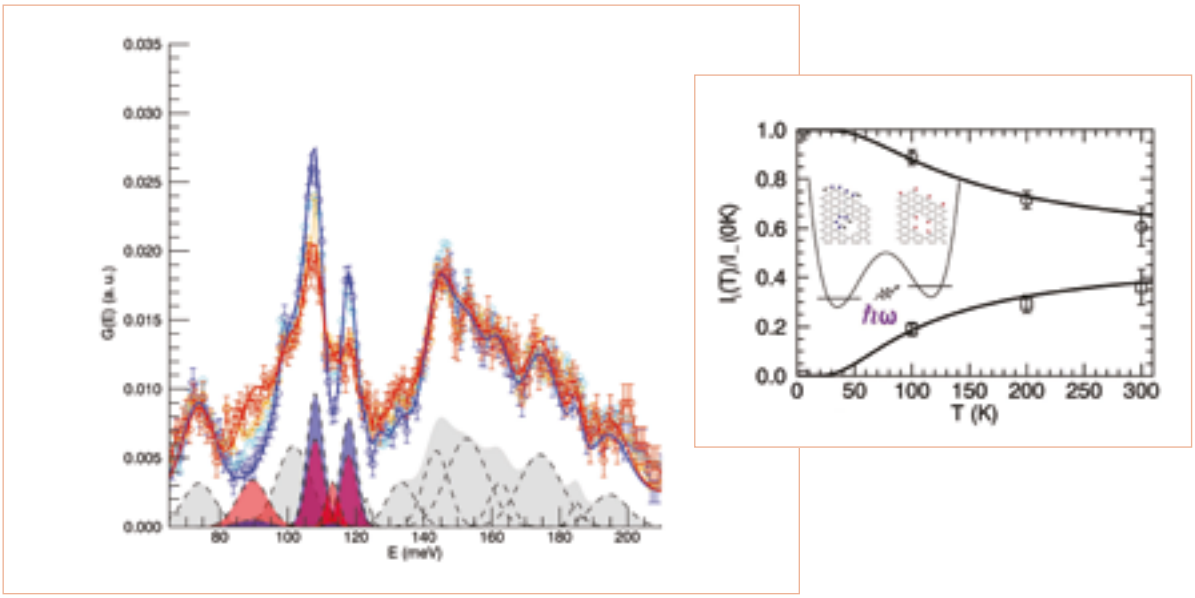

Figure 2

IN1-LAGRANGE spectra in the bending mode region measured at 1.5 K (blue), 100 K (cyan), 200 K (yellow) and 300 K (red). The spectra were fitted to a sum of Gaussian peaks (dashed lines): the grey area is kept constant at all temperatures, while the blue and red features are contributions respectively losing or gaining intensity with increasing T. **Inset)** T evolution of the red (open squares) and blue (open circles) surfaces. The full lines are the predicted evolutions for a model where the H atoms tunnel from a "compact" configuration (blue) to a "diluted" configuration (red), the quantum jump being sustained by phonons of the graphene surface with an energy $\hbar\omega$ ~ 30 meV.

Graphene-based materials, prepared from the exfoliation of graphite oxide, have been used as a model of interstellar carbon dust as they contain a relatively large amount of reactive atomic defects, either at the edges of the carbon flakes or on their surface. These defects are thought to be such that the C-H bond formed thereafter allows the H atom to be released easily to recombine with another H atom flying nearby into one H_2 molecule.

We have successfully combined neutron spectroscopy and density functional theory (DFT) to characterise the local environment of hydrogen atoms chemically bound at the surface of defected graphene flakes [2]. The vibrational spectrum measured on IN1-LAGRANGE at the ILL revealed a series of peaks which have been attributed one by one to C-H bending modes with H atoms bound either at the edges or inside structural voids at the surface (**figure 1**), with a ratio of ~ 1:1. The surprisingly strong temperature dependence of the spectrum (**figure 2**) at modest temperatures could only be reproduced with a scenario involving hydrogen 'quantum hopping' from one carbon atom to another in its direct vicinity, tunnelling through energy barriers which could not be overcome in the cold interstellar environment. This movement is sustained by the fluctuations of the graphene structure, which could catalyse the recombination process by bringing the H atoms into unstable regions and allowing the release of the chemically bound H atom.

For the first time ever, this study showed 'quantum tunnelling' in graphene-based systems, allowing the H to explore relatively long distances at temperatures as low as those in molecular clouds. Therefore, it is believed that quantum tunnelling facilitates the recombination reaction and opens new prospects for the formation of molecular H_2 in the interstellar media.

Oxyhalides – a new class of multiferroic materials with high critical temperature

Two-axis diffractometer D1B and high-resolution diffractometer D2B

AUTHORS

L. Zhao, **L.H. Tjeng** and **A.C. Komarek** (Max Planck Institute for Chemical Physics of Solids, Dresden, Germany)
M.T. Fernández-Díaz (ILL)

REFERENCES

[1] L. Zhao, M.T. Fernández-Díaz, L.H. Tjeng and A.C. Komarek, Sci. Adv. 2 (2016), e1600353
[2] M. Nishiyama, A. Oyamada, T. Itou, S. Maegawa, H. Okabe and J. Akimitsu, J. Phys. Conf. Ser. 320 (2011) 012030

Spin-induced multiferroic materials are interesting due to their high potential for applications in electronic devices. This interest is based on potentially high magnetoelectric effects arising from the intrinsic coupling between magnetic and ferroelectric ordering parameters. To date, such a spin-driven multiferroicity is found mainly in oxides, as well as in a few halogenides. We observed multiferroic properties for synthetic melanothallite Cu_2OCl_2, which is the first discovery of multiferroicity in a transition metal oxyhalide. Our neutron diffraction results reveal an incommensurate magnetic structure indicative of a spin-induced multiferroic material.

For next generation data storage devices, the fast switching of magnetic states by applying electrical fields (voltage) would be highly desirable. This switching could be realised in so-called magnetoelectric or spin-driven multiferroics. In general, multiferroic materials can be simultaneously electrically polarised (ferroelectric) and magnetically ordered. However, typical multiferroics with high ferroelectric ordering temperature do not exhibit a strong coupling of magnetic and electric properties. Also, in such materials the magnetic ordering temperature and the ferroelectric onset temperatures are very different from each other. This already indicates the strong independence of these two phenomena in such multiferroics. Therefore, any macroscopic magnetoelectric response in multiferroics with conventional ferroelectricity is, if existent at all, very small.

A few years ago, it was a great surprise to observe the magnetic control of the ferroelectric polarisation in a manganese oxide ($TbMnO_3$) below 28 K. In such magnetoelectric multiferroics, the ferroelectricity arises from the magnetic structure itself. Therefore, the ferroelectric properties are intimately coupled to the magnetic properties, resulting in large magnetoelectric effects that are desirable for possible future applications. Often, incommensurate spiral magnetic structures give rise to ferroelectric properties in these magnetoelectric multiferroics. These spiral magnetic structures typically arise from the competition between exchange interactions of neighbouring and next-nearest neighbouring spins in such a way that it is difficult to align all spins parallel or antiparallel (ferro- or antiferromagnetically), leading to so-called frustration in the system.

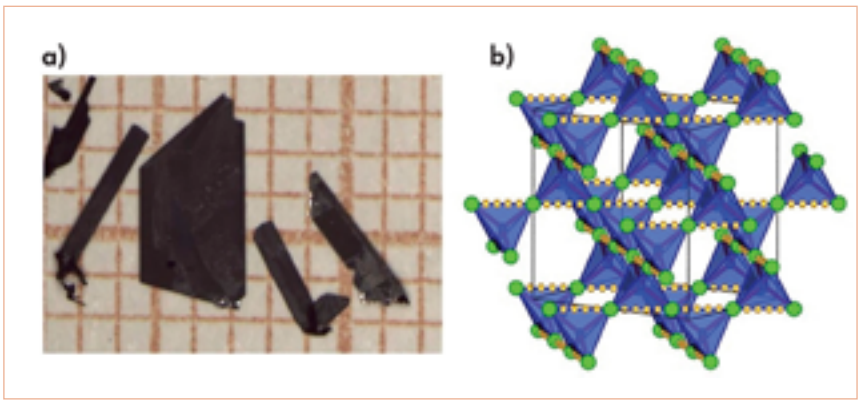

Figure 1

a) Typical plate-like single crystals of Cu_2OCl_2 grown by chemical vapour transport;
b) Pyrochlore-like crystal structure of melanothallite Cu_2OCl_2. In this figure only the OCu_4 tetrahedra are shown, while for the sake of simplicity the Cl ions which fill the free space in-between have been omitted (blue/green spheres: O/Cu ions). In such a structure, frustration effects can appear.

Figure 2

Rietveld refinement of our powder neutron data. The magnetic peaks can all be indexed with a propagation vector k = [0.827(7), 0, 0]. Thus, the recently claimed "all-in–all-out" spin structure can be excluded.

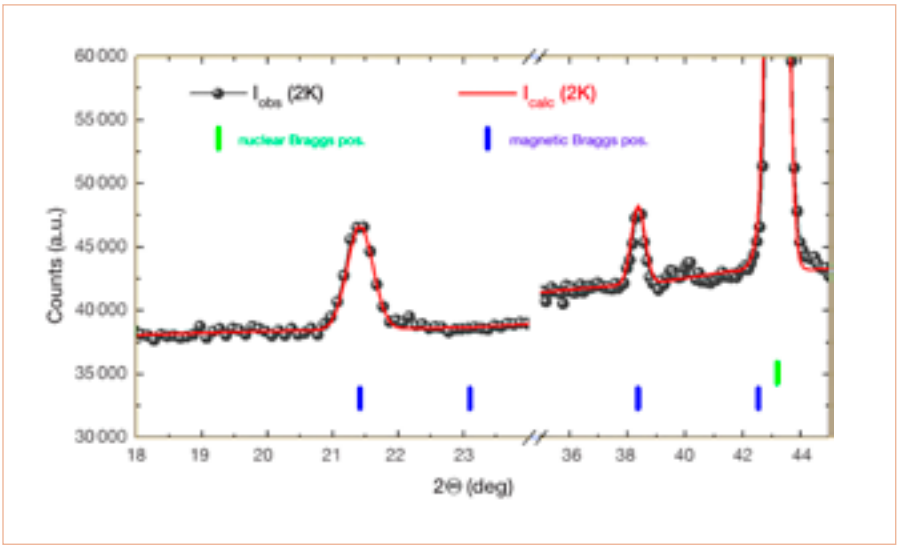

We have found a new class of magnetoelectric multiferroics with high critical temperature – transition metal oxyhalides with melanothallite structure (**figure 1**).

In addition to measurements of pyrocurrent and the dielectric constant in Cu_2OCl_2 that reveal ferroelectricity below its Néel temperature of ~ 70 K, we have performed powder neutron diffraction experiments [1]. The evolution with temperature of the diffracted intensity shows evidence of an incommensurate magnetic structure below T_N for which all magnetic reflections can be indexed with a propagation vector [0.827(7), 0, 0] (**figure 2**). This finding allows us to discard the claimed pyrochlore-like "all-in–all-out" spin structure for Cu_2OCl_2 [2], and instead, together with the fact that ferroelectricity appears at T_N, indicates that this transition metal oxyhalide is indeed a spin-induced multiferroic material.

Thus, transition metal oxyhalides with melanothallite structure are a new class of multiferroic materials with an exceptionally high critical temperature. Moreover, the magnetic origin of ferroelectricity in this class of materials in general is a promising property for sizeable magnetoelectric effects, opening up the search for new high-performance multiferroic materials through various possible substitutions in this ternary system.

Our findings also point to the importance of sizeable exchange interactions within a frustrated magnetic structure for the emergence of magnetoelectric multiferroicity with high critical temperature. Moreover, it also links the field of multiferroics with another important field of contemporary solid state physics – that of high-temperature superconducting cuprates, in which frustration effects have also been discussed in recent years.

Magnetoelectric effect and phase transitions in CuO in external magnetic fields

Single-crystal diffractometer D23

CuO is so far the only known binary multiferroic compound, and at 230 K it has a higher transition temperature into the multiferroic state than that of any other known material in which the electric polarisation is induced by spontaneous magnetic order. However, until now no magnetoelectric effect has been observed as direct crosstalk between bulk magnetisation and electric polarisation counterparts. In this study we combine neutron diffraction and macroscopic experiments under high magnetic fields of up to 50 T, which unambiguously prove that even modest magnetic fields are able to alter the magnetic structures and therefore dramatically affect the electric polarisation [1].

Perspective view of the spin cycloid propagating along q = [0.509 0 -0.483] in the multiferroic AF2 phase in CuO. The magnetic moments rotate within a plane defined by the monoclinic *b*-axis and a direction within the *a*-*c* plane 28 ° from the *c*-axis.

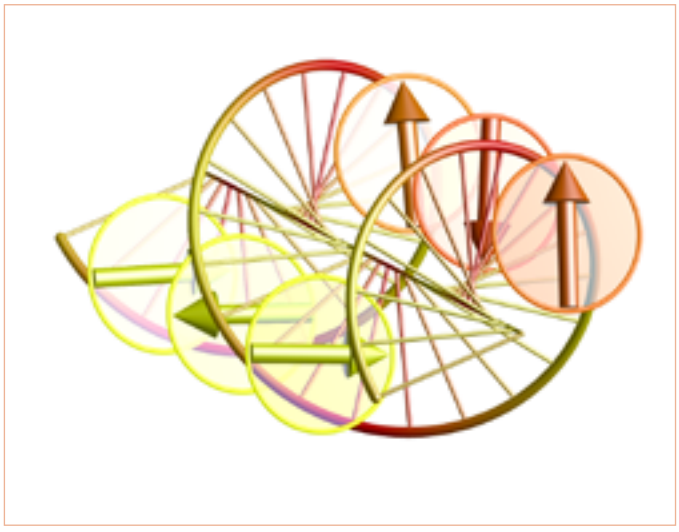

AUTHORS

N. Qureshi (ILL)
Z. Wang and **S. Zherlitsyn** (Hochfeld-Magnetlabor Dresden, Helmholtz-Zentrum Dresden-Rossendorf, Germany)
E. Ressouche (SPSMS, UMR-E CEA/UJF-Grenoble, France)
A.A. Muhkin (Prokhorov General Physics Institute, Russian Academy of Sciences, Moscow, Russia)
V. Skumryev (Departament de Física, Universitat Autònoma de Barcelona/ICREA, Spain)

REFERENCES

[1] Z. Wang, N. Qureshi, S. Yasin, A. Mukhin, E. Ressouche, S. Zherlitsyn, Y. Skourski, J. Geshev, V. Ivanov, M. Gospodinov and V. Skumryev, Nat. Commun. 7 (2016) 10295
[2] J.B. Forsyth, P.J. Brown and B.M. Wanklyn, J. Phys. C. Solid State Phys. 21. (1988) 2917
[3] P.J. Brown, T. Chattopadhyay, J.B. Forsyth, V. Nunez and F. Tasset, J. Phys. Condens. Matter 3 (1991) 4281
[4] P. Monod, A.A. Stepanov, V.A. Pashchenko, J.P. Vieren, G. Desgardin and J. Jegoudez, J. Magn. Magn. Mater. 177-181 (1998) 739

Multiferroics are materials that combine at least two of the ferroic states, e.g. (anti)ferromagnetism and ferroelectricity. In improper multiferroics the electric polarisation appears as a by-product of the magnetic ordering and therefore the two phenomena are intimately coupled. This ability to control the magnetic properties by an electric field and *vice versa*, the so-called magnetoelectric effect, renders these compounds highly interesting for use as data storage devices.

Below the Néel temperature of 230 K, CuO reveals a complex magnetic structure with an incommensurate cycloidal modulation of the magnetic moments in a plane defined by the monoclinic *b*-axis and a direction within the *a*-*c* plane (AF2 phase). This peculiar spin configuration breaks inversion symmetry and is able to induce a uniform shift in the oxygen positions *via* the inverse Dzyaloshinskii-Moriya effect, therefore rendering the material ferroelectric. At 213 K a magnetic phase transition takes place into a collinear commensurate antiferromagnetic and paraelectric structure where the spins point along the *b* direction (AF1 phase) [2, 3].

We have investigated the field-induced phase transitions at the single-crystal diffractometer D23 by applying an external magnetic field along the *b*-axis. At 2 K a clear change in the integrated intensities at about 12 T suggests a spin-reorientation transition, which is in agreement with our susceptibility measurements. This field-induced magnetic structure (HF1 phase) was solved using symmetry-adapted spin configurations revealing a spin-flop transition, where the spins flop from one axis of the cycloidal envelope (*b*-axis) to the other (within the *a*-*c* plane 28 ° from the *c*-axis).

Figure 1

Electric polarisation as a function of the applied magnetic field along the *b*-axis revealing two magnetic phase transitions (AF1→AF2 at lower field and AF2→HF1 at higher field).

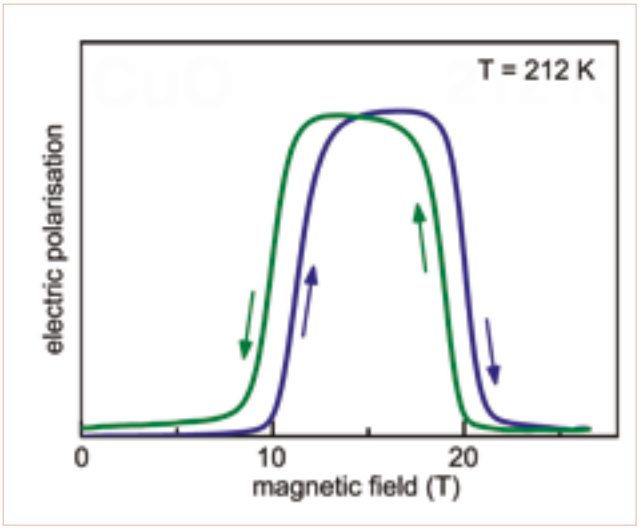

Figure 2

Magnetoelectric phase diagram of CuO for H||b based on pyrocurrent (blue dots), capacitance (green dots), magnetostriction (pink dots), sound velocity (red dots) and bulk magnetisation data (black dots). Dashed lines are expected hypothetical phase boundaries.

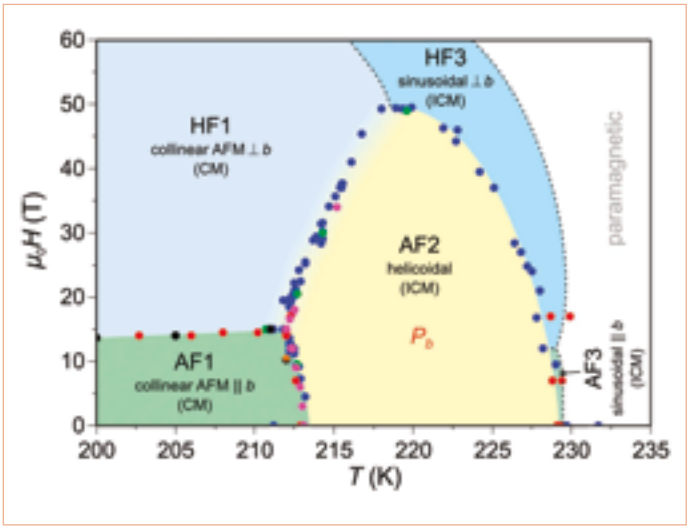

Surprisingly, we have found that at 212 K, i.e. just below the spontaneous AF1-AF2 transition, an induced first-order commensurate-to-incommensurate magnetic phase transition takes place at 10.5 T. The analysis of magnetic Bragg reflections collected within the in-field phase confirmed that even at moderate fields a transition from the paraelectric AF1 phase to the multiferroic AF2 phase can be induced, which therefore constitutes evidence of a magnetoelectric effect.

In the search for magnetic phase transitions at higher magnetic fields we employed pyrocurrent, capacitance, magnetostriction, sound velocity and magnetisation measurements at the High Magnetic Field Laboratory in Dresden, by applying magnetic fields of up to 50 T along the main axes of the cycloidal envelope. The field-induced transition into the AF2 phase mentioned above is seen as a peak in the pyrocurrent along the *b*-axis, which corresponds to the rise of the electric polarisation (**figure 1**). However, we observe a second peak with inverted sign at fields at 20 T. This observation is related to a further magnetic phase transition into the HF1 phase where the electric polarisation is suppressed. At T ≈ 220 K a magnetic field of 50 T is necessary to destroy the multiferroic cycloid, and at higher temperatures our magnetostriction data suggest an incommensurate-to-incommensurate phase transition. However, in the high-field phase HF3 the electric polarisation is not observed along any other axis, which rules out the flop of the spin cycloid and favours a sinusoidally modulated spin structure with moments perpendicular to *b*.

The fact that the spin cycloid (AF2) can only be stabilised in one plane and that the moment direction in the collinear phases AF1 and HF1 coincides with the main axes of that cycloid leads to the conclusion that CuO should be considered an *easy plane* antiferromagnet, which is in agreement with antiferromagnetic resonance data [4]. The magnetoelectric phase diagram (**figure 2**) of this high-temperature, magnetically induced, multiferroic has been sketched, unveiling unknown transitions and important magnetoelectric features.

Observation of magnetic fragmentation in spin ice

Single-crystal diffractometer D23, diffuse scattering spectrometer D7 and time-of-flight spectrometer IN5.

AUTHORS

S. Petit (LLB, Saclay, France)
E. Lhotel (Institut Néel, Grenoble, France)
A. Wildes, **H. Mutka** and **J. Ollivier** (ILL)
E. Ressouche (CEA, Grenoble, France)

REFERENCES

[1] M.E. Brooks-Bartlett, S.T. Banks, L.D.C Jaubert, A. Harman-Clarke and P.C.W. Holdsworth, Phys. Rev. X 4 (2014) 011007

[2] S. Petit, E. Lhotel, B. Canals, M. Ciomaga Hatnean, J. Ollivier, H. Mutka, E. Ressouche, A.R. Wildes, M.R. Lees and G. Balakrishnan, Nat. Phys. 12 (2016) 746 [doi: 10.1038/NPHYS3710]

The evidence for fractionalised quasiparticles that emerge from a many-body system is one of the most appealing recent discoveries in condensed matter physics. Fractionalised quasiparticles have been shown to exist in a large variety of systems, from 2D electron gases and graphene to spinons and magnetic monopoles in magnetic systems. However, the fractionalisation in these systems concerns the excited states that develop above a specific ground state. The question that immediately arises is therefore: could fractionalisation exist in the degrees of freedom of the system themselves? A series of neutron scattering experiments performed recently at the ILL leads us to conclude that the answer is yes. Indeed, we have observed the fragmentation process of the magnetic degrees of freedom in the context of highly frustrated magnets, and more precisely in the spin ice candidate $Nd_2Zr_2O_7$. As the first observation of the fragmentation process in a real material, our work marks an important breakthrough in the field of magnetism and opens the way to a wide field of research.

Spin ice is an unusual magnetic material in which the combination of strong local Ising anisotropy and ferromagnetic interactions imposes a local constraint to the magnetic moments, the "ice rule" (**figure 1a**). The magnetic ground state remains disordered but with specific local correlations. It belongs to the class of Coulomb phases, an original state of matter where the ground state is disordered and the local constraint can be interpreted as the flux conservation law of an "emergent" electromagnetic field.

Classical excitations in spin ice, called magnetic monopoles, are defects that locally violate the ice rule by reversing the orientation of a moment (**figure 1b**), and thus induce a magnetic charge in the electromagnetic field. When the monopole density is large enough, and if monopoles experience a Coulombic interaction, an outstanding effect has been predicted by Brooks-Bartlett

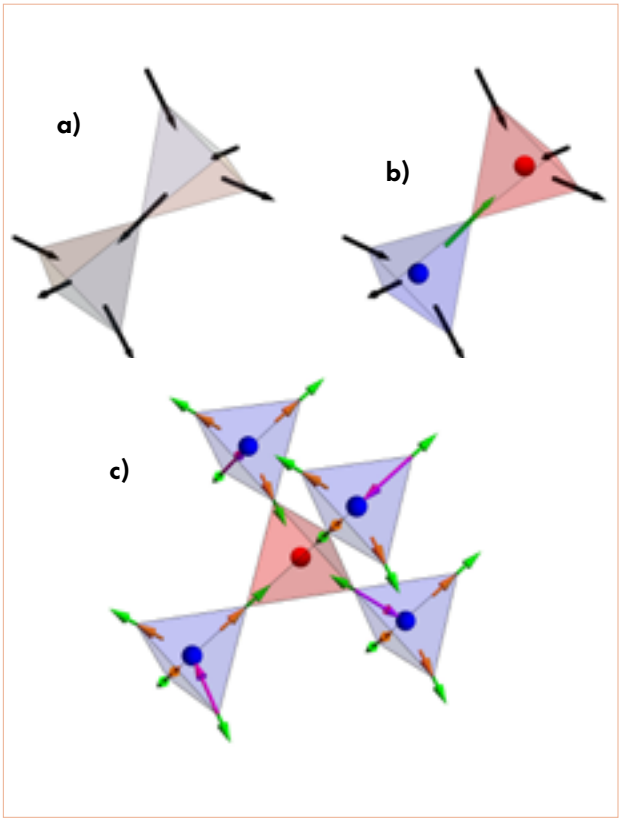

Figure 1

a) The spin ice "two-in two-out" configuration of the spins (arrows); **b)** A spin flip (green arrow) creates two magnetic monopoles in the centre of the tetrahedra (red and blue dots); **c)** The fragmented moments superimposed on the lattice. They are composed of "all-in all-out" (green arrows) moments from the crystallised monopoles and of the fluctuating (orange and purple arrows) spins from the (spin-liquid) Coulomb phase.

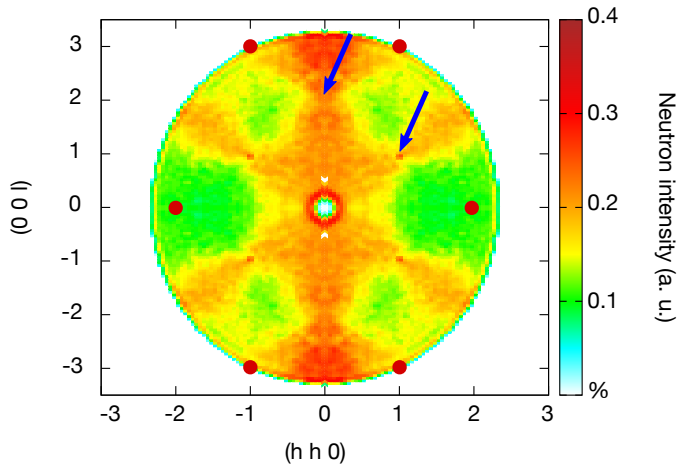

Figure 2

Iso-energy inelastic intensity (E = 50 μeV) showing the pinch points characteristic of the fluctuating fragment.

et al. [1]: the emergent charged field can fractionalise into two parts, where the first fragment is a crystal of monopoles with a half charge and the second is a novel Coulomb phase (**figure 1c**).

In the spin ice candidate $Nd_2Zr_2O_7$, the fragmentation mechanism manifests experimentally as the striking coexistence between an antiferromagnetic ordered state and a new Coulomb phase with ferromagnetic-like correlations: magnetic Bragg peaks, characteristic of the ordered phase, coexist with a "pinch point pattern", characteristic of the new Coulomb phase (**figure 2**). Moreover, our inelastic neutron scattering experiments show that the pinch point pattern is a dynamical effect, hence suggesting that quantum effects are at play [2].

The fragmentation in spin ice is based on the Helmholtz decomposition of the emergent, electromagnetic charged field. This decomposition is a classical concept, commonly used to make flow analysis in geophysics, turbulence or even imaging and robotics. Our findings demonstrate that the emergent electromagnetic field is "real" in these magnetic materials. Our observation of a dynamical Coulomb phase emphasises the need for further theoretical study of quantum fragmentation, which might also lead to the discovery of new states of matter.

The work could only be achieved through a series of neutron scattering techniques performed at very low temperature (T = 60 mK): neutron diffraction on the D23-CEA-CRG diffractometer to observe the ordered fragment, and polarised diffuse scattering and inelastic scattering on the D7 and IN5 spectrometers to observe the fluctuating part and the inelastic process. It is a collaboration between the LLB (CEA-CNRS-Univ. Paris-Saclay), Institut Néel (CNRS Grenoble), Warwick University, CEA Grenoble and the ILL.

Field-induced spin-density wave beyond hidden-order in URu_2Si_2

Three-axis spectrometer IN22

URu_2Si_2 is one of the most enigmatic, strongly correlated electron systems and offers a fertile testing ground for new concepts in condensed matter science [1]. In spite of more than thirty years of intense research, no consensus on the order parameter of its low-temperature hidden-order phase exists. Here, thanks to neutron diffraction under pulsed magnetic fields up to 40 T, we identify the field-induced phases of URu_2Si_2 as a spin-density wave state [2]. The transition to the spin-density wave represents a unique touchstone for understanding the hidden-order phase.

Figure 1

Three-axis spectrometer IN22 (CRG-CEA) with the 40 T cryomagnet and the 1 MJ pulsed-field generator.

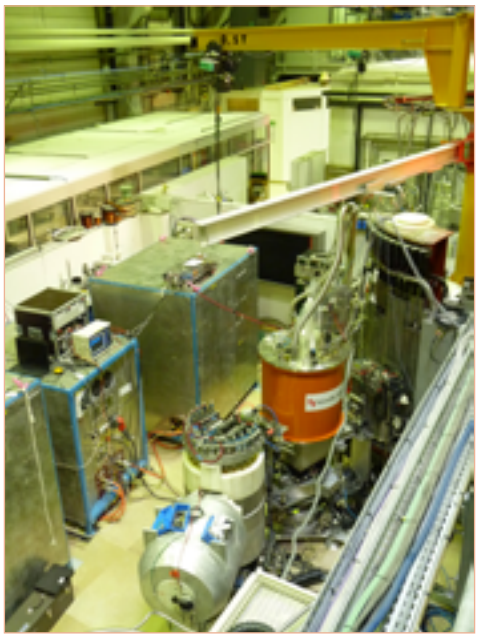

AUTHORS

W. Knafo, **F. Duc**, **J. Billette** and **P. Frings** (Laboratoire National des Champs Magnétiques Intenses, Toulouse, France)
F. Bourdarot and **J. Flouquet** (CEA, Grenoble, France)
K. Kuwahara (Ibaraki University, Mito, Japan)
H. Nojiri (Tohoku University, Sendai, Japan)
D. Aoki (CEA, Grenoble, France/Tohoku University, Ibaraki, Japan)
L.-P. Regnault, **X. Tonon** and **E. Lelièvre-Berna** (ILL)

REFERENCES

[1] J.A. Mydosh and P.M. Oppeneer, Rev. Mod. Phys. 83 (2011) 1301
[2] W. Knafo *et al.*, Nat. Commun. 7 (2016) 13075
[3] F. Bourdarot *et al.*, Physica B 359-361 (2005) 986
[4] A. Villaume *et al.*, Phys. Rev. B 78 (2008) 012504
[5] D. Aoki *et al.*, J. Phys. Soc. Jpn. 78 (2009) 053701
[6] H. Ikeda *et al.*, Nat. Phys. 8 (2012) 528

The application of extreme conditions permits the ground state of a system to be modified in order to gain new insights about it. In URu_2Si_2 under pressure, the hidden-order state is replaced by an antiferromagnetic phase whose order parameter is a moment aligned antiferromagnetically along **c** with the wavevector $\mathbf{k}_0$ = (0 0 1) [3]. Under a high magnetic field applied along **c**, a cascade of first-order phase transitions at the fields $\mu_0 H_1$ = 35 T, $\mu_0 H_2$ = 36 / 37 T (rising / falling fields), and $\mu_0 H_3$ = 39 T, leads to a polarised paramagnetic regime above H_3. Here, thanks to a new cryomagnet (developed by the LNCMI-Toulouse, the CEA-Grenoble, and the ILL) allowing neutron diffraction up to 40 T (**figure 1**), we have determined the magnetic structure of URu_2Si_2 in fields between 35 and 39 T.

After testing different wavevectors, a magnetic signal has been detected at $\mathbf{k}_1$ = (0.6 0 0). **Figure 2a** shows the time profile of a magnetic field pulsed up to 38 T, as well as the time dependence of the diffracted neutron intensities recorded during 38 T pulses at the momentum transfers **Q** = (0.6 0 0) and (1.6 0 -1), which are satellites of wavevector $\mathbf{k}_1 = \mathbf{Q} - \boldsymbol{\tau}$ around the structural Bragg positions $\boldsymbol{\tau}$ = (0 0 0) and (1 0 -1), respectively. **Figure 2c** emphasises, in the window 32-41 T, the field-dependence of the diffracted neutron intensities. The enhancement of the intensity at T = 2 K, absent at T = 18 K, shows that long-range ordering with wavevector $\mathbf{k}_1$ is established at high field and low temperature. At T = 2 K, the intensity with wavevector $\mathbf{k}_1$ is enhanced in fields higher than $\mu_0 H_1$ = 35 T and drops down to the background level in fields higher than $\mu_0 H_3$ = 39 T. *Via* a normalisation on the nuclear Bragg peak (1 0 -1), the magnetic intensity has been associated with a Fourier component $m(\mathbf{k}_1) = 0.25\ \mu_B$ / U.

Figure 3 presents the magnetic phase diagram of URu_2Si_2 under pressure and magnetic field, over a wide range of temperatures up to 75 K. In the hidden-order state, the magnetic fluctuations peaked at the hot wavevectors $\mathbf{k}_0$ and $\mathbf{k}_1$, indicating the proximity of quantum phase transitions associated with long-range ordering with the same wavevectors. With pressure [3], the disappearance of the hidden-order coincides with a transfer of weight from magnetic fluctuations with wavevector $\mathbf{k}_0$ into antiferromagnetic order with the same wavevector [4, 5].

Figure 2

a) Time profile of a magnetic field pulsed up to 38 T, and corresponding time-dependence of the neutron diffracted intensity at **Q** = (0.6 0 0) and **Q** = (1.6 0 -1).

b) Magnetisation versus magnetic field at T = 1.5 K and magnetic-field-temperature phase diagram of URu_2Si_2.

c) Field dependence of the neutron diffracted intensities in fields up to 40.5 T.

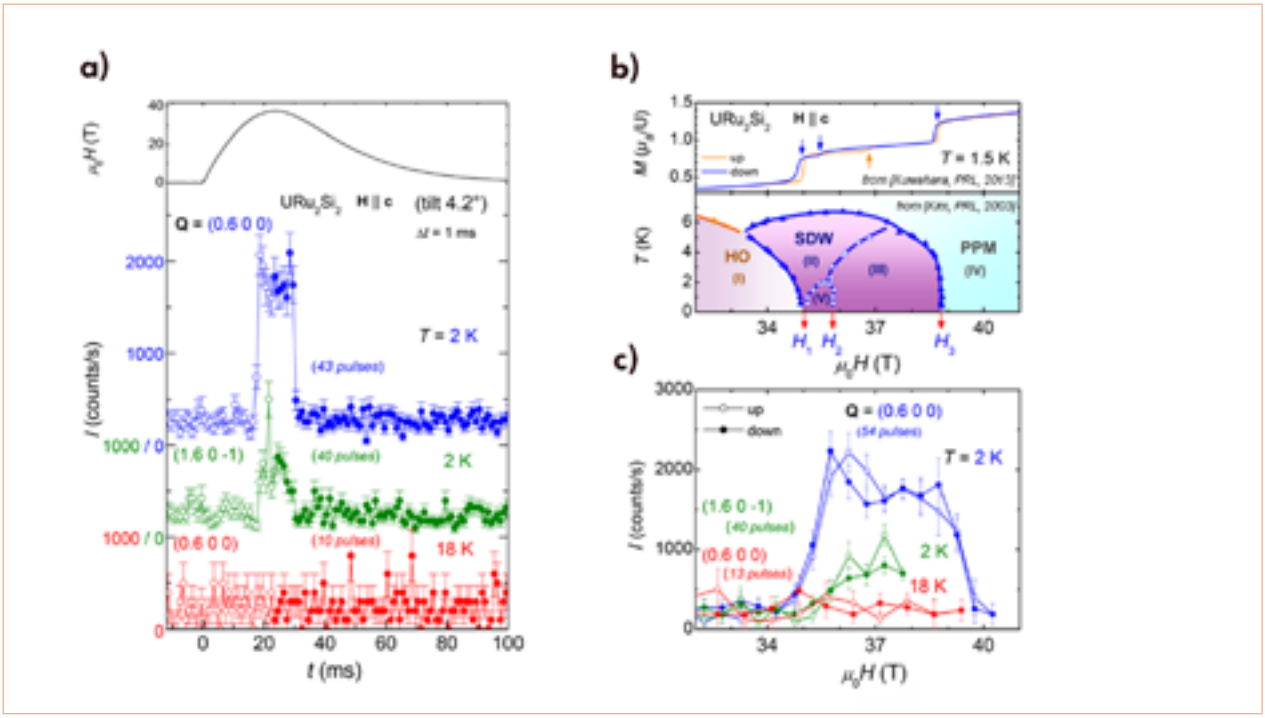

With magnetic field, we have observed that a spin-density wave is stabilised with the wavevector $\mathbf{k}_1$, which may coincide with a loss of intersite magnetic fluctuations, as indicated by the enhanced magnetisation (**figure 2b**).

In an itinerant picture of magnetism, long-range magnetic ordering with a wavevector $\mathbf{k}_m$ can be related to a partial or complete nesting of two parts of the Fermi surface. In URu_2Si_2, *5f* electrons hybridise with electrons from the conduction bands. Modifications of the Fermi surface and carrier mobility accompany the establishment of the hidden-order phase at the temperature T_0, and Fermi surface nestings with the wavevectors $\mathbf{k}_0$ and $\mathbf{k}_1$ can be identified [6]. However, no long-range magnetic order has been reported yet in URu_2Si_2 in its hidden-order phase. Resulting from the Fermi surface reconstruction at H_1, the nesting with $\mathbf{k}_1$ is probably reinforced, leading to the onset of the spin-density wave with the wavevector $\mathbf{k}_1$.

Our observation of a spin-density wave in magnetic fields between 35 and 39 T will certainly push to develop models incorporating on equal basis the Fermi surface topology and the magnetic interactions. With the aim of describing competing quantum instabilities between the hidden-order and long-range-ordered phases, such models will be a basis for solving the hidden order problem.

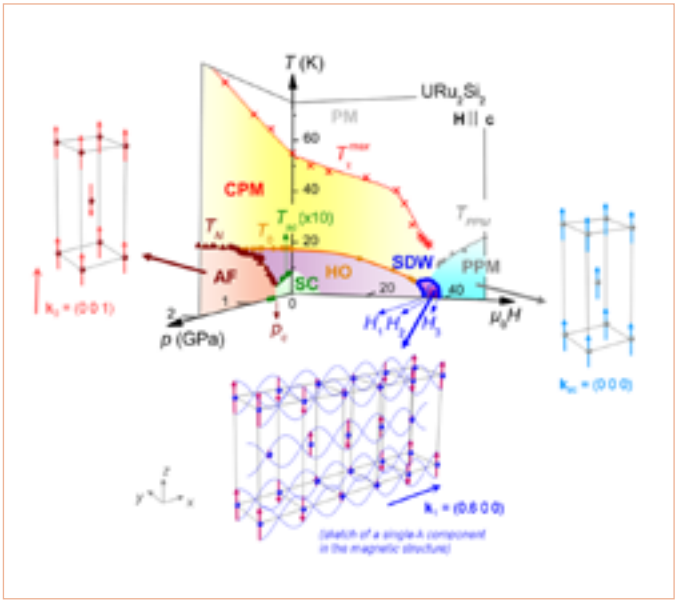

Figure 3

Temperature-magnetic field and temperature-pressure phase diagrams of URu_2Si_2.

Complex field-induced states in linarite $PbCuSO_4(OH)_2$ with a variety of high-order, exotic, spin-density wave states

Single-crystal, four-circle diffractometer with three-axis energy analysis D10

AUTHORS

B. Willenberg (TU Braunschweig and Helmholtz-Zentrum Berlin for Materials and Energy, Germany)
M. Schäpers, **A.U.B. Wolter**, **S.-L. Drechsler**, **B. Büchner** and **S. Nishimoto** (IFW Dresden, Germany)
M. Reehuis and **J.-U. Hoffmann** (Helmholtz-Zentrum Berlin for Materials and Energy, Germany)
A.J. Studer and **K.C. Rule** (Nuclear Science and Technology Organisation, Kirrawee, Australia)
B. Ouladdiaf (ILL)
S. Süllow (TU Braunschweig, Germany)

REFERENCES

[1] A.U.B. Wolter *et al.*, Phys. Rev. B 85 (2012) 014407
[2] J. Sudan, A. Lüscher and A.M. Läuchli, Phys. Rev. B 80 (2009) 140402
[3] B. Willenberg *et al.*, Phys. Rev. Lett. 116 (2016) 047202
[4] A. Smerald and N. Shannon, Phys. Rev. B 88 (2013) 184430

Detecting and understanding novel types of quantum phases is a core topic of modern condensed matter physics. A prime example is the search for spin-nematic and higher-order multipolar phases. These phases do not show dipolar order, making them notoriously difficult to establish experimentally. Now, we have found evidence for the existence of such multipolar phases in the mineral linarite, $PbCuSO_4(OH)_2$. Combining neutron diffraction and nuclear magnetic resonance reveals a competition of an unconventional spin-density wave phase with one of dominant multipolar character, providing a testing ground for these elusive phases.

The natural mineral linarite $PbCuSO_4(OH)_2$ has been known to mineralogists for its shiny blue colour for two hundred years. Only recently, the material was established in a different context, as a low-dimensional, frustrated quantum magnet. Within the monoclinic crystal structure, the Cu^{2+} ions are arranged in a chain-like fashion, leading to a magnetic coupling scheme of a competition between nearest-neighbour ferromagnetic exchange $J_1 \sim 100$ K and next-nearest-neighbour antiferromagnetic exchange $J_2 \sim 36$ K along the chain [1]. In spite of these coupling constants in the order of 100 K, the material orders magnetically only below $T_N = 2.7$ K, this way attesting both to the magnetic frustration and the low-dimensionality of the magnetic coupling.

A major prediction for the model of a frustrated spin chain with competing nearest-neighbour ferromagnetic and next-nearest-neighbour antiferromagnetic interactions is the occurrence of novel, high-field quantum phases of multipolar character, which compete with unconventional spin-density wave phases [2]. Various tools of experimental magnetism allow the spin-density wave to be observed,

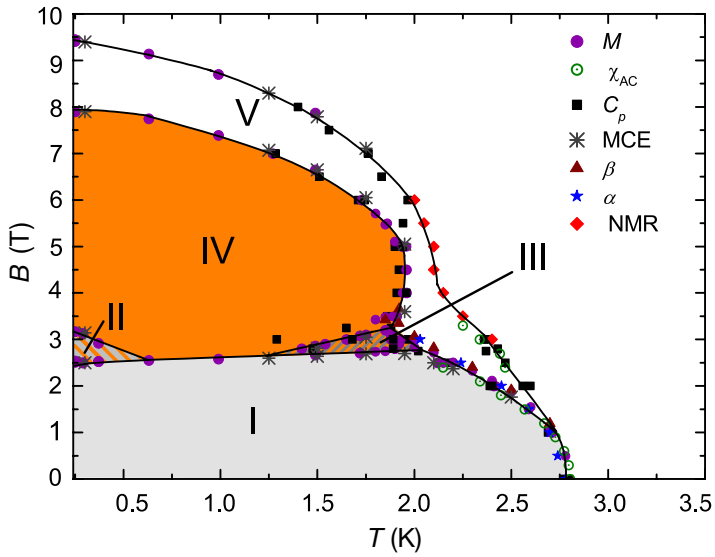

Figure 1
The phase diagram of linarite $PbCuSO_4(OH)_2$ for the magnetic field B aligned along the crystallographic b-axis.

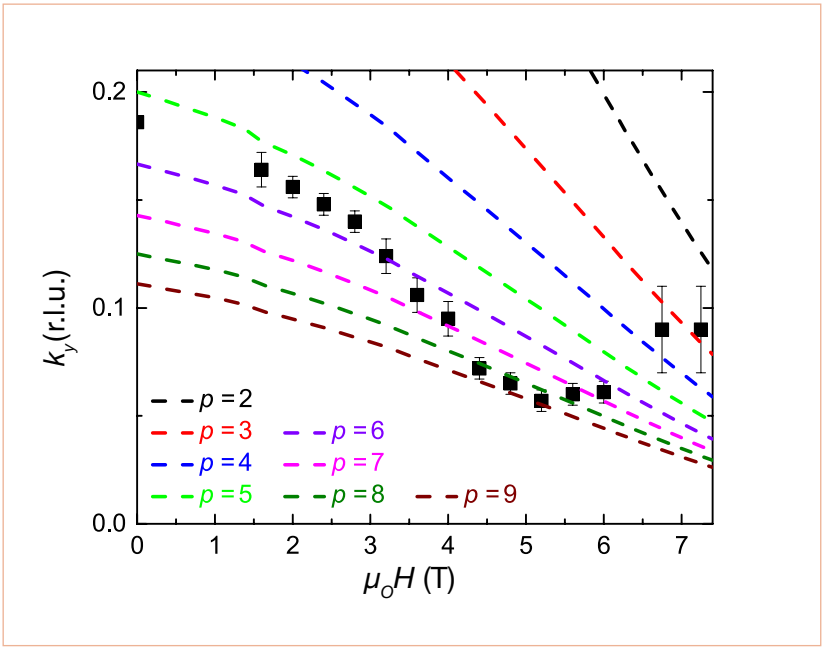

Figure 2

The field dependence of the incommensurability vector k_y of linarite in the spin-density wave phase V.

but the multipolar phases are notoriously difficult to detect because of a lack of dipolar order. Yet, it is possible to detect multipolar phases indirectly, by studying their competition with the spin-density wave.

Therefore, we have extensively characterised the zero-field and field-induced phases of linarite using a multitude of micro- and macroscopic experimental techniques. As a result we have fully established the magnetic phase diagrams, that for the magnetic field B aligned along the crystallographic b-axis being particularly rich (**figure 1**). Furthermore, we have determined the symmetry of the magnetic moment arrangement on the Cu^{2+} ions in the thermodynamic phases I to V, by means of neutron scattering [3]. Most remarkably, we find in phase V the formation of an unconventional spin-density wave with ordering vector $\vec{q}$ =(0,k_y,0.5). Notably, the incommensurability vector k_y of the spin-density wave depends strongly on the magnetic field, as is predicted by the theory of the field-induced multipolar phases in these frustrated chain systems (**figure 2**). The figure illustrates how the field evolution of the incommensurability vector k_y compares with theoretical predictions for multipolar phases of different polar number p between 2 and 9. Clearly, no single value p accounts for the observed field-dependent behaviour of the incommensurability vector k_y. This observation led us to the conclusion that in linarite we are dealing with a variety of highly unusual multipolar phases of different polar number p.

Next, in high magnetic fields $B > 6$ T, by means of nuclear magnetic resonance experiments we have established a phase separation in phase V into the spin-density wave and a phase component that lacks conventional dipolar order. Such a phase volume without dipolar order is predicted to occur for multipolar states [4], and thus we attribute it to spatial regions in the material with multipolar correlations occurring within phase V in high magnetic fields.

Finally, *via* numerical theoretical methods, we can relate our experimental observations to a minimum spin model for linarite within the framework of the frustrated ferromagnetic J_1-J_2 chain by incorporating a small, residual interchain coupling. In result, the interchain coupling modifies the essential properties of the chain model to the extent that linarite is shifted towards a quantum critical point within the J_1-J_2 phase space. In other words, linarite represents a unique material allowing the experimental study of a multitude of new topics within the context of quantum magnetism.

Evidence for charge stripes in a layered cobalt oxide

Three-axis spectrometer IN20

A key challenge in materials physics is to understand how certain layered antiferromagnets evolve into high-temperature superconductors on addition of charge carriers. Many such systems pass through an intermediate phase in which the added charge condenses into stripes. In this work we found evidence for disorderly charge stripes in a layered cobalt oxide. The finding provides an explanation for the unusual hourglass shape of the magnetic spectrum of this material, and also offers insight into the magnetic behaviour of the related copper oxide high-temperature superconductors.

AUTHORS

P. Babkevich (EPFL, Switzerland)
P.G. Freeman (UCLan, UK)
M. Enderle (ILL)
D. Prabhakaran and **A.T. Boothroyd** (University of Oxford, UK)

REFERENCES

[1] D.X. Yao, E.W. Carlson and D.K. Campbell, Phys. Rev. Lett. 97 (2006) 017003
[2] A.T. Boothroyd, P. Babkevich, D. Prabhakaran and P.G. Freeman, Nature 471 (2011) 341
[3] Y. Drees, Z.W. Li, A. Ricci, M. Rotter, W. Schmidt, D. Lamago, O. Sobolev, U. Rütt, O. Gutowski, M. Sprung, A. Piovano, J.P. Castellan and A.C. Komarek, Nat. Commun. 5 (2014) 5731
[4] P. Babkevich, P.G. Freeman, M. Enderle, D. Prabhakaran and A.T. Boothroyd, Nat. Commun. 7 (2016) 11632

Stripe phases are a form of complex matter involving coupled spin and charge order. They are observed in certain doped antiferromagnetic oxides containing copper, nickel or manganese ions arranged on a square lattice. Some theoreticians believe that stripe fluctuations are important to the mechanism of superconductivity in the copper oxide family of high-temperature superconductors. A key piece of evidence for this idea is the universal form of the magnetic spectrum of hole-doped copper oxide superconductors, as measured by neutron scattering, which is in the shape of an hourglass. This type of spectrum emerges naturally from a stripe-ordered ground state [1].

In 2011, experiments performed at the ILL revealed that the magnetic spectrum of an insulating, layered cobalt oxide $La_{5/3}Sr_{1/3}CoO_4$ also has an hourglass shape (**figure 1** [2]). The result was considered significant because it provided an experimental demonstration of how an hourglass spectrum could arise from a stripe-ordered ground state, the existence of which had been inferred indirectly from measurements of the magnetic order.

Up until now, however, direct evidence for charge-stripe order in $La_{5/3}Sr_{1/3}CoO_4$ has been missing. Indeed, attempts to observe charge stripes in layered cobalt oxides with synchrotron x-ray diffraction and unpolarised neutron diffraction were unsuccessful. The apparent absence of charge stripes motivated a proposal for an alternative, stripe-free, model to explain the hourglass spectrum of $La_{5/3}Sr_{1/3}CoO_4$ based on a nanoscale coexistence of two types of short-range magnetic order [3].

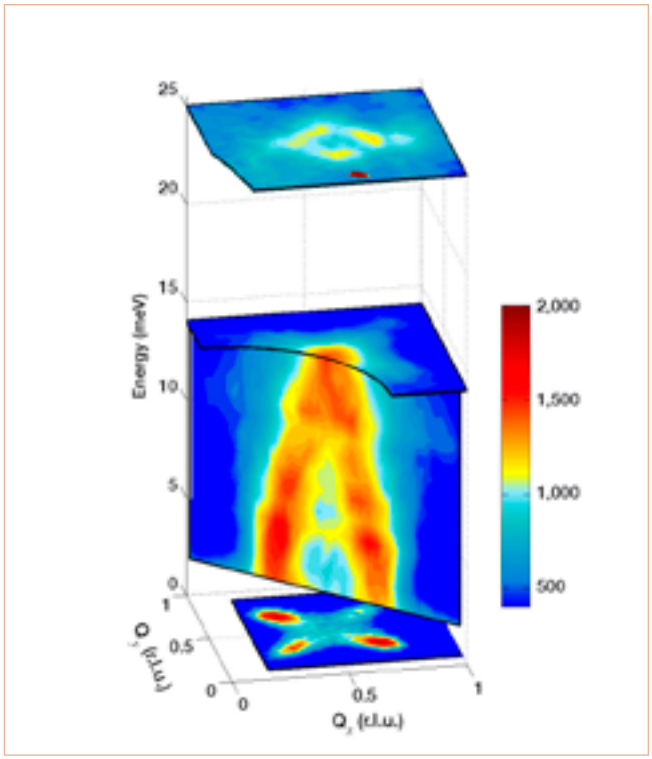

Figure 1

Hourglass magnetic spectrum measured by three-axis neutron spectroscopy at the ILL [2].

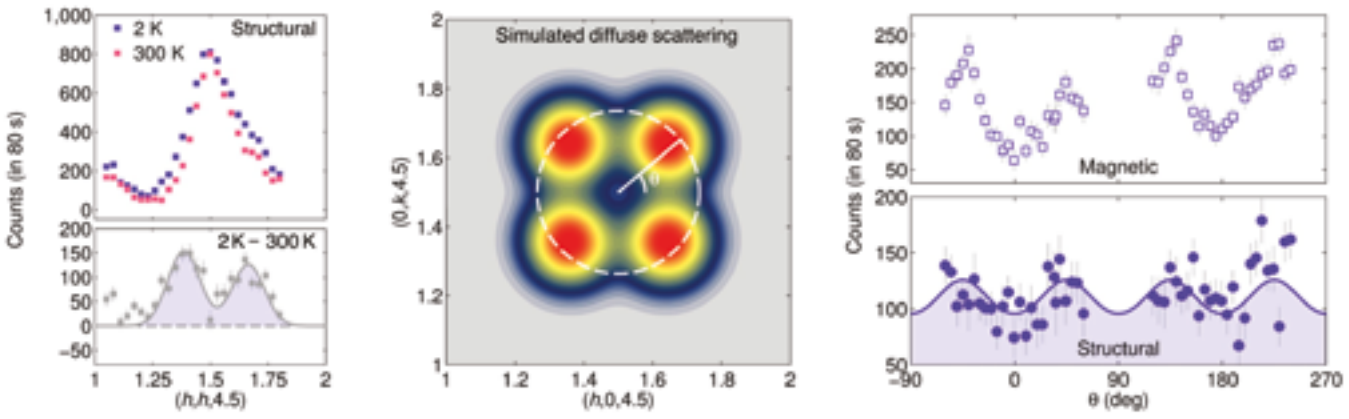

Figure 2

Structural and magnetic diffuse scattering from $La_{5/3}Sr_{1/3}CoO_4$. At low temperatures additional structural diffuse scattering is present, which is highlighted by the difference between the data recorded at 2 K and 300 K (**left**). A model for spin and charge stripes predicts a fourfold pattern of diffuse scattering (**centre**). The observed magnetic and structural diffuse scattering around a circular path (**right**) is consistent with the simulation for the stripe model. The path is shown by the dashed line in the centre panel.

In our new work [4] we employed polarised neutron diffraction on IN20 at the ILL to search for the signature of charge stripes in $La_{5/3}Sr_{1/3}CoO_4$. This compound exhibits short-range magnetic order at temperatures below about 100 K. Polarisation analysis made it possible to separate structural diffuse scattering associated with charge order from magnetic diffuse scattering.

At room temperature, $La_{5/3}Sr_{1/3}CoO_4$ contains patches of checkerboard charge order, in which Co^{2+} and Co^{3+} alternate like the black and white squares on a chess board [3]. On cooling to low temperatures, however, we observed a build-up of non-magnetic diffuse scattering on the flanks of the checkerboard charge order peaks (**figure 2**). This additional structural diffuse scattering has the same fourfold pattern as that of the magnetic diffuse scattering, consistent with a model of period-3 spin and charge stripes as shown in **figure 3**.

The results show that the magnetic ground state is more complicated than initially thought, comprising a nanoscale coexistence of (i) spin- and charge-stripe order and (ii) checkerboard charge order. The presence of the stripe-ordered component identified in this work reinforces the stripe model as the underlying mechanism for the hourglass magnetic spectrum in the cobalt oxides. The data also provide an experimental basis for theories that assume a ground state with static or slowly fluctuating stripes in order to explain the hourglass spectrum exhibited by many, if not all, copper oxide superconductors.

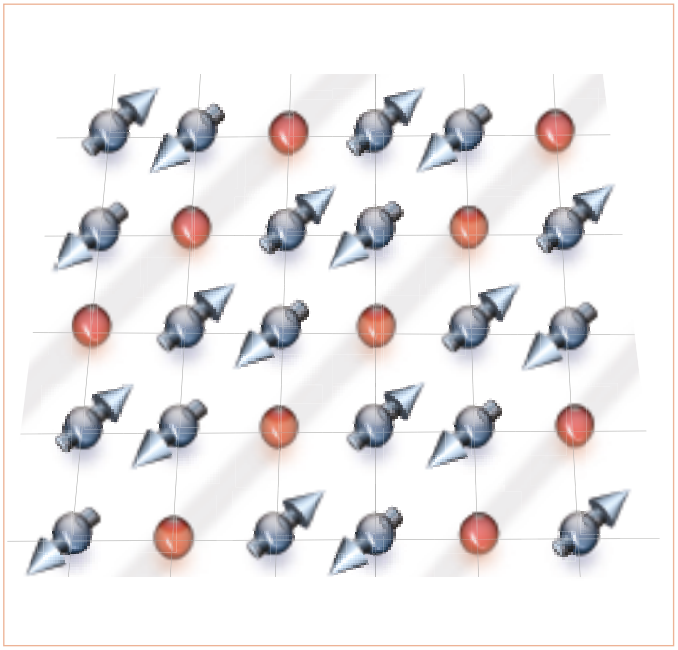

Figure 3

Model for ideal period-3 spin and charge stripes. The blue arrows are the spins and the red spheres are the condensed charge carriers.

Transition from sign-reversed to sign-preserved Cooper-pairing symmetry in sulphur-doped iron selenide superconductors

Three-axis spectrometer IN8

In most unconventional superconductors, the low-energy spin excitation spectrum is dominated by a peculiar excitation, often known as a resonant mode, which only appears when the superconducting gap exhibits a sign reversal. Here we observed a transition from sign-reversed to sign-preserved Cooper-pairing symmetry in S-doped iron selenide superconductors $K_xFe_{2-y}(Se_{1-z}S_z)_2$. Our data show that a sharp resonant mode well below the superconducting gap (2Δ) in the undoped sample is replaced by a broad hump structure above 2Δ under 50 % S-doping. These findings suggest that multiple channels are required to understand the superconductivity in this system.

AUTHORS

Q. Wang, **Y. Feng**, **Y. Shen**, **Y. Hao**, **B. Pan** and **J. Zhao** (Fudan University, Shanghai, China)
J.T. Park (MLZ, Garching, Germany)
J.W. Lynn (NIST, Gaithersburg, USA)
A. Ivanov (ILL)
S. Chi, **M. Matsuda** and **H. Cao** (Oak Ridge National Laboratory, Tennessee, USA)
R.J. Birgeneau (University of California, Berkeley, USA)
D.V. Efremov (IFW Dresden, Germany)

REFERENCES

[1] P. Dai, Rev. Mod. Phys. 87 (2015) 855
[2] S. Onari, H. Kontani and M. Sato, Phys. Rev. B 81 (2010) 060504 (R)
[3] S. Onari and H. Kontani, Phys. Rev. Lett. 109 (2012) 137001
[4] G. Yu, Y. Li, E.M. Motoyama and M. Greven, Nat. Phys. 5 (2009) 873

In conventional BCS superconductors, electron-phonon coupling gives rise to a sign-preserved s-wave pairing. In high-temperature superconductors, weak coupling theories suggest that superconductivity is mediated by spin fluctuations which lead to a sign reversal between the superconducting order parameters on different parts of the Fermi surfaces. Strong evidence for this comes from the observation of a sharp magnetic resonant mode below 2Δ in the spin excitation spectrum [1]. Recently, it was pointed out that in the case of the sign-preserved order parameter there is a redistribution of the magnetic spectral weight below *Tc*, due to the opening of a superconducting energy gap in the spin excitation channel, which leads to a non-resonance broad peak above 2Δ [2, 3]. Therefore the observation of the peak either below or above 2Δ allows identification of the relative sign of the order parameter.

In the present experiment we used the three-axis spectrometer IN8 at the ILL to study the effect of isovalent S-doping on the spin dynamics and its relationship with superconductivity in $K_xFe_{2-y}(Se_{1-z}S_z)_2$. **Figures 1a–c** show the evolution of the resonant mode as a function of S concentration. The spectra of the undoped sample exhibit a sharp resonant mode (**figure 1a**). Interestingly, in the $z = 0.4$ sample, in addition to the resonant excitation below 2Δ the spectra exhibit a shoulder on the higher energy side above 2Δ (**figure 1b**). With increasing S concentration to $z = 0.5$, the resonant mode is completely replaced by a broad hump structure above 2Δ (**figure 1c**). The absence of magnetic resonant mode below 2Δ and the pile up of states above 2Δ suggest that the superconducting order parameter no longer has a sign reversal at this doping level.

The scattering of the resonant mode and the hump structure above 2Δ displays an order parameter-like temperature dependence with an onset at *Tc* (**figure 1d–g**), suggesting that the redistribution of the spin excitation spectra is intimately associated with superconductivity.

Figure 2 summarises the doping dependence of the *Tc*, the superconducting gap (2Δ) and the superconductivity-induced magnetic peak energy (E_p). The magnetic peak energy (E_p) barely changes from $z = 0$ to $z = 0.4$, and

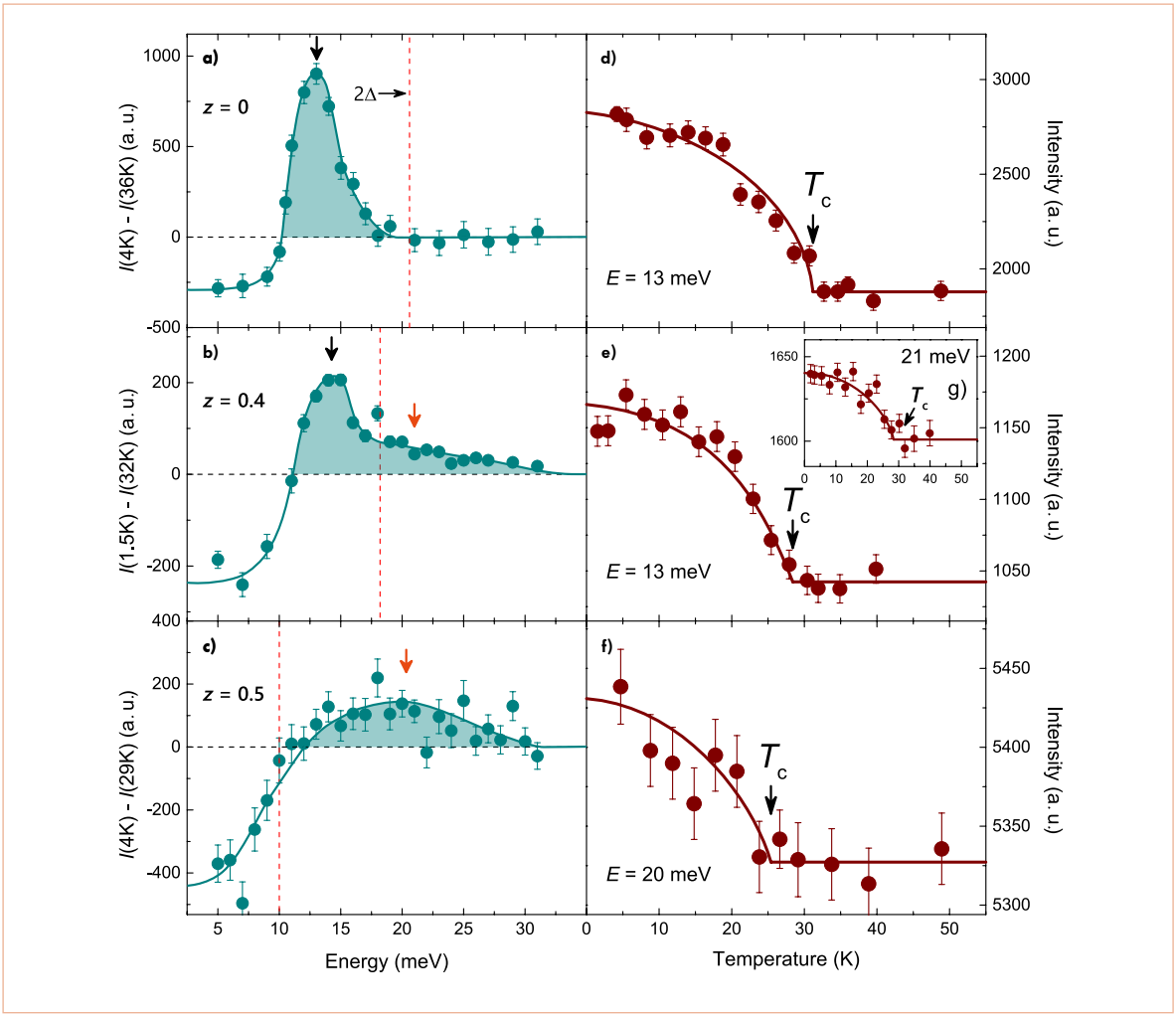

Figure 1

Temperature dependence of the spin excitations and their doping evolution in $K_xFe_{2-y}(Se_{1-z}S_z)_2$ (z = 0, 0.4, 0.5) below and above *Tc*. **(a)-(c)** Energy dependence of the intensity difference between the superconducting and the normal state in the vicinity of Q = (0.5, 0.75, 0). The dashed lines represent 2Δ determined by ARPES measurements. **(d)-(g)** Temperature dependence of the spin excitations measured at the indicated energies.

suddenly shifts to higher energy at $z = 0.5$. For $z = 0$, 0.25 and 0.4, the ratio $E_p = 2\Delta$ is close to the empirical universal ratio of ~ 0.64 for magnetic superconductors [4], which meets the requirement that the resonant mode is a bound state below the superconducting gap in a sign-reversed pairing state. This ratio jumps to 2.03 at $z = 0.5$, which obviously violates the primary criteria of the magnetic resonant mode.

Our results cannot be readily explained by simple spin fluctuation-exchange pairing theories and, therefore, multiple pairing channels are required to describe superconductivity in this system. It is possible that $K_xFe_{2-y}(Se_{1-z}S_z)_2$ is close to an intermediate pairing state. The predominant effect of S-doping is to decrease progressively the electronic correlations. This may, in turn, change the balance between various fluctuations and pairing instabilities.

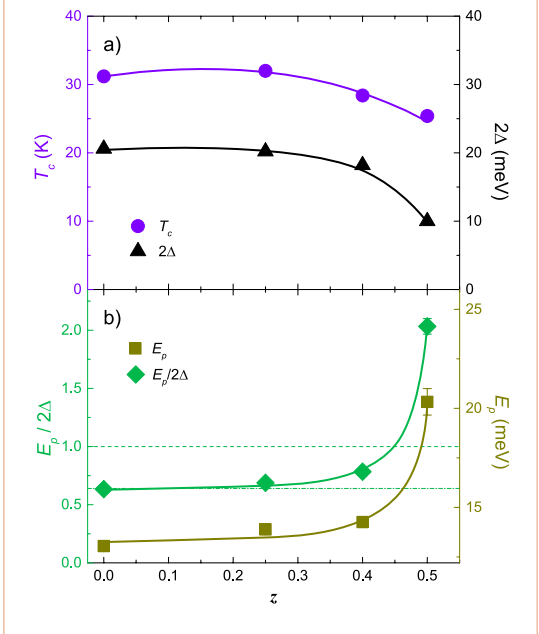

Figure 2

Doping dependence of *Tc*, the superconducting gap (2Δ), and the superconductivity-induced magnetic peak energy (E_p).

Competing coexisting phases in two-dimensional water

Time-of flight spectrometer IN5
Time-of flight spectrometer Mibémol at LLB

The properties of bulk water come from a delicate balance of interactions on length scales encompassing several orders of magnitude: i) the hydrogen bond (H-Bond) at the molecular scale; and ii) the extension of this H-Bond network up to the macroscopic level. What happens when the three-dimensional extension of the H-Bond network is frustrated, so that the water molecules are forced to organise in only two-dimensions (2D)?

AUTHORS

J.-M. Zanotti and **M.-C. Bellissent-Funel** (LLB, CEA Saclay, France)
P. Judeinstein (Université Paris-Saclay and LLB, CEA Saclay, France)
S. Dalla Bernardina, **G. Creff**, **J.-B. Brubach** and **P. Roy** (Synchrotron SOLEIL, France)
M. Bonetti (SPEC, CEA, CNRS, Université Paris-Saclay, France)
J. Ollivier (ILL)
D. Sakellariou (NIMBE, CEA, CNRS, Université Paris-Saclay, France)

REFERENCES

[1] J.-M. Zanotti *et al.*, Sci. Rep. 6 (2016) 25938 doi: 10.1038/srep25938
[2] H.E. Stanley and J. Teixeira, J. Chem. Phys. 73 (1980) 3404
[3] S. Combet and J.-M. Zanotti, Phys. Chem. Chem. Phys. 14 (2012) 4927
[4] D. Champion, C. Loupiac, D. Russo, D. Simatos and J.-M. Zanotti, J. Therm. Anal. Calorim. 104 (2011) 365
[5] N. Malikova *et al.*, Phys. Rev. Lett. 101 (2008) 265901
[6] I.M. Briman *et al.*, J. Phys. Chem. C 116 (2012) 7021

A striking hint that this situation might be interesting is provided by calorimetry. Compared with bulk hexagonal ice, interfacial water shows a large specific heat suggesting specific dynamical modes at low temperature. And indeed, synchrotron-based far and near infra-red spectroscopy evidences phases and/or dynamical transitions in the 160, 220 and 250 K regions. Solid-state quadrupolar NMR reveals a strong dynamical heterogeneity of this interfacial water due to the coexistence of a liquid-like and a solid-like phase. The temperature dependence of those two phases can be directly inferred from the NMR spectra.

On more theoretical ground we show that, while simple, a purely analytical mean-field percolation model is robust enough to account, in a coherent manner, for this whole set of experimental structural, dynamical and thermodynamical data on an extended temperature range from 150 to 300 K [1].

Figure 1

In two-dimensions on a hydrophilic silica surface, the ideal tetrahedral organisation of the bulk H-Bond network **a)** is frustrated. **b)** A water molecule may only engage three "classical" H-Bonds with neighbouring molecules lying on the surface and a much more long-lived/stable one with a Si-OH group on the surface. **c)** Temperature dependence of the probability, *p*, to form a H-Bond. This quantity is directly derived from time-of-flight quasi-elastic data (**figure 2a**).

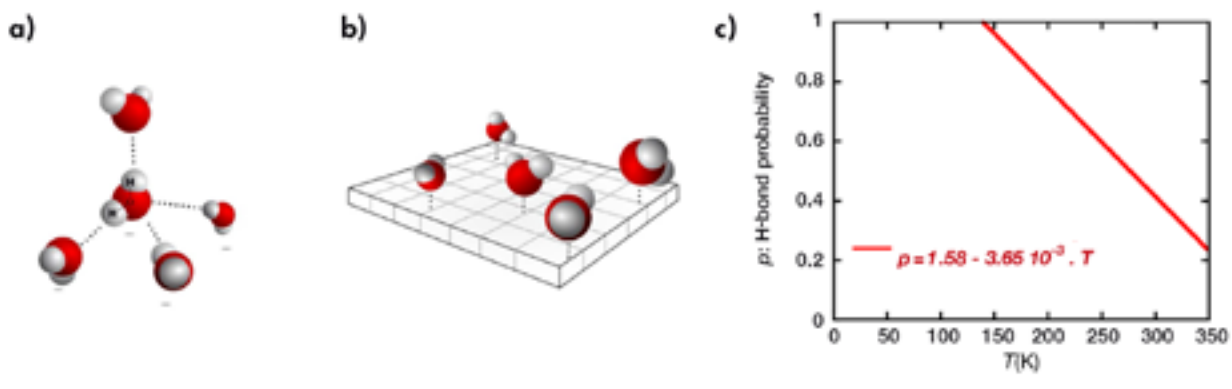

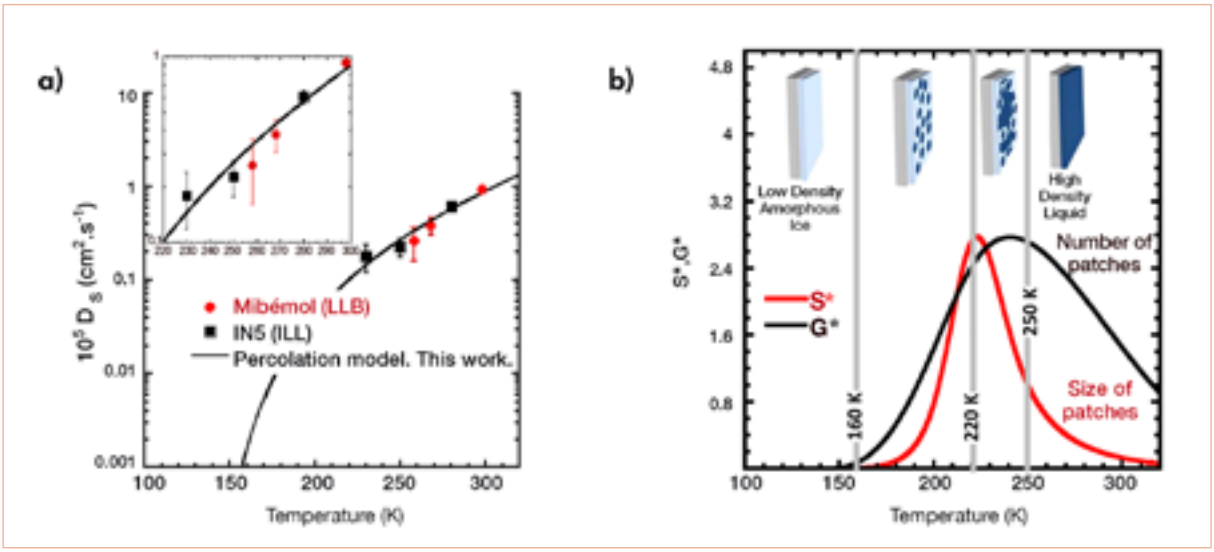

Figure 2

a) To tune, *p*, the probability to form a H-Bond, we use the temperature dependence of the self-diffusion coefficient of a monolayer of water as measured by QENS. **b)** Two-dimensional water is a heterogeneous system where a low-density (light blue) and a high-density (dark blue) phase coexist. This system shows unexpected physical properties: a glass transition at 165 K, a dynamic transition at 220 K and a liquid-liquid transition at 250 K.

Following Stanley and Teixeira [2], the essence of our approach is to point out that the local density around a given water molecule is ruled by the number of short-lived H-Bonds this molecule experiences. Two extreme situations can be described: the presence of a molecule engaged in four H-Bonds induces a local, *ice-like* low density, while the density is maximum if the molecule is transiently "free", i.e. not bound to any neighbouring molecule. As the H-Bond is a transient interaction (typically a few picoseconds (ps) at room temperature), an assembly of water molecules experiences constant density, hence entropy, fluctuations. The basic building block of the model is *p*, the probability, to form a hydrogen bond.

To tune *p(T)*, the temperature dependence of *p*, we measure *Ds*, the translational self-diffusion coefficient of interfacial water as inferred at the local scale by quasi-elastic neutron scattering (QENS) (**figure 2a**): $D_s(T) = C.ln(3p(T) - 3p(T)^2 + p(T)^3)$, where *C* is a constant. What do we learn? At very low temperatures all water molecules are frozen within a low density, amorphous ice phase. As the temperature increases, several transitions are observed (**figure 2b**). Starting at temperatures as low as 160 K, water molecules are found capable of breaking hydrogen bonds. These mobile and liquid-like molecules have a strong tendency to cluster, forming transient patches. These patches grow and at 220 K percolate, i.e. they form a connected surface. In the end a single patch emerges that covers the whole surface. The source of this particular water behaviour in two dimensions is the frustration of the natural bulk tetrahedral local geometry and the underlying very significant increase in entropy of the interfacial water molecules: ΔS = 48 J / mol / K in 2D *vs* 21.6 J / mol / K in bulk.

The results of this study on the original structural and dynamic properties of interfacial water have relevance in all areas where water is in a monolayer situation, such as in the fields of biophysics [3], the food industry [4] or in materials [5] and nuclear science [6] (storage of long-lived waste).

Neutrons tell us how water dipoles relax

Time-of-flight spectrometer IN5

Quasi-elastic neutron scattering results on H_2O reflecting H dynamics and on D_2O delivering the dynamic structure factor around the intermolecular peak and at intermediate length scales, reveal three processes (diffusive, local relaxational and vibrational) at frequencies below 3 THz, to which the contributions commonly invoked in dielectric studies can be directly mapped. We achieve a unified description of the results from both techniques, clarifying the nature of the molecular motions involved in the dielectric spectra and their impact on the structural relaxation.

AUTHORS

A. Arbe, **P. Malo de Molina**, **F. Alvarez** and **J. Colmenero**
(Materials Physics Centre, San Sebastián, Spain)
B. Frick (ILL)

REFERENCES

[1] W.J. Ellison, K. Lamkaouchi and J.M. Moreau, J. Mol. Liq. 68 (1996) 171
[2] N.Q. Vinh, M.S. Sherwin, S.J. Allen, D.K. George, A.J. Rahmani and K.W. Plaxco, J. Chem. Phys. 142 (2015) 164502
[3] A. Arbe, P. Malo de Molina, F. Alvarez, B. Frick and J. Colmenero, Phys. Rev. Lett. 117 (2016) 185501; J. Teixeira, Physics 9 (2016) 122
[4] A. Arbe, D. Richter, J. Colmenero and B. Farago, Phys. Rev. E 54 (1996) 3853
[5] J. Qvist, H. Schober and B. Halle, J. Chem. Phys. 134 (2011) 144508

Exploiting the permanent dipole of water molecules as a marker for molecular orientation, dielectric spectroscopy has been used for about a century to study water dynamics – of paramount importance in many areas of research and industrial applications [1]. However, the dynamic hydrogen-bond network in water imprints collectivity on the dielectric relaxation and therefore cannot be associated with any single-molecule (dipole) reorientation. Thus, the microscopic nature of its main component (the so-called Debye peak) and other weaker contributions phenomenologically introduced to account for the high-frequency data (**figure 1a** [2]) still remain elusive. Coherent and incoherent neutron scattering has allowed the identification of water's nuclei motions, the direct monitoring of the structural relaxation and clarification of the origin of the dielectric response [3]. This work also opens up a new way of approaching water dynamics under different conditions (supercooled, confined, etc.), as well as that of other hydrogen-bonded liquids.

Our time-of-flight experiments on protonated and heavy water covered the interesting frequency range for the dynamics at room temperature, revealing single-nuclei (H) motions and collective dynamics respectively, with space-time resolution around the main structure factor peak ($Q_{max} \approx 2$ Å^{-1} for water) and at intermediate length scales. Proper renormalisation with the Bose factor delivered corresponding susceptibilities. In these functions we can directly distinguish three processes (**figures 1b** and **1c**): (i) the one dominating at low frequencies shows dispersion in Q, indicating diffusive behaviour; (ii) at the other extreme of the spectra, the relevant process is Q-independent and with a rather high characteristic frequency (≈ THz), indicating an inelastic vibrational origin; (iii) a third, intermediate process – more evident in the low-Q coherent data – shows, if any, a very weak Q-dependence.

Assuming for the relaxational component – as in a model used for polymer dynamics [4] and also proposed for H_2O [5] – the simultaneous occurrence of a local process and diffusion, the intermediate contribution would reflect such a local process affected by diffusive motions (i.e. an 'effective local' process). This scenario provides an excellent description of all the experimental data (**figures 1b** and **1c**).

Figure 1

Imaginary part of water susceptibility at 298 K: **a)** dielectric spectroscopy results [2]; **b)** and **c)** incoherent and coherent neutron scattering results respectively, at the Q-values indicated in Å^{-1}.

Solid lines are the fits obtained in this work. The components are represented for Q = Q* = 0.7 Å^{-1} in **a)** and **b)** and for Q = Q_{max} = 2.0 Å^{-1} in **c)**: diffusive 'd' (red), effective local 'ℓd' process (green) and vibrational 'v' (blue) processes. Grey dashed-dotted lines in **(a)** show the components reported from a phenomenological analysis [2].

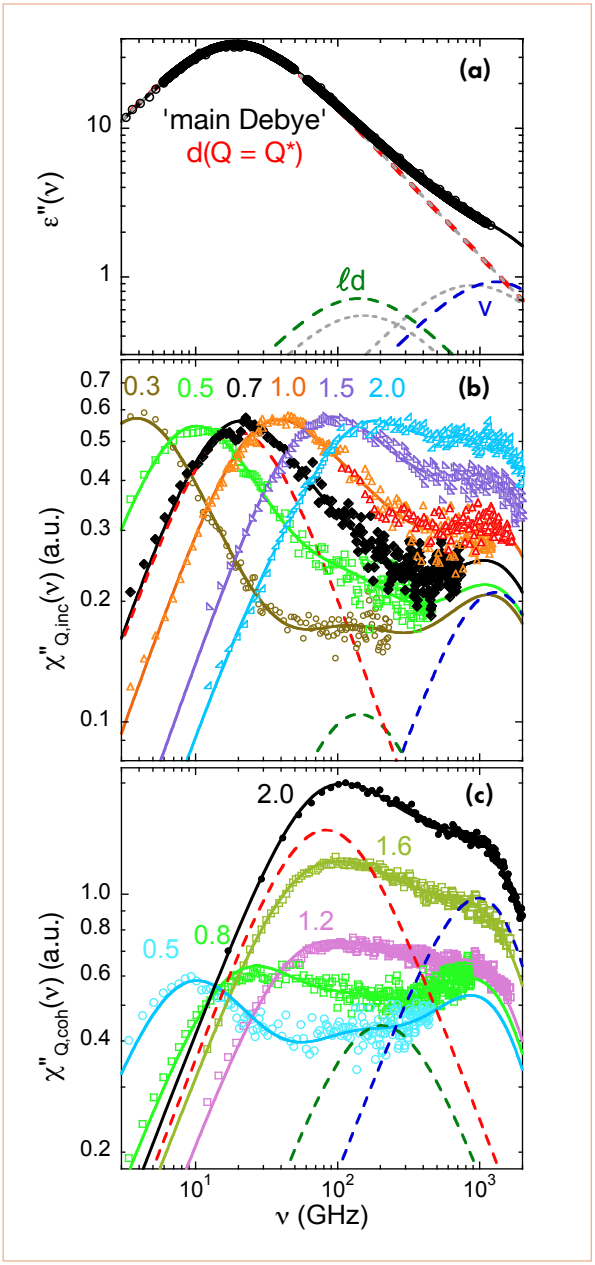

We find a coincidence of the main Debye dielectric peak (centred at τ_D = 8.37 ps) with the diffusive process at Q = Q* ≈ 0.7 Å^{-1}. In fact, the whole dielectric spectrum can be perfectly described by the same model used for the neutron susceptibility at Q* with relative amplitudes rather similar to those usually found in phenomenological dielectric studies, as can be seen in **figure 1a**. Thus, the collective dipolar relaxation is mainly

Figure 2

'Mean displacement' experimentally obtained for Hs (different symbols for different Q-values in the range 0.19 ≤ Q ≤ 2.0 Å^{-1}) and calculated from the simulations for Hs (solid line) and Os (dashed-dotted line). Dotted lines mark the co-ordinates corresponding to τ_D, τ_ℓ, τ_V (inverse frequencies of the susceptibility components' maxima).

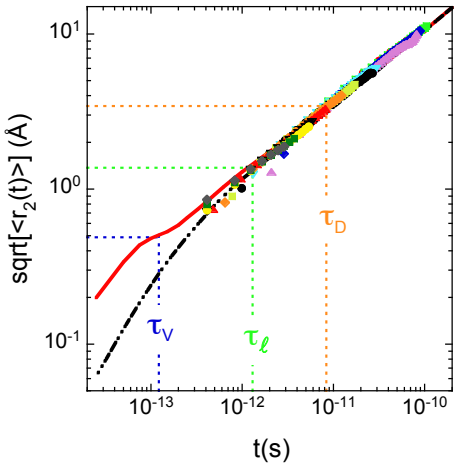

driven by translational diffusion, and the additionally invoked low-amplitude high-frequency processes can be mapped into the vibrational and localised processes also resolved by neutrons. Q* constitutes a link between molecular diffusion and dipolar relaxation. It can be expressed as Q* ≈ [(2/3) a^2G_K/J_K]$^{-1/2}$, i.e. in terms of a 'single-molecule' magnitude – the effective radius, a – and the ratio between the Kirkwood static and dynamical coupling parameters, G_K/J_K, measuring the strength of many-body effects on dipolar relaxation.

Interestingly enough, thanks to the experiments on D_2O, the structural relaxation is directly accessible as the relaxational contribution of coherent susceptibility at Q_{max}. As shown in **figure 1c**, the structural relaxation has contributions from both the diffusive and the effective local process; however, we can conclude that it is largely dominated by diffusion.

How far do atoms move at the time scales of the different processes? Applying the Gaussian approximation, incoherent scattering provides this information for H nuclei. We have complemented it with molecular dynamics simulation results [3], which also access O-trajectories (**figure 2**). The collective dipolar relaxation can only take place when the atoms move in average large distances (the displacement at τ_D is ≈ 3.4 Å), which are comparable or slightly larger than intermolecular distances. Hydrogens' trajectories show a first vibrational 'cage' around τ_V, where the decaging would likely involve hydrogen bond breaking and which is hardly reflected for Os. A second cage is less defined, likely due to the convolution of local and diffusive processes, in the range of the local process. Delocalisation from this cage leads to pure diffusive behaviour. Since the total reorientation of the dipole moment (collective Debye peak) requires large O-displacements, the motions inside this cage would only contribute to hindered rotations of the dipole moment, which translate into the low amplitude dipolar relaxation observed in this short-time/high-frequency range.

Double-difference isotope substitution on liquid $Ca_3Al_2O_6$

Disordered materials diffractometer D4

Understanding the atomic-scale characteristics of oxide liquids which promote glass formation represents a long-standing problem in condensed matter physics. Their high melting temperatures and the inherent disordered nature of liquids has meant that experimental measurements of the structure of oxide melts are limited. To overcome these problems, we have applied the method of neutron diffraction with isotope substitution, together with aerodynamic levitation using laser heating, to unravel the complex overlapping atom-atom correlations in the glass-forming liquid $Ca_3Al_2O_6$ [1].

AUTHORS

J.W.E. Drewitt, **A.C. Barnes**, **S.C. Kohn** and **M.J. Walter** (University of Bristol, UK)
S. Jahn (University of Cologne, Germany)
A. Novikov (CNRS-IPGP/Sorbonne Paris and CEMHTI-CNRS/University of Orléans, France)
D.R. Neuville (CNRS-IPGP/Sorbonne Paris, France)
H.E. Fischer (ILL)
L. Hennet (CEMHTI-CNRS/University of Orléans, France)

REFERENCES

[1] J.W.E. Drewitt *et al.*, Phys. Rev. B 95 (2017) 064203
[2] J.W.E. Drewitt *et al.*, Phys. Rev. Lett 109 (2012) 235501
[3] H.E. Fischer, A.C. Barnes, and P.S. Salmon, Rep. Prog. Phys. 69 (2006) 233
[4] J.W.E. Drewitt *et al.*, J. Phys.: Condens. Matter 23 (2011) 155101

The CaO-Al_2O_3 glass-forming system has a diverse range of applications, from aluminous cements and bioceramics to optoelectronic glass, as well as being an important component of natural magmas [2]. Detailed knowledge of the structural role of aluminium and calcium in these refractory melts is important to improve our understanding of the rheology of magmas and the mechanisms of crystallisation and glass formation. To this end, we have made neutron diffraction with isotope substitution (NDIS) [3] measurements of liquid $Ca_3Al_2O_6$ at the ILL diffractometer D4. Three structurally identical samples were prepared using either Ca in its natural isotopic abundance, predominantly ^{44}Ca, or a 50:50 mixture of the two. *In situ* neutron diffraction measurements were made for the samples levitated in a stream of argon and heated to 2 073 K by two CO_2 lasers.

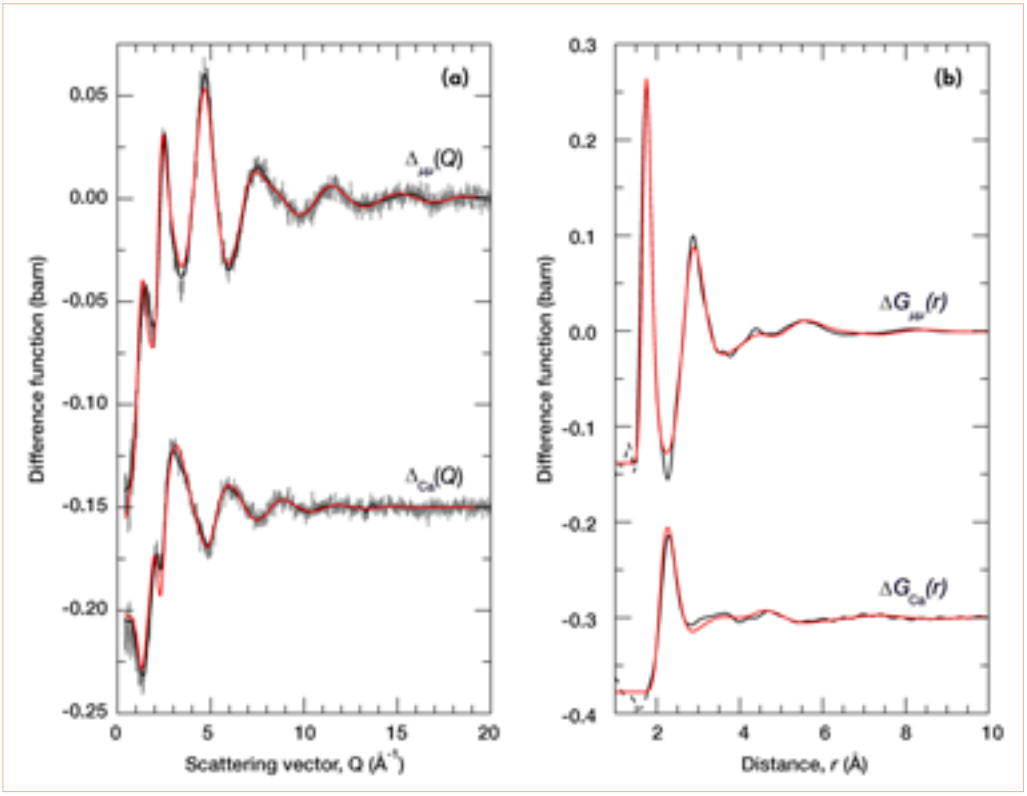

Figure 1

a) Reciprocal-space difference functions $\Delta_{\mu\mu}(Q)$ and $\Delta_{Ca}(Q)$. The vertical bars represent the statistical errors, the black curves are the Fourier back-transforms of the corresponding real-space functions in **(b)** after the un-physical features below the first interatomic distance were set to the theoretical $r = 0$ limit. **b)** Real-space difference functions $\Delta G_{\mu\mu}(r)$ and $\Delta G_{Ca}(r)$ (black curves). The dashed black curves show the extent of the un-physical low-r features. The red curves in **(a)** and **(b)** are from MD simulations [4].

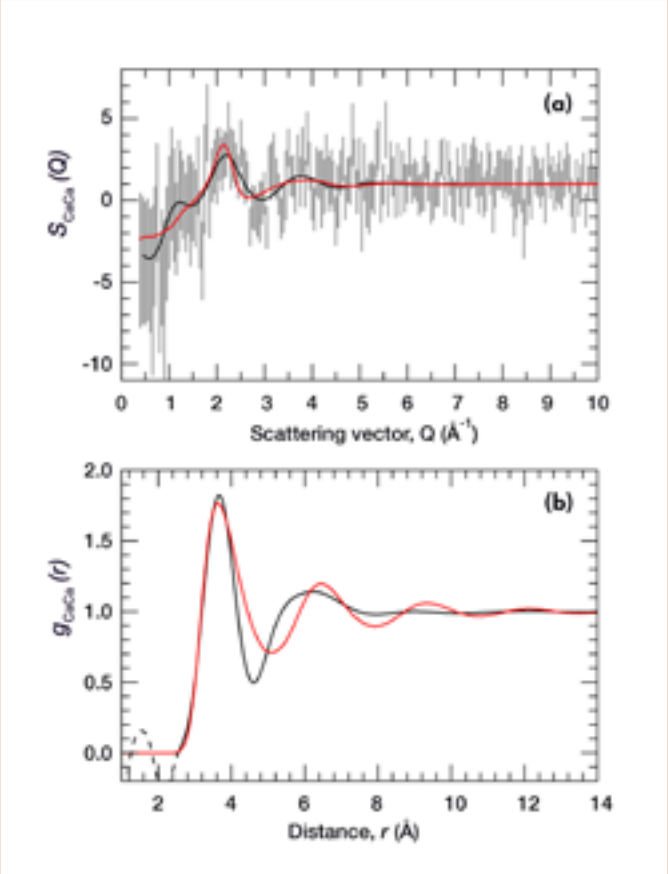

Figure 2

a) Partial structure factor $S_{CaCa}(Q)$. The vertical bars represent the statistical errors, the black curve is the Fourier back-transform $g_{CaCa}(r)$ after the un-physical features below the first interatomic distance were set to the theoretical limit $g_{CaCa}(r = 0) = 0$. **b)** Pair-distribution function $g_{CaCa}(r)$ (black curve). The broken black curve shows the extent of the un-physical low-r features. The red curves in **(a)** and **(b)** are the results from MD simulations [4].

The contrast in neutron scattering lengths for ^{nat}Ca (4.70 fm) and ^{44}Ca (1.45 fm) means that the pair correlations involving calcium atoms receive different weightings in the total structure factors $^{nat}F(Q)$, $^{44}F(Q)$, and $^{mix}F(Q)$. Specific pair correlations may be eliminated by linear combination of the structure factors. The first-order difference functions are shown in **figure 1a**, where $\Delta_{Ca}(Q)$ contains only Ca-Ca and Ca-μ (μ = Al, O) correlations, and $\Delta_{\mu\mu}(Q)$ contains only μ-μ correlations. The corresponding real-space $\Delta G_{Ca}(r)$ and $\Delta G_{\mu\mu}(r)$ Fourier transforms are shown in **figure 1b**. The first peak in $\Delta G_{Ca}(r)$ at 2.29(2) Å, arising from Ca-O bonds, gives a Ca-O co-ordination of 5.5(3). The first peak in $\Delta G_{\mu\mu}(r)$ at 1.75(1) Å corresponds to the Al-O bond length and gives an Al-O co-ordination of 4.2(1).

By combining all three $^{nat}F(Q)$, $^{44}F(Q)$, and $^{mix}F(Q)$ measurements, the second-order (or "double") difference has allowed for the direct determination of the $S_{CaCa}(Q)$ and $g_{CaCa}(r)$ partials in liquid $Ca_3Al_2O_6$ (**figure 2**).

The results of molecular dynamics (MD) simulations [4] are in excellent agreement with the experimental data. Our results reveal that calcium has a wide distribution of 4- to 7-fold co-ordination sites, where higher co-ordinated Ca preferentially bonds to bridging oxygen atoms. Although significantly de-polymerised, liquid $Ca_3Al_2O_6$ is still largely composed of AlO_4 tetrahedra, most of which belong to an infinite corner-shared network. The MD simulation model reveals the presence of about 10 % unconnected Al_2O_7 and AlO_4 monomers and dimers in the liquid. The number of these isolated units is expected to increase with CaO concentration, such that the upper value of the glass-forming composition could be described in terms of a percolation threshold at which the glass can no longer support the formation of an infinitely connected AlO_4 network.

Smart nanogels at the air/water interface: structural studies by neutron reflectivity

Horizontal reflectometer FIGARO

Nanomaterials are receiving increased attention in fundamental and applied studies, for example in biomedical applications [1]. Nanogels are covalently cross-linked polymers, characterised by their small size and high surface-to-volume ratio, combining properties of typical colloids with the soft character and responsiveness of gels [2]. The development of nanogels that exhibit a switchable phase transition close to the normal physiological temperature of 37 °C is of key interest [3]. Their structures at interfaces, however, require a better understanding before they can be used in applications.

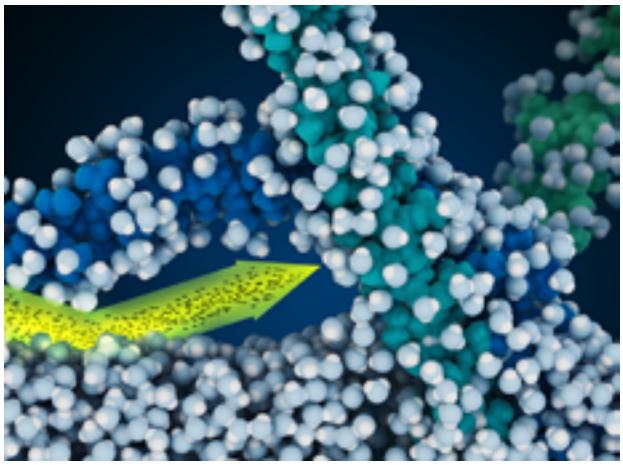

AUTHORS

K. Zielińksa, **H. Sun**, **A. Zarbakhsh** and **M. Resmini** (Queen Mary University of London, UK)
R.A. Campbell (ILL)

REFERENCES

[1] O.V. Salata, J. Nanobiotechnology 2 (2004) 3
[2] R. Pelton, Adv. Colloid Interf. Sci. 85 (2000) 1
[3] B.R. Saunders, N. Laajam, E. Daly, S. Teow, X. Hu and R. Stepto, Adv. Colloid Interf. Sci. 147–148 (2009) 251

Poly(*N*-isopropyl acrylamide) (PNIPAM) is a polymer that has a phase transition, called the lower critical solution temperature, at around 32 °C. This transition temperature can be tailored to different values through the addition of cross-linkers. PNIPAM has potential therefore as a "smart" delivery vehicle, where the release of a drug can be triggered by changes in temperature, which in turn can be tuned by the degree of cross-linker incorporated into the polymer matrix. Like conventional short-chain surfactants, PNIPAM nanogels lower the surface tension of water. However, because of the lack of well-defined hydrophobic and hydrophilic regions, they form more complex structures at the air/water interface.

Understanding how nanogels stabilise interfaces, what surface pressures they generate and which are their conformations at the surface, are important questions that need to be answered before such materials can be considered for widespread use in applications. For that reason a project was started, involving neutron measurements on the FIGARO reflectometer at the ILL, to understand the relation between the surface tension and interfacial structure with respect to the degree of cross-linker in a nanogel. The structure of PNIPAM nanogels with 0-30 % content of N,N'-methylenebisacrylamide (MBA) was studied at the air/water interface at 37 °C. Normal and deuterated nanogels were synthesised specifically for this work, to maximise the sensitivity of the measurements to fine details of the interfacial structure. In-depth structural studies on a molecular length scale of these systems at an interface had not previously been attempted.

The use of neutrons in this work was of paramount importance. The non-equilibrium nature of these systems means that it is not possible to apply a normal surface tension analysis to estimate the amount of a nanogel at an interface. Neutron reflectivity measurements with isotopic contrast variation, however, provide a sensitive means to determine the adsorbed amount directly. Furthermore, analysis of measurements recorded in different isotopic contrasts leads to the resolution of complex structures. The technique also allows the changes in the volume fraction of nanogels at the interface to be followed with time as more material reaches the interface. Additionally, it can be used to reveal changes in conformation, which is important in relating the structure-to-function for this class of materials.

Examples of the neutron reflectivity data recorded for the deuterated nanogels are shown in **figure 1a**, with the resulting volume fraction profiles shown in **figure 1b**. A three-layer model was found to describe the structures formed: first a densely packed layer in contact with air, then a second layer of solvated polymer, and lastly a third layer of diffuse polymer chains extending into the solution. Interestingly, the content of water in the first layer increases with percentage of cross-linker in the gels. This is attributed to a reduction in the ability of the nanogel to change conformation and repel water from the polymer network when there is a higher degree of cross-linking. This was the first experimental evidence of structural changes of nanogels as a function of the degree of cross-linking at the air/water interface. The three distinct regions of the surface structure with respect to the degree of cross-linking are sketched in **figure 2**.

The structural data also suggest an extensive rearrangement of the conformation of the nanogel particles at the interface during the adsorption process, resulting in structural deformation. The degree of deformation also diminishes with increasing percentage of cross-linker. Furthermore, as the percentage of cross-linker incorporated in the nanogels was increased, more rigid matrices were obtained and the adsorbed amount increased. Although the differences in conformations between the bulk and the liquid/liquid interface for PNIPAM-based microgels had previously been hypothesised, this study is the first to provide supporting experimental evidence at a fluid interface.

The data presented are an important input into understanding the behaviour of nanogels at interfaces. Already the project has been extended to measurements with respect to temperature as well as measurements at the oil/water interface. It is hoped that the insight gained may lead to achievement of the rational, smart design of new materials for biomedical applications.

Figure 1

a) Neutron reflectivity data of PNIPAM-MBA nanogels at the air/water interface recorded with different amounts of the cross-linker; the data are offset for clarity in the main panel with the differences highlighted in the **inset**; **b)** The resulting volume fraction profiles normal to the interface showing three distinct regions.

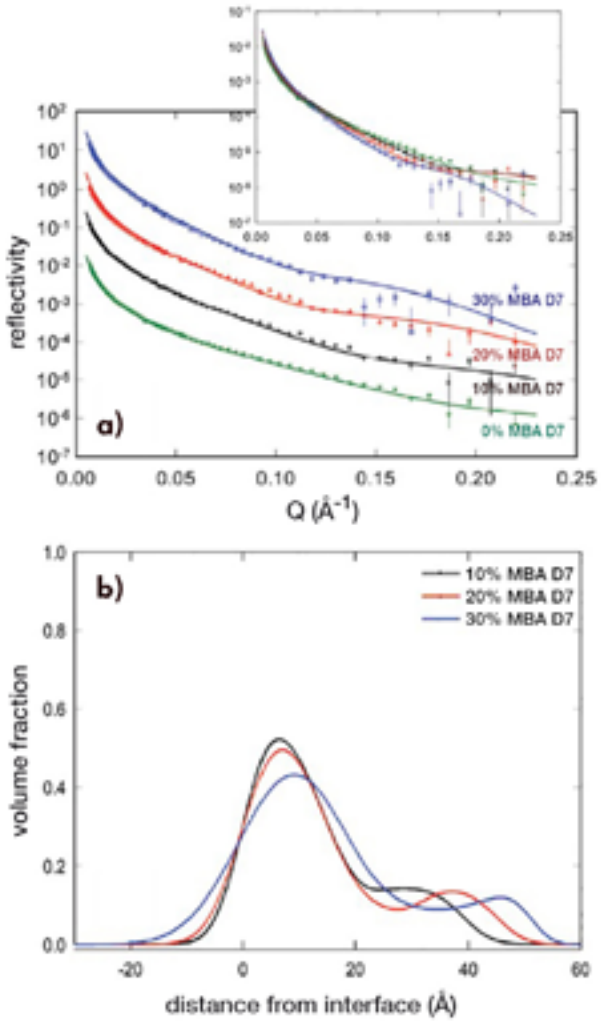

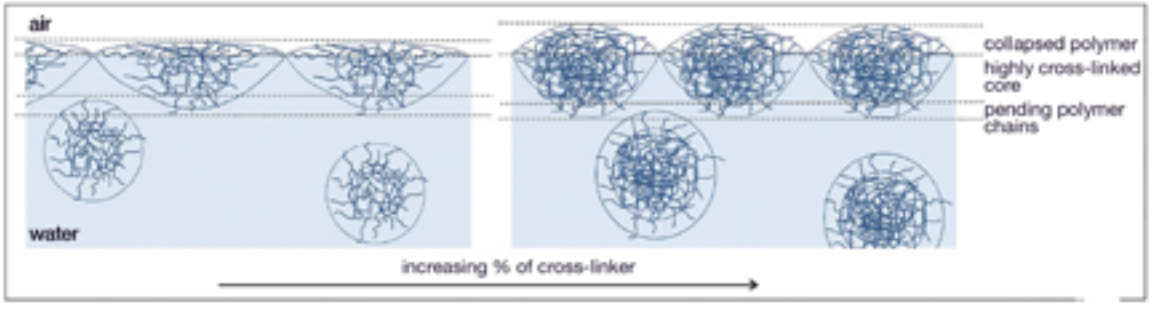

Figure 2

Schematic of the structure of PNIPAM-MBA nanogels at the air/water interface with respect to the amount of cross-linker.

Structural features of reconstituted wheat wax films

Reflectometer D17

Cuticular waxes are essential for the wellbeing of all plants, from controlling the transport of water and nutrients across the plant surface to protecting them against external environmental attacks [1, 2]. Despite their significance, current understanding regarding the structure and physiochemical properties of the cuticular wax film, which allows them to carry out their functions, is limited. In this study we formed representative reconstituted wax film models of controlled thicknesses which facilitated an *ex-vivo* study of plant cuticular wax film properties by neutron reflection (NR) using the D17 instrument at the ILL. Solid-liquid NR measurements were also carried out to investigate the interaction of, and changes to, the structural properties of cuticular wax films when in the presence of water. This study provides a useful structural basis that underlies the function of the epicuticular waxes in controlling the water transport of crops.

AUTHORS

E. Pambou, **Z. Li** and **J.R. Lu** (University of Manchester, UK)
M. Campana, **A. Hughes** and **L. Clifton** (STFC ISIS, UK)
P. Gutfreund (ILL)
J. Foundling and **G. Bell** (Jealott's Hill International Research Centre, Bracknell, UK)

REFERENCES

[1] W. Barthlott, C. Neinhuis, D. Cutler, F. Ditsch, I. Meusel, I. Theisen and H. Wilhelmi, Bot J Linn Soc. 126 (1998) 237
[2] G. Bianchi, in Waxes: Chemistry, Molecular Biology and Functions, R.J.Hamilton (ed), The Oily Press, Dundee (1995)
[3] Y. Yoneda, Phys Rev. 131 (1963) 2010

The cuticular wax film models used in this study were produced *via* the isolation of *Triticum aestivum L.* (wheat) waxes from wheat straw samples using two distinct extraction methods. Waxes extracted from harvested field-grown wheat straw using supercritical CO_2 are compared with waxes extracted from laboratory-grown wheat straw *via* wax dissolution by chloroform rinsing. Chloroform solutions of the two samples were subsequently spin-coated onto silicon substrates to produce the reconstituted films.

Together with spectroscopic ellipsometry, atomic force microscopy (AFM) and cryo scanning electron microscopy (cryo-SEM) imaging revealed that the two reconstituted wax film models are ultra-thin and porous with characteristic nanoscale extrusions on the outer surface, mimicking the structure of epicuticular waxes found upon adaxial wheat leaf surfaces (**figure 1**). Off-specular neutron reflection "Yoneda" peaks were also encountered using D17, which provided our first indication of regularly ordered crystalline extrusions upon the wax surface [3]. On the basis of solid-liquid NR, carried out under three neutron scattering contrasts (D_2O, water contrast matched to air, and water contrast matched to silicon), and solid-air NR and ellipsometric measurements, the wax films could be modelled into two representative layers: the diffuse underlying layer fitted with thicknesses ranging from ~ 65-70 Å, while the surface extrusion region reached heights exceeding 200 Å.

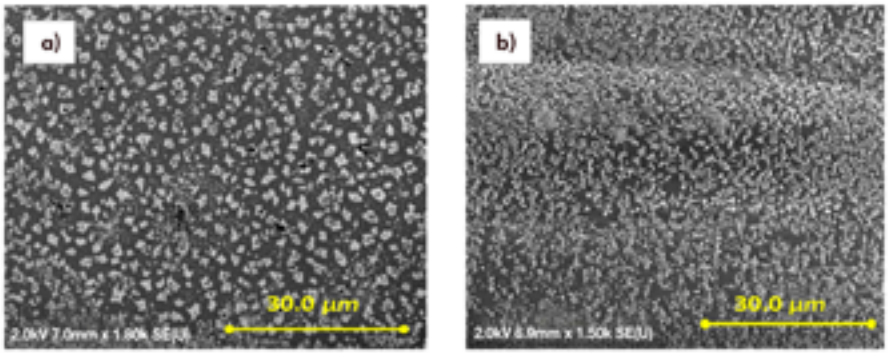

Figure 1
Cryo-SEM images of
a) a reconstituted wheat wax film surface and
b) that of an adaxial surface of an excised wheat leaf; 2-week old glasshouse-grown plant (scale bars = 30 *µm*).

Figure 2

Tomographic visualisation of a wax film immersed in water caused by water penetration. The colour gradient describes the amount of water penetration.

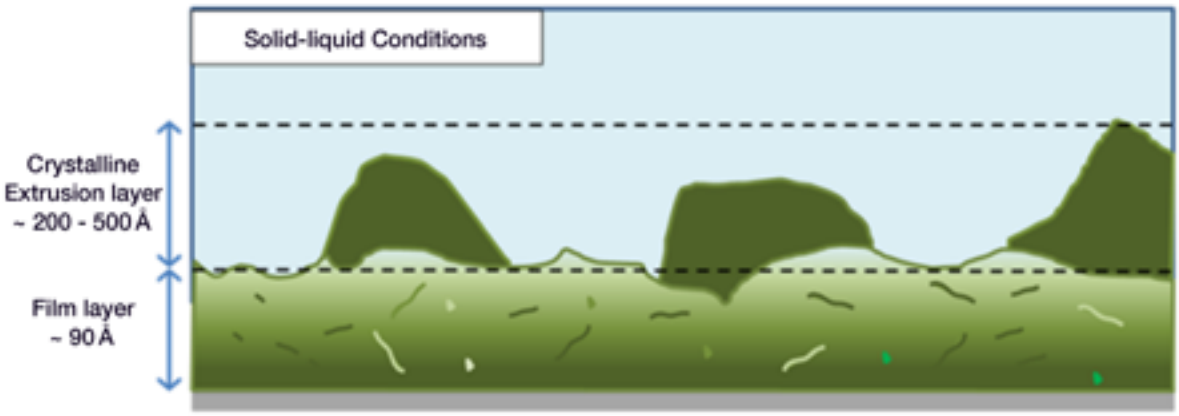

Moisture-controlled NR measurements carried out in dehydrated, ambient and saturated humidity conditions indicated that water penetrates extensively into the wax films measured under saturated humidity and under water, causing them to hydrate and swell significantly with up to 50 % of the underlying film occupied by water. These swollen wax films could return to their basic structural feature upon drying. NR measurements carried out in a moisture-saturated environment show that it is particularly easy for water vapour to penetrate and become trapped within the underlying wax films (**figure 2**). A steady increase in water content with interfacial distance was observed as the water vapour readily penetrates the wax near the surface of the underlying film, as confirmed by spectroscopic ellipsometry. Despite moisture penetration and swelling observed under hydrated conditions, wax films are significantly thinner than when immersed in water at the solid-liquid interface. Exposure to the bulk water could be said to cause more substantial swelling to the underlying wax film, as was evident from the increase in film thickness measured by ellipsometry and NR. Comparison of the films measured under ambient and dehydrated environments shows little noticeable effect upon the basic wax film structure feature and film thickness. It can be inferred that an unhydrated cuticular wax film will be significantly thinner than its hydrated counterpart.

In conclusion, this work has demonstrated that the main leaf surface could be mimicked, in terms of its main characteristics, by reconstituted films, thus opening up the prospect of further investigations using cuticular wax models by elaborate physical techniques. The general perception is that plant cuticular waxes form part of the hydrophobic, waterproof surface coating whose primary function is to act as a water-repellent barrier against external environmental attacks. While this is apparent on the macroscopic scale, our findings from the behaviour of reconstituted cuticular wax films show a significantly different behaviour at the molecular level. Measurements carried out in moisture-saturated solid-air and solid-liquid environments point towards a highly porous and diffusive underlying wax film which allows a significant amount of water penetration. Furthermore, to our best knowledge this is the first study to report the swelling and dehydrating of the cuticular plant wax films as a way of controlling water transportation from the reconstituted wax films. It is highly likely that the same mechanism works across real plant surfaces.

Solvent extraction: structure of the liquid/liquid interface containing a diamide ligand

Horizontal reflectometer FIGARO

Interfaces between immiscible liquids are ubiquitous in chemistry and biology, and are the site of numerous physico-chemical processes such as sorption, solvation and complexation. Electron, electrolyte, molecule, or colloid transfer through liquid interfaces are relevant for domains like chemistry, electrochemistry-driven solvent extraction [1], nanoparticle synthesis and heterogeneous catalysis. In solvent extraction using amphiphilic ligands to separate ions, the ion partitioning between immiscible phases is significantly enhanced by the ligand/ion complex formation on one side of the interface. The role of metal-ligand interaction and ligand supramolecular aggregation is essential in the distribution and separation factors. Here, the combined application of X-ray and neutron reflectivity measurements [2] represents a key milestone in the determination of the interfacial structure from two different lipophilic ligands.

Quartz liquid-liquid cell developed at the ILL and used for neutron reflectivity experiments. The cell is filled in the bottom with water and on top (above the internal quartz edge) with dodecane. The neutron beam passes through 3.5 cm of water.

AUTHORS

E. Scoppola (CEA/CNRS/ENSCM, University of Montpellier, France and ILL)
O. Diat, **J.-F. Dufrêche** and **L. Girard** (CEA/CNRS/ENSCM, University of Montpellier, France)
E.B. Watkins (Los Alamos National Laboratory, USA and ILL)
R.A. Campbell and **G. Fragneto** (ILL)
O. Konovalov (ESRF)
G. Ferru (Argonne National Labororatory, USA)

REFERENCES

[1] A. Berduque, A. Sherburn, M. Ghita, R.A.W. Dryfe and D.W.M. Arrigan, Anal. Chem. 77 (2005) 7310
[2] J. Daillant and A. Gibaud, Springer, Berlin (2009) 770
[3] Q.Z. Tian and M.A. Hughes, Hydrometallurgy 36 (1994) 79
[4] G. Benay and G. Wipff, J. Phys. Chem. B 118 (2014) 3133

We show that the determination of the ligand and ion distributions across the water/oil interface can help our understanding of the dynamics for ion transfer in a solvent extraction system. Only a few experimental techniques that probe a buried liquid interface are available to access this specific concentration profile. In particular, reflectivity techniques have already demonstrated their power in numerous interfacial characterisations because the explored domain, defined in Fourier space by the amplitude and direction of the scattering wave vector Q, fits perfectly with the nanometre range of spatial information.

For our study two systems were selected, involving diamide lipophilic ligands DMDOHEMA and DMDBTDMA and which we have labelled EXT1 and EXT2, respectively. These lipophilic ligands are currently used in the nuclear industry to separate f-elements from high-level radioactive liquid waste by liquid-liquid (LL) extraction processes (the DIAMEX process), as well as in the more conventional field of hydrometallurgy to recycle rare-earth elements [3]. We worked with ligands in dodecane contacted with aqueous solutions of neodymium and lithium nitrate.

The combination of X-rays and neutrons is very helpful for understanding the microscopic structure at the LL interface. X-rays reveal the distribution of higher electron density aqueous solutes (salts, nitric acid), and neutrons are the perfect probes to quantify the structuration of protonated solvents and ligand molecules thanks to the use of isotopic substitution.

Our work is the first to report neutron measurements at the interface of two bulk liquids. It was made possible not only by the high flux of FIGARO, which allowed us to cross between 3.5 and 5 cm of deuterated liquid, but also by its ability – unique in the world – to reach the interface from the bottom side, which allowed us in this case to cross heavy water at the bottom of the interface and in the oil phase to use hydrogenated ligands that would lower the transmission of neutrons if neutrons crossed that phase.

In **figure 1** the results of our analysis are plotted for two sets of reflectivity measurements of the two biphasic systems described above and registered at the equilibrium state. The main observation for the EXT1 system is an increase of the ligand adsorption at the interface when approaching its concentration in the organic phase, as expected for a surface active molecule. The evolution of ligand adsorption for the EXT2 system looks rather different. At low molar content, the ligand is localised in a more defined region at the boundary between the oil and water phases, as expected for a surfactant molecule.

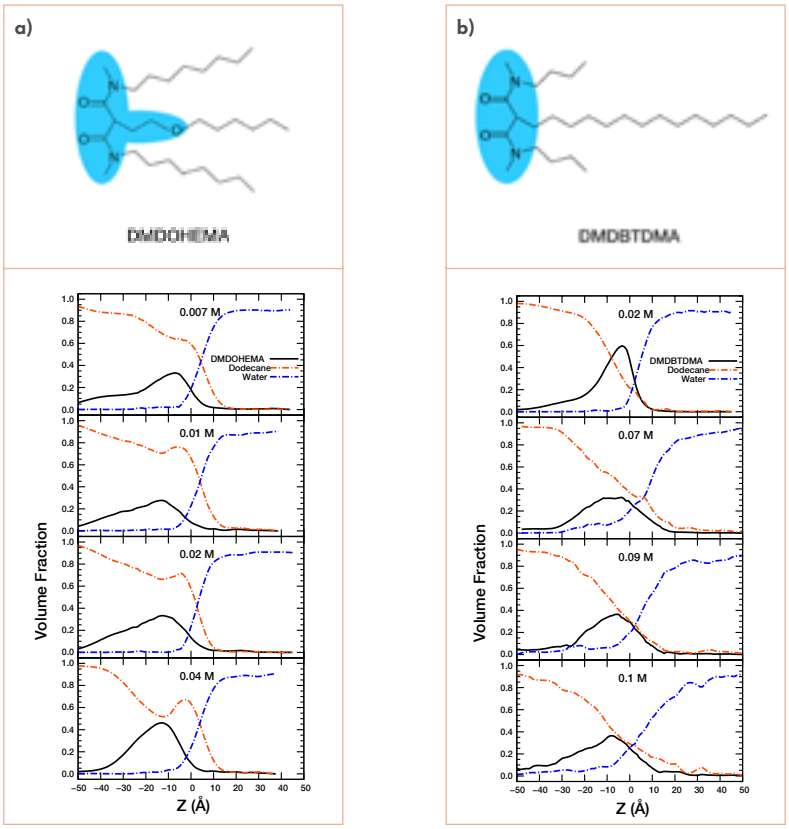

Figure 1

a) Concentration profiles across the LL interface (z-co-ordinate) of water, oil and ligand at four concentrations of DMDOHEMA or EXT1 (0.007, 0.01, 0.02 and 0.04 mol/L) with the chemical structure of the ligand;
b) Concentration profiles across the LL interface of water, oil and ligand at four concentrations of DMDBTDMA or EXT2 (0.02, 0.07, 0.09 and 0.1 mol/L). The light blue-coloured region over the structures defines the polar part of the molecules.

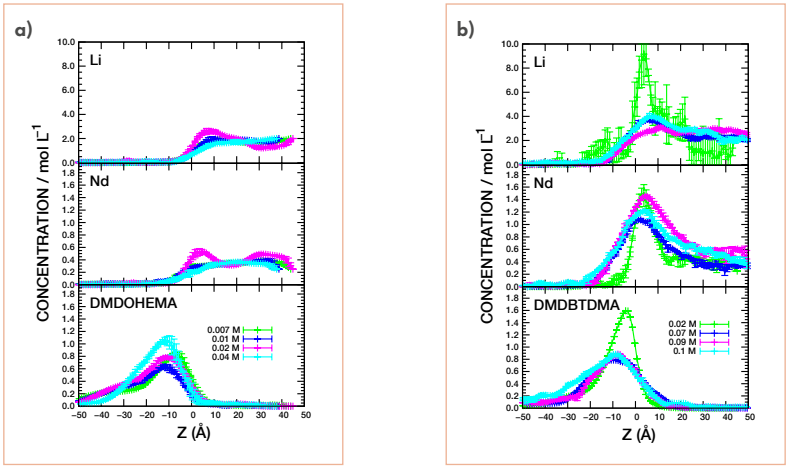

Figure 2

a) Concentration profiles across the LL interface of lithium, neodymium cations and ligand at four concentrations of DMDBTDMA or EXT2 (0.02, 0.07, 0.09 and 0.1 mol/L). Negative values of z correspond to the oil phase, positive values to the aqueous phase. The vertical lines correspond to z = 0 and are guides for the eyes to visualise the mixing between organic and aqueous species at the interface.

b) Concentration profiles in mol/L across the LL interface (z-co-ordinate) of lithium, neodymium cation and ligand at four concentrations of DMDOHEMA or EXT1 (0.007, 0.01, 0.02 and 0.04 mol/L).

In **figure 2**, the concentration profiles of the cations are plotted and compared with those of the ligand profiles for the four selected ligand concentrations. For both systems we observe different ion distributions with respect to the type of ligand. For the EXT1 system, the ion concentration profiles are rather constant and the ions are located exclusively in the aqueous phase. For the EXT2 system the profiles of lithium are still rather constant with respect to the ligand concentration, there is only a small excess at the interface compared with the bulk concentration in the aqueous phase, and there is a smooth decay towards the oil phase extending beyond 1 nm. However, for neodymium a significant increase close to the interface was determined, with a smooth decay towards the oil phase that largely overlaps the ligand distribution.

For both ligands we clearly observe an adsorption of the molecules at the interface with a local concentration much higher than in the bulk. In the case of DMDOHEMA, the ligand has an interfacial behaviour resembling a surfactant and the ligand layer at the interface forms a barrier to the various cations. In the case of DMDBTDMA, we observe a thick interface that apparently allows an incursion of the hydrated pairs of ions that can be complexed by the ligand.

To conclude, by coupling different neutron and X-ray reflectivity measurements we were able to determine the distribution of salts and ligands across a composite liquid interface. The work has also allowed us to make a link between experiments and simulation in such systems [4]. These results should serve as a basis for further understanding the extraction mechanism in order to improve the efficiency and kinetics of existing processes and to develop new ones. These methodological developments will also allow the study of other liquid interfaces.

Static and dynamic behaviour of responsive graphene oxide-poly (N-isopropyl acrylamide) composite hydrogels

Spin-echo spectrometer IN11 and small-angle scattering diffractometer D22

AUTHORS

B. Berke (ILL and Budapest University of Technology and Economics, Hungary)
O. Czakkel and **L. Porcar** (ILL)
E. Geissler (CNRS and Université Grenoble Alpes, France)
K. László (Budapest University of Technology and Economics, Hungary)

REFERENCES

[1] T. Tanaka, Phys. Rev. Lett. 40 (1978) 820
[2] L. Ionov, Mater. Today 17 (2014) 494
[3] F. Mezei, Neutron Spin Echo, in Lect. Notes Phys., ed. F. Mezei (1980) vol. 128

Responsive hydrogel composites have enormous potential in applications such as sensors, actuators and drug delivery vectors, but current understanding of their structure and swelling behaviour falls below that of industrial design requirements. The scarcity of appropriate methods of measurement, particularly at the nanoscale level, is a barrier to characterising these composite hydrogels. Neutron scattering offers a non-destructive means of gaining information about both the static and the dynamic behaviour of these complex systems.

Thermo-responsive hydrogels are three-dimensional polymer networks with high water content that exhibit a reversible volume phase transition (VPT) when the temperature changes. Within this group, those based on poly(N-isopropyl acrylamide) (PNIPAM) are outstanding for their peculiar VPT temperature at around 34 °C, close to that of the human body [1].

Unfortunately, poor mechanical strength and uncontrolled thermal response often limit their usefulness in applications. Composites may be a means of overcoming these constraints. Polymer nanocomposites have been widely studied in the past, but gel nanocomposites are a new class of materials and their behaviour is largely uncharted.

Carbon nanoparticles, widely used as polymer fillers, immensely improve both the physical and the chemical properties of composites. Nanocomposites composed of members of the graphene family have become the focus of intense interest. Graphene is a carbon monolayer with the thickness of a single atom. It has

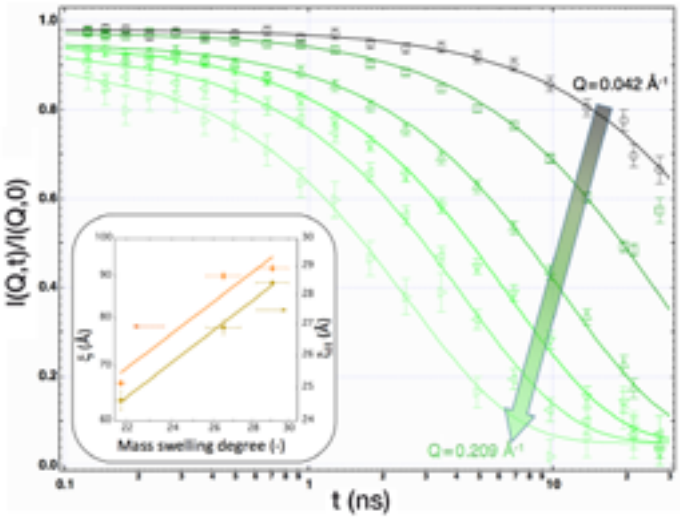

Figure 1

Experimental intermediate scattering functions from neutron spin-echo (NSE) at different values of momentum transfer Q, measured on IN11, with the corresponding single exponential fits for a GO-containing PNIPAM hydrogel nanocomposite. **Inset** shows the static (ξ, obtained from small-angle neutron scattering on different GO-containing samples) and hydrodynamic (ξ_H, obtained from NSE) correlation lengths at 25 °C, as a function of the mass swelling degree of the gels.

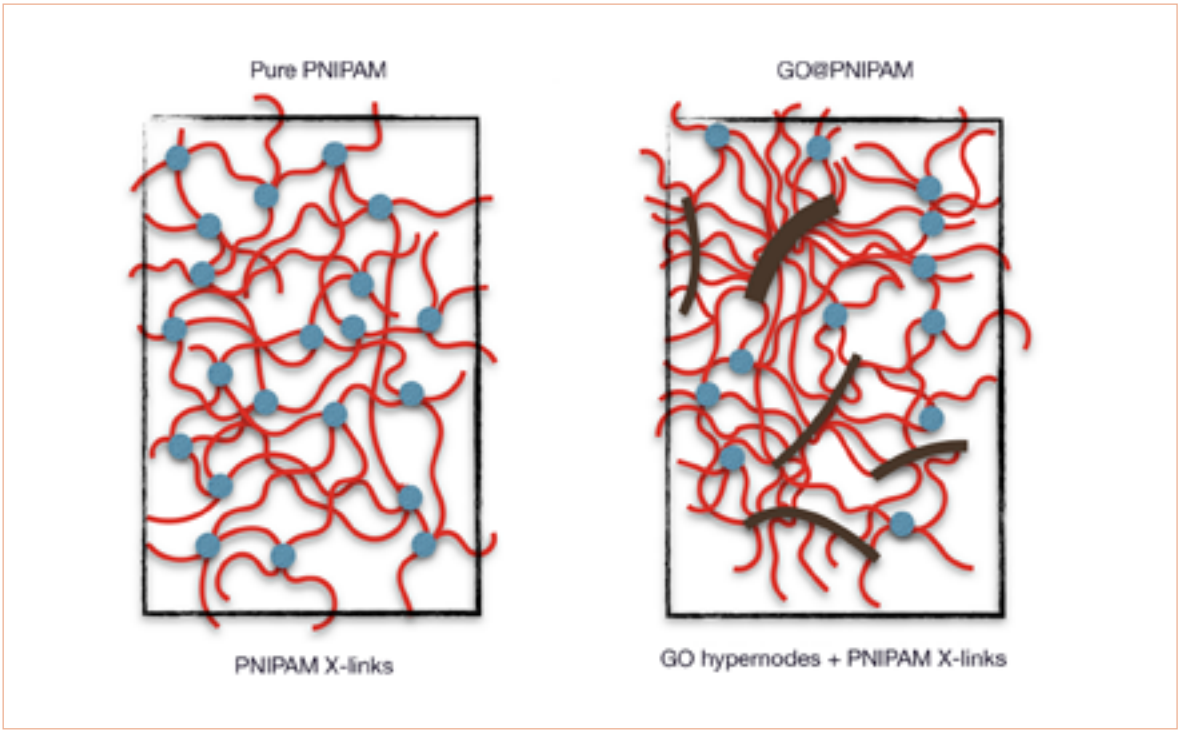

Figure 2

Representation of the structure of pure PNIPAM and GO-containing PNIPAM hydrogels as revealed by a combination of neutron scattering and macroscopic measurements.

outstanding electrical conductivity and mechanical strength. Its hydrophobic surface, however, jeopardises applications that involve aqueous systems. Graphene oxide (GO), by contrast, is a graphene layer decorated with oxygen-containing functional groups. Its hydrophilic character and dispersibility in water facilitate its preparation in composites. For biomedical applications GO fulfils the basic requirements of non-toxicity and biocompatibility. It has also recently been discovered that its thermal conductivity in GO-filled composites moderates their response to visible or infrared light. This opens the way to IR-controlled microvalves, artificial muscles and actuators [2].

In these applications the dynamics of the hydrogels is of paramount importance. Since they are strongly light absorbing, GO@PNIPAM hydrogel composite systems cannot be studied by dynamic light scattering. Neutron spin-echo (NSE) spectroscopy offers a means to solve this problem [3].

In the low temperature swollen state, the hydrodynamic properties of the network chains measured by NSE spectroscopy are consistent with those of the unfilled polymer gels. The resulting correlation functions (**figure 1**) display, in addition, a static component that corresponds to network chains in the gel that are immobilised on the GO surface. Small-angle neutron scattering observations show that as the gel de-swells with increasing GO content, the static polymer–polymer correlation length decreases according to scaling theory.

As the GO content increases the elastic modulus of the gels also increases, but their swelling capacity diminishes much faster than expected. This behaviour is due to a qualitative change in the architecture of the polymer gel: increasing GO concentration in the precursor solution gives rise to a primary interpenetrating network, within which the polymer matrix develops *via* chain nucleation at the surface of the GO platelets (**figure 2**).

Differential scanning microcalorimetry observations show that the volume phase transition temperature of the PNIPAM segments is unaffected by the GO, but an increasing fraction of the polymer does not participate in the phase transition.

In the high temperature collapsed state GO accelerates evacuation of water, which in pure PNIPAM otherwise remains trapped in the network in the form of microscopic droplets. This implies that collapsed PNIPAM chains are oriented by the GO surfaces. The GO filler has a major impact both on the gel structure and on the kinetics of its collapse. Unlike pure PNIPAM hydrogels, where macroscopic de-swelling is limited by their sponge-like structure, the rate of de-swelling in the composites is governed by ordering of the interpenetrating GO network.

Studying drying processes using acoustic levitation

Small momentum transfer diffractometer with variable vertical focusing D16 and small-angle scattering diffractometer D33

Small-angle X-ray scattering diffractometer SWING at SOLEIL

The drying phase is the last stage in various manufacturing processes and has a critical influence on the quality of the final product. It can be improved by better understanding the biophysical mechanisms involved during the process. In this work, acoustic levitation was combined for the first time with small-angle neutron scattering and also associated with small-angle X-ray scattering to probe large-scale structural fluctuations and interactions of lysozyme (model protein) in aqueous solution as a function of the concentration in drying conditions.

AUTHORS

V. Cristiglio and **I. Grillo** (ILL)
S. Brassamin, **L. Hennet** and **A. Novikov** (CNRS-CEMHTI, Orléans, France)
M. Fomina (University of Palermo, Italy)
J. Pérez, **M. Réfrégiers** and **F. Wien** (Synchrotron SOLEIL, Gif-sur-Yvette, France)
E. Shalaev (Allergan Inc., Irvine, USA)

REFERENCES

[1] J.C. Lee and S.N. Timasheff, J. Biol. Chem. 256 (1981) 7193
[2] G.B. Strambini and M. Gonnelli, Biophys. J. 92 (2007) 2131
[3] R.J.K. Weber *et al.*, Rev. Sci. Instrum. 80 (2009) 083904
[4] J. Leiterer *et al.*, Anal. Bioanal. Chem. 391 (2008) 1221

The freeze-drying method (lyophilisation) is commonly used in the pharmaceutical industry to preserve the integrity and the bioactivity of protein drugs, minimising chemical and physical degradation during their shelf life. Various pharmaceutical formulations are also developed to avoid protein degradation and irreversible aggregation during freeze-drying and storage [1]. However, it has been observed that storage in freeze-dried states does not guarantee long-term stability, and aggregation effects are often observed after freeze-thaw or the reconstitution of freeze-dried powder. In particular, the formation of ice can have a destabilising effect on protein molecules during freezing [2].

To gain a better knowledge of the process it is thus important to use tools that will allow the monitoring of protein behaviour in freeze-drying conditions. Our ultimate objective is therefore to develop an appropriate experimental set-up that will enable time-resolved structural analysis during the process. As a first step, we focused our interest on the study of the structural evolution of protein solutions up to supersaturation conditions. These are created by partial evaporation of the solvent to mimic the drying process. The sample environment used to reproduce the evaporation conditions is critical, and we chose to work with acoustic levitation. Using this contactless method, the liquid drop (~ 45 μl) was positioned in the surrounding medium (ambient air or

Figure 1
Acoustic levitation apparatus installed on the D33 **(a)** and D16 **(b)** instruments.

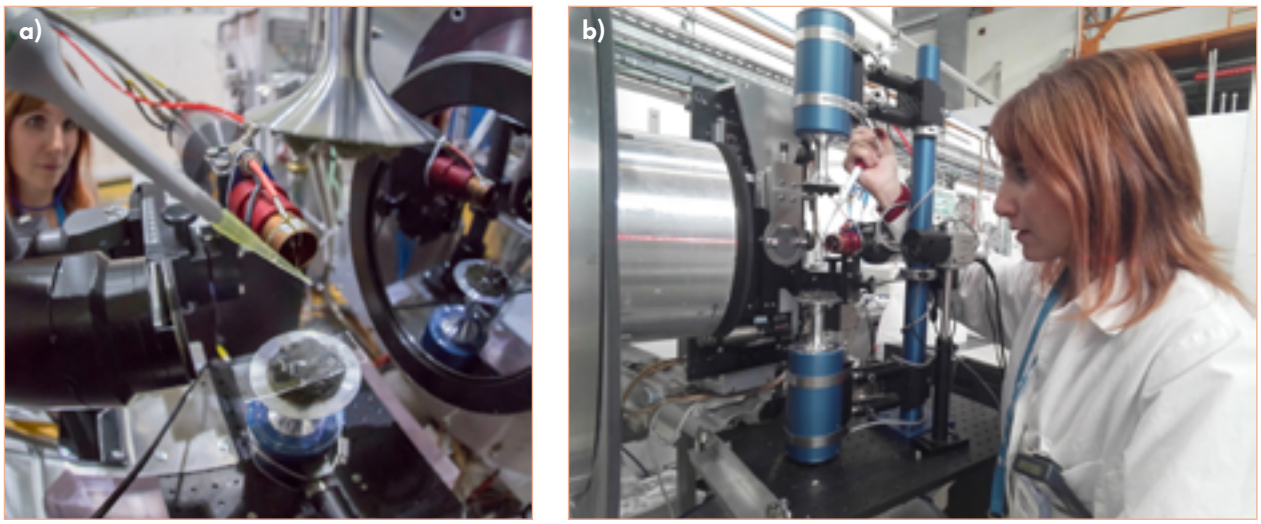

defined gas) at a node of the standing ultrasonic wave (22 kHz) created by two opposite transducers (see [3] for more technical details). Evaporation of the solvent during levitation gradually decreases the volume of the droplet and therefore increases the corresponding concentration of the solute. The evolution of the droplet volume (concentration) during the drying process was estimated from video images following a procedure described in [4].

The small-angle neutron and X-ray scattering (SANS and SAXS) experiments were carried out on the D33 and D16 instruments at the ILL and on the SWING beamline at the SOLEIL synchrotron. Photos of the levitation set-up installation in the neutron instruments are shown in **figure 1**. In this study, lysozyme solutions were prepared by directly dissolving lysozyme powder (from chicken egg white) into pure D_2O at various protein concentrations (C = 10, 30, 60 and 90 mg/ml for SAXS and 58 mg/ml for SANS). The evolution with time of the measured SANS scattering profiles is plotted in **figure 2a**. From these scattering curves we were able to monitor structural changes looking at the evolution of the interaction peak of the lysozyme particles with the solvent evaporation. In particular, we observed a peak shift towards higher q values. The same trend was observed in the SAXS measurements (**figure 2b**) on the sample at 60 mg/ml. In both cases, we observed an intensity decrease and a broadening of the interaction peak. For SANS, due to a decrease of the D_2O content the signal is mainly dominated by the incoherent contribution coming from the hydrogen present in the sample. Hence, the interaction peak of the lysozyme disappears faster compared with the SAXS measurements which are not affected by the incoherent contribution. The signal was also too weak to see the form factor peak visible with SAXS at all concentrations (**figure 2b**).

The evolution of the interaction peak position q_p derived from the SAXS measurements is presented as a function of $C^{1/3}$ for the four studied lysozyme solutions in **figure 3**. The evolution is quasi-linear up to approximately 150 mg/ml, showing that we retain an ideal solution up to this concentration. The decrease observed above 230 mg/ml is not clear at the moment.

This study demonstrated that acoustic levitation can be combined with SANS measurements to monitor the evolution of the protein structure with time during the drying process. In a second step, a cryostream device enabling work at lower temperature will be integrated and an adapted chamber to preserve the sample from external conditions implemented. Both enhancements will permit the introduction of a new procedure of working at low temperature and reproducing the freeze-drying process. This SAXS/SANS approach should give new insights into crystallisation and self-assembly phenomena of biological compounds, with promising potential applications in pharmaceutical, food and cosmetics industries.

Figure 2

SANS **(a)** and SAXS **(b)** signal measured during the evaporation of a 45 µl droplet of lysozyme in D_2O solution (initial concentration about 60 mg/ml). In the SAXS measurement, the form factor peak is clearly visible for all concentrations.

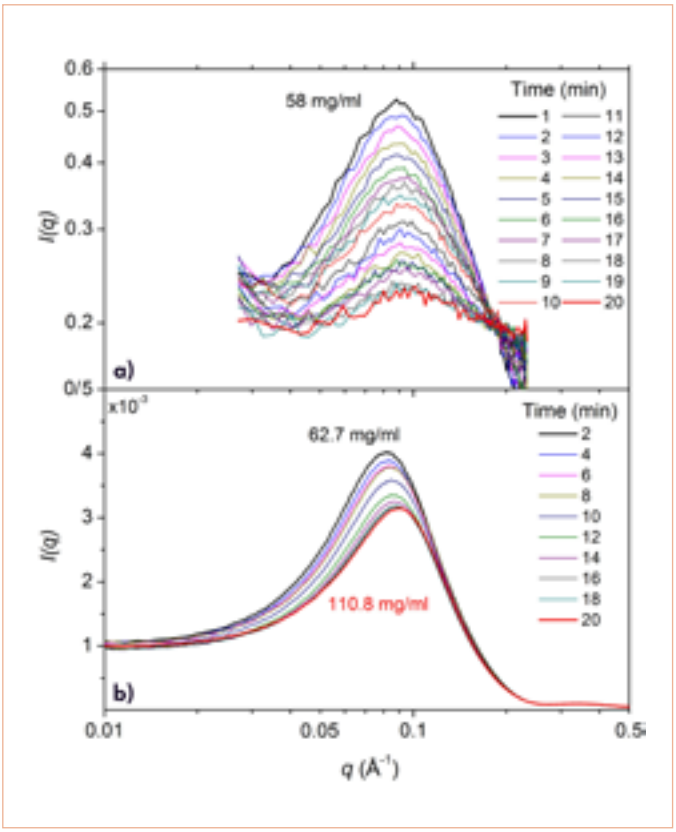

Figure 3

Evolution of the peak position q_p derived from SAXS measurements on solutions with various initial protein concentrations (10, 30, 60 and 90 mg/ml).

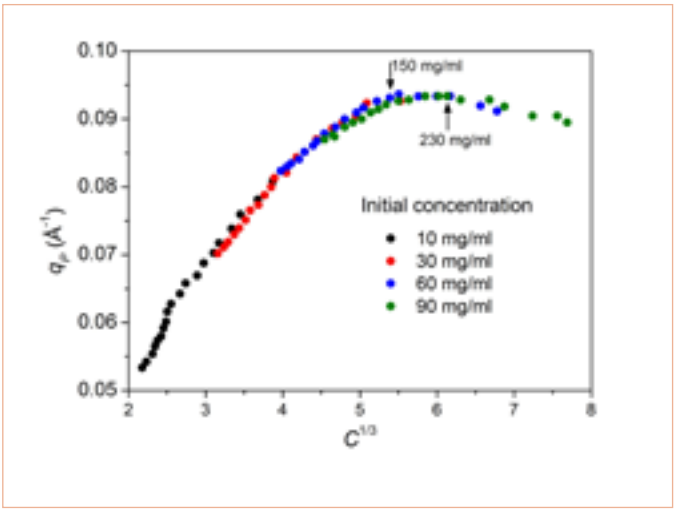

New insights into the Alzheimer's β-peptides interaction with membrane rafts, provided by neutron reflectivity

Reflectometer D17

In 2013 the UN published a report estimating that by 2050 over 20 % of the world's population will be 65 or older – the advance of medicine and the increase in global living standards means that the human race is living longer than ever before. An ageing population means that more of us are being diagnosed with age-related illnesses such as Alzheimer's. In 2015, there were 46.8 million people living with dementia, costing the world economy over $800 billion. With an estimated 131.5 million Alzheimer's sufferers by 2050, understanding Alzheimer's is more important than ever.

AUTHORS

V. Rondelli, **P. Brocca**, **S. Motta**, **L. Cantù** and **E. Del Favero** (Università degli Studi di Milano, Italy)
M. Messa, **L. Colombo** and **M. Salmona** (Istituto di Ricerche Farmacologiche 'Mario Negri', Milano, Italy)
G. Fragneto (ILL)

REFERENCES

[1] D.H. Small and R.A. Cappai, J. Neurochem. 99 (2006) 708
[2] A. Kakio *et al.*, Biochem. 41 (2002) 7385
[3] V. Rondelli *et al.*, BBA Biomembranes 1818 (2012) 2860

The mechanisms underlying Alzheimer's disease are not completely understood, but genetic, pathological and biochemical observations indicate that the progressive production and accumulation of β-amyloid peptides (Aβ), proteolytic fragments of the membrane-associated amyloid precursor protein (APP), play a pivotal role [1]. Neurons release these peptides in a soluble form that progressively generates different molecular assemblies, from oligomeric to multimeric structures, ending up as fibrillar aggregates. In particular, soluble oligomers are considered the main actor for the onset and progression of the cognitive dysfunction. One of the peculiar properties of soluble Aβ oligomers is that they are a "membrane-active" species that can promote membrane puncturing and increase its permeability. Within membranes, the interaction sites for either APP or Aβ are localised at those domains, such as rafts and caveolae, enriched in cholesterol and GM1-ganglioside. It is suggested that GM1, within rafts, participates in Aβ interactions with the membrane and acts as a templating spot for Aβ aggregation [2]. Several processes have been hypothesised, in connection with different theories from biochemistry, microscopy and simulation experiments. Population imbalance, favouring either labile or structured oligomers, is a fascinating route, yet the designation of the species as potentially more effective in promoting the disease is not so clear. This is a topic of importance where, as well

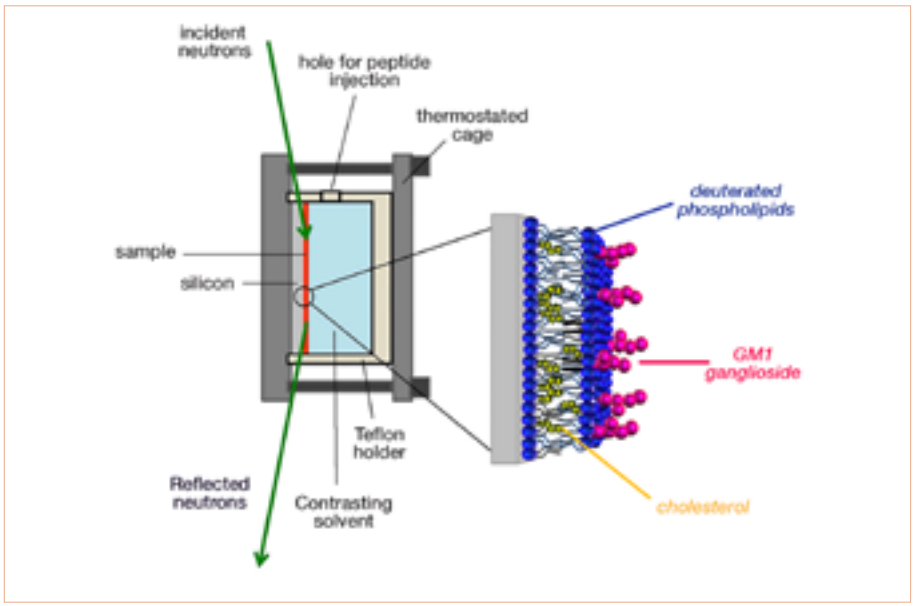

Figure 1
Schema of the experimental set-up.

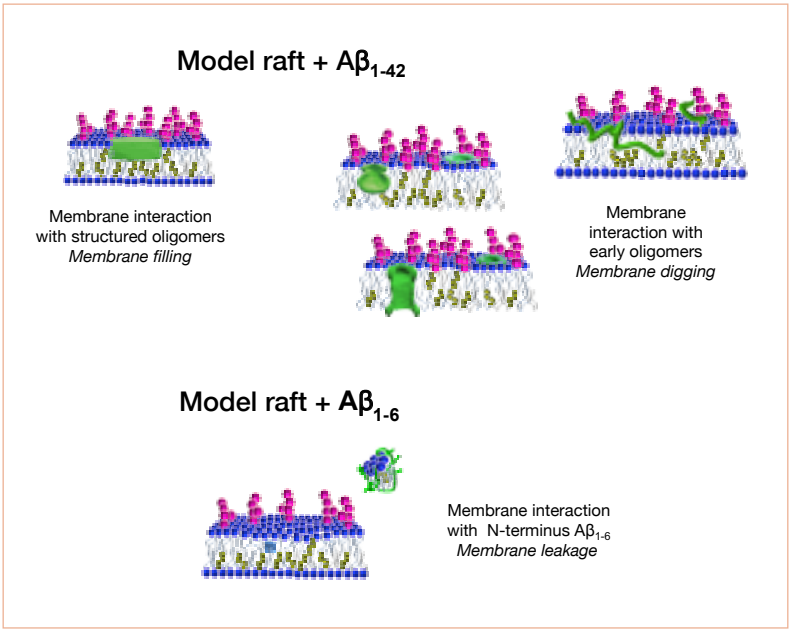

Figure 2

Pictorial sketch of a model raft interacting with Aβ peptides.

as attempting to understand the basic phenomena, a therapeutic strategy is being pursued in order to prevent progression or promote regression of the disease.

To this end we performed experiments on the D17 reflectometer aimed at revealing the existence and extent of the interaction between Aβ peptides at different aggregation states and synthetic membranes imitating the outside layer of neurons found in the brain. We have in fact recently developed a model for lipid rafts that is suitable for structural investigation by neutron reflectometry [3]. We prepared and characterised lone, macroscopic membranes (nanometre single-bilayer thickness, centimetre lateral extension) with biosimilar composition in phospholipid, GM1 and cholesterol and, notably, with asymmetric distribution of components, a distinctive property of cell membrane rafts (**figure 1**). We focused on two conditions: 1) when the $A\beta_{1-42}$ reaches the raft-mime surface already in the membrane-active, structured-oligomer state; and 2) when early, unstructured $A\beta_{1-42}$ forms are administered and peptide oligomerisation possibly takes place at the membrane.

The neutron reflectometry technique reveals the transverse structural details of a bilayer, discriminating regions at different depths within the membrane, avoiding radiation damage. Moreover, the contrast variation strategy allows the visibility of the H-containing peptides in interaction with the deuterated phospholipids membrane to be enhanced. Thanks to the H-D neutron contrast enhancement, the use of fluorescent dyes at the N-terminus of the peptides, as commonly used in microscopy techniques, can be avoided. The binding of fluorescent groups to the N-terminus of Aβ peptides is generally considered non-invasive. Nonetheless, a modification of the specific properties of this end environment cannot be discounted. This portion has been recently proved to play a critical role in the $A\beta_{1-42}$ supramolecular assembly. In fact, a point-mutation in this region (A2V), correlated with early-onset AD only in homozygous carriers, was found to induce a more prompt formation of structured oligomers and amyloid fibrils.

In our study we also tested the membrane-interaction ability of the N-terminal sequence of the $A\beta_{1-42}$ peptide, namely, the $A\beta_{1-6}$ fragment. We found that the structured oligomer of $A\beta_{1-42}$, its most acknowledged membrane-active state, is embedded as such into the external leaflet of the membrane. Conversely, the $A\beta_{1-42}$ unstructured early-oligomers deeply penetrate the membrane, likely mimicking the interaction at neuronal cell surfaces, when the $A\beta_{1-42}$ is cleaved from APP protein and the membrane constitutes a template for its further structural evolution. The smaller $A\beta_{1-6}$ fragment was seen to remove lipids from the bilayer. This finding suggests that the terminal part of the whole peptide ($A\beta_{1-42}$) plays a central role in membrane leakage, favouring peptide recruitment (**figure 2**).

We conclude that both claimed membrane-active species of Aβ, namely early-labile and structured oligomers, interact with the membrane, their association being neither peripheral nor purely electrostatic. Nonetheless, differences exist in the extent and depth of interaction, interestingly pointing to unexpected, relative impacts on the membrane. An eventual deeper impact of monomers as opposed to oligomers is surprising, based on current concepts. A peculiar profile suggests that Aβ organisation, starting from enclosed monomers, is templated by the membrane into a forming pore. Furthermore, we hypothesise a role for the 1-6 N-terminal sequence of Aβ, namely in membrane destabilisation and then in facilitating Aβ recruitment.

These results push us towards developing peptidomimetic compounds as a way of effectively modulating both amyloid aggregation promptness and stability, and amyloid interaction with cell membranes, and hence towards the identification of new drug targets.

Neutrons capture a two-proton transfer event in an enzyme catalytic site

Quasi-Laue diffractometer LADI IMAGINE diffractometer at Oak Ridge National Laboratory

AUTHORS

O. Gerlits, **T. Wymore**, **J.M. Parks**, **J.C. Smith**, **K.L. Weiss**, **P. Langan** and **A. Kovalevsky** (Oak Ridge National Laboratory, Tennessee, USA)
A. Das (BARC, Mumbai, India)
I.T. Weber and **C.-H. Shen** (Georgia State University, Atlanta, USA)
M.P. Blakeley (ILL)
D.A. Keen (ISIS, UK)
J.M. Louis (National Institutes of Health, Maryland, USA)

REFERENCES

[1] O. Gerlits, T. Wymore, A. Das, C.-H. Shen, J.M. Parks, J.C. Smith, K. Weiss, D.A. Keen, M.P. Blakeley, J.M. Louis, P. Langan, I. Weber and A. Kovalevsky, Angew. Chem. Int. Ed. 55 (2016) 4924

Proton transfer is a fundamental chemical reaction which is at the heart of most biochemical processes, such as enzymatic catalysis. The mechanism of proton transfer by relay, or proton "hopping", is a widely accepted concept first put forward by Grotthuss over two hundred years ago. To observe proton transfer experimentally, and to study structures of the reactants and products of this chemical process, is very challenging. Therefore, previously no crystallographic experiments have been performed in which the protons could be unequivocally located before and after the transfer. However, recently published results [1] demonstrated that macromolecular neutron crystallography is capable of detecting a two-proton transfer event in the confined environment of an enzyme active site, providing accurate structural information on the reactants and products.

This research used HIV-1 protease, a key enzyme drug target for HIV/AIDS therapy, to locate and reveal movement of hydrogen atoms between catalytic aspartic acid residues and a hydroxyl group of the clinical drug darunavir. For this study, neutron crystallographic experiments were carried out on the LADI diffractometer at the ILL and the IMAGINE diffractometer at the High Flux Isotope reactor at Oak Ridge National Laboratory. Neutron crystallography provides a direct means of accurately determining the locations of hydrogen atoms in a macromolecular structure. To directly visualise hydrogen atoms before and after the proton transfer, neutron structures of HIV-1 protease were obtained at two different pHs: 6.0 and 4.3.

The conventional catalytic mechanism for aspartic proteases such as HIV-1 protease involves a symmetrically bound H_2O in the catalytic site, which consists of two aspartic acid (Asp) residues. One of these catalytic aspartates is believed to be protonated, with the proton presumably located halfway between the carboxylic oxygen atoms of the Asp residues, as depicted in **figure 1**. How the strong hydrogen bond between the two Asp residues believed to exist in the substrate-free active site is broken, and how this hydrogen atom is transferred to the outer oxygen for the catalysis to ensue, was not known. Now, the two neutron structures of HIV-1 protease go some way towards providing the answers.

Figure 1

Proposed positions of hydrogen atoms in the catalytic site of HIV-1 protease and their movement upon substrate binding.

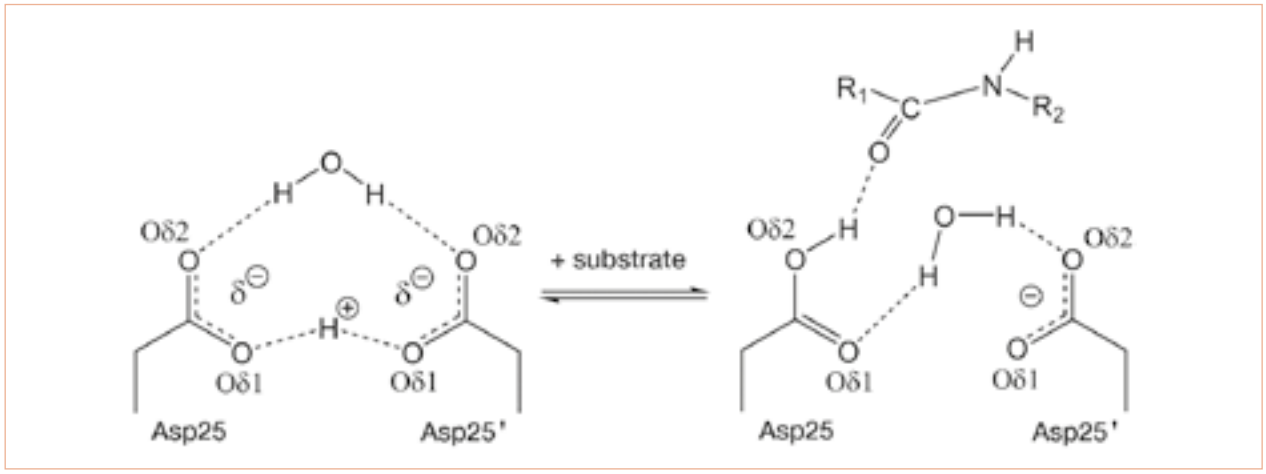

Figure 2

Two-proton transfer event, occurring due to changes in the protonation states of HIV-1 protease surface residue upon lowering the pH in the crystal, is detected using neutron crystallography.

The neutron structure of HIV-1 protease at pH 6.0 showed the presence of two hydrogen atoms in the catalytic site: one shared as a hydrogen cation located exactly in the middle between the carboxylic group of Asp25′ and the hydroxyl of darunavir; and the other, covalently bound to the drug's hydroxyl group facing the other aspartate, Asp25 (**figure 2**). When the crystal was acidified to lower the pH to 4.3, four residues, two aspartates and two glutamates on the protease surface accepted protons from the solvent and thus changed their protonation states from negatively charged to neutral. These changes in electrostatics at the protease surface triggered a two-proton transfer in the catalytic site of the enzyme, in which the hydroxyl hydrogen of darunavir is transferred to Asp25 and, concurrently, the hydrogen on Asp25′ shifts to the hydroxyl of darunavir (**figure 2**). Molecular simulations provided evidence that this proton transfer at the catalytic site is triggered by an external stimulus, i.e. the change in the surface charge of the protease, and that the configuration of hydrogen atoms in the catalytic site at pH 4.3 is only stable when four surface residues are protonated. These results demonstrate that neutrons represent a superb probe for obtaining structural details relating to hydrogen, paving the way for neutron crystallography studies of other important proton transfer reactions in biological systems.

Probing the secrets of extremophile bacteria

Disordered materials diffractometer D4, small momentum transfer diffractometer D16, small-angle scattering diffractometer D22, backscattering spectrometer IN16B and deuteration laboratory D-Lab

Micro-organisms represent the most numerous life forms on earth, and understanding how they behave is integral to our own survival and well-being. Microbial life has an amazing flexibility for adapting to extreme environments — niches that are extraordinarily hot or cold, acidic or basic, salty as in the Dead Sea or at high pressure in great ocean depths. These organisms are known as extremophiles. Understanding how they adapt to extreme environments remains a challenge of high biotechnological potential in important areas such as health care, bioremediation and waste management.

AUTHORS

G. Zaccai (ILL, CNRS, IBS, CEA and Université Grenoble Alpes, France)
G. Cuello and **V.M Galván Josa** (ILL)

REFERENCE

G. Zaccai, I. Bagyan, J. Combet, G.J. Cuello, B. Demé, Y. Fichou, F.X. Gallat, V.M. Galvan Josa, S. Von Gronau, M. Haertlein, A. Martel, M. Moulin, M. Neumann, M. Weik and D. Oesterhelt, Sci Rep, 6 (2016) 31434

Among the extremophiles, bacteria isolated from salt marshes or marine environments include a variety of interesting species of high biotechnological potential, such as the rust-producing *Halomonas titanicae*, recently discovered in the hull of the sunken RMS Titanic (**figure 1**). *Halomonas* are halotolerant, in that their cells can cope without bursting with salt concentrations from 0.5 to 25 % NaCl (on average, sea water has a salt concentration of 3.5 %). They do this by producing ectoine to the appropriate concentration to counterbalance the outside osmotic pressure. Ectoine is called a *compatible solute*; its occurrence within the internal material of the cell does not interfere with cellular biochemistry or metabolism. Ectoine, which displays an indirect stabilising effect on proteins and membranes and a related inhibitory effect on inflammation in mammalian cells, has itself been discovered to have broad cosmetic and clinical applications through its hydration, stabilisation and inflammation reducing properties, e.g. for the treatment of allergies, atopic dermatitis and cough and cold symptoms. With the aim of understanding the behaviour of ectoine a range of experiments conducted at the ILL, in collaboration with the Max Planck Institute of Biochemistry, Bitop biotechnology company and the Institut de Biologie Structurale, explored its interactions with water and protein.

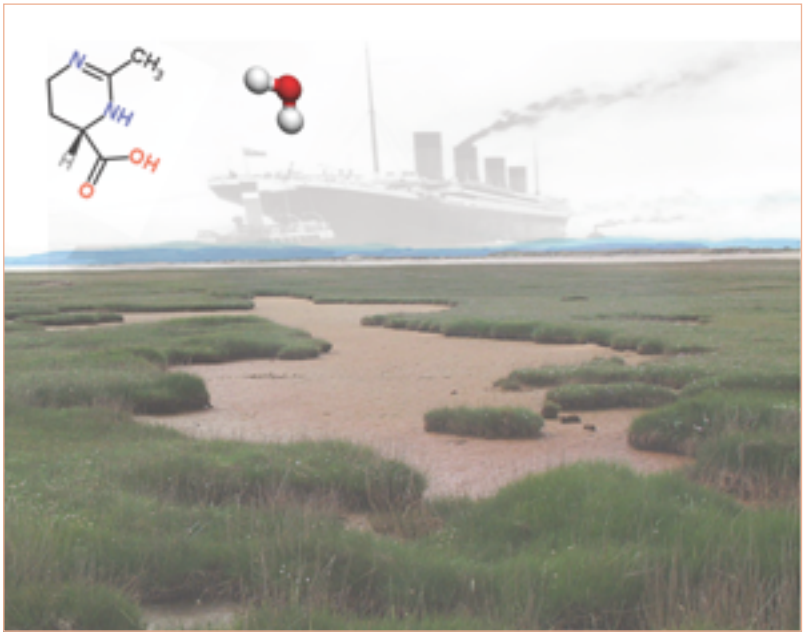

Figure 1

Ectoine and water molecules above a salt marsh, with the ghost of RMS Titanic.

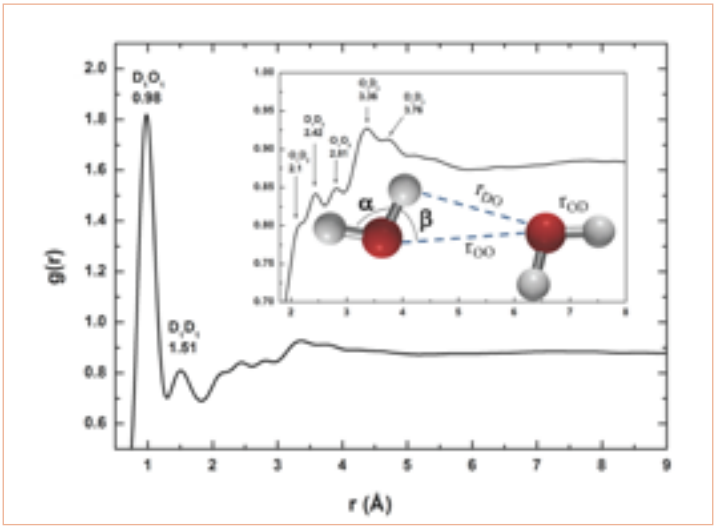

Figure 2

Liquids diffraction of ectoine solutions. The radial distribution function g(r), obtained by Fourier transformation of the experimental structure factor S(Q) for sample 1.5 M D-ectoine/D_2O. The inter-molecular region, beyond r = 2 Å, is expanded in the **inset**, which also shows the H-bonding scheme between two adjacent D_2O molecules.

The experiments, using D4, D16, D22, IN16 and samples prepared at the D-Lab, have illustrated how ectoine acts by leaving the shell of water on protein and membrane surfaces, which is essential to their biological activity, intact. H_2O molecules in liquid water interact with each other through a highly dynamic, fluid network of hydrogen bonds (H-bonds) between the O and H atoms of adjacent molecules. The presence of other substances in the water can hamper this organisation. In order to explore the effect of molar concentrations of ectoine on water structure, aqueous solutions of 1.5 M ectoine were examined on the D4 liquids diffractometer: natural abundance ectoine in heavy water (D_2O) (H-ectoine/D_2O), and D-labelled ectoine in D_2O (D-ectoine/D_2O). Structure modifications of H-bonding in water were studied through the radial distribution functions, g(r), obtained by Fourier transformation of the experimental structure factors S(Q). The mean geometrical distances and angles obtained by neutron diffraction for the ectoine solutions established a significantly more bent average water-water intermolecular H-bond configuration than that found in bulk water (**figure 2**), i.e. a larger proportion of weaker H-bonds in the presence of ectoine favour greater configuration exchange in the water H-bond structure, thus contributing entropy to the thermodynamic preference for ectoine to be excluded from the surface of proteins and membranes. Combined, the neutron, infrared spectroscopy (IR) and molecular dynamics (MD) results favour a model in which the modification of water structure by ectoine appears to be similar to that of water confined in reverse micelles, in which were observed strong water-polar group H-bonds as well as a larger proportion of inter-water H-bonds with energetically unfavourable angles compared with that found in bulk water. The neutron experiments went on to describe the effects of ectoine on water H-bond dynamics, revealing how ectoine's protective characteristics do not interfere with the cell metabolism. In fact rather than hindering, ectoine enhances the remarkable dynamic properties of H-bonds in water-properties that are essential for water's unique solvent capabilities and vital for the proper organisation, stabilisation and function of proteins, lipids, membranes, RNA and DNA.

The search for life on Mars and elsewhere in the universe is guided by a search for liquid water. This is because liquid water is essential for all life. Its remarkable properties are based on dynamic H-bond networks that play vital roles in macromolecular folding and interactions, which in turn determine their biological functions. Because of their rich scattering interaction with protons and deuterons, neutrons provide the ideal tool for studying water.

The results of this study illustrate how the osmolyte behind the halotolerance response in micro-organisms induces compensating effects on water H-bonding that respect these essential biological properties. Each of the instruments used in the study provided complementary structural information on different molecular length and time scales, ranging from crucial hydrogen-bonding at the atomic level to the larger protein and membrane structures. Although many spectroscopic and thermodynamic investigations have been done before on ectoine, this is the first study that has allowed, through the use of neutrons, a direct experimental characterisation of ectoine-water-protein and ectoine-water-membrane structures to explain the mode of action of this very interesting and useful molecule.

Structural analysis of the clock protein KaiB–KaiC complex by iCM-SANS

Small-angle scattering diffractometer D22

AUTHORS

M. Sugiyama and **R. Inoue** (Research Reactor Institute, Kyoto University, Japan)
H. Yagi (Graduate School of Pharmaceutical Sciences, Nagoya City University, Japan)
A. Martel and **L. Porcar** (ILL)

REFERENCES

M. Sugiyama *et al.*, Sci Rep. 6 (2016) 35567

Many physiological phenomena display an approximate 24-hour cycle. This means that every life has a circadian clock in its body. Cyanobacteria have one of the simplest biological clocks, consisting of only three proteins: KaiA, KaiB and KaiC. This system displays ATP-dependent complex formation and dissociation within a 24-hour period. It has been clarified that KaiC controls the clock phase by auto-phosphorylation and -dephosphorylation. It is therefore crucial to clarify the complex structure in relation to the phosphorylation state of KaiC.

Figure 1 provides an overview of the latest standard model of the clock system of Cyanobacteria. KaiC forms a hexameric ring consisting of two rings: C1 and C2. The fully dephosphorylated KaiC (I) starts phosphorylation through the interaction of KaiA to the C2 ring (II) and induces conformational change of C1/C2 rings (III). Then, KaiB sequentially connects with the C1 ring and promotes KaiC dephosphorylation. Finally, KaiB (and KaiA if it is connecting to KaiC) disconnect(s) from the dephosphorylated KaiC (IV) and the system returns to the initial state (I). The formation of the KaiB–KaiC complex precludes the direct KaiA–KaiC interaction by promoting direct binding of KaiA to KaiB in the complex, thereby initiating a phase proceeding in the circadian cycle. Furthermore, KaiB competes with SasA for binding to the KaiC hexamer. SasA is a histidine kinase that operates as a major clock-striking protein during the regulation of circadian transcription. Hence, the KaiB–KaiC interaction is a key event during oscillation of the system. In this work, we focused on clarification of the structure of the KaiB–KaiC complex.

Figure 1

Overview of the oscillation scheme of the circadian clock of Cyanobacteria. Three proteins, KaiA, KaiB, and KaiC, periodically repeat association and dissociation depending upon the phosphorylation state of KaiC.

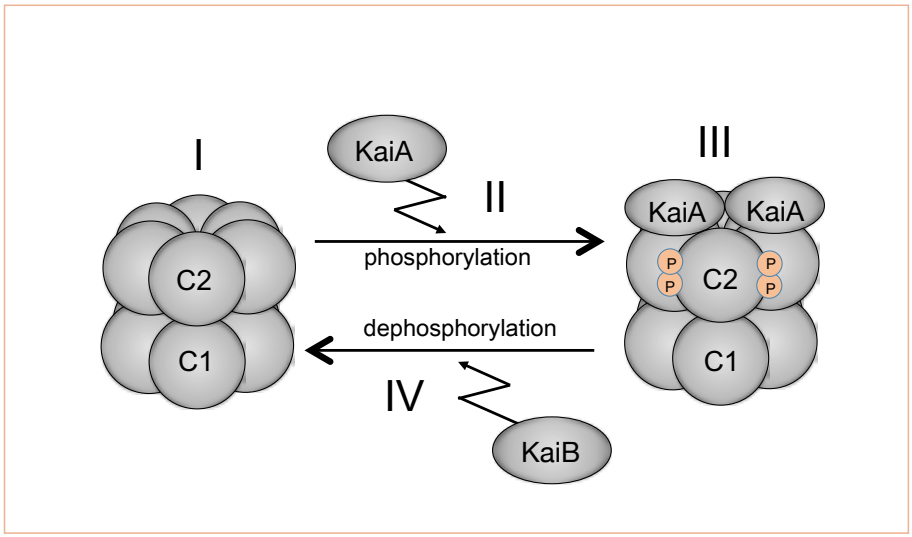

Figure 2

SANS profiles in iCM-SANS. The closed circles show the SANS profile of 72d-KaiC$_{DT}$–h-KaiB complex with the 6:6 stoichiometry in 97 % D_2O solvent. In this solvent 72d-KaiC$_{DT}$ is expected to be invisible due to the contrast matching with the solvent. The red line shows the calculated SANS profile from the complex model (the inset figure).

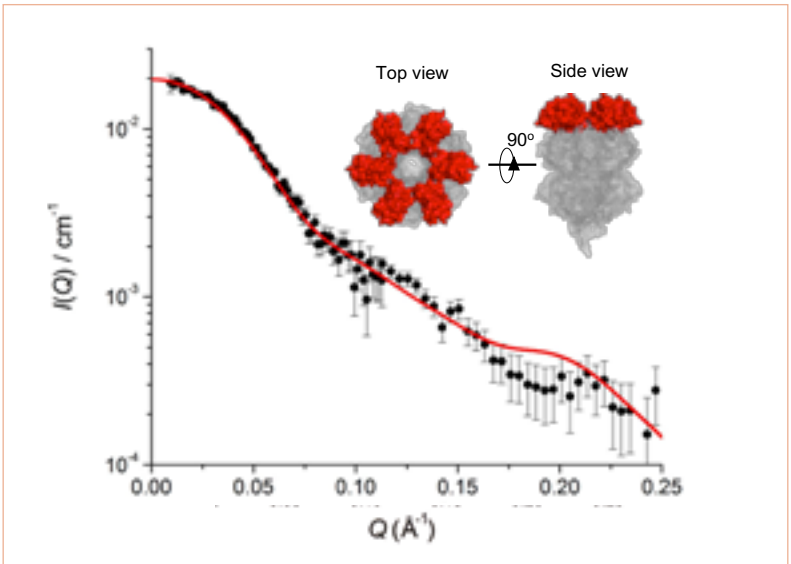

Two residues, S431 and T432, in the C2 ring are periodically phosphorylated and dephosphorylated in a 24-hour period, as follows:
KaiC-S/T → KaiC-S/pT → KaiC-pS/pT → KaiC-pS/T → KaiC-S/T
– where 'p' represents the phosphorylated residue. Since KaiC$_{DT}$, which is a mono-phosphorylated KaiC mimic at Ser431, exhibited the highest binding affinity to KaiB, we prepared a KaiB–KaiC$_{DT}$ complex. First, we examined a stoichiometry of KaiB–KaiC$_{DT}$ complex with native mass-spectroscopy (nMS). The nMS data indicated that the KaiC$_{DT}$ hexamer formed a uniform complex with a molecular mass of 428,600 ± 410 Da, corresponding to a 6:6 stoichiometry of KaiB–KaiC$_{DT}$.

Next, the spatial arrangement of the KaiB subunits in the complex should be revealed in an aqueous solution. Even though small-angle X-ray scattering is a powerful method for analysing an overall structure of protein in an aqueous solution, it is difficult to distinguish only structural information about KaiB from the scattering profile of the complex due to the more intensive scattering from KaiC than from KaiB: KaiC's molecular mass is almost six times that of KaiB. In addition, the structure of KaiC hexamer in the complex should be known in order to extract the spatial arrangement of the KaiB subunits from the whole complex structure. However, the structure of KaiC hexamer in the complex, which is supposed to be modulated from that of the solo hexamer, has not been clarified.

Our strategy for overcoming this difficulty was to weaken or erase scattering from the KaiC subunits in the complex by small-angle neutron scattering using inversed contrast matching (iCM-SANS). Considering scattering contrast, the partial deuteration of protein (around 75 % deuterated) becomes scatteringly invisible in D_2O solvent, whose incoherent scattering is lower than that of H_2O solvent. Therefore, we prepared 72.2 % deuterated KaiC$_{DT}$ (72d-KaiC$_{DT}$) and experimentally confirmed that 72d-KaiC$_{DT}$ was invisible in 97 % D_2O solvent. We also prepared the 6:6 KaiB–KaiC complex, consisting of the 72d-KaiC$_{DT}$ subunits and the non-deuterated KaiB (h-KaiB) subunits (72d-KaiC$_{DT}$–h-KaiB complex).

The iCM-SANS experiments were performed on the small-angle scattering instrument D22 at the ILL. The scattering profile of the 72d-KaiC$_{DT}$–h-KaiB complex in 97 % D_2O solvent approximately followed the Q^2 power law, indicating that the six KaiB subunits were arranged in a disk-like shape. Then, we constructed several structural models of the complex in which the arrangements of KaiB had disk-like shapes and also six-fold symmetry (C1-ring). By comparing the calculated scattering spectra of the models with the experimental one, the best compromised arrangement of the KaiB subunits in the complex was obtained, as shown in **figure 2**. In the model complex, the KaiB subunits form a hexameric ring on the top of the C1-ring. The distance between the centre of mass of each KaiB component and the six-fold axis of KaiC$_{DT}$ becomes minimal with avoidance of steric hindrance between the KaiB subunits. In this model, the hexameric KaiB subunits cover the top surface of the C1 ring, including the interaction site of SasA. Therefore, it is conceivable that the co-operative binding of KaiB as a competitive inhibitor against SasA promotes the synergistic release of this clock-output protein from the KaiC hexamer.

Macromolecular structure phasing by neutron diffraction

Single crystal diffractometer D19

We have shown for the first time that neutron anomalous dispersion can be used in a routine way to determine experimental phases of a protein crystal structure. The approach was demonstrated using the D19 monochromatic neutron thermal diffractometer at the ILL in combination with a crystal of perdeuterated protein in order to minimise the level of hydrogen incoherent scattering and to enhance the visibility of the anomalous signal. The results are likely to be of interest for use at existing and emerging spallation neutron sources where time-of-flight instruments provide inherent energy discrimination.

AUTHORS

E. Mossou and **T. Forsyth** (ILL)
M. Cuypers (Faculty of Natural Sciences, Keele University, UK)
E. Mitchell (ESRF)

REFERENCES

[1] M.P. Blakeley, Crystallogr. Rev. 15 (2009) 157
[2] B.P. Schoenborn, Nature 224 (1969) 143
[3] M.G. Cuypers *et al.*, Sc. Rep. 6 (2016) 31487
[4] M. Haertlein *et al.*, Methods Enzymol. 5 (2016) 113

In recent years, neutron protein crystallography has emerged as a powerful technique that yields unique information of central importance for an understanding of macromolecular function. Neutron protein crystallography allows the visualisation of protonation states and water networks surrounding biological macromolecules, which has been a longstanding challenge in structural biology. The insights provided are crucial for understanding enzymatic catalysis, redox reactions and protein engineering relevant to areas such as bio-fuel cells, biosensors and biochips, and drug design. At the ILL, major developments continue for neutron protein crystallography using both Laue and monochromatic instruments [1]. However, despite the increasing interest in neutron protein crystallography, the application of neutron anomalous diffraction differences has not been considered a serious alternative to X-ray phasing. Their use was first suggested in the 1960s for crystals containing atoms such as ^{113}Cd, ^{149}Sm, ^{151}Eu and ^{157}Gd, with Schoenborn and co-workers [2] demonstrating the phasing approach using cadmium derivatives of myoglobin. However, at that time neutron data collection required very large crystals and very long data collection times, making anomalous experiments very expensive in neutron beamtime and hence far from tenable as a realistic phasing method for proteins. Since then neutron sources have evolved, becoming more brilliant and using increasingly efficient detector systems. With this, and the availability of perdeuterated proteins, the possibility now exists for using neutron anomalous dispersion to phase protein crystal structures in a standard way.

Figure 1

Plot of the anomalous signal to noise ratio (<d''/sig>) obtained from SHELXC (red line) and correlation coefficient as a function of resolution (blue line, from CCP4).

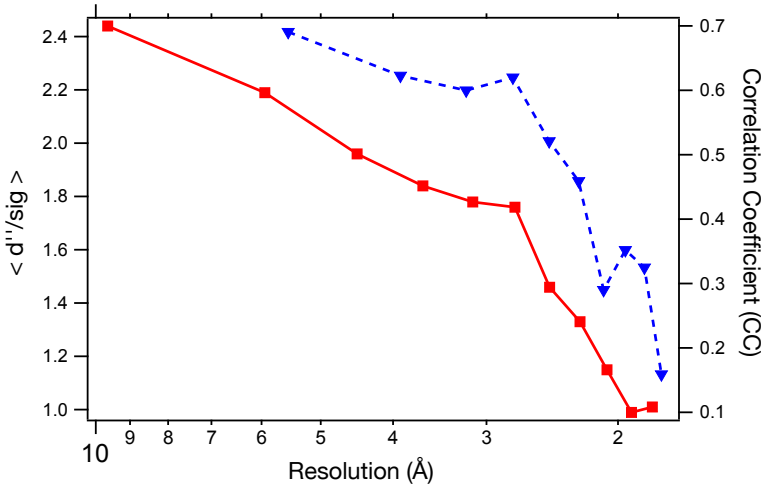

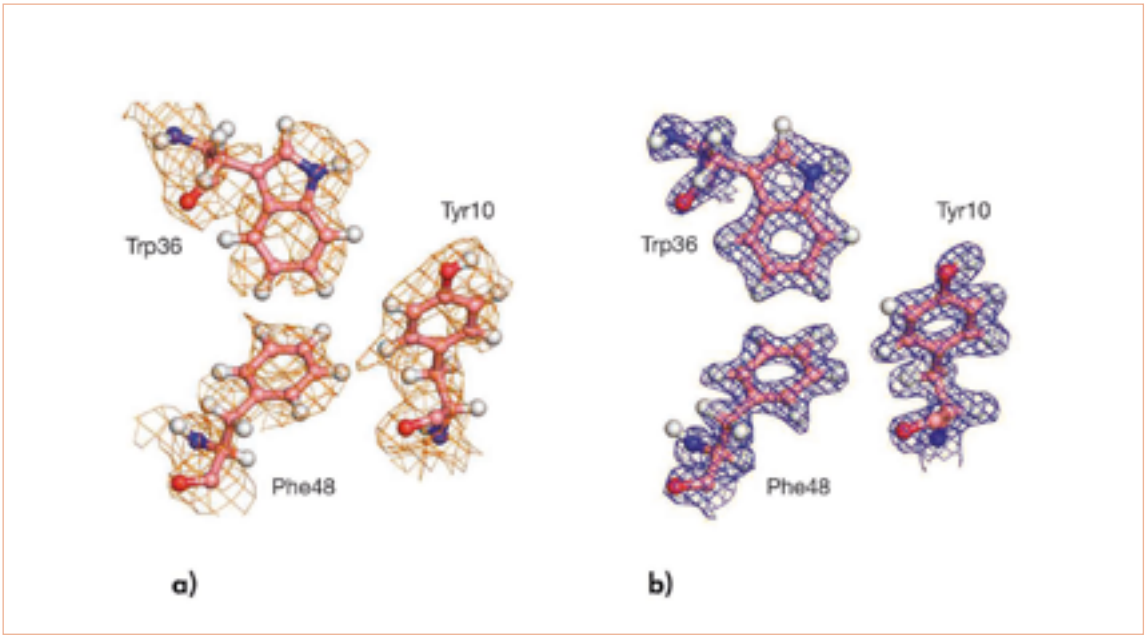

Figure 2

Neutron scattering density maps near the hydrophobic core of *Pf* rubredoxin (Trp36, Tyr10, Phe48) showing: **a)** the experimental phased map from SHELXE (2.30 Å resolution, contoured at 0.8 sigma in orange); and **b)** the 2Fo-Fc map from the refined, final model (1.75 Å resolution, contoured at 1.5 sigma in blue).

Here we demonstrated the feasibility of this approach using perdeuterated rubredoxin [3]. Rubredoxins are small, monomeric redox proteins found in prokaryotes and some eukaryotes. For the purpose of this study, ^{113}Cd replaced the Fe^{3+} at the iron-sulphur site. Large perdeuterated crystals were obtained and high quality data were collected on the high intensity monochromatic neutron instrument D19 using a wavelength of 1.17 Å. This wavelength was selected on the basis of a compromise between the proximity to the cadmium absorption resonance and the difficulty of resolving Bragg reflections at short wavelength. A high anomalous signal to noise ratio was present across most of the resolution range, as shown in **figure 1**. The data were analysed using standard crystallographic software packages. The high quality, experimentally phased, neutron density map obtained shows clear features from the protein backbone structure (**figure 2a**). Using the phased diffraction data, an initial model of 38 residues out of a total of 54 was built. Cycles of manual construction and refinement gave a final model consisting of all 54 residues and 49 D_2O molecules with R/Rfree of 23.3/28.6 %. Typical residues of the refined map are displayed in **figure 2b**.

The development of new neutron sources (e.g. tuneable spallation neutron sources), high-performance detectors and ready access to perdeuterated proteins [4] is paving the way for practical perspectives on neutron phasing methods. The relative simplicity of the method, as demonstrated here with standard software packages and relatively fast neutron data collection, can easily be applied to other protein systems. This method may provide a useful complement to X-ray anomalous phasing approaches – particularly where structure determination at room or physiological temperature is advantageous or relevant to the *in vivo* context of the protein system. In addition, neutron beam exposure does not normally result in radiation damage effects – this is particularly important for redox proteins, given that X-ray experiments may easily alter the redox state of the protein being studied. This approach, and the data processing requirements, could easily be fully integrated into standard data analysis packages and made more widely available to the scientific community.

The neutron lifetime puzzle

Ultra-cold neutron facility PF2

The best experiments in the world cannot agree on how long free neutrons live before decaying into other particles. Two main types of experiment are underway: bottle-like traps count the number of neutrons that survive after various intervals of storage time, while beam experiments look for one of the particles into which neutrons decay. Resolving this question is vital to answering a number of fundamental questions about the universe.

AUTHORS

G.L. Greene (University of Tennessee and Spallation Neutron Source at Oak Ridge National Laboratory, USA)
P. Geltenbort (ILL)

REFERENCES

[1] A. Serebrov *et al.*, Phys. Lett. B 605 (2005) 72
[2] A.T. Yue *et al.*, Phys. Rev. Lett. 111 (2013) 222501
[3] Z. Berezhiani and L. Bento, Phys. Rev. Lett. 96 (2006) 081801
[4] G.L. Greene and P. Geltenbort, Sci. Am. 314 (2016) 36

Within a nucleus, a neutron may be completely stable; but removed from the nucleus it will radioactively decay in about fifteen minutes. While this instability is unimportant for neutron scattering applications where the neutron time-of-flight is measured in milliseconds, the fact that free neutrons decay is of profound importance. The average decay time for a neutron (its "lifetime") sets the scale for the strength of one of the four fundamental forces of nature – the weak force. It also determines the rate of energy production in the sun and, in part, determines the relative abundances of light chemical elements (up to lithium) created in the big bang nucleosynthesis. Not surprisingly, nuclear and particle physicists have for decades been expending considerable efforts on its accurate determination.

About ten years ago, two independent experimental teams – one working at the ILL [1], the other at the National Institute of Standards and Technology (NIST) in the USA [2] – published measurements of the neutron lifetime. The two experiments used completely different techniques and, to the surprise and consternation of the experiment teams as well as the broader scientific community, the two measurements disagreed. This discrepancy remains today and has become known as the neutron lifetime problem.

HOW TO DETERMINE A LIFETIME

As a fundamental quantum mechanical process, neutron decay is not deterministic. There is no way to predict exactly when a particular neutron will decay. When one speaks of the neutron lifetime, it is only in the context of an average. As such, one can only measure the lifetime of an unstable particle by studying the decay of many such particles.

An obvious way to measure a lifetime is to start with a known number of particles and measure how many are left after a given time. If the process is repeated a number of times, one can effectively create a "plot" of the decay curve and then determine the time constant. This method is, however, only practical if one can maintain a sample for a time comparable to or longer than the lifetime. For neutrons, this method can be applied using ultra-cold neutrons stored for periods of up to one hour or even more. This method, known as the "Bottle Method", was used at the ILL and is explained in **figure 2**.

There is an alternative method, which involves shorter observation times. One collects an ensemble containing a known number of particles. Then, rather than counting the surviving particles one measures the number of decays occurring over a short period. In many cases, this can be done quite accurately because the decay process creates energetic particles that are relatively easy to detect. In a

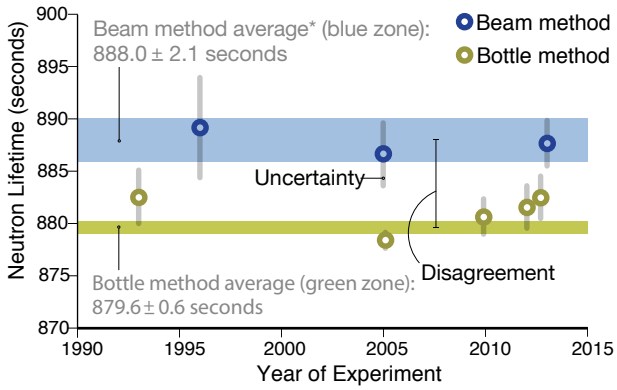

Figure 1

The history of recent neutron lifetime measurements. The green band represents the one standard deviation uncertainty for the average of all "Bottle" experiments. The blue band illustrates the same for all "Beam" experiments.

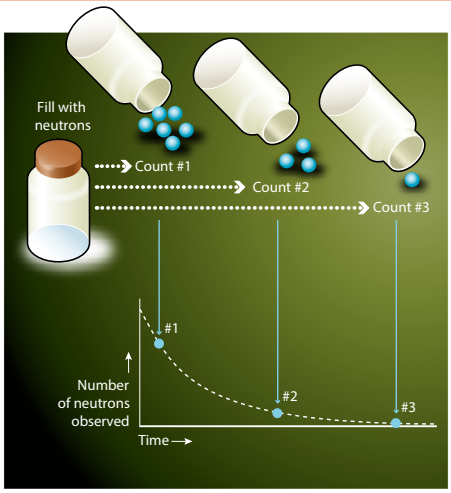

Figure 2

The Bottle Method: One way to measure how long neutrons live is to fill a container with neutrons and empty it after various time intervals under the same conditions to see how many remain. These tests fill in points along a curve that represents neutron decay over time. From this curve, scientists use a simple formula to calculate the average neutron lifetime. Because neutrons occasionally escape through the walls of the bottle, scientists vary the size of the bottle as well as the energy of the neutrons – both of which affect how many particles will escape from the bottle – to extrapolate to a hypothetical bottle that contains netrons perfectly with no losses.

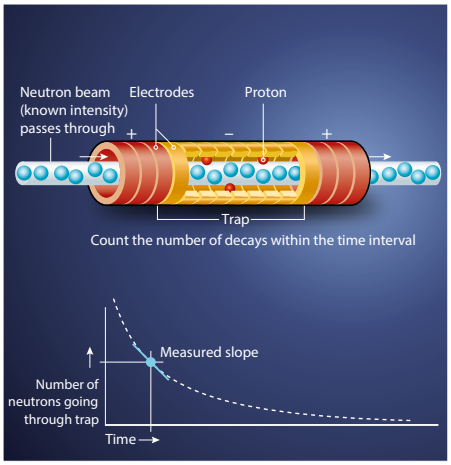

Figure 3

The Beam Method: In contrast to the bottle method, the beam technique looks not for neutrons but for one of their decay products, protons. Scientists direct a stream of neutrons through an electromagnetic 'trap' made of a magnetic field and ring-shaped high-voltage electrodes. The neutral neutrons pass right through, but if one decays inside the trap, the resulting positively charged protons will get stuck. The researchers know how many neutrons were in the beam, and they know how long they spent passing through the trap, so by counting the protons in the trap they can measure the number of neutrons that decayed in that span of time. This measurement is the decay rate, which is the slope of the decay curve at a given point in time and which allows the scientists to calculate the average neutron lifetime.

sense, this method determines the slope of the decay curve rather than its shape. This method requires that the number of particles and the number of decays be determined absolutely. This was the method used at NIST. In that experiment, the ensemble of neutrons was an intense beam of cold neutrons passing through a well-defined decay detection volume. While each individual neutron spent less than a millisecond in the detection volume, there is always an approximately constant density of neutrons in that volume. This method is known as the "Beam Method" and is depicted in **figure 3**.

THE NEUTRON LIFETIME "PUZZLE"

Figure 1 shows the history of recent neutron lifetime measurements. The green band represents the one standard deviation uncertainty for the average of all "bottle" experiments. The blue band illustrates the same for all "beam" experiments. It is interesting to note that while the bottle and beam methods disagree by more than eight seconds or by almost four standard deviations, there is reasonably good agreement among experiments of each type.

One exciting possibility is that the difference is real and reflects a new physical process. For example, imagine that in addition to normal beta decay, neutrons decayed via some previously completely unknown process that is not beta decay and does not create a low energy proton. The bottle experiment would attribute this process to beta decay and conclude that the lifetime was shorter than that due to beta decay alone. On the other hand, the beam experiment would dutifully record only beta decays and get a larger value for the lifetime. It has been suggested [3] that free neutrons may "oscillate" into a "mirror neutron", a hypothetical, no-interacting particle that might be a component of cosmic dark matter. While quite stimulating, this idea remains highly speculative.

Much more likely is the possibility that one (or perhaps, both!) of the experiments has underestimated or overlooked one or more systematic effects. Indeed, the only way to be totally confident that a measurement has not missed something is to check it with an independent measurement(s) of comparable accuracy. Ideally the measurement(s) should use different methods that do not share systematic effects. Viewed in this fashion, the magnitude of the difference between the different results provides an objective measure of the uncertainty. In the case of the neutron lifetime, while the experiments mentioned above are the most accurate to date, there are several other independent determinations underway and the overall agreement between them (or lack thereof) will give a good indication of the state of the art.

This article provides a brief outline of the fuller review of the "neutron enigma" published by Scientific American [4] and its international editions.

The intriguing interplay between collective and single-particle excitations in the exotic nucleus ^{133}Sb

Cold neutron beam facility PF1B

AUTHORS

G. Bocchi and **S. Leoni** (University of Milano and INFN, Italy)
B. Fornal (Institute of Nuclear Physics, PAN, Krakow, Poland)
EXILL collaboration
U. Köster (ILL)

REFERENCES

[1] G. Bocchi *et al.*, Phys. Lett. B 760 (2016) 273
[2] R.A. Broglia, G. Colò, G. Onida and H.E. Roman, Solid State Physics of Finite Systems, Springer, Germany (2004)

The exotic, one-valence proton nucleus ^{133}Sb was produced by neutron-induced fission of ^{235}U and ^{241}Pu targets, during the EXILL campaign. Its γ decay was measured by a large, high-purity Ge multi-detector array coupled to fast scintillators. The experimental analysis provides new insights into the fundamental coupling between collective and single-particle structures in exotic nuclei.

Atomic nuclei are complex systems composed of many strongly interacting particles. As a consequence, their structure can be viewed from two general and complementary perspectives: a microscopic one, focusing on the motion of individual nucleons in a mean-field potential created by all constituents; and a mesoscopic perspective that concentrates on the collective behaviour. Ideal systems to investigate this duality are nuclei composed of one valence particle and a doubly magic core, in which the coupling between collective core excitations (phonons) and the valence nucleon strongly influences their structure. In general, coupling phenomena between phonons and particles are basic ingredients entering the description of interacting fermionic many-body quantum systems, in both nuclear physics and condensed matter physics.

Figure 1

Partial level scheme of the exotic, one-valence proton nucleus ^{133}Sb **(a)** produced by neutron-induced fission of ^{235}U and ^{241}Pu targets. The γ decay reveals a large difference between consecutive magnetic dipole transition probabilities – a clear signature of complex excitations. **(b)** The experimental result cannot be described in the framework of "pure shell model" configurations and points to a hybrid nature of excitations: the valence proton can couple to excitations of the ^{132}Sn core of both genuine phonon type and less collective character [1].

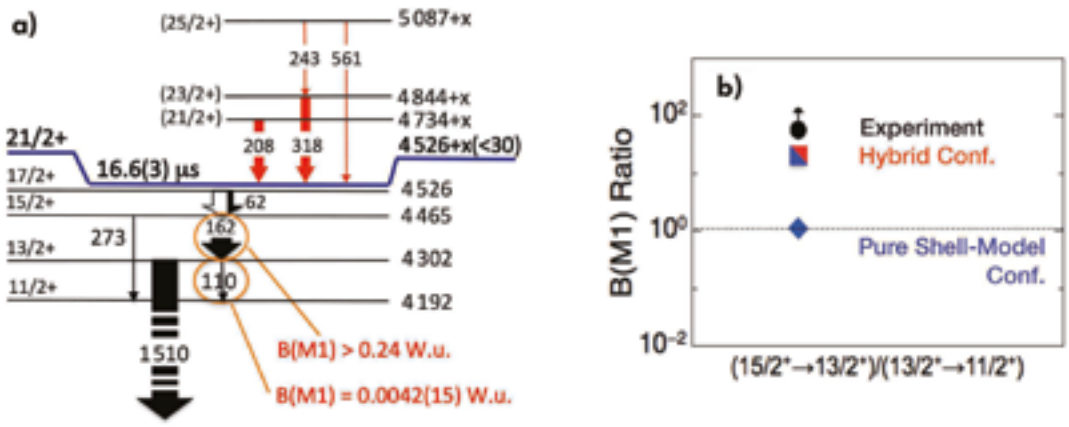

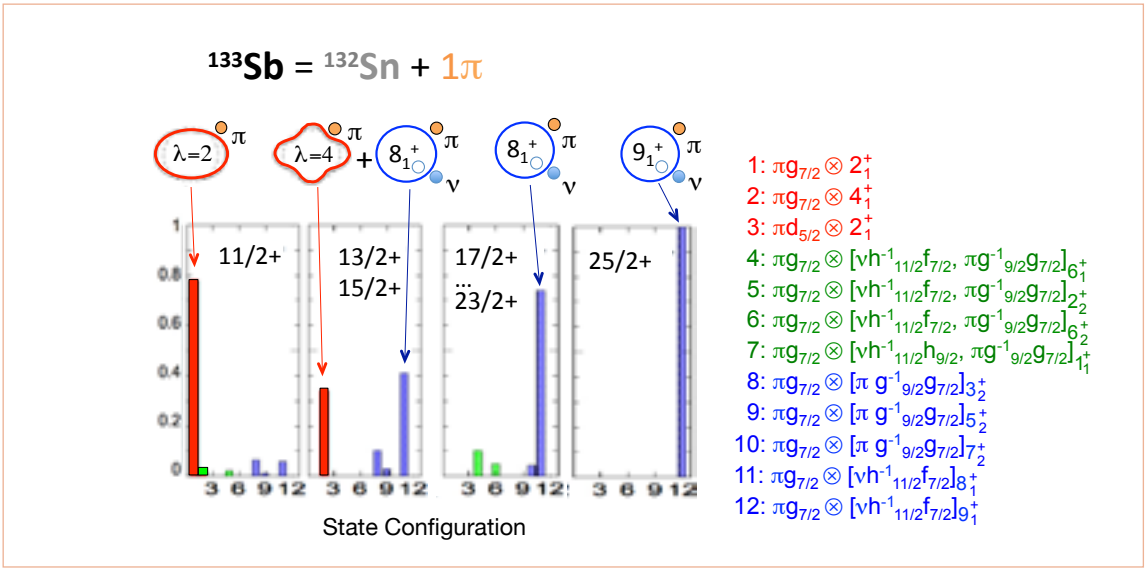

Figure 2

Composition of the lowest states of ^{133}Sb (in the spin range 11/2+ – 25/2+), considering components with amplitude larger than 0.01 (listed in the legend), as predicted by the "Hybrid" Model [1] and illustrated by cartoons on top of the figure (red for phonons and blue/green for less collective excitations of the ^{132}Sn core).

In a recent campaign at the ILL, a European collaboration set up an advanced detection system to study the spectrum of γ rays emitted from excited nuclei produced by the fission of ^{235}U and ^{241}Pu targets, induced by the capture of slow neutrons. This was the first time a large array of high-purity Ge detectors had been placed in front of a high-intensity neutron beam such as the one delivered by the ILL reactor at the PF1B cold neutron beam facility. The so-called EXILL campaign lasted two reactor cycles, allowing a wealth of data to be accumulated. A valuable result of the campaign, published in a recent paper [1], concerns the investigation of the nature of the nuclear excitations in the "exotic" nucleus ^{133}Sb, which has ten neutrons more than the heaviest stable isotope ^{123}Sb. The nucleus of ^{133}Sb is ideal for testing the aforementioned interplay between single particle excitations and phonons, because its immediate neighbour, ^{132}Sn, is a doubly magic nuclide. At first, the spectrum of ^{133}Sb was extended in excitation energy, up to more than 5 MeV. As shown in **figure 1a**, γ transitions feeding the long-lived 16.6 μm isomers were observed, for the first time, reaching angular momenta as high as 25/2. Next, taking advantage of the fast scintillator detectors present in the set-up, the lifetimes of selected excited states were measured and the speed of the electromagnetic decay between excited states deduced: the large difference between consecutive magnetic dipole transition probabilities (i.e. the B(M1) values reported in **figure 1a**) is a clear signature of fast changes in the nature of the excitations of ^{133}Sb, with increasing spin. As shown in **figure 1b**, the experimental results cannot be described within the framework of "pure shell model" configurations, while they can be satisfactorily reproduced by a newly-developed, quantitative theoretical approach that points to a hybrid nature of excitations. In the model, couplings between the valence proton and excitations of the ^{132}Sn core, of both genuine phonon type and less collective character, coexist.

The hybrid nature of the excitations in ^{133}Sb is illustrated by the histograms of **figure 2**, giving the composition of the state configuration sketched on the corresponding cartoons on top of the figure. As can be seen, the added proton cannot change its state in isolation but will be more or less coupled to the deformations of the nuclear core. Hybridisation phenomena of the type reported here are well known in all branches of physics, including condensed matter: there, electrons and plasmons in metals, for example, [2] are the counterparts of the proton and collective excitation of the ^{132}Sn core, in the ^{133}Sb nucleus.

Helium surface as a mirror for ultra-cold neutrons

AUTHORS

P.D. Grigoriev (Landau Institute, Moscow, Russia)
A.D. Grigoriev (Samara State University, Russia)
T. Ziman (ILL and CNRS, France)
O. Zimmer (ILL)

REFERENCES

[1] D. Dubbers and M.G. Schmidt, Rev. Mod. Phys. 83 (2011) 1111
[2] P.D. Grigoriev, O. Zimmer, A.D. Grigoriev and T. Ziman, Phys. Rev. C 94 (2016) 025504

Neutrons are known as "ultra-cold" when their energies are so low that they can be reflected by the surfaces of materials acting as mirrors with average potentials of up to a few hundred nano (10^{-9}) eV. If we place the mirror surface horizontally and introduce the neutrons from above, they can remain in states that are determined by the repulsive potential below and the linear gravitational potential above, which in comparable units is of strength 100 neV per metre. These states extend in the vertical direction over a distance of 6 μm and the binding energies are tiny: pico (10^{-12}) eV. "Neutron bottles" made by these and other means, including magnetic fields, are exploited for high-precision experiments [1], for example to probe gravitational interactions over a scale of micro-metres or in the longstanding search for a non-vanishing electric dipole moment of the neutron.

In past experiments the mirrors have been made of polished quartz. As well as being expensive and fragile they are limited in size, at most several tens of centimetres in scale. The mirror must be made exactly level and extremely flat if the vertical motion is to remain bound over the lifetime of the free neutron, i.e. for many hundreds of seconds. A new idea is to use the different optical potentials between the neutron in the vacuum and in the liquid helium to make a cold, reflecting "lake" surface which could be much larger than that obtained from polished quartz or self-levelling. Even at a temperature of a degree Kelvin, the helium is much warmer (~10^{-4} eV) than the energy scale of bound states, so we have to estimate how quickly the neutrons will be unbound in the vertical direction. To do this, we have to consider which excitations of the helium "lake" will limit the lifetimes of neutron bound states.

Figure 1

A winter lake naturally provides a large horizontal surface that can reflect light. Similarly, a helium "lake" can provide a large reflecting mirror for ultra-cold neutrons with ripplons, quantised excitations of the surface profile and vaporised helium atoms limiting bound states of the neutrons [2].

Figure 2

Lifetime at low temperatures estimated from scattering of free helium atoms (vapour) and quantised surface waves (ripplons) from the lowest bound state of a neutron above the helium surface [2].

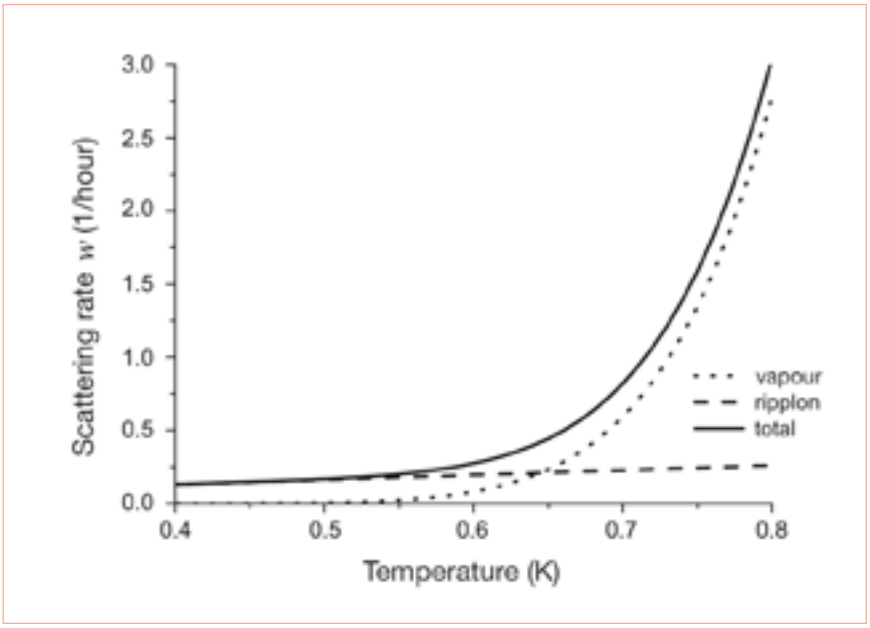

LIMITING PROCESSES FOR THE LIFETIME OF BOUND STATES OF NEUTRONS NEAR A SURFACE OF LIQUID HELIUM

Just as the cold winter lake of **figure 1** is not a perfectly flat, reflective surface for light – there may be ripples propagating at the surface and water vapour in the air above – a surface of the quantum liquid helium has quantised surface excitations ("ripplons") and thermally excited helium atoms in the near vacuum above [1]. We have calculated the effects of the scattering of these and other excitations (e.g. bulk phonons and other proposed surface modes called "surfons"), and it is only the vaporised helium atoms and ripplons that limit the lifetime of the vertically bound states of neutrons. Bulk excitations of the helium contribute very weakly, since the neutron bound states penetrate only a very short distance into the helium bath. These scattering calculations are rather unusual in that the neutrons, while bound in the vertical direction, still have a relatively large kinetic energy in the horizontal plane. In **figure 2** we show the calculated scattering lifetimes for the two dominant processes: it can be seen that above 0.65 K it is the vaporised helium atoms that limit the lifetime of the bound state, but at lower temperatures the number of such atoms decreases exponentially. The ripplons, which have a small, gapless dispersion just like capillary waves, vary as $\omega \sim q^{3/2}$ for small q, then provide limiting value. The encouraging result for further implementation of helium mirrors is that the total scattering rate is less than the inverse neutron lifetime at 0.7 K and reduces even further at lower temperatures. It is fitting that while for decades neutrons have been used to probe the physics of the condensed phases of helium, we may now be able to use helium liquid to study fundamental aspects of neutrons.

Sub-diffusion and population dynamics of water confined in soft environments

How does water behave when restricted in soft charged confining environments? The question is relevant for systems ranging from natural assemblies like proteins, to synthetic nano-structured materials like the proton-conducting membranes used in fuel cells. We provide information for a possible answer based on molecular dynamics simulation. We clarify the dynamical nature of water adsorbed in ionic surfactant phases, and discuss the implications for the analysis of spectroscopy experiments with neutrons.

AUTHORS

S. Hanot (ILL)
S. Lyonnard and **S. Mossa** (Université Grenoble Alpes, CNRS, CEA, INAC-SYMMES, France)

REFERENCES

[1] M.-C. Bellissent-Funel *et al.*, Chem. Rev. 116 (2016) 7673
[2] S. Hanot, S. Lyonnard and S. Mossa, Nanoscale 8 (2016) 3314
[3] Q. Berrod *et al.*, Macromolecules 48 (2015) 6166
[4] J.-C. Perrin, S Lyonnard and F. Volino, J. Phys. Chem. C 111 (2007) 3393

Confinement at the nano-scale and interaction with interfaces alter the structure and dynamics of bulk water. Highlighting the details of these modifications at the molecular level is a primary scientific challenge, crucial in contexts such as biology [1], among others. It is also important for the development of advanced materials employed in modern technologies, including novel energies applications. This is certainly the case for proton-conducting, polymer electrolyte membranes (e.g. Nafion) used as separators in fuel cells. Being able to control the above modifications is key to optimising the performance of these devices. Transport of protons, in fact, correlates with the dynamical state of the adsorbed water. This latter, in turn, affects the morphology and functional response of the confining soft medium. Insight into this interplay comes from spectroscopy, including quasi-elastic neutron scattering (QENS), pulsed-field gradient nuclear magnetic resonance (PFG-NMR) techniques and computer simulation.

We performed molecular dynamics simulation of a self-assembling model for ionic surfactants [2] at different values of λ, the number of water molecules per surfactant (**figure 1**, **bottom**). These materials are efficient, simplified templates for the nano-scale organisation of the significantly more complex Nafion ionomer [3]. By following the time evolution of water molecules confined in phase-separated environments with tuneable topology (**figure 1**, **top**), we have also analysed their dynamics in terms of quantities measured in neutron scattering experiments.

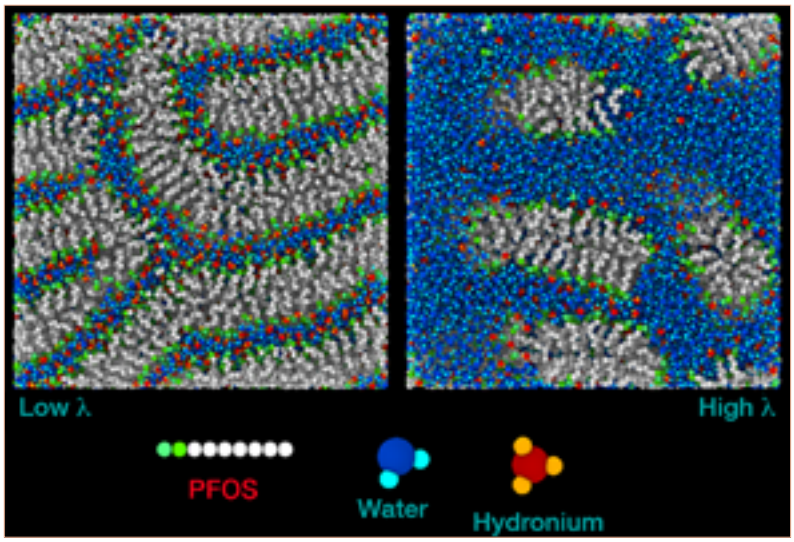

Figure 1

Top) Simulation snapshots of the studied ionic surfactants, at low (lamellae) and high (micelles) water content. The hydrophobic section of surfactants is represented by grey beads, the charged hydrophilic units by green ones. Water molecules are indicated in blue, hydronium cations in red. **Bottom)** Details of the coarse-grained representation of the surfactants, and all-atoms structure of the water molecules and hydronium ions.

Figure 2

Top) Mean-squared displacements of the water oxygen atoms, at the indicated values of λ. The solid lines are the power-law fits described in the text, the dashed lines indicate the limiting Fickian (**top**) and highly sub-diffusive (**bottom**) limits, respectively. In the **inset** we show the hydration dependence of the power-law exponents. **Bottom)** Diffusion coefficients obtained by PFG-NMR (open circles) and QENS (open squares), together with the corresponding simulation data (closed symbols) determined, as described in the text.

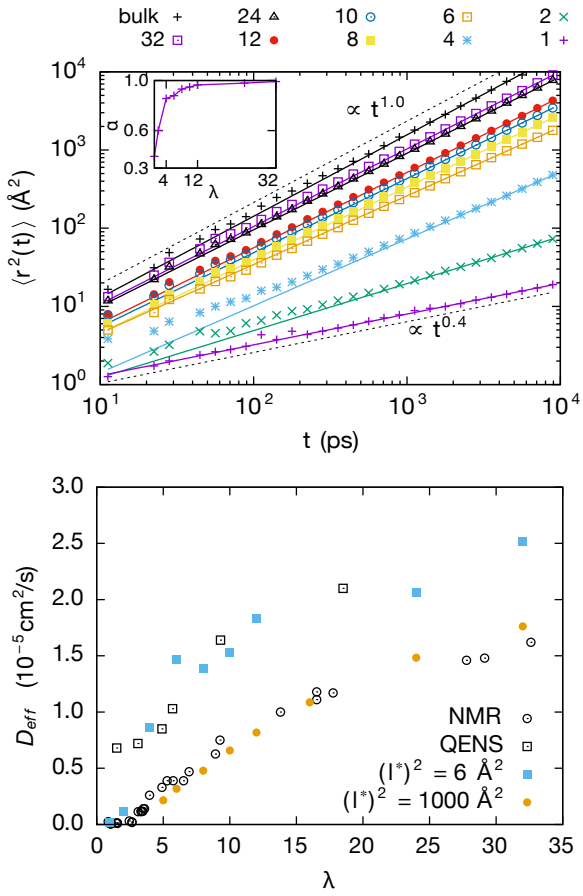

The mean-squared displacement (MSD) of water oxygens is a particularly instructive quantity. In **figure 2**, **top**, we show the results of our calculations at the indicated values of hydration. We were able to represent these data at long-times by power laws with exponents decreasing continuously with λ (see **inset**), from an almost bulk-like behaviour (α = 1), to extremely confined cases (α < 1). This is an unambiguous hallmark of sub-diffusion. Our model therefore turns out to be an efficient tool for both underlining this remarkable feature (substantially overlooked in previous studies) and continuously tuning its strength, ranging from Fickian to strongly anomalous diffusion, by simply varying hydration.

We have also clarified the origin of the observed anomalous behaviour, an exercise only possible through simulation. This is the result of a heterogeneous and space-dependent dynamics characterising water molecules at different distances from the phase boundaries. In particular, we have demonstrated that molecules close to the interfaces and in direct interaction with the latter, move more slowly than those with a bulk-like character lying further away from the confining matrix. This partition directly identifies water populations with different instantaneous dynamics, a picture also provided indirectly by the modelling of QENS data [4]. A quite technical study of the long-tailed probability distribution of residence times at the interfaces, reminiscent of continuous-time random walks, delivers the complete picture. The observed average anomalous dynamics can ultimately be related to an exchange mechanism between molecules pertaining to these dynamical populations. The details of this process depend on water content determining the observed variable degree of sub-diffusivity.

An alternative representation of the data in **figure 2**, **top**, also allowed us to reproduce water diffusion coefficients determined by different spectroscopies, as shown in **figure 2**, **bottom**, as a function of hydration. QENS (open squares) typically probes displacements of a few angstroms, on time-scales ranging from one to a few hundred picoseconds. PFG-NMR (open circles), in contrast, measures the self-diffusion of water over large distances, of the order of the micrometre, with typical time-scales of a few milliseconds. The experimental observation that the two sets of data do not coincide has been rather artificially explained by introducing coefficients characterising different types of dynamics valid over the corresponding time-scales. Simulation provides a complementary picture. When anomalous transport is involved, the constant Fickian diffusion coefficient must be replaced by a time- and length-scale-dependent effective diffusion coefficient, D_{eff}, defined from the local slope of the MSD. Sampling the simulation data for D_{eff} at length-scales similar to those associated with the experimental probes, we obtain the closed symbols shown in the same figure. Surprisingly, the simulation points convincingly reproduce the hydration dependence of both experimental data sets, without any complex fitting procedure. From this perspective, PFG-NMR and QENS turn out to determine different values of the same D_{eff}, probing it at different length- (time-) scales.

We are currently working to extend this picture to experimental and simulation data collected for Nafion. This work will also allow us to clarify some aspects of the interpretation of QENS measurements and establish connections with other research domains, including biology and advanced issues in statistical mechanics.

MODERNISATION PROGRAMMES AND TECHNICAL DEVELOPMENTS

78 MODERNISATION PROGRAMME

80 INSTRUMENTS AND TECHNICAL DEVELOPMENTS

84 NEW EXPERIMENTAL TECHNIQUES

The ILL's Projects and Techniques Division (DPT) has the proud responsibility of ensuring that the institute's scientific installations adapt and retain their potential for discovery. We will ensure that the ILL maintains its fifty-year tradition of innovation, unrolling technology for the future of neutron science. I shall attempt in the following to give a brief overview of the Division's areas of expertise and the services it provides for the ILL's scientific users.

Let us start with detectors. Over the years, the Detector Service has developed helium-3 detectors whose outstanding dimensions and count rates have completely modified the shape of the ILL instruments. The reliability of these detectors has significantly reduced time previously lost on detector problems. This explains the high demand for the ILL's helium-3 detectors from all over the world. There is, nevertheless, a need today for new technology on diffraction instruments such as the ILL's XtremeD. We are therefore collaborating on two major projects, with ICMA of Zaragoza and FRMII in Munich, to produce large, high-resolution, high-count-rate detectors. These technologies will also be of service to other diffraction instruments, including D19, just as our highly successful IN5 technology is being extended to Panther. But the Detector Service has other irons in the fire: in collaboration with the ESS its work on boron detectors will provide count rates, background and spatial resolutions for the ILL's Rainbows project that cannot be achieved through existing technologies.

If we now move upstream, towards the instrument, let us note the importance for all new instruments of advanced monochromator technology and polarisation. The production of polarising super-mirrors for WASP was a real challenge for the ILL that was nevertheless successfully met. The ILL's T-REX machine produces polarised helium-3 and is a real breakthrough in polarisation analysis for ILL users. Its reliability and success led directly to the development of the ILL's polarisation analysis set-up PASTIS. It should be noted that there is no actual polarisation project in the first phase of the ESS's instrument programme and that this is a very challenging domain for pulsed polychromatic sources.

As for the instrument itself, it is the DPT's role to maintain and develop instrument electronics and instrument control facilities. The reference for instrument control at the ILL is NOMAD, the software with a user-friendly interface developed by our Instrument Control Service. The Service's instrument electronics, including detector electronics, have been standardised over the years for easier and less costly management and upgrade.

From the user point of view it is of course the sample that counts, and the data generated. SANE is the Science Division's "advanced neutron environment" service, with a history of advanced and reliable, low-background set-ups for users' samples. Sample environment is one of the most important and reliable features cited by users working at the ILL and the current NESSE project in the Endurance Programme will ensure that the ILL maintains these standards. NESSE will also extend our sample environment facilities for soft matter and high pressure experiments.

As for data processing and reduction, the DPT's IT staff have developed tools for data reduction over the years and are now working on BASTILLE: the ILL's framework for coherent and efficient data analysis systems, capable of handling and transforming the ever-increasing flows of data being generated.

The IT Service has also recently undertaken a major initiative in terms of research data management for the ILL's users and committees. We are thus playing a leading role at international level on the question of access to research data and publications, data standards, archiving and good practice. The Service will continue to collaborate with other research organisations on this and other data-related issues (remote data analysis for users, for example).

Finally, it would not be possible to develop our installations without the resources and expertise of our Installations and Maintenance Service (SAE). In 2016 the SAE combined a programme of seismic reinforcement with exploits such as the opening and re-closure of the guide hall roof for the delivery of supersized magnet coils. At the same time our Design office, engineers and technicians deployed their expertise in instrument construction and guide optimisation to make scientists' dreams come true.

The Millennium Programme on all these fronts was a real success. It will end in 2017 with the commissioning of the wide-angle spin-echo machine WASP, which will offer new capabilities in soft-matter high-resolution spectroscopy. But projects and techniques do not stop there – the Endurance Programme has already started to make its mark on neutron science, as you can see from the next article of this report.

Charles Simon
Associate Director,
Head of the Projects and Techniques Division

MODERNISATION PROGRAMME

Endurance: the new ILL Modernisation Programme

AUTHORS
C. Dewhurst and C. Simon (ILL)

The ILL is modernising and developing instrumentation and infrastructure around its neutron source within the framework of the Endurance Programme. Phase 1 of Endurance is currently running from 2016 to 2019, with a second phase foreseen to run between 2020 and 2023.

ENDURANCE PHASE 1 is well underway. During the period September 2015 to June 2016, all projects passed from their feasibility to execution phases following the preparation of detailed project plans, review and validation by the PMC (project management committee) board. The projects are in varying stages of advancement as a function of parameters such as their complexity, modularity, expenditure and, most importantly, interdependence with other logistical boundaries such as guide renewal, reactor function and the H1-H2 in-pile guide replacement.

The first tangible results from Endurance 1 have arrived in the form of the new fission fragment gamma-ray spectrometer, **FIPPS**, which received its first neutrons and users during the last days of the reactor cycle in December 2016. The **Bastille** project sees the ILL join and contribute to the international Mantid software development for neutron data treatment. A rollout of software work packages for time-of-flight (TOF) and backscattering data treatment began in October 2016, with work beginning on packages for small-angle neutron scattering (SANS) and reflectometry in 2017. The **Nesse** project is already delivering new and upgraded sample environments, capabilities and support infrastructure such as humidity chambers, stopped-flow observation heads, liquid pressure cells, fast and low background cryostats and precision orientation goniometer sample sticks. The **SuperSUN** project will provide a source of ultra-cold neutrons (UCN) with densities one order of magnitude greater than the UCN sources available today, paving the way for the next generation of fundamental physics experiments such as those defining the limits on the neutron electric dipole moment. The first manufacturing of cryogenic components for **SuperSUN** is also underway, funded in the first instance by an additional ANR grant, and should begin to produce the first ultra-cold neutrons in 2018.

The largest single instrument project, **Panther**, replacing the existing IN4 instrument, has been scheduled with a view to providing the first commissioning data and results before the end of 2018. **Panther** will be equipped with a large position sensitive detector, offering a much greater solid angle of detection along with the ability to work with single crystal samples. Dramatic improvements in signal-to-noise are expected with the replacement and addition of background choppers, better-defined neutron optics and significant shielding of the new detectors. Detailed technical designs for the major instrument components are close to completion, with manufacturing and procurement due to proceed through 2017.

The new fission fragment gamma-ray spectrometer – FIPPS.

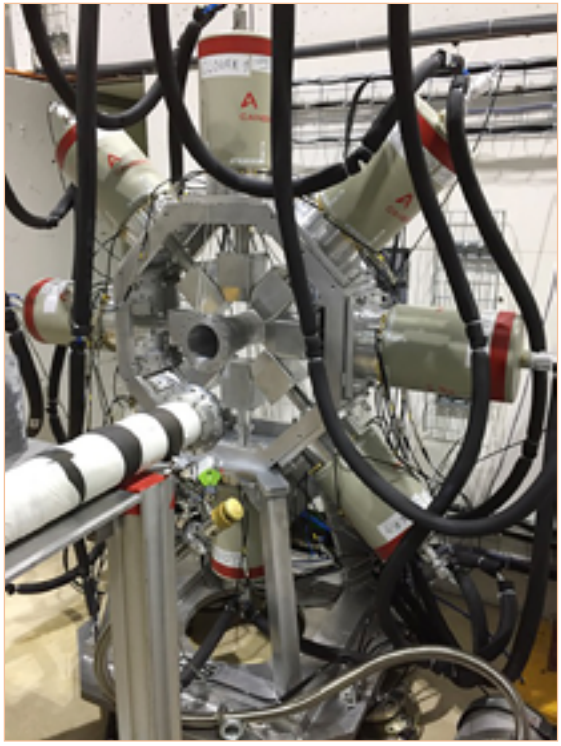

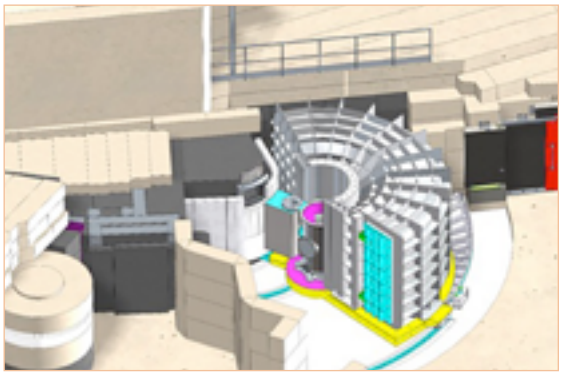

Model of the new thermal TOF spectrometer – Panther.

The Chartreuse projects are underpinned by the renewal of the **H24** thermal neutron guide by way of a multiple branch guide delivering high performance end-of-guide positions to the new or upgraded instruments **XtremeD**, **D10+** and **IN13+**. The test and sample orientation instruments **CT2**, **Cyclops** and **Orient Express** are also to be relocated on to the end of one branch of the **H24** guide. All Chartreuse instrument and guide projects are phased for completion with the renewal of the **H1–H2** beam tube and in-pile guides at the end of 2019. Conceptual design work for **D10+** and **XtremeD** is close to completion, with detailed engineering drawings in progress and manufacturing and procurement of components to begin in 2017. The existing D10 will benefit in the immediate term from the new, larger and higher resolution Bidim100 detector for **D10+** to be installed and commissioned during 2017. **D10+** is expected to deliver gains in neutron flux of approximately one order of magnitude over the existing instrument due to the rebuilt and higher critical angle **H24** guide, dedicated end of guide position and rebuilt and optimised monochromators. **XtremeD** is a flagship instrument within the Endurance Programme and will be operated as a Spanish CRG. A separate working group has been established by the Spanish CRG team to define and provide "extreme-conditions" sample environments, such as high-pressure cells and high magnetic fields, for use on the instrument. Endurance will also see the **IN13+** backscattering CRG instrument repositioned on its own dedicated branch of the new **H24** guide. A separate CRG project to renew the complex gradient monochromators is underway, to capitalise on the new high performance guide and associated gain in performance of the instrument.

ENDURANCE PHASE 2: A shortlist of new or upgraded instrument concepts was established in 2014, with the first projects launched as part of Endurance Phase 1 (2016-2019). It is now timely to review the remaining projects and make a further call to the neutron user community for propositions for new or upgraded instrumentation. One focus of Endurance 2 is likely to be the upgrade of the Vercors side of the ILL 7 guide hall, with the renewal of one or more cold neutron guides and instrumentation complementing the renewal of thermal neutron guides and instrumentation under Endurance 1. In December 2016 the ILL invited further expressions of interest for flagship instruments to exploit the full scientific potential of the ILL's high flux reactor and help define a coherent scientific strategy and capabilities within the landscape of existing and emerging neutron sources. A strategy for Endurance 2 is rapidly taking shape.

Model of the new extreme conditions powder and single crystal diffractometer – XtremeD.

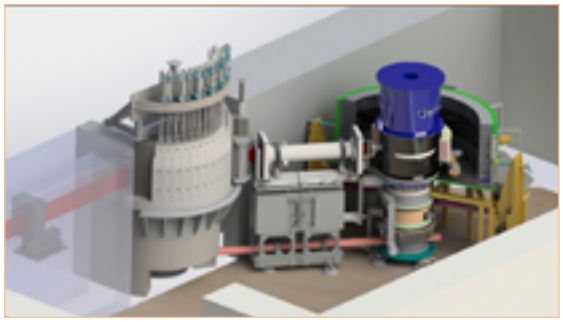

INSTRUMENTS AND TECHNICAL DEVELOPMENTS

The IN15 upgrade

The old IN15 used to be the flagship neutron spin-echo instrument of the ILL. It had the highest intensity and highest energy resolution (spin-echo time) of any such instrument in the world. Nevertheless, there was a demand from users to improve the instrument, and the instrument scientists had ideas on how to do it. The upgrade was funded jointly by BMBF, the ILL and Forschungszentrum Jülich. The BMBF funding (FKZ05K13KT1) was brought in by Professor Gradzielski of TU Berlin. The new components were installed during the 2014 long shutdown, with user operation resuming in September 2015.

AUTHORS

B. Farago, **P. Falus**, **F. Thomas** and **C. Gomez** (ILL)
I. Hoffmann and **M. Gradzielski** (TU Berlin, Germany)

REFERENCES

[1] C.M.E. Zeyen, P.C. Rem, R.A. Hartmann and L.J.M. van de Klundert, IEEE Trans. Magn. 24 (1988) 1540

Neutron spin-echo (NSE) can detect very slow motions in materials by coding the speed of neutrons using their spin precession in a magnetic field. The higher the field the neutrons encounter, the more rotations they make and the more sensitive is the measurement. In order to obtain a successful measurement it is not enough just to have a high magnetic field, the field also has to be very homogeneous. For any possible neutron path before and after the sample, the field integral has to be identical up to ppm precision. Due to Maxwell's laws, for finite beam sizes solenoids cannot produce such homogeneous precession fields, and flat correction coils (so called Fresnels) have to be inserted in the beam path. While they make measurements possible, they also attenuate and scatter the beam. Robust correction coils can correct a lot of magnetic field but in turn attenuate the neutron beam a lot. Thinner coils attenuate less but have limited correction capabilities. It was quickly recognised that the quest for the highest resolution NSE is not limited by the precession fields. The highest field in the old IN15 coils was only 0.2 T. What really limits us is our ability to correct these fields.

For a given field integral the amount of correction depends on the field profile. The more abrupt the field changes between zero and maximum, the more correction is needed. For very thin beams it was first shown by Zeyen [1] that the optimum field is $\cos^2$-shaped. For large, diverging, conical beams a more asymmetric shape is better. The new, optimised IN15 coils (**figure 1**) need a factor 2 less correction than the old ones for the same field integral. New, more transparent, and twice as strong Fresnel coils were manufactured at the ILL. In total, the field integral was increased fourfold with marginal loss of beam intensity. The new precession coils are made up of 11 individual coils of different diameters. They are wound from hollow copper wires that are water-cooled from the inside. The two coil assemblies weigh 5 t each. The precession coils were manufactured by Sigmaphi (Vannes, France) and the power supplies, which can run up to 1 375 A current through the coils, were made by Danfysik (Taastrup, Denmark).

The longest spin-echo time achievable is proportional to the field integral and the neutron wavelength cubed ($t \propto \lambda^3 \int Bdl$). To achieve higher resolution we can increase the field integral or use longer wavelength neutrons. In the range used by IN15 the neutron intensity drops with $I \propto \lambda^{-5}$. To reach the same spin-echo time with the new instrument we can use 1.6 times shorter wavelengths which in turn will have ten times higher intensity. Thus, the new instrument can either have four times better resolution at the same wavelength (**figure 2**) or aim for the same resolution as before but at shorter wavelength and profit from the tenfold intensity gain.

Figure 1
The new IN15.

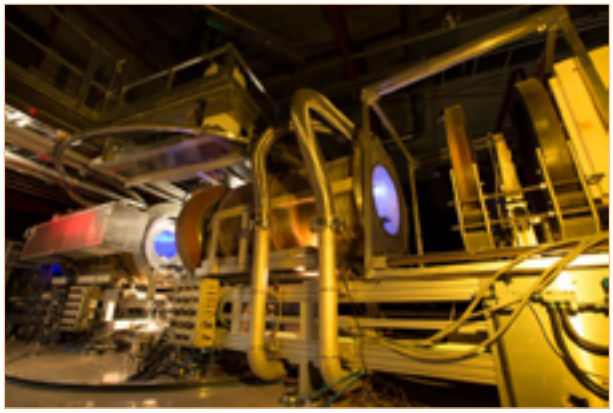

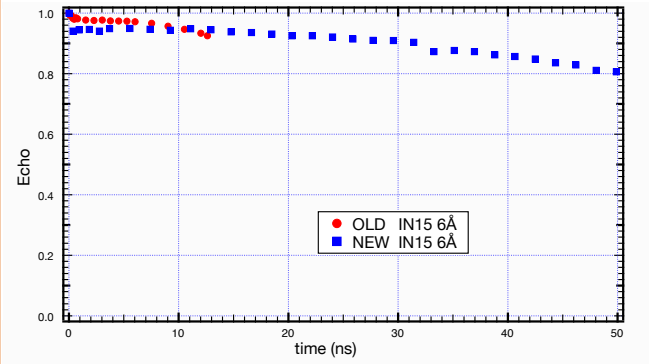

Figure 2

With the new IN15, four times longer spin-echo times can be obtained using the same wavelength.

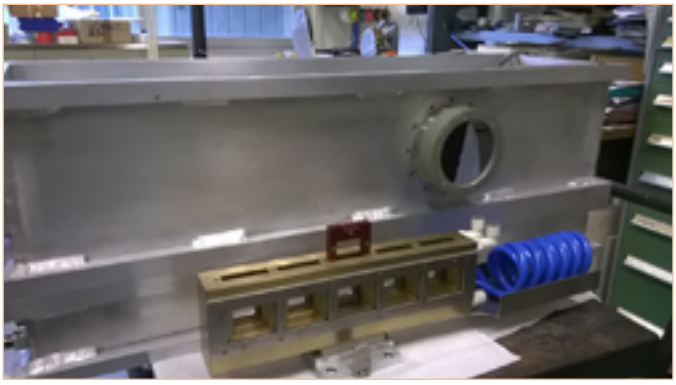

Figure 3

The new 5-position sample changer for quartz cells.

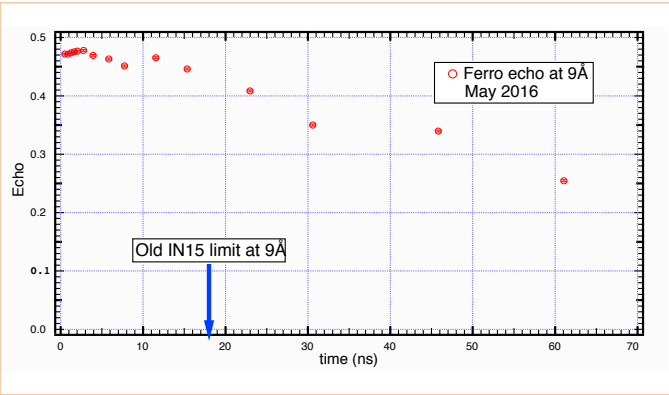

Figure 4

Resolution of the ferro echo option at the new IN15.

Thanks to this gain, samples are measured in a few hours rather than days. This high throughput called for a sample changer. Since the majority of samples at IN15 are solutions, a five positions water bath-controlled sample changer was built which is now our standard sample environment (**figure 3**). For biological samples where the sample is scarce, ten times higher intensity means ten times less sample is necessary for a measurement. Thus now, 10 mg/ml protein concentration is sufficient for meaningful results.

All previous IN15 options are tested and available. The 'small echo' option gives 10^4 dynamical range for the same wavelength – for example at 10 Å we can cover NSE times from 20 ps to 200 ns. For magnetic samples, the paramagnetic and ferromagnetic echo options are available with 4 times longer NSE time than before (**figure 4**). The new instrument has been tested with the non-magnetic furnaces, standard ILL cryostat and cryofurnace, and a 500 bar pressure cell.

As complementary methods the sample changer offers *in situ* turbidity and light scattering monitoring. The ILL support laboratories have been equipped with field gradient NMR and dynamic light scattering facilities (R. Schweins) which is the auxiliary equipment most frequently used by our users.

Although IN15 is back to normal operation, the neutron spin-echo upgrades are not completed. The new wide-angle spin-echo instrument WASP is advancing in leaps and bounds, and the first neutrons are expected in 2017.

Development of a new 2D curved ^{3}He detector for XtremeD: the Trench-MWPC

The future XtremeD instrument, due to start operation in 2019, will be equipped with a large area 2D detector for the study of powder and crystal samples under extreme conditions of pressure and magnetic field. A new concept of ^{3}He detector, called the Trench-MWPC (Multi-Wire Proportional Chamber), has been developed to match the experimental conditions of the instrument.

AUTHORS

SDN and XtremeD team (ILL)

REFERENCES

[1] J.C. Buffet *et al.*, Nucl. Instrum. Methods, A 554 (2005) 392

[2] J. Fried *et al.*, Nucl. Instrum. Methods, A 478 (2002) 415

Although scintillation detectors have gained strong interest in neutron scattering science due to the ^{3}He shortage, the detection efficiency and counting rate capability associated with this technique are below the requirements of XtremeD. Another ^{3}He alternative technique, called Multi-blade [1] is based on ^{10}B-films embedded in a MWPC. This technique is promising but still requires some development before its reliability and performance can compare with that of ^{3}He detectors. ^{3}He recycling and the use of alternative technologies for homeland security have been established in recent years to secure ^{3}He availability for scientific applications. As a result, ^{3}He's price has been stable for more than two years, at less than 2.000 $ / litre. As a matter of fact, ^{3}He MWPC detectors offer a good compromise between technical performance, development effort and cost for small- or medium-size detectors.

To cope with a flux of 10^8 n.cm^{-2}s^{-1} at the sample position, the counting rate limit of the XtremeD detector has been specified as follows: assuming a maximum counting deviation of 10 %, the detector must be able to count 2 MHz for a uniform irradiation and 50 kHz for the irradiation of one single channel along the horizontal axis. These values are above those accessible with the curved ^{3}He 2D multi-wire proportional chambers currently in operation on D19 [1]. The D19 detector contains 40 glass plates of 4 cm x 40 cm, each one having 400 horizontal chromium strips connected together with a resistive line. The counting rate limit of the D19 detector, of 20 kHz per angular sector of 6 °, comes from the 5 µsec duration of the analogue signals which is determined by the RC time constant of the cathodes.

A way of improving the counting rate of such a detector is to use individual channel electronics instead of charge division. Assuming typical values for individual readout, namely 2 µsec for the analogue signal time development and 200 ns for the XY coincidence window, a counting rate of 500 kHz per angular sector and 50 kHz per wire is easily accessible. In this case, dividing the sensitive area of the detector into four independent sectors of 30 ° is intrinsically sufficient to reach 2 MHz global counting rate for XtremeD, but because of mechanical constraints it was decided to use nine sectors. Other specifications of XtremeD have been specified as follows: sample to detector distance = 76 cm; angular coverage: horiz >= 120 ° and vert >= 18 °; angular resolution: horiz = 0.15 ° and vert = 0.2 °; and detection efficiency = 80 % @ 2.5 Angstrom.

An important benefit of individual channel electronics is that the detector is operated at lower amplification gain – 50 instead of 500 – which expands its lifetime. A further improvement of its robustness will come from the replacement of CF_4 by Ar-CO_2 in the gas mixture. Although the D19

Figure 1

Schematic view of the Trench-MWPC: the teeth between the anode wires help to reduce space-charge effect due to ion feedback, resulting in better uniformity of response, lower gain operation and higher counting.

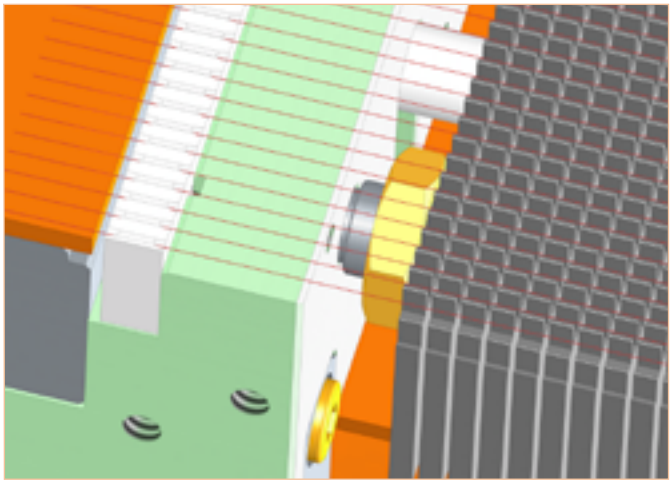

Figure 2

Amplification gain and counting efficiency versus flux for the two versions of the detector presented in this paper: without (blue) and with (red) teeth between the anode wires. Data are divided by the value measured at low flux.

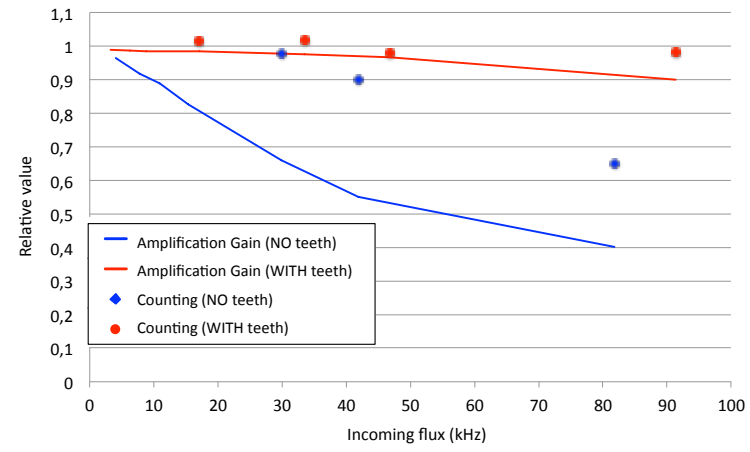

Figure 3

Image measured with a Cd mask.

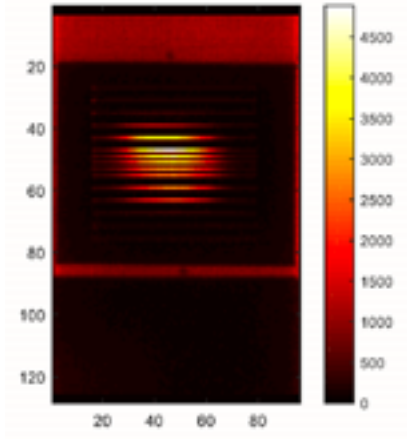

detector showed acceptable reliability during twelve years of continuous operation, we had to open it four times during that period to fix several technical problems: instability of a cathode contact, current leak on the drift electrode, one cathode failure, and one broken anode. As a result of this experience, we imposed severe constraints on the design of the XtremeD detector in order to improve reliability and maintainability: replacement of the glass electrodes by a robust metallic electrode, no drift electrode, and no cathode wires on top of the anode wires. It should be noted that, in addition to the development of the XtremeD detector, the ILL participates in a collaboration with FRM-II and PSI to convert a curved BNL-type detector [2] to an individual readout detector with a position resolution of 1.6 mm x 1.6 mm.

The XtremeD detector will contain nine identical modules mounted side by side in a cylindrical pressure vessel to cover a continuous angular coverage of 129.6 ° horizontally. Each module contains 96 anode wires mounted vertically at a pitch of 2 mm, and 128 curved aluminium blades stacked vertically at a pitch of 2.5 mm, corresponding to a sensitive area of 172 cm x 32 cm. Ceramic spacers are used to separate the aluminium blades mechanically and electrically. Two ceramic combs are used to guide the anode wires with a precision better than 50 µm. Anode wires and cathode blades are connected individually to electrical feedthroughs by means of polyimide flex-rigid circuits. Several prototypes containing only one module of 14.4 ° have been mounted and tested over more than a year. In one of them, called the Trench-MWPC, teeth are machined precisely every 2 mm in the aluminium blades so as to provide separations between the anode wires (**figure 1**).

Experimental results show that this design fulfils all the requirements of XtremeD. In particular, by exposing one module to a large beam with neutron absorber plates of different thicknesses, the limit of 10 % counting deviation is reached at 550 kHz, corresponding to an expected counting rate of 5 MHz for a uniform irradiation of the nine modules. Furthermore, the local irradiation of one anode wire with a vertical slit showed no counting deviation up to 50 kHz. The local counting rate capability was investigated with a beam of 5 mm x 5 mm; both versions of the same prototype, MWPC and Trench-MWPC, have been compared experimentally. The Trench-MWPC showed better performance for all detection parameters, in particular:

- The average multiplicity on the cathodes is reduced from 3.5 to 2
- The operational amplification gain is reduced by a factor of 2
- The amplification gain measured along the anode wires is more uniform (+-5 % against +-50 %)
- As illustrated in **figure 2**, the local counting rate capability is improved by at least a factor of 3.

The amplification gain and the local counting rate have been measured as a function of the incoming flux, with (red) and without (blue) teeth between the anode wires. The benefit of the Trench-MWPC is clearly visible: we observed no deviation at 92 kHz (18 kHz per pixel), whereas for the standard MWPC without teeth, 10 % counting deviation was measured at 42 kHz (8 kHz per pixel). Furthermore, 10 % reduction of the amplification gain was observed at a flux ten times larger for the Trench-MWPC.

This good performance is attributed to the fast collection of the positive ions on the cathode teeth, which minimises the space-charge effect as in a micro-strip gas chamber. **Figure 3** shows an image measured with the Trench-MWPC prototype covered with a Cd mask and having 0.5 mm horizontal slits spaced every 5 or 10 mm.

Compared with existing curved 2D detectors, the Trench-MWPC is more robust, its maintainability is easier and its performance is better. In particular, the counting rate capability, both local and global, is increased significantly. Following these encouraging results, this technique has been selected for the design of the future XtremeD instrument.

NEW EXPERIMENTAL TECHNIQUES

One order of magnitude better signal-to-noise ratio for neutron backscattering

AUTHORS

M. Appel (ILL and FAU Erlangen-Nürnberg)
B. Frick (ILL)

REFERENCES

[1] M. Appel and B. Frick, Rev. Sci. Instr. (2017), accepted for publication

With the community recently celebrating the 50th anniversary of neutron backscattering, it has become clear once again how its application has benefited from the enormous improvement in count rate over the last decades. While this helps users to achieve better counting statistics in shorter experiments, the sensitivity expressed in the signal-to-noise ratio has only been moderately improved. With a new acquisition mode available on IN16B, this ratio can now be increased by about one order of magnitude to unprecedented values of above 10 000 for standard samples.

The high energy resolution provided by neutron backscattering spectrometers is frequently used to investigate nanosecond dynamics in a wide range of science, e.g. investigation of energy-related materials (for H-storage, batteries, fuel cell membranes, etc.), biologically relevant systems, local polymer dynamics, glass transition phenomena, liquid crystals, dynamics in confinement and others. The IN16B spectrometer at the ILL is at the cutting edge of the development of reactor-based neutron backscattering spectrometers providing highest neutron count rates, where up until now signal-to-noise ratios (SNRs) near 2 000 were reached for standard user samples.

We have recently conceived and implemented a new acquisition mode on IN16B, further improving the SNR by one order of magnitude at the moderate cost of reducing neutron count rate by 37 % [1]. The ability of this mode to attain unprecedented SNRs is shown in **figure 1a**, using a strongly scattering PET sample for benchmarking

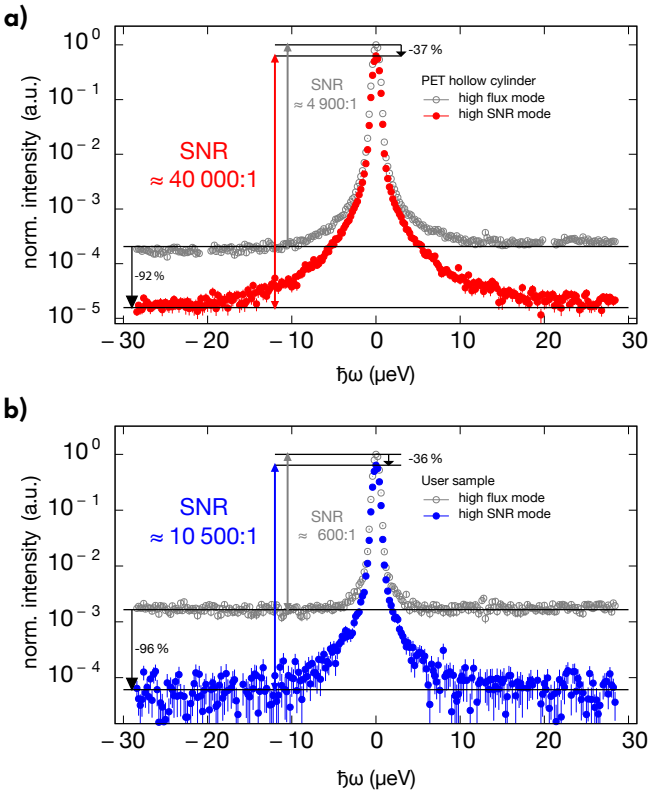

Figure 1

Energy transfer spectra summed over all large-angle detectors of IN16B comparing the signal-to-noise ratio in "high flux mode" and "high SNR mode" for **(a)** a very strong PET scatterer with > 85 % scattering at 2 K, and **(b)** an absorbing user sample with ~ 12 scattering and 50 % transmission at 2 K.

Figure 2

Schematic layout of modern neutron backscattering spectrometers such as IN16B. See text for a description of the labelled components.

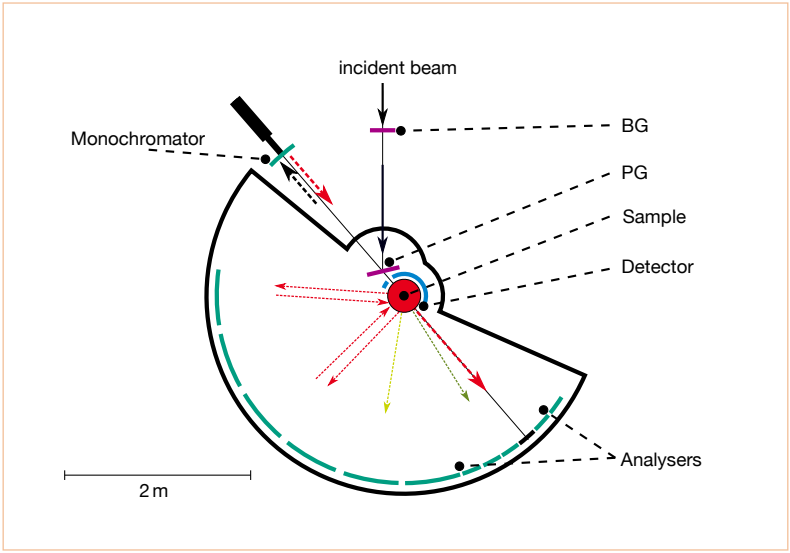

purposes. The SNR is calculated as the ratio between peak height and flat background. While the conventional "high flux mode" yields an already competitive value of 4 900, the sensitivity can be boosted even more in the new "high SNR mode", achieving a ratio of 40 000. An even more important improvement could be observed in a subsequent user experiment shown in **figure 1b** using a more common scatterer of ~ 12 %, though with comparably large absorption (50 % transmission). The "high SNR mode" reduces the background by 96 %, improving the initial SNR of 600 to more than 10 000! This makes the method much more sensitive for its usual applications of detecting quasi-elastic scattering or weak inelastic peaks, especially when their intensities come close to the background level.

In order to understand how and why this new acquisition method works, we have to recall the layout and functioning of modern neutron backscattering spectrometers such as IN16B. **Figure 2** shows the schematic layout with labels for all essential instrument components. The incoming beam in the top of the figure contains a preselected wavelength band of neutrons. A background chopper (BG) is optionally used to produce long neutron pulses with 50 % duty cycle phased with the subsequent deflector chopper (PG). The deflector chopper is equipped with pyrolytic graphite crystals to deflect the neutron beam towards the monochromator crystals (Mono), where a highly monochromatic portion of the beam is selected in backscattering corresponding to a Bragg angle of 90 °. The geometry and chopper speeds are matched to the neutron flight time such that the monochromatic pulses are transmitted through open segments of the PG chopper towards the sample. Scattering from the sample is analysed and backscattered from the crystal analysers (Ana) covering a large solid angle and sent to the detectors (Det) located very close around the sample. The pulsed operation of the spectrometer enables discrimination of analysed neutron pulses in the detector from those scattered directly from the sample into the detector. Now, by moving the monochromator back and forth, the energy of the incident neutrons on the sample is modulated due to the Doppler shift. Recording analysed neutrons as a function of Doppler velocity allows us to obtain energy transfer spectra such as shown in **figure 1**.

The folded beam path allows neutrons to be scattered back from the monochromator and analysers, returning by the same path they arrived on. This is crucial to the high-energy resolution – hence the name 'backscattering spectroscopy'. But it also leads to a big challenge in terms of background suppression, as the detector needs to be sensitive down to count rates < 10 n/s within the exact time frame that the PG chopper is deflecting 10^{10} n/s in just about 30 cm distance! The idea introduced here for the "high SNR mode" is as simple as it is effective: the background chopper is rotated at half its usual speed, suppressing every second pulse and avoiding a high intensity pulse impinging on the PG chopper during the counting time frame of the detector. This would usually lead to an intensity decrease of 50 %, but in the case of IN16B the length of the counting time frame could be slightly increased to limit the loss to 37 %.

After introducing the optional "high SNR mode" in August 2016, numerous experiments immediately benefited from the increased sensitivity. It is to be expected that this new method will be highly valuable for many users, maybe even enabling experiments that were deemed to fail due to weak signals that would otherwise remain undetectable.

INDUSTRIAL ACTIVITIES

The ILL provides industrial users with access to state-of-the-art neutron instrumentation and the expertise of its scientific and technical staff.

Contact: industry@ill.fr
https://www.ill.eu/industry/

Industrial and cultural heritage activities at the ILL

AUTHORS
J. Beaucour, D. Atkins, C. Boudou, V. Duchastenier T. Pirling and J. Segura (ILL)

The Industry Liaison Unit (ILU) is the priviledged point of contact for industry looking to use the ILL's suite of instruments for proprietary research. The ILU matches the needs of industrial customers, directs them towards the technique and instrument best suited for their purposes and provides administrative support. The Unit thus ensures fast and confidential access for clients. The ILU may also initiate dedicated partnerships for technological R&D with consortia including academic and industrial partners. During 2016 the ILU dealt with an intense and extremely varied workload, due to the launch of operations on the new industrial instrument D50 of the Platform for Advanced Characterisation – Grenoble (IRT-Nanoclec), the start of the ILL's industrial activities in the SINE2020 Industrial Consultancy initiative[1] and the ILU's ongoing efforts to attract European industry to the unique possibilities at the ILL for research and innovation.

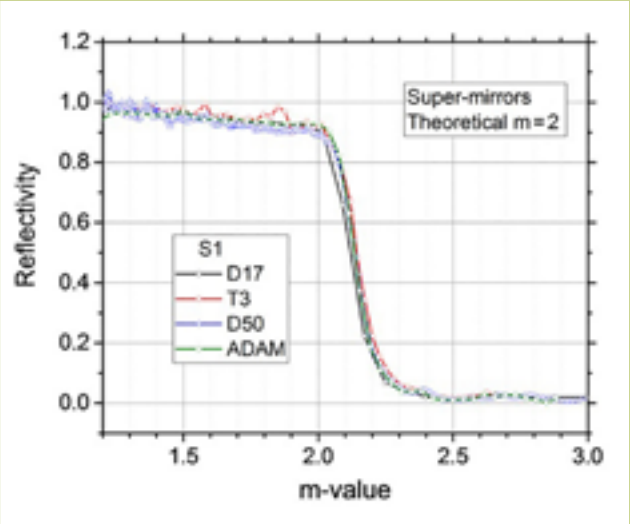

Figure 1
Comparative reflectivity measurements of m = 2 super-mirrors on different ILL reflectometers.

Satisfactory results have already been achieved on the D50 reflectometer set-up, thanks to the innovative Rainbows reflectivity technique used to characterise the mirrors provided by the neutron guides manufacturers. These measures are in good agreement with those obtained on other reflectometers at the ILL (**figure 1**), and further improvements to the instrument are planned in order to provide reflectometry services for the characterisation of neutron guide mirrors in 2017. Moreover, several experiments and feasibility tests were carried out on D50 in 2016. We can cite, as examples of its first industrial users, a microelectronics company and a client working on the development of new radiation shielding materials.

Besides reflectometry, the D50 neutron irradiation set-up was successfully validated and used by a team of experts from **Airbus** to perform single event upset (SEU) tests for electronic reliability purposes. The robustness of on-board electronic circuits exposed to atmospheric neutrons produced by cosmic radiation is a major safety concern in the space and aeronautical industries. The tests on D50 demonstrated the appropriateness of thermal and cold neutrons for the analysis of SEU and we are therefore expecting to attract new clients from aerospace companies.

At the end of 2015 work started on an imaging option for D50 in collaboration with the Université Grenoble Alpes (UGA). The project has been boosted by financial support from TOTAL and EDF. This has enabled UGA to provide the capital and operational costs for the imaging station, including a dedicated scientist and several doctoral students for its day-to-day operations. The applied research fields being targeted are very wide and include CO_2 sequestration, soil stability during earthquakes and advanced concretes (porous media) for long-term nuclear waste storage. Very promising first tomography results were obtained by the UGA/ILU team. The collaboration, baptised **NEutron and X-ray Tomography** (NEXT – Grenoble), has attracted significant interest from academic and industrial quarters. During the instrument's commissioning phase in the late autumn of 2016, experiments were performed for **TOTAL**, **EDF** and the **CEA** as well as for bio-mechanical research (see **figures 2–3**).

[1] http://www.sine2020.eu/industry.html

Figure 2

Neutron radiographies of a hydrogen fuel cell (approximately 10 x 10 cm^2) taken on the D50 tomography set-up. The images (from left to right, top to bottom) show secondary H_2O formation *in operando*. A. Morin (CEA), D. Atkins (ILL) and A. Tengattini (UGA).

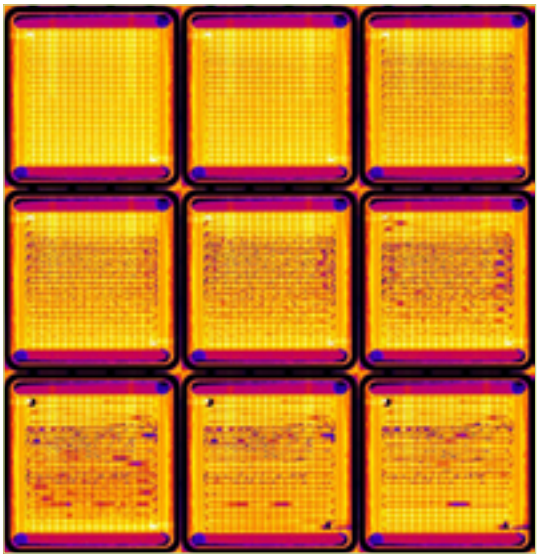

Figure 3

Rendering of neutron tomography data of an animal bone with a titanium screw. Traction pull-out tests coupled with imaging were carried out to quantify the resistance of a bio-mechanical bone/implant and apply these results to human prosthetics. S. Le Cann, E. Tudisco (Lund University), A. Tengattini (UGA).

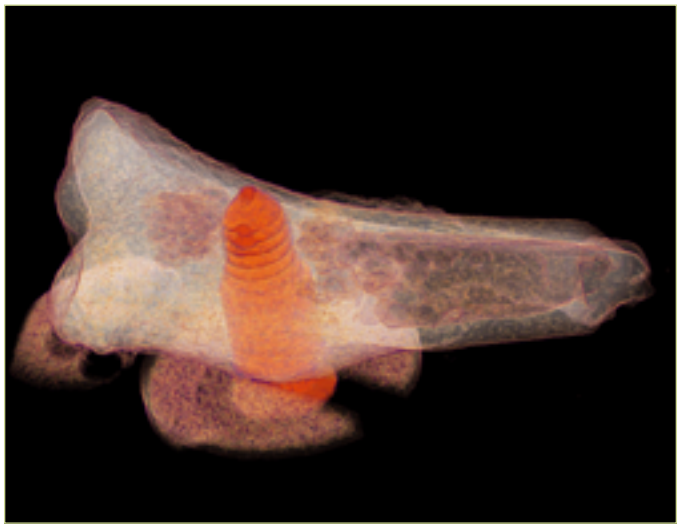

Neutron imaging, along with other techniques such as NAA, PGAA and stress scanning, played a role in various cultural heritage studies carried out by the ILU in 2016, including collaborations with other European neutron centres (HZB Germany, NPI Czech Republic and LLB France) and in experiments involving ILL scientists and health physics experts. This type of project is not only of major societal interest; by highlighting the power of neutron techniques it reinforces the ILL's outreach to industry and the general public. Close relationships were also established with the 3SR (UGA, CNRS) INP-Grenoble Phelma and SIMaP (INP, UGA, CNRS) laboratories for complementary X-ray tomography (see **figure 4** for an example) and metallurgical measures, including a very successful ILU studentship that culminated in a paper being presented at the Synchrotron and Neutrons for Art and Archaeology conference. On the theme of neutrons in cultural heritage, Loic Bertrand (IPANEMA) was invited to the ILL to present *"An overview of the European Research Infrastructure for Heritage Science (ERIHS); current status in France and potential role of Large Scale Facilities"*. His talk outlined the status of this major European initiative, which was accepted for the European Strategy Forum on Research Infrastructure Roadmap 2016. The ILL has expressed its interest in the ERIHS project and looks forward to participating in future initiatives.

The ILU is playing a key role in the Industry Consultancy work package of the European Union's Horizon **SINE2020 programme**. A full-time Industrial Liaison Officer, financed by SINE2020 for three years, started at the ILL on 1st March 2016 with the remit of raising awareness amongst European companies of the added value that neutron methods can bring to Research and Innovation, as well as developing the industrial client portfolio at the ILL. SINE2020 offers in addition, funded neutron feasibility tests to private companies and several experiments have been successfully carried out at the ILL this year involving small-angle scattering (D33) and stress scanning measurements (SALSA).

Within this framework, SALSA (the Stress Analyser for Large Scaled engineering Applications) performed around ten studies for industrial applications, predominantly for the space industry where mechanical specifications are extremely stringent and materials and structures, often operating in extreme conditions, must be optimised in terms of weight, stiffness, lifetime and reliability. Aerospace R&D is a driver of new technologies and SALSA, with its ability to measure stress profiles within real components, can provide crucial answers for the development of new products. An example of this is the mounting structure of a sunlight sensor for space satellites shown in **figure 5**. The device is produced by additive layer manufacturing (ALM), or "3-D printing". This is an extremely attractive method since it allows products to be built up in layers of different thickness (e.g. in the areas where forces are expected). This provides for dramatic reductions in weight (and cost) without compromising stiffness. However, the 3-D printing of complex metallic components can result in high residual stresses, leading to cracks and eventual failure. Non-destructive stress determination is essential for the development and optimisation of ALM, and SALSA has performed comprehensive analyses of different techniques such as wire feed laser melting and blown powder direct deposition, linked to the ESA-driven project AMAZE.

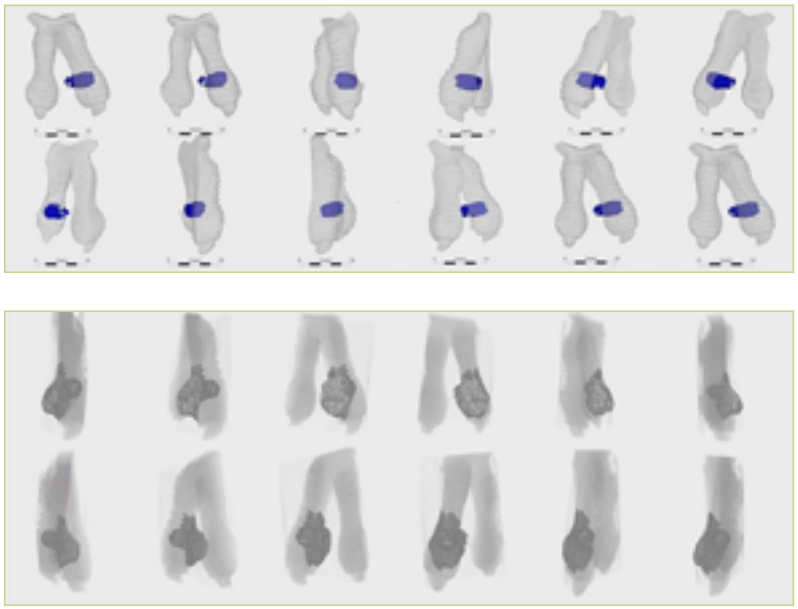

Figure 4

Comparison of tomographic analyses of a Napoleonic eagle talon in brass, found on the site of the battle of Berezina (courtesy of the Centre d'Études Napoléoniennes, France and the Institute of History – National Academy of Sciences of Belarus). The X-ray CT reconstructions (upper series) revealed the inclusion of an object in one of the claws (blue); the central series of images shows the same artefact under neutron tomography; the lower frame shows two views of what was established as an iron screw using both methods – we see the rusted hydrogen-rich surface with neutrons, and the un-corroded centre with X-rays. N-images: D. Atkins (ILL) and N. Kardjilov (HZB); X-images: E. Andò (3SR) and D. Atkins (ILL).

Figure 5

Stress measurements on SALSA, on the support structure of a sun detector used on space satellites.

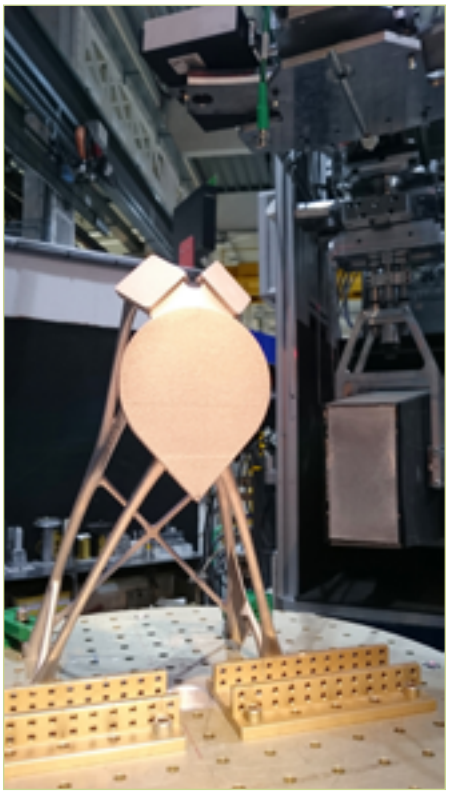

For the object in **figure 5** produced by Thales Alenia Space and Renishaw, SALSA successfully provided 3-D stress profiles of the legs and mounting plates, thus helping to achieve a weight reduction of 50 % in the final structure.

Finally, during 2016 ILU staff liaised with several major French, German and UK companies, with the support of a team of ILL scientists. The prospects are promising. The techniques in demand from potential clients are predominantly diffraction stress analysis, SANS and imaging, along with neutron irradiation. The first of these underlines the importance of SALSA for the ILL's attractiveness to industry; the other techniques will benefit greatly from the new developments on D50 and cover areas such as new energies (hydrogen fuel cells and lithium batteries) and transport (safety studies for aerospace electronics). With these instruments and the diffractometers such as D20 and SANS, the ILL's suite of characterisation techniques is second to none. It offers industrial users unique R&D opportunities for tomorrow's world.

EXPERIMENTAL AND USER PROGRAMME

92 USER PROGRAMME

94 USER AND BEAMTIME STATISTICS

98 INSTRUMENT LIST

Neutron beams and instrument facilities are free of charge for proposers of accepted experiments. Scientists affiliated to the institute's member countries will also, in general, be assisted with necessary travel and daily subsistence for a limited period. The User Support team makes all arrangements for accommodation and will process claims for expenses after users have completed their experiments.

The ILL User Support team (SCO) is dedicated to helping all visiting researchers to make the most of its facilities. If you are coming to the ILL to carry out experiments, the SCO is here to give you the organisational and administrative support you need to successfully perform your experiments.

Our users can now flip through our User Handbook (with practical information for their stay) at: **http://www.ill.eu/fileadmin/users_files/documents/users/user_guide/User_Handbook_web.swf**.

For further information about the institute's facilities, applications for beamtime, user support and the experimental programme, please visit our website at **http://www.ill.eu/users**.

The ILL is firmly committed not only to building high-performance instruments but also to offering the best scientific environment to the user community.

USER PROGRAMME

THE ILL USER CLUB

All administrative tools and information for our scientific visitors are grouped together and directly accessible on the web, courtesy of our user-friendly, online User Club. Club members can log on using their own personal identification to gain direct access to all the information they need. Users with particular responsibilities have privileged access to other tools, according to their role.

https://userclub.ill.eu/userclub/

PROPOSAL SUBMISSION

There are different ways of submitting a proposal to the ILL:

- Standard submission – twice a year – *via* the Electronic Proposal Submission system (EPS)
- Long-Term Proposals (LTPs) – once a year – *via* the EPS system
- Easy access system (EASY) – throughout the year – *via* our User Club website
- Director's Discretionary Time (DDT) – throughout the year – *via* the Head of Science Division
- Special access for proprietary research and industrial users.

Submission of a standard research proposal

Applications for beamtime should be submitted electronically, *via* our Electronic Proposal Submission system (EPS) available on the User Club website. Proposals can be submitted to the ILL twice a year, usually in February and in September. The web system is activated two months before each deadline. Submitted proposals are divided amongst the different colleges (**see box below**) according to their main subject area.

THE ILL SCIENTIFIC LIFE IS ORGANISED INTO 10 COLLEGES:

College 1	Applied Metallurgy, Instrumentation and Techniques
College 2	Theory
College 3	Nuclear and Particle Physics
College 4	Magnetic Excitations
College 5A	Crystallography
College 5B	Magnetic Structures
College 6	Structure and Dynamics of Liquids and Glasses
College 7	Spectroscopy in Solid State Physics and Chemistry
College 8	Structure and Dynamics of Biological Systems
College 9	Structure and Dynamics of Soft-condensed Matter

Proposals are judged by a Peer Review Committee of the subcommittees of the ILL Scientific Council. Subcommittee members are specialists in relevant areas of each College. Two proposal review rounds are normally held each year, approximately eight weeks after the deadline for submission of applications. Before each meeting, the subcommittee receives a report from the appropriate College on the technical feasibility and safety of a proposed experiment. The subcommittee evaluates the proposals for scientific merit and recommends that the ILL Management award beamtime to the highest-priority proposals.

More detailed information on application for beamtime and deadlines is given on our website, at **http://www.ill.eu/users/applying-for-beamtime/**.

Easy access system

The easy access system (EASY) grants diffraction beamtime to scientists from ILL member countries who need a rapid structural characterisation of samples and data analysis. Access is open all year long and allows applicants to bypass the ILL's standard proposal round and consequent peer review process.

The system offers applicants one neutron day per cycle, on two instruments (D2B and D16), in which to perform very short experiments at room temperature. The users are not invited to the ILL but send their samples to one of two designated ILL scientists who are responsible for the measurements and sample radiological control. The ILL ships back the sample once the measurement is finished. Interested parties can apply for EASY beamtime through the User/Visitors' Club. More information is available at **http://club.ill.eu/cvDocs/EASY_Guidelines.pdf**.

Long-Term Proposals

Users from ILL member countries can also apply for extended periods of beamtime by submitting a Long-Term Proposal (LTP). The purpose of this process is to facilitate the development of instrumentation, techniques or software that could be beneficial to the ILL community as a whole, through the award of beamtime over several cycles. The total amount of beamtime that may be allocated to LTPs on any particular instrument is capped at 10 %, and beamtime is not awarded to LTPs to perform science beyond essential testing. LTPs can be submitted once a year at the autumn proposal round, using the specific LTP application form. The length of LTP projects is expected to be three years typically, with continuation approved at the end of each year, based on an annual report; a final report is also required at the end of the project.

More details are given at **http://www.ill.eu/users/applying-for-beamtime/**.

Submission of a proposal for Director's Discretionary Time

A total of 5 % of ILL beamtime is reserved for proposals that do not fall within the usual rules of proposal submission. Primarily these proposals concern urgent experiments that cannot wait for the twice-yearly proposal rounds. Proposals can be submitted at any time and will be reviewed by the chairperson and relevant members of the proposal subcommittee concerned, and the ILL science director. If successful, beamtime on the requested instrument will then be awarded as soon as possible.

In the future, DDT may also be used to award beamtime to excellent proposals that do not satisfy the rule that two-thirds of the proposers must come from the ILL's Associate and Scientific Member countries (see the two-thirds rule below). Such proposals can therefore be submitted by any team with an excellent idea for an experiment, although this must be done through the usual proposal rounds so that the level of excellence can be assessed against that of other proposals.

Experimental reports

Users are asked to complete an experimental report on the outcome of their experiments. The submission of an experimental report is compulsory for every user who is granted ILL beamtime. Failure to do so may lead to the rejection of any subsequent continuation proposals.

All ILL experimental reports are archived electronically and searchable via the web server as PDF files (under **https://userclub.ill.eu/userclub/reportSearch**).

COLLABORATIVE RESEARCH GROUP INSTRUMENTS

The ILL provides a framework in which Collaborative Research Groups (CRGs) can build and manage instruments at the ILL to carry out their own research programmes. CRGs represent a particularly successful form of long-term international scientific collaboration. They are composed of scientists from one or two research disciplines, are often multinational and involve carrying out a joint research programme centred around a specific instrument. CRGs enjoy exclusive access to these instruments for at least half of the beamtime available. The CRGs provide their own scientific and technical support, and cover the general operating costs of these instruments. If there is demand from the user community, and the resources are available, the beamtime reserved for the ILL can be made accessible to users via the subcommittees.

There are currently three different categories of CRG instruments.

- In the **CRG-A** category, external groups lease an instrument owned by the ILL. They have 50 % of the beamtime at their disposal and for the remaining 50 % they support the ILL's scientific user programme.
- In the **CRG-B** category, groups own their instrument and retain 70 % of the available beamtime, supporting the ILL programme for the other 30 %.
- Finally, in the **CRG-C** category instruments are used full time for specific research programmes by the external group, which has exclusive use of the beam.

Support laboratories

The opportunities we offer to our users extend beyond the privilege of access to the world's leading suite of neutron instruments. The ILL – in collaboration with the European Synchrotron Radiation Facility (ESRF) and other institutes – is actively responding to the needs of scientists unfamiliar with neutron techniques and in need of training and support facilities. New support facilities have been already set up on the ILL site. For more information see p.106.

INDUSTRY-SPONSORED ACADEMIC RESEARCH AND INDUSTRIAL USERS

In a research and innovation environment it is essential to demonstrate the long-term impact of academic research, and the medium- and short-term impact of research with industry. Neutrons have significant, specific applications for industry (like the doping of silicon crystals for the semiconductor industry), for pharmaceutical and chemical companies and the production of radio-isotopes for imaging and therapy. Neutron beamtime can be sold directly to industry for proprietary research, in which case the experimental data are not made publicly available. This access mechanism accounts for less than 1 % of beamtime. The Industry Liaison Unit (ILU) is the single point of contact for industry looking to use the ILL's neutron scattering instruments (see p.86).

According to a recent study at the ILL the use of neutrons by industry *via* academia is, however, estimated to be much higher, possibly 25 %. The experimental data from these experiments is publicly available and the results of successful experiments may be published. Given the volume of this industry-relevant access to neutron beamtime, from now on the ILL will measure more accurately the number and nature of industry *via* academia experiments with a view to promoting this use of neutrons and potentially enhancing it in the future. Users are therefore strongly encouraged to specify in their proposal any direct links between their academic research and industry (*via* industry sponsorship, for example, of students or samples).

USER AND BEAMTIME STATISTICS

THE ILL USER COMMUNITY

The ILL welcomed 1 306 users in 2016, including 323 from France, 229 from Germany and 242 from the UK (**figure 1**). Many of our visitors were received more than once (giving a total of 1 801 user visits).

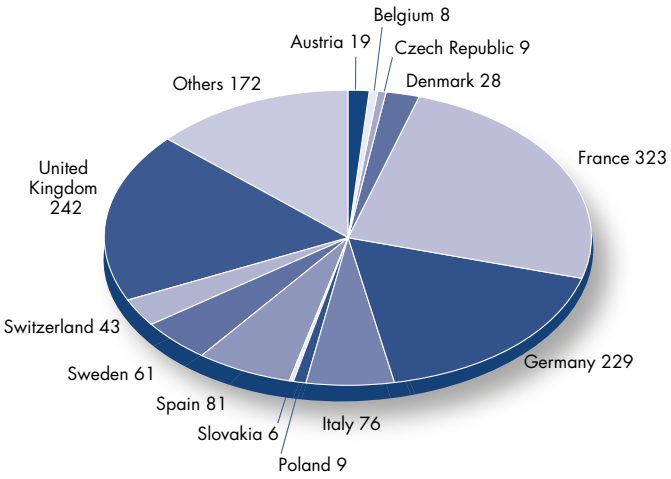

Figure 1: National affiliation of ILL users in 2016.

We value feedback from our users as an indicator of how well our facility is fulfilling their needs and to initiate action when this is not the case (**figure 2**). The *User Satisfaction Form* is a means of finding out what our users think of the facility. Users who have just finished an experiment at the ILL are asked to share their views on different topics by completing the questionnaire through the User Club. User comments are made available to managers for action where appropriate. User feedback rate was close to 70 % in 2016.

INSTRUMENTS

The instrumental facilities at the ILL are shown in the schematic diagram on page 98. The list of operational instruments as of December 2016 is summarised below. Besides the 28 ILL instruments there are nine Collaborative Research Group (CRG) instruments (marked with an asterisk *):

- powder diffractometers: D2B, D20, SALSA, D1B*
- disorder materials diffractometer: D4
- single-crystal diffractometers: D3, D9, D10, D23*
- large-scale structures diffractometers: D16, D19, LADI,
- small-angle scattering diffractometers: D11, D22, D33
- reflectometers: D17, FIGARO, SuperADAM*
- diffuse scattering and polarisation analysis spectrometer: D7
- three-axis spectrometers: IN1-LAGRANGE, ThALES, IN8, IN20, IN12*, IN22*
- time-of-flight spectrometers: IN4, IN5, IN6, BRISP*
- backscattering and spin-echo spectrometers: IN11, IN15, IN16B, IN13*
- nuclear physics instruments: PN1, PN3
- fundamental physics instruments: PF1, PF2, S18*

IN15 has special status since it is a joint venture of the ILL with FZ Jülich. GRANIT* is not listed above because as a CRG-C instrument it is not available as a 'user' instrument. Details of the instruments can be found on our website at **http://www.ill.eu/instruments-support/instruments-groups/**.

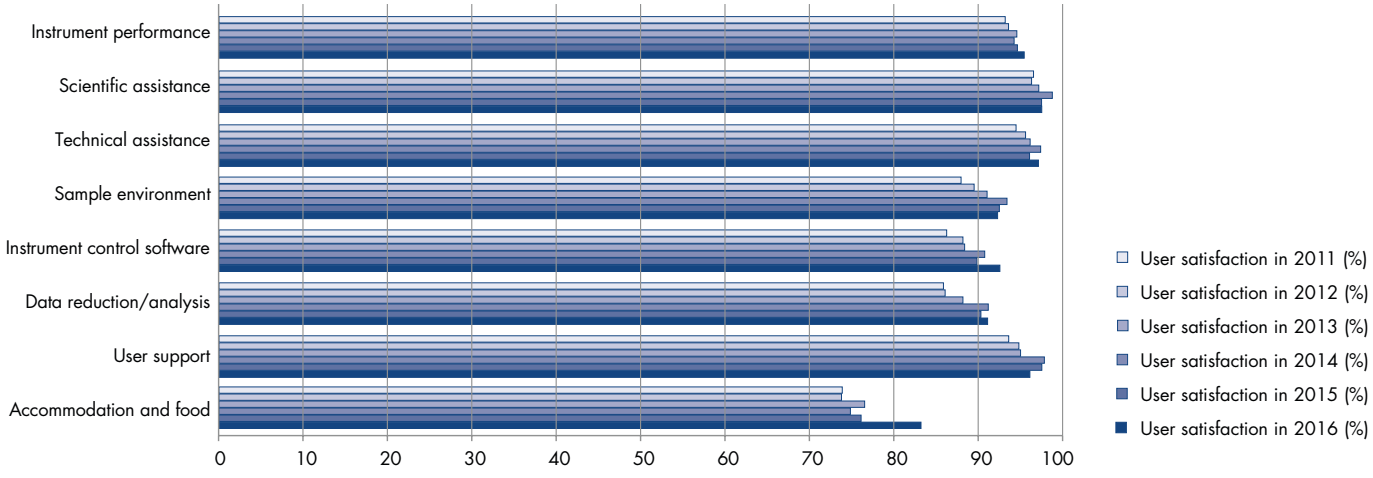

Figure 2: User satisfaction survey results for 2016, compared with those obtained in previous years.

BEAMTIME ALLOCATION AND UTILISATION FOR 2016

During 2016 the reactor operated for 3 cycles, representing 156 days of neutrons (see § Reactor Operation, p.102).

Overall, the subcommittees of the Scientific Council examined 717 proposals requesting 4 404 days in 2016. Of these, 538 proposals received beamtime, requiring the allocation of 2 815 days of beamtime on the different instruments[1]. A total of 595 experiments were scheduled in 2016. The distribution of accepted proposals amongst the different research areas and colleges is given in **figure 3**.

In 2016, the member countries of the ILL were as follows: France, Germany, UK, Austria, Belgium, the Czech Republic, Denmark, Italy, Poland, Slovakia, Spain, Sweden and Switzerland.

Figure 3: Beamtime allocation in 2016: distribution amongst the different research areas (**a**) and colleges (**b**).

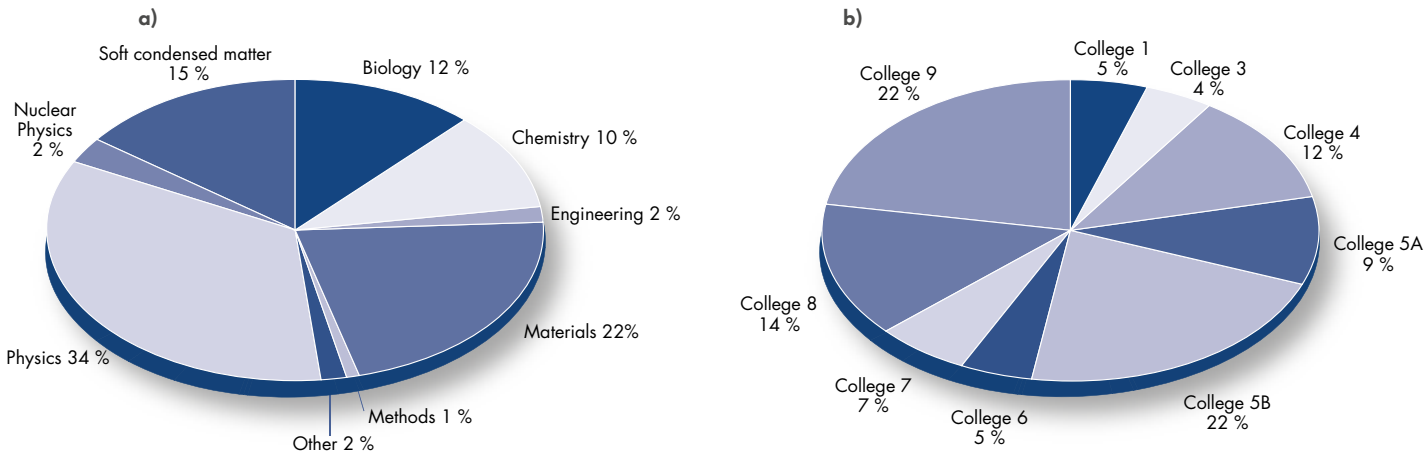

Table 1: Distribution amongst the Associate and Scientific Member countries of beamtime requested and allocated in 2016 during the subcommittees of the Scientific Council. *Proposals from purely non-member countries and from purely ILL or ESRF proposals do not appear in this table and therefore the total request and allocation is different in Table 2.*

	Request days	Request %	Allocation days	Allocation %	Allocation days	Allocation %
Member countries only			Before national balance		After national balance	
AT	167.09	3.82	90.45	3.23	90.40	3.24
BE	23.38	0.53	14.85	0.53	14.72	0.53
CH	266.01	6.08	209.87	7.50	198.51	7.11
CZ	80.23	1.83	57.81	2.07	57.80	2.07
DE	1 132.87	25.90	699.55	25.01	693.87	24.85
DK	59.19	1.35	35.09	1.25	35.05	1.25
ES	175.74	4.02	117.02	4.18	129.10	4.62
FR	1 105.79	25.28	691.22	24.71	688.16	24.64
GB	840.64	19.22	598.67	21.40	603.01	21.59
IT	297.99	6.81	153.93	5.50	153.24	5.49
PL	3.50	0.08	0.00	0.00	0.00	0.00
SE	202.72	4.64	116.55	4.17	116.51	4.17
SK	18.23	0.42	12.16	0.43	12.14	0.43
Total	**4 373.39**	**100.00**	**2 797.16**	**100.00**	**2 792.52**	**100.00**

[1] Yearly statistics are based on the experiments scheduled during the year, e.g. calculated taking into consideration the figures corresponding to the previous year's fall round and current year's spring round. As there was no proposal round in the fall of 2015, these statistics correspond to the spring 2016 round figures, which cover the entire 2016 scheduling period (3 cycles).

USER AND BEAMTIME STATISTICS

Table 1 gives the beamtime distribution amongst the different **member** countries (request and allocation in 2016). In calculating the statistics of beamtime per country, the attribution is based on the location of the laboratory of the proposers, not their individual nationality. For a proposal involving laboratories from more than one member country, the total number of days is divided amongst the collaborating countries and weighted by the number of people from each. Local contacts are not counted as proposers, except when they are members of the research team. The beamtime requested by and allocated to scientists from the ILL, ESRF or EMBL is allocated to the member countries according to a weighting system based on the fractional membership of the country of the institute concerned. When a proposal involves collaboration with a non-member country, the allocated time is attributed entirely to the collaborating member country (or countries), and weighted by the number of people from each member country. Proposals in which all proposers are from non-member countries therefore do not appear in this table. This explains why the total number of allocated days shown here differs from that in **table 2**.

A more complete view of beamtime use is given in **table 2**. Requests for and allocation of beamtime, as well as the number of scheduled experiments, refer to standard submissions to the subcommittee meetings. The effective number of days given to our users also takes into account Director's Discretionary Time and CRG time for CRG instruments.

INSTRUMENT PERFORMANCE

Table 2 also gives a summary of instrument performance for 2016. For each cycle a record is kept of any time lost from the total available beamtime and the reasons for the lost time analysed, for all the instruments. The table gives a global summary for the year.

Overall 4 089 days were made available to our users in 2016 on ILL and CRG instruments, which represents about 73 % of the total days of operation. A total of 339 days were used by the ILL scientists to carry out their own scientific research. About 14 % of the total beamtime available on the ILL instruments was allowed for tests, calibrations, scheduling flexibility, recuperation from minor breakdowns and student training.

Beam days given to science in 2016 amounted to 4 428 (used for users and internal research).

In 2016, 362 out of 5 604 days were lost as a result of various malfunctions, which represents 6 % of the total available beamtime.

Figure 4: Use of ILL beamtime

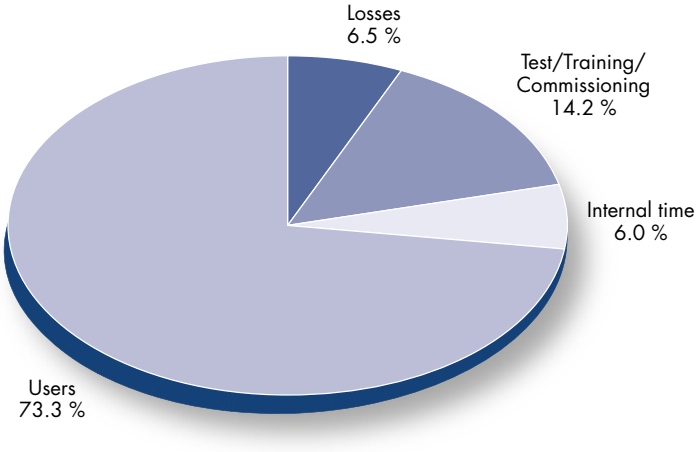

Table 2: Beamtime request/allocation (via standard subcommittees and Director Discretionary Time – DDT together) by instrument and instrument performance. CRG instruments are in blue.

* 'days allocated' refers to only those days reviewed by the subcommittees (i.e., excluding CRG days and DDT)

**'days used' refers to the total number of days given to users (i.e., including CRG days and DDT)

PF2 consists of different set-ups where several experiments are running simultaneously. The values given are averages for these positions.

D4 and IN1 share the same beam port and cannot be run simultaneously.

Instrument	Days requested	Days allocated*	Number of scheduled experiments	Available days	Days used for users**	Days lost	Days for test/ commissioning /training	Days for internal research
BRISP	29	25	3	156	50.0	11.0	45.0	50.0
D1B	58	55	20	155	117.0	5.0	31.0	2.0
D10	107	110	18	156	149.0	7.0	0.0	0.0
D11	141	86	37	156	106.0	2.0	42.0	6.0
D16	123	93	19	156	115.0	3.0	21.0	17.0
D17	199	99	28	156	102.0	11.0	17.0	26.0
D19	148	122	14	156	136.0	8.0	12.0	0.0
D2B	107	77	37	156	131.0	4.0	7.0	14.0
D20	143	103	41	156	140.0	1.0	8.0	7.0
D22	153	84	46	156	101.0	3.0	43.0	9.0
D23	109	38	7	156	145.0	2.0	9.0	0.0
D3	82	88	11	156	93.0	4.0	46.0	13.0
D33	126	92	35	156	103.0	4.0	25.0	24.0
D4	62	43	8	73	61.0	4.0	4.0	4.0
D7	141	99	16	156	130.0	3.0	20.0	3.0
D9	177	93	14	156	116.0	1.0	34.0	5.0
FIGARO	196	104	34	156	121.0	7.0	24.0	4.0
IN1	63	46	8	83	62.0	6.0	8.0	7.0
IN11	149	88	11	156	84.0	0.0	31.0	41.0
IN12	65	43	7	156	125.0	4.0	22.0	5.0
IN13	65	26	3	156	57.0	27.0	12.0	58.0
IN15	151	42	8	156	98.0	13.0	45.0	0.0
IN16B	172	72	21	156	142.0	2.0	7.0	5.0
IN20	77	80	12	156	114.0	33.0	11.0	0.0
IN22	65	36	5	156	120.0	12.0	24.0	0.0
IN4	84	76	18	156	132.0	2.0	11.0	12.0
IN5	247	113	25	156	136.0	2.0	14.0	4.0
IN6	140	90	21	156	131.0	0.0	22.0	3.0
IN8	130	58	10	156	31.0	59.0	66.0	0.0
LADI	221	135	9	156	152.0	0.0	4.0	0.0
PF1B	47	47	4	121	107.0	0.0	6.0	8.0
PF2/4	86	86	3	156	89.0	50.0	16.0	0.0
PN1	93	61	5	156	130.0	13.0	13.0	0.0
PN3 - GAMS 6	91	70	4	156	78.0	10.0	11.0	11.0
SALSA	85	49	9	156	79.0	1.0	42.0	4.0
SUPERADAM	44	40	6	156	125.0	1.0	25.0	5.0
S18	66	66	2	156	130.0	26.0	0.0	0.0
THALES	177	90	16	156	129.0	31.0	23.0	3.0
Total	**4 419**	**2 825**	**595**	**5 580**	**4 089.0**	**362.0**	**790.0**	**339.0**
Percentage of the total beamtime					73.3 %	6.5 %	14.2 %	6.0 %

INSTRUMENT LIST

INSTRUMENT LIST

ILL INSTRUMENTS		
D2B	powder diffractometer	operational
D3	single crystal diffractometer	operational
D4 (50 % with IN1-LAGRANGE)	liquids diffractometer	operational
D7	diffuse-scattering spectrometer	operational
D9	single crystal diffractometer	operational
D10	single crystal diffractometer	operational
D11	small-angle scattering diffractometer	operational
D16	small momentum-transfer diffractometer	operational
D17	reflectometer	operational
D19	single crystal diffractometer	operational
D20	powder diffractometer	operational
D22	small-angle scattering diffractometer	operational
D33	small-angle scattering diffractometer	operational
FIGARO	horizontal reflectometer	operational
FIPPS	fission project prompt x-ray spectrometer	commissioning
IN1-LAGRANGE (50 % with D4)	three-axis spectrometer	operational
IN4	time-of-flight spectrometer	operational
IN5	time-of-flight spectrometer	operational
IN6	time-of-flight spectrometer	operational
IN8	three-axis spectrometer	operational
IN11	spin-echo spectrometer	operational
IN16B	backscattering spectrometer	operational
IN20	three-axis spectrometer	operational
PF1	neutron beam for fundamental physics	operational
PF2	ultra-cold neutron source for fundamental physics	operational
PN1	fission product mass-spectrometer	operational
PN3 – GAMS	gamma-ray spectrometer	on hold
SALSA	strain analyser for engineering application	operational
ThALES	three-axis spectrometer	operational
WASP	wide-angle spin-echo spectrometer	under construction

CRG INSTRUMENTS		
BRISP	Brillouin spectrometer	CRG-B operational
D1B	powder diffractometer	CRG-A operational
D23	single crystal diffractometer	CRG-B operational
GRANIT	gravitation state measurement	CRG operational
IN12	three-axis spectrometer	CRG-B operational
IN13	backscattering spectrometer	CRG-A operational
IN22	three-axis spectrometer	CRG-B operational
SuperADAM	reflectometer	CRG-B operational
S18	interferometer	CRG-B operational

JOINTLY FUNDED INSTRUMENTS		
LADI (50 %)	Laue diffractometer	operated with EMBL
IN15	spin-echo spectrometer	operated with FZ Jülich
GRANIT	gravitation state measurement	operated with LPSC (UJF, CNRS)

TEST AND CHARACTERISATION BEAMS	
CT1, CT2	detector test facilities
CYCLOPS	Laue diffractometer
TOMOGRAPHY	neutrography
OrientExpress	Laue diffractometer
T3	neutron optics test facility
T13A, C	monochromator test facility
T17	cold neutron test facility

INSTRUMENT LAYOUT JANUARY 2017

NEUTRON GUIDE HALL/ILL22

REACTOR BUILDING/ILL5 "NIVEAU D"

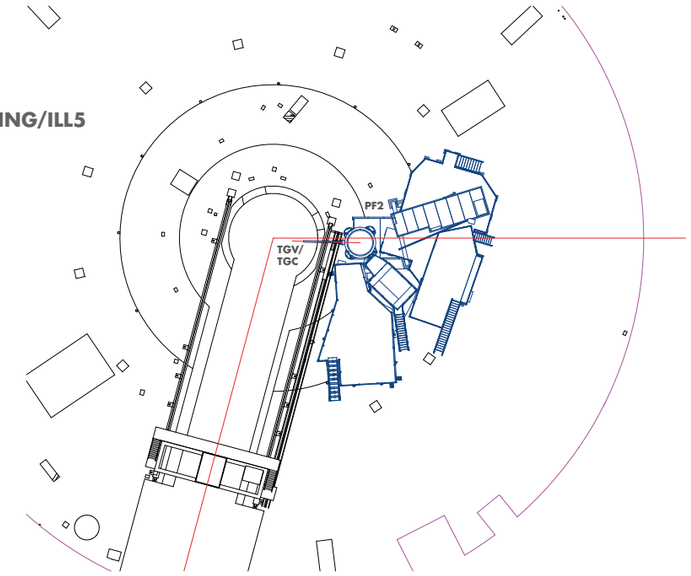

REACTOR HALL/INCLINED GUIDE H4

NEUTRON GUIDE HALL/ILL 7 – VERCORS SIDE (WEST)

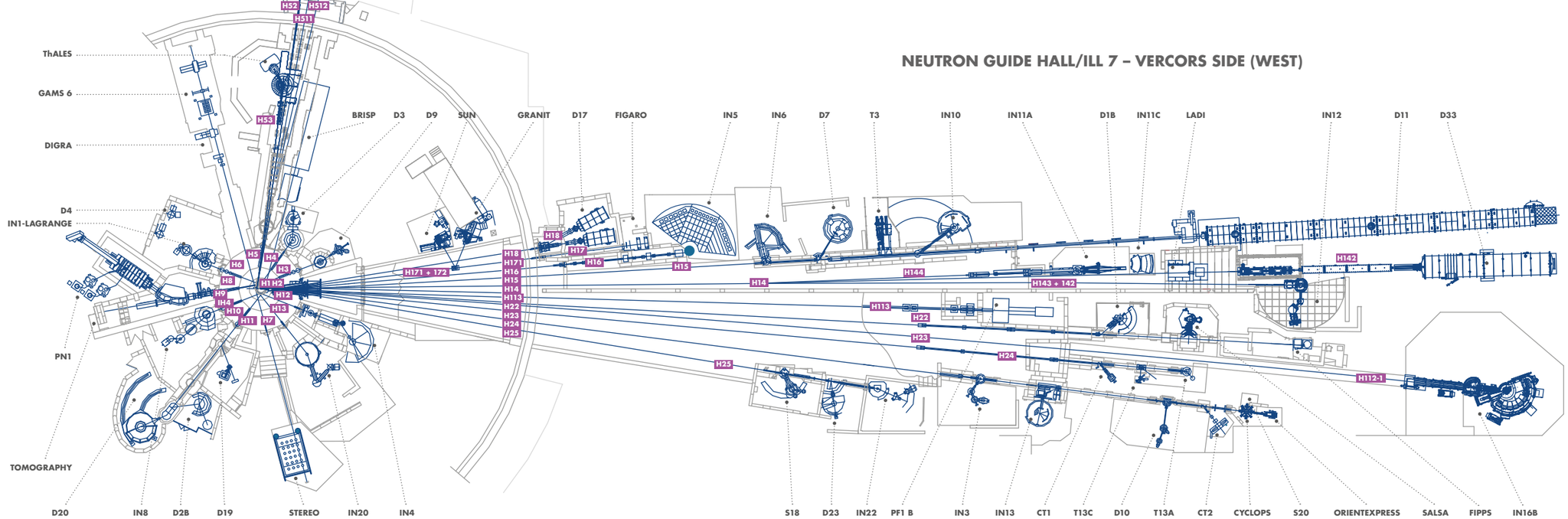

REACTOR HALL ILL 5/EXPERIMENTAL LEVEL (C)

NEUTRON GUIDE HALL/ILL 7 – CHARTREUSE SIDE (EAST)

REACTOR OPERATION

102 REACTOR OPERATION IN 2016

The ILL's High-Flux Reactor (HFR) produces the most intense neutron flux in the world: (1.5 x 10^{15} neutrons per second per cm^2), with a thermal power of 58.3 MW. The reactor normally operates 4 reactor cycles per year. At the end of each cycle there is a shutdown period during which the fuel element is changed and a number of checks are carried out. Occasional longer shutdowns are scheduled to allow for equipment maintenance.

At maximum power, the reactor's fuel element can provide 46 days of operation per cycle. For almost the last ten years our "contract" with our scientific users has been to provide 200 days of operation per year (excluding maintenance and upgrade work). At nominal power this allows for 4.5 cycles per year. For obvious practical reasons, this number of annual cycles is not ideal: for the Reactor Division it involves the same amount of work as having 5 operating cycles, since the tests to be carried out and fuel loading operations are the same before every start-up irrespective of the length of the cycle. As the performance of the instruments has generally been increased by a factor of 20 thanks to the Millennium Programme, we have recently decided to provide the 200 days of operation over 4 50-day cycles, at slightly lower power.

Following the nuclear disaster at Fukushima in 2011, the French nuclear safety authority (ASN) ordered the carrying out of additional safety assessments on all French basic nuclear installations (INBs), including the ILL. This additional safety review has had a major impact on the ILL and its budget over the past few years. Studies were performed by the Reactor Division teams to analyse the behaviour of the ILL reactor under extreme conditions, in particular an earthquake scenario involving major damage to Grenoble and the failure of all the dams on the river Drac – a scenario that would leave the city centre under ten metres of water.

We have been making the necessary improvements to our facility since 2012. The whole programme is due to last six years (from 2012 to 2017) and is being carried out without causing any major disruption to the ILL user programme.

The ILL's High-Flux Reactor (HFR) produces the most intense neutron flux in the world.

REACTOR OPERATION

Reactor operation in 2016

Three reactor cycles were completed in 2016 using three fuel elements. A total of 156 days of scientific activity were provided.

Cycle n°	Start of cycle	End of cycle	Number of days of operation	Number of days scheduled	Power in MW	Number of unscheduled shutdowns
178	19.05.16	16.07.16	58	58	45	0
179	23.08.16	12.10.16	50	50	52.8	0
180	04.11.16	22.12.16	48	48	55.8	0
Total			**156**	**156**	**51 on average**	**0**

The three reactor cycles in 2016 were completed without incident.

The winter shutdown allowed us to complete final commissioning of:

- The seismic depressurisation circuit (part of the "hardened safety core" helping to provide the fourth level of defence-in-depth, namely mitigation through containment); and the seismic annular space pressurisation system, which guarantees the stability of the metal containment even in the event of an extreme earthquake as defined in the additional safety review performed following the accident at Fukushima
- The instrumentation and control racks for the containment system (part of the "hardened safety core") in the reactor control room and the remote reactor control room
- The seismically resistant reactor shutdown system
- The power supply cut-off on reaching the second seismic threshold.

The winter shutdown was also used to remove the new pumps of the shutdown cooling system in order to replace their bearings, to install new electrical distribution racks and to begin the first phase of work on upgrading fire alarm systems in order to ensure their compliance.

A spectacular operation was also carried out in 2016. As part of the extreme earthquake scenario considered under the ILL's post-Fukushima reinforcement programme, we were unable to demonstrate the stability of the reactor's 45-metre high chimney stack. The best option in the end was to remove the top 30-metre stretch of the chimney that was built in concrete, and rebuild it with much lighter steel parts. Calculations show that the new chimney will resist extreme earthquake conditions and pose no threat to the nearby PCS3 control room (see photos).

A few photos of a spectacular operation: the replacement of the reactor's 45-metre high chimney stack.

THE KEY REACTOR COMPONENTS (KRC) PROGRAMME

The aim of the KRC programme is to upgrade or replace some of the reactor's most important components in order to guarantee its safety and reliability for the coming years of operation.

The programme, which was launched in 2005, is ongoing.

The main work still to be completed under the KRC programme includes:

- The replacement of beam tubes
- The upgrade of the out-of-pile part of the horizontal cold source, including its instrumentation and control system
- The putting into service of a hafnium safety rod
- The procurement of replacement cells for the cold sources.

MAIN WORK PLANNED FOR 2017

Maintenance operations:

- Heavy maintenance of main diesels.

Work on the Key Reactor Components:

- Putting into service of a prototype safety rod made of hafnium (safety rods are currently manufactured using a silver-indium-cadmium alloy)
- Replacement of beam tubes H3 and H8 and removal of through-going beam tube H6/H7.

Work following the post-Fukushima safety assessment:

- Commissioning of the groundwater circuit, involving modifications to the emergency core reflood system, which will bring to an end the post-Fukushima programme. These systems form the third level of defence-in-depth, namely prevention by guaranteeing the water inventory around the reactor core and hence the efficiency of cooling by natural convention.

RADIOACTIVE WASTE AND EFFLUENTS

The ILL's activities in 2016 generated waste and effluents respecting the regulatory limits applicable to our installation, as follows:

Evacuation of radioactive waste	Quantity
Decay bin (60 l)*	0
5 m^3 pre-concreted crate (low and intermediate level waste)	0
5 m^3 crate (low and intermediate level waste)	6
200 l HDPE drums of "incinerable" waste	47
120 l HDPE drums of "incinerable" waste	41
120 l HDPE drums (laboratory waste)	8
30 l cylinders (liquid)	3

** The decay bins contain high-level waste. After a period of interim storage in dedicated facilities they will be transferred to ANDRA's deep disposal site CIGEO, once it is operational.*

Gaseous effluents	Released in 2016 (TBq)
Tritium	4.9
Rare gas	0.92
Carbon-14	0.36
Iodine	0.0000041
Aerosols	0.00000013

Liquid effluents	Released in 2016 (TBq)
Tritium	0.038
Carbon-14	0.00022
Iodine	0.00000063
Other activation products	0.00022

MORE THAN SIMPLY NEUTRONS

106 PARTNERSHIPS
108 TRAINING AND OUTREACH

In order to maintain their ranking on the international scene, European research institutes must optimise their resources and develop synergies at every level.

The ILL is firmly committed not only to building high-performance instruments but also to offering the best scientific environment to the user community. We have established successful collaborations with neighbouring institutes over the years, and launched many successful scientific and support partnerships.

In addition, the ILL and the ESRF have transformed our joint site into a research campus – the European Photon and Neutron science campus, or EPN-campus for short – with a truly international reputation. The EPN science campus is a unique, international science hub in Grenoble, hosting three major European institutes – EMBL, ESRF and the ILL – along with the IBS (**http://www.epn-campus.eu/**).

Last but not least, training and outreach forms a major part of the ILL programme, and happens in a wide variety of ways. The ILL Graduate School and PhD programme are intended to train the next generations of neutron users. In parallel, schools, training sessions and local initiatives for Masters and PhD students are organised throughout the year. Through regular open days on the EPN-campus and yearly participation in the local science festival, we also hope to inspire new vocations in science disciplines or at least to broaden the general public's awareness of science.

The EPN science campus is a unique, international science hub in Grenoble, hosting three major European institutes – EMBL, ESRF and the ILL – along with the IBS.

PARTNERSHIPS

PARTNERSHIP FOR SOFT CONDENSED MATTER

The Partnership for Soft Condensed Matter (PSCM) is a joint ILL-ESRF initiative that provides enhanced support services to ESRF and ILL users addressing contemporary challenges in soft matter research, including nanomaterials, environmental and energy sciences, biotechnology and related fields. The PSCM offers on-site sample preparation and characterisation facilities located in the Science Building, which is physically connected to both the ILL and ESRF experimental halls. The collaborative development of specialised sample environments and instruments enables cutting-edge experiments for investigating the structure and dynamics of bulk and interfacial soft matter systems.

In addition to daily users' support, the PSCM is continually seeking to strengthen the soft matter research community through the search for new collaborative partners and the establishment of long-term collaborations between academic and industrial research groups and the experimental teams developing the ESRF beamlines and ILL instruments. The resulting enhanced research capabilities and methodological developments are made available to the entire user community.

In 2016, the PSCM hosted around 150 ILL users and 15 visiting scientists and students.

The PSCM is located on the 2nd floor of the Science Building, alongside the Soft Matter Science and Support Group (SMSS).

Users wishing to use the PSCM laboratories and equipment in conjunction with neutron measurements should indicate this when submitting their request for beamtime. Further details can be found at **http://www.epn-campus.eu/pscm/**.

PARTNERSHIP FOR STRUCTURAL BIOLOGY

The Partnership for Structural Biology (PSB) contains a powerful set of technology platforms that are contributed by the various partner institutes (ILL, ESRF, EMBL, IBS and the unit for host-pathogen interactions). These platforms include advanced capabilities that strongly complement the neutron scattering facilities available to ILL users: synchrotron X-rays, electron microscopy, nuclear magnetic resonance (NMR), high-throughput methods (e.g. soluble expression and crystallisation), and a range of biophysical techniques such as isothermal calorimetry and surface plasmon resonance. The PSB includes the Deuteration Laboratory (see below) as a user platform and the joint SANS/SAXS platform. In addition, there is strong connectivity and collaboration between the ILL and ESRF life sciences/structural biology and industry groups.

The aim of the PSB is to enhance the interdisciplinary capabilities of each of the facilities co-located on the site. The Carl-Ivar Brändén building (CIBB) is the principal site for the PSB and its partner organisations. Further details are provided on the PSB website **http://www.psb-grenoble.eu/**.

DEUTERATION LABORATORY (D-LAB)

The D-Lab user programme uses *in vivo* recombinant expression approaches to provide deuterated analogues of proteins and lipids for the study of structure (crystallography, SANS, fibre diffraction) and dynamics (EINS) using neutron scattering. The platform is therefore of central importance to the activities of biological work relating to all the ILL instrument groups. The group is involved in a wide variety of externally funded programmes that exploit the capabilities of the PSB as well as promoting interdisciplinary structural biology. It also interacts strongly with industry. Each year the group takes a small number of undergraduate placement students who are trained in many of these techniques and contribute to method development activity.

Access to the D-Lab platform is managed through a rapid, peer-review proposal system (**http://www.ill.eu/deuteration**). Successful applicants from ILL Member state countries are provided with deuterated material without charge if the neutron experiment is carried out using ILL facilities. Other applicants are expected to contribute to the costs involved.

CHEMISTRY LABORATORIES

The Chemistry Laboratories, together with the PSCM Laboratories, are managed by the Soft Matter Science and Support Group (SMSS). The main goal is to provide ILL Users with the ability to prepare and characterise their samples during their neutron experiments, but also to support the in-house research conducted by instrument scientists and PhD students.

The main facilities are based in the Science Building, while a further three sample preparation labs can be found in the guide halls ILL7 and ILL2. The laboratory next to D11 in ILL7 has been completely renewed and will be ready for operation with the first cycle in 2017.

The laboratories are stocked with basic equipment, glassware, consumables and the chemicals necessary to prepare samples for a variety of different neutron experiments. More specific equipment, such as high-temperature furnaces, a glovebox or an enclosure for handling nano-powders, are also available. Different methods for sample characterisation, such as UV-Vis, FTIR, light scattering and more, are offered by the PSCM laboratories. Further information on the Chemistry Laboratories can be found on **http://www.ill.eu/instruments-support/labs-facilities/chemistry-laboratories/home/**.

MATERIALS SCIENCE SUPPORT LABORATORY

The joint ILL-ESRF Materials Science Support Laboratory (MSSL) provides a range of support to users, from advice with experiment proposals, through sample preparation to the performance of the experiment. We provide equipment for tensile testing, hardness testing and microscopy as well as the fabrication of specialised sample holders. In particular, the Laboratory works with users to optimise the experimental methodology before the start of an experiment. This takes the form of standardised specimen mounting, digitisation of samples and definition of measurement macros. It is recommended that users contact us well in advance and arrive at the ILL a day or two prior to the start of an experiment, to enable these off-line preparations to be performed.

More information may be found on the MSSL's website **http://www.ill.eu/sites/mssl/**.

COMPUTATION LABORATORY (C-LAB)

The Computation Lab offers support to ILL users for atomistic simulations using classical and *ab initio* methods. Typical applications for simulations are structure, phonons and (some) magnetism in crystals, and structure and dynamics in (partially) disordered systems ranging from liquids and glasses to macro/bio-molecular systems. As samples become more complex, simulations can provide key, complementary information that helps to interpret experimental data and understand how systems behave. Scientists and thesis students at the ILL benefit from the software, hardware and expertise of the C-Lab, while users can benefit *via* their local contacts.

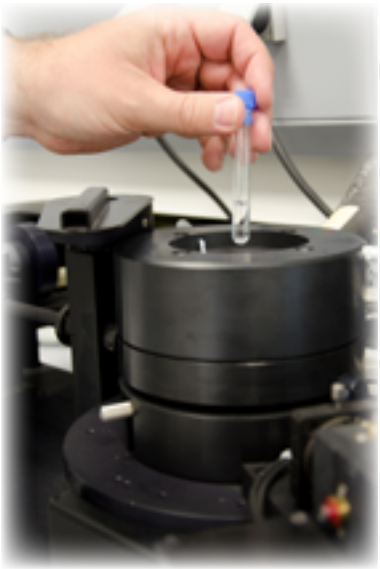

TRAINING AND OUTREACH

STUDENTS TRAINING

Through the **ILL PhD programme**, the **ILL Graduate School** has grown in strength over recent years. It currently involves around 40 students, of many different nationalities, who are wholly or partially supported by the ILL or, in a few cases, financed by other sources. In the recent 2016 call for proposals for PhD projects some 47 applications were submitted, of which ten full-time equivalent projects will be selected in spring 2017 and students subsequently recruited.

Since the students work in different disciplines, their annual **clip session** gives them the opportunity to exchange ideas and get to know one another better. This is also an occasion for the ILL staff at large to meet the students and learn about their projects. The 2016 clip session on 6 June, once again challenged the students to present their work in five minutes. This event was entertaining as ever, with some presenting on their levitating samples as fast as their mouths could go and others attempting to discuss all the data from their thesis in the given time! It is a tradition to grant a diploma and prize to the best presentation of each year of thesis work.

Running throughout the year a set of seminars (titled "**All you need is neutrons**" in 2015-2016) is held on a weekly basis. The speakers are the PhD students themselves and the topics cover aspects of neutron science and current PhD projects.

In 2016, the ILL again offered Masters and PhD students from the local university, "Université Grenoble Alpes" (UGA), the opportunity to take part in real neutron scattering experiments, within the framework of the so-called **TP CESIRE**. Co-ordinated by Paul Steffens, and thanks to the support of a number of ILL scientists interested in this project, experiments with appropriate topics and experimental set-up are constantly selected for this purpose. This year, 13 UJF (Université Joseph Fourier) Masters students participated in some TP CESIRE experiments performed on both ILL and CRG instruments.

TRAINEES

The ILL welcomed a total of 78 trainees in 2016 (10 from the ILL ESRF summer school, 2 from the UGA-ILL summer school, 7 from the STFC), of 24 different nationalities (including 12 German, 30 French, 14 British and 11 from other ILL Member countries).

The ILL PhD students after their clip session on 6 June.

HERCULES SCHOOL

This one-month course, co-ordinated by the "Université Grenoble Alpes", is designed to provide training for students and postdoctoral and senior scientists from European and non-European universities and laboratories in the field of neutron and synchrotron radiation for condensed matter studies (biology, chemistry, physics, materials science, geosciences and industrial applications). It includes lectures, practicals and tutorials, visits to large facilities and a poster session (each participant puts up a poster about her/his thesis or research topic for a day). A special seven-day programme is included, hosted in a partner institution (including the ILL). In 2016, the school took place from 29 March to 29 April. More information is available at **http://hercules-school.eu/**.

SCIENCE FESTIVAL

On Saturday 8 October, the four EPN-campus institutes took a stand at the French Science Festival "Fête de la Science". We welcomed most of the 2 800 curious and enthusiastic visitors who came to the Grenoble "Parvis des Sciences" that day. The public discovered the different activities and research carried out on the EPN Science Campus guided by more than 30 passionate volunteers from the four institutes, demonstrating once again their complementarity and the importance of geographical proximity.

Half of the stand highlighted the large-scale facilities (ILL/ESRF) and their wide range of scientific activities. The other half was dedicated to structural biology, with many hands-on activities coming from EMBL Heidelberg. A great success, without a doubt.

Top: Photo Science festival.

Bottom: Young visitor playing with carbon allotropes.

WORKSHOPS AND EVENTS

111 CHRONICLE
112 SCIENTIFIC EVENTS
114 A YEAR IN PHOTOS

ILL CHRONICLE 2016

12 JANUARY
Visit by Christophe Ferrari (Métro)

27 JANUARY
Visit by a delegation from Lund

16 FEBRUARY
Visit by a delegation from Japan

2 MARCH
STFC/ILL/ESRF Directors' meeting

10 MARCH
Visit by the Préfet of the Isère region

12-15 APRIL
Meetings of the ILL Scientific Council and its Subcommittee meetings

10-11 MAY
Meeting of the Subcommittee on Administrative Questions (SAQ)

26 MAY
Visit by a delegation from PANASONIC

21-22 JUNE
Meeting of the Steering Committee

27 JUNE
Visit by Madame Rector of the Academy of Grenoble, Claudine Schmidt-Lainé

28 JUNE
Visit by Eric Piolle, Mayor of Grenoble

7 JULY
Visit by a delegation from Luxembourg

11 JULY
Visit by Vincent Berger (Director of Fundamental Research at CEA)

12 JULY
Visit by a delegation from the Institute of Nuclear Physics, Republic of Kazakhstan

18-19 OCTOBER
Meeting of the Subcommittee on Administrative Questions (SAQ)

22-25 NOVEMBER
Meetings of the ILL Scientific Council and its Subcommittee meetings

30 NOVEMBER – 1 DECEMBER
Meeting of the Steering Committee

SCIENTIFIC EVENTS IN 2016

Scientific events

In 2016, the ILL organised (or jointly organised) **10 scientific events** (workshops, conferences and schools). Short reports on the ILL workshops can be found on the ILL News for Reactor Users (June and December 2016 issues) – **http://www.ill.eu/quick-links/publications/ill-news/**.

Workshops websites can be found at **http://www.ill.eu/news-events/past-events/**.

18 JANUARY
Biology day

7-11 MARCH
ADD 2016 – School and Conference on Analysis of Diffraction Data in Real Space

30-31 MARCH
Workshop on Neutron Spectroscopy in Condensed Matter Physics (to mark Louis Pierre Regnault's retirement)

2 MAY
Homage to Bernard Jacrot

9-14 MAY
FullProf School 2016

6 JUNE
PhD students clip session

28 AUGUST – 2 SEPTEMBER
ECOSS 2016 – European Conference on Surface Science

28 AUGUST – 23 SEPTEMBER
X-Ray and Neutron Science – International Student Summer School 2016

12-16 SEPTEMBER
ISMC2016 – 4th International Soft Matter Conference

12-16 DECEMBER
Workshop on New Trends in Magnetic Structure Determination

1

2

3

1. Participants at the School and Conference on Analysis of Diffraction Data in Real Space (ADD 2016).
2. The EPN campus stand at the European Conference on Surface Science (ECOSS 2016).
3. Participants at the 4th International Soft Matter Conference.

ILL seminars organised in 2016

51 general seminars were organised at the ILL in 2016, in addition to **7 colloquia**.

The list of colloquia can be found at
https://www.ill.eu/press-and-news/colloquia-seminars-talks/ill-colloquium-series/2016/.

11 January H. Gunnlaugsson
Emission Mössbauer spectroscopy at ISOLDE/CERN

14 January H. Kohlmann
A sapphire single-crystal cell for *in situ* neutron powder diffraction of solid-gas reactions

19 January A.K. Petoukhov
Towards a broad-band solid polariser with flipping ratio of thousands

26 January E. Bahn
Molecular diffusion on surfaces of carbon materials

26 January C. Bousige
Structure and dynamics of model carbon systems and other less model systems

26 January I. Calvo-Almazán
2D diffusion of poly-aromatic hydrocarbons (PAH) on graphite

26 January C. Cavallari
Local structure and dynamics of hydrogen in defective graphene

26 January A. Lazzarini
Structural and surface characterisation of activated carbons through multi-technical tools

26 January T. Lorne
Study of covalent grafting of Fluorescein Isothiocyanate on double-walled carbon nanotubes

26 January S. Mamone
Spectroscopy of light-molecule endofullerenes

26 January A.C. Selvati
Photo-active molecules encapsulated inside single-walled carbon nanotubes

28 January R. Reifarth
Measurements of neutron-induced reactions in inverse kinematics

1 February R. Boffy
Irradiation ageing of alkali-borosilicate neutron guides

4 March A.N. Andreyev
Low-energy fission and beta-delayed fission with radioactive beams

11 March B. Frandsen
A new spin on pair distribution function analysis: Introducing magnetic PDF

16 March J. Akola
Quantum confinement effects and atomic-scale simulations of interactions in biological environments

24 March B. Vestergaard
Structural analysis of amyloid-like protein fibrillation using SAXS as a central tool

29 March I.A. Zaliznyak
Spin-liquid polymorphism in a correlated electron system on the threshold of superconductivity

5 April E. Pierre
Status of the KEK/RCNP/TRIUMF UCN/nEDM project

6 April M. Jentschel
The PN3 ultra-high resolution gamma spectrometry facility

7 April P. Bender
Polarised SANS as advanced characterisation technique within the NanoMag project

28 April R. Palacin
Batteries beyond Li-ion: Viability of alternative chemistries

9 May L. Pusztai
Neutron diffraction of hydrogenous materials: Measuring incoherent and coherent intensities separately

19 May S. Holbein
Magnetic excitations in the chiral multiferroic $TbMnO_3$

24 May L. Falvelo
Reaction and proton transport dynamics in non-porous molecular crystals

3 June P. Niga
Anaesthetic drug interaction with the phospholipid membrane

7 June M. Johnson
Ultrathin organic films for protection against atmospheric corrosion

15 June S. Degenkolb
Precision measurements with noble gases: Magnetometry and EDM searches

15 June L. Piculell
Complex salts: Controlling love and hate

28 June M. Pedrosa
Radiobiology data for improving BNCT treatment planning

22 July T. Coetzer and M. Papathanasopoulos
Host pathogen interactions in malaria and HIV infection: A SANS/SAXS study

25 August D. Ciumac
Selective interactions of a short antimicrobial peptide with model lipid monolayers

26 August I.R. Evans
Structural chemistry of functional materials: Complexity in the solid state

29 August P. Arnold
Organometallic f-block complexes with multiple-electron reductive activation reactivity

12 September V.V. Voronin
Test of the equivalence of inertial and gravitational neutron masses by Laue diffraction

19 September Y. Hasegawa
Quantum paradoxes emerging in neutron interferometer experiments

27 September G. Zaccai
Ectoine effects on water H-bonding and hydration around a soluble protein and a cell membrane

12 October R. Dos Santon Morais
Membrane – interfacial protein interactions: SAXS, SANS and molecular modelling analysis of dystrophin 3D structure in the presence of membrane lipids.

16 October P. Butler
A new collaborative computational project for the atomistic or coarse-grained modelling of SANS and SAXS data

18 October J.W. Brady
Probing water structure with neutron scattering and computer simulation

04 November I. Dhiman
Current status of CG-1D imaging beamline at ORNL

19 November L. Ciano
Degradation of cellulose by lytic polysaccharide monooxygenases

22 November B. Clément
Status and perspectives of the GRANIT facility

28 November J. Li
The observation of the oxygen-oxygen interactions in ices

30 November D. Deamer
Combinatorial chemistry in the prebiotic environment

2 December M.P. Krafft
Dynamic self-assembly induced by fluorocarbons: Applications in medicine

2 December O. Petrenko
Low-temperature magnetism in the honeycomb systems SrRE2O4

15 December M. Wolff
New light on an old problem: The solid-liquid boundary condition

16 December M. Roth
Can lasers complement or even replace particle accelerators for radiation facilities?

A YEAR IN PHOTOS

Visits and events

1

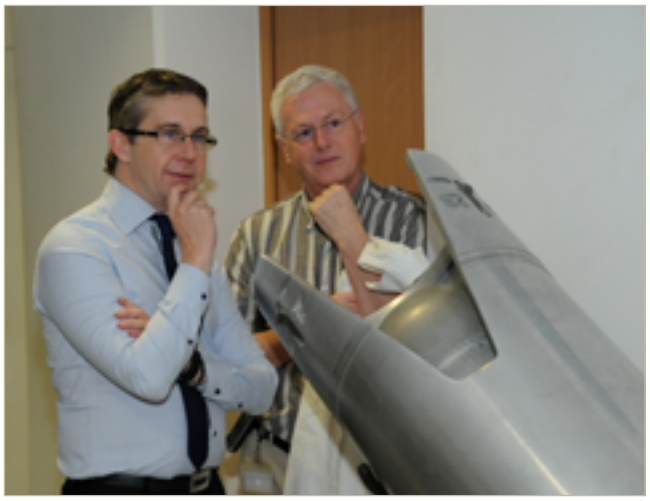

2

3

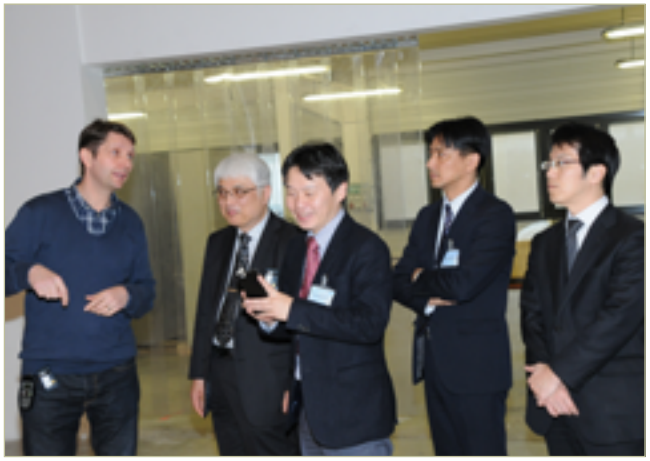

4

5

6

Goodbye Bill and Manuel!

7

8

9

10

On Thursday, 29 September, the ILL celebrated the retirements of Manuel Rodriguez-Castellano, Head of Administration since 2012, and Bill Stirling, after a tenure of 33 months as Director-General of the ILL.

On 1 October, Helmut Schober became the new Director of the ILL, with Mark Johnson the new Science Director and Alexandre Durand the new Head of Administration.

1. Bruno Desbrière (ILL, right) at the fuel element mockup with Christophe Ferrari, president of the Métro, Grenoble Alpes during his visit on 12 January.

2. Colin Carlile (former ILL Director and now professor at Lund University) accompanying a delegation from Lund during a visit to the ILL on 27 January.

3. Bruno Demé (ILL, left) accompanying Mr. Mitsuyuki Ueda (Ministry of Education, Culture, Sports, Science and Technology, Japan), Mr. Tetsuya Ishikawa and Mr. Makina Yabashi (RIKEN SPring-8 Center, Japan), alongside Mr. Ichiro Ikeda (Embassy of Japan in Paris) during a visit on 16 February.

4. Visit by a delegation from PANASONIC on 26 May.

5. Helmut Schober (ILL Director) welcoming Mrs Claudine Schmidt-Lainé, the Rector of the Academy of Grenoble.

6. A delegation from the Institute of Nuclear Physics of the Republic of Kazakhstan accompanied by Valery Nesvizhevsky during a visit to the ILL on 12 July.

7. Bill Stirling (left) and Helmut Schober (right), former and present Director of the ILL, respectively.

8. Manuel Rodriguez-Castellano, Head of ILL Administration from 2012 to 2016.

9. From left to right: Bill Stirling, Miriam Perrin (ESRF), Jenny (Bill's spouse), Patricia Cuccari, Jutta Burat, Marie Mucci (ESRF) and Manuel Rodriguez-Castellano.

10. The new ILL Management Board, from left: Charles Simon, Mark Johnson, Helmut Schober, Alexandre Durand and Hervé Guyon.

A YEAR IN PHOTOS

Happy users

1

2

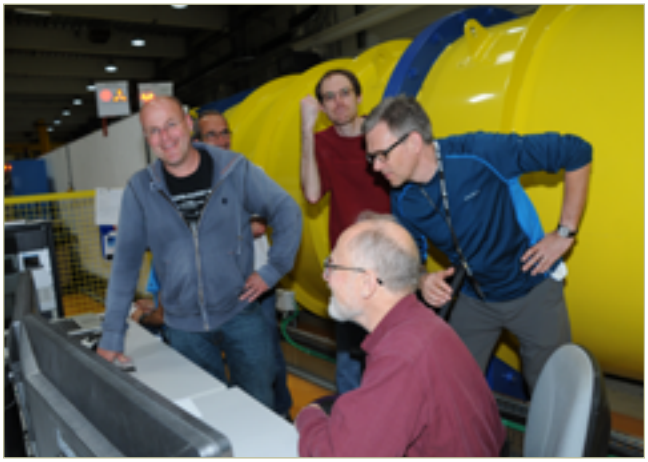

3

4

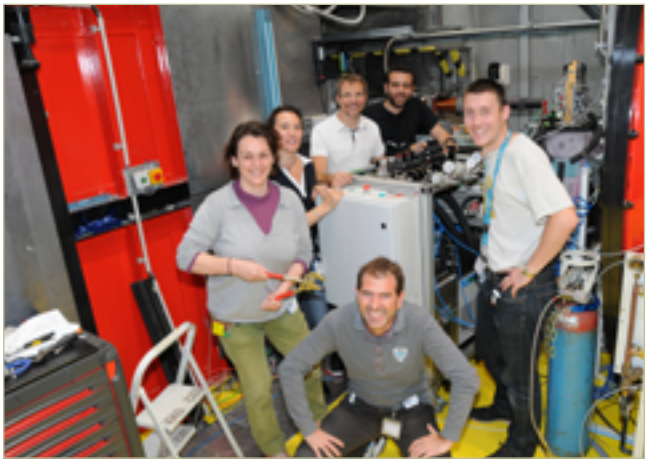

5

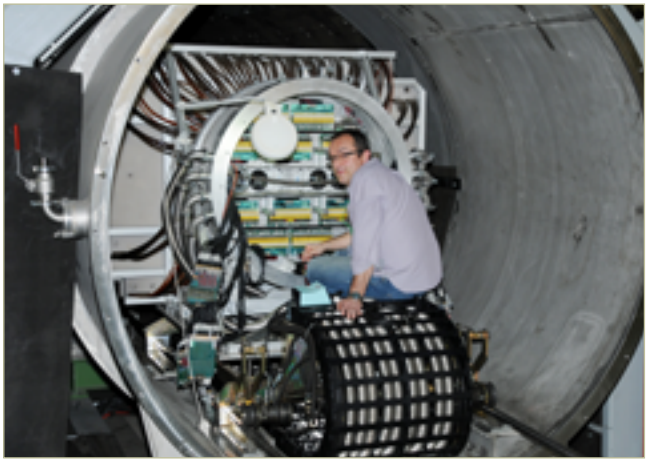

1. Sine Larsen (University of Copenhagen) during an experiment on D19.
2. Charles Dewhurst, Michel Bonnaud (ILL), Bill Halperin, Keenan Avers (Northwestern University, USA) and Morten Eskildsen (Notre Dame University, USA) on D11.
3. Happy User Kristina Vlášková (Charles University) with Marek Koza (ILL).
4. Sandrine Lyonnard (CEA-DRF/INAC), Sylvie Escribano, Arnaud Morin (CEA-DRT/LITEN), Nicolas Martinez (CEA-DRF/INAC), Laurent Jacqmin (CEA-DRT/LITEN) with Lionel Porcar (ILL) on D22.
5. Paolo Mutti (ILL Instrument Control Service) reparing the BRISP detector.

6

7

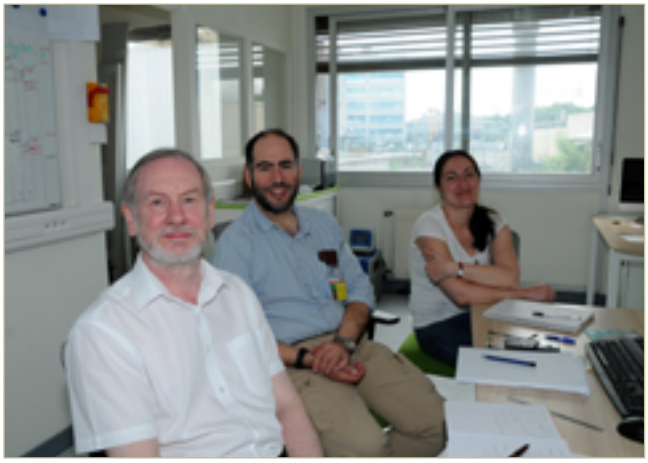

8

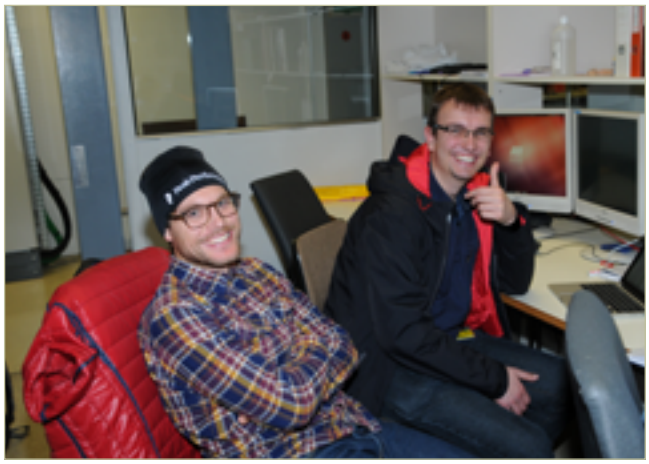

9

10

6. Stéphane Pailhes, Valentina Giordano (Université Lyon), Frédéric Bourdarot (CEA Grenoble INAC/SPSMS) and Marc de Boissieu (SIMAP – GRENOBLE INP).

7. David Barlow (King's College) and his team during their experiment on membrane rafts.

8. Gerard Perren (left) and Johannes Moeller (ETH Zürich) during their experiment on IN5.

9. Jano Heppt, Tilo Schmutzler, Torben Schindler (University of Erlangen) during an experiment on D11.

10. Meriem Chrifi-Alaoui, Gilles Despaux, Emmanuel Le Clézio (Université Montpellier) visiting the ILL with Yoann Calzavara (ILL).

FACTS AND FIGURES

119 FACTS AND FIGURES

121 PUBLICATIONS

122 ORGANISATION CHART

STAFF ON 31/12/2016

486.5 people including 70 experimentalists in the scientific sector and 38 thesis students.

343 French, 44.5 German, 38.5 British, 44 scientific participating countries and 16.5 others.

Country		%
French	343.0	70.50 %
German	44.5	9.15 %
British	38.5	7.91 %
Member countries	44	9.04 %
Others	16.5	3.39 %
Total	**486.5**	**100 %**

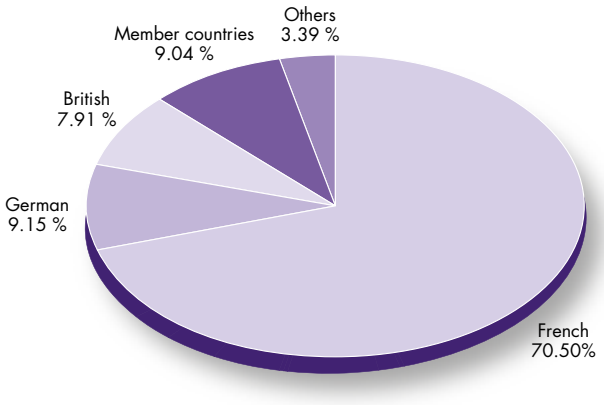

REVISED BUDGET 2016: 98,136 M€ (excluding taxes)

Income	M€	%
Income from Associates (incl. Fukushima & Millennium Progamme & add. nuclear tax)	65.607	66.85 %
Income from Scientific Members	19.616	19.99 %
Own income	2.719	2.77 %
Carry forward from 2015	3.408	3.47 %
Reserve	6.786	6.91 %
Cashflow		0.00 %
Total	**98.136**	**100.00 %**

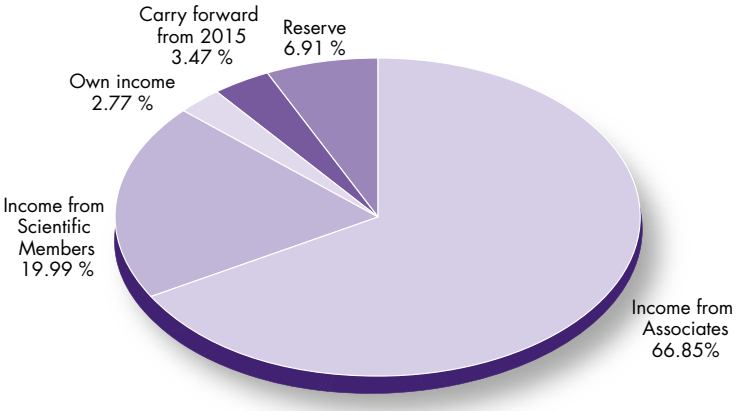

Expenditure	M€	%
Staff costs	44.447	45.29 %
Operating costs	19.201	19.57 %
Investment costs	14.908	15.19 %
Fuel cycle	19.580	19.95 %
Total	**98.136**	**100.00 %**

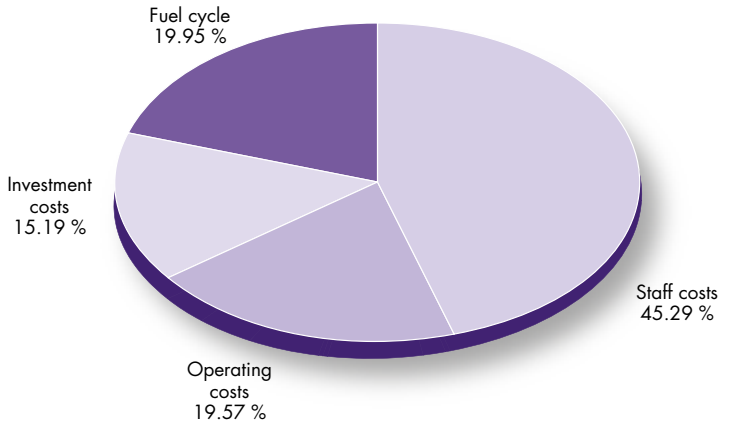

PURCHASING STATISTICS (Figures 2016 to end of August 2016)

	M€	%
France	8.959	55.94 %
Germany	3.9225	24.49 %
United Kingdom	0.537	3.35 %
Scientific Members	1.424	8.89 %
Others	1.174	7.33 %
Total	**16.017**	**100.00 %**

France captif market	9.181	
Total captif/non captif	**25.198**	

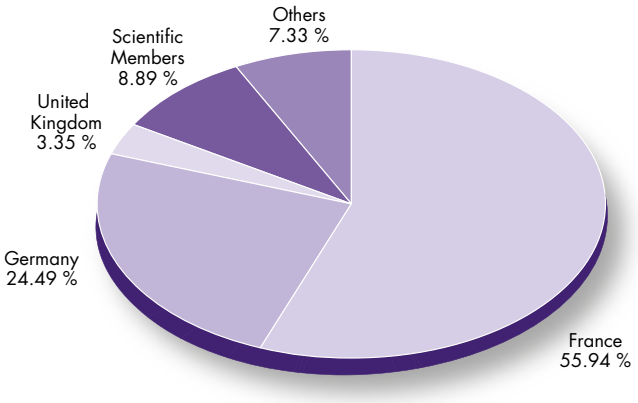

FACTS AND FIGURES

NAME

Institut Max von Laue-Paul Langevin (ILL).

FOUNDED

17 January 1967.

Intergovernmental Convention between France, Germany and United Kingdom (19/07/1974).

ASSOCIATES

France

Commissariat à l'Energie Atomique et aux Energies Alternatives (CEA).

Centre National de la Recherche Scientifique (CNRS).

Germany

Forschungszentrum Jülich (FZJ).

United Kingdom

Science & Technology Facilities Council (STFC).

COUNTRIES WITH SCIENTIFIC MEMBERSHIP

Spain

MINECO Ministerio de Economia y Competitividad.

Switzerland

Staatssekretariat für Bildung, Forschung und Innovation (SBFI).

Italy

Consiglio Nazionale delle Ricerche (CNR).

CENI (Central European Neutron Initiative)

Consortium composed of:

- Austria: Österreichische Akademie der Wissenschaften.
- Czech Republic: Charles University of Prague.
- Slovakia: Comenius University Bratislava.

TRANSNI

(Belgian-Danish-Swedish Transnational Neutron Initiative Consortium)

- Belgium: Belgian Federal Science Policy Office (BELSPOL).
- Sweden: Swedish Research Council (VR).
- Denmark: Danish Agency for Science, Technology and Innovation (DASTI).
- Poland: ILLPL Consortium of Polish Scientific and Research Institutions.

SUPERVISORY AND ADVISORY BODIES

- Steering Committee, which meets twice a year.
- Subcommittee on Administrative Questions, which meets twice a year.
- Audit Commission, which meets once a year, and statutory auditor.
- Scientific Council with 9 Subcommittees, which meets twice a year.

REACTOR

Operating 3 cycles in 2016.
156 days in total, average power 51.2 MW (p.102).

EXPERIMENTAL PROGRAMME

- 595 experiments (allocated by Subcommittees) on 28 ILL-funded and 9 CRG instruments.
- 1 306 visitors from 42 countries.

Publications in 2016

In 2016, the ILL received notice of 534 publications by ILL staff and users.

They are listed on the ILL website: www.ill.eu/science-technology/scientific-publications/list-of-publications/

THE DISTRIBUTION BY SUBJECT IS AS FOLLOWS

Applied Physics, Instrumentation and Techniques	45
Biology	46
Crystallography and Chemistry	52
Liquids and Glasses	32
Magnetic Excitations	32
Magnetic Structures	76
Materials Science and Engineering	48
Nuclear and Particle Physics	58
Theory	20
Soft Matter	91
Spectroscopy in Solid State Physics	33
Other	1

ILL PHD STUDENTSHIPS

PhD students at ILL in 2016*	44
PhD theses completed in 2016*	8
PhD theses completed in 2016**	3

* *Receiving a grant from ILL.*
** *Receiving an external grant.*

ORGANISATION CHART IN DECEMBER 2016

REVIEW PANELS

Key
Chair/focus group Chair
ILL college secretary/focus group secretary
ILL specialist

APPLIED METALLURGY, INSTRUMENTATION AND TECHNIQUES
D.J. Hughes (WMG, Warwick University, UK)
E. Farhi
T. Pirling

NUCLEAR AND PARTICLE PHYSICS
W. Heil (University of Mainz, Germany)
T. Jenke
P. Geltenbort

MAGNETIC EXCITATIONS
T.G. Perring (ISIS, UK)
J. Ollivier
B. Fåk

CRYSTALLOGRAPHY
C. Masquelier (CNRS Amiens, France)
E. Mossou
C. Ritter

MAGNETIC STRUCTURES
F. Damay (LLB Saclay, France)/**F. Ott** (LLB Saclay, France)
N. Qureshi/T. Saerbeck
J. Rodriguez Carvajal

STRUCTURE AND DYNAMICS OF LIQUIDS AND GLASSES
L. Bove (Pierre and Marie Curie University, Paris, France)
G. Cuello
T. Seydel

SPECTROSCOPY IN SOLID STATE PHYSICS AND CHEMISTRY
D. Djurado (CEA Grenoble, France)
A. Piovano
M. Zbiri

STRUCTURE AND DYNAMICS OF BIOLOGICAL SYSTEMS
R. Biehl (JCNS and ICS-1 Jülich, Germany)
A. Martel
M. Blakeley

STRUCTURE AND DYNAMICS OF SOFT CONDENSED MATTER
R. Jacobs (Oxford University, UK)/**F. Cousin** (LLB Saclay, France)
O. Czakkel/Y. Gerelli
R. Schweins

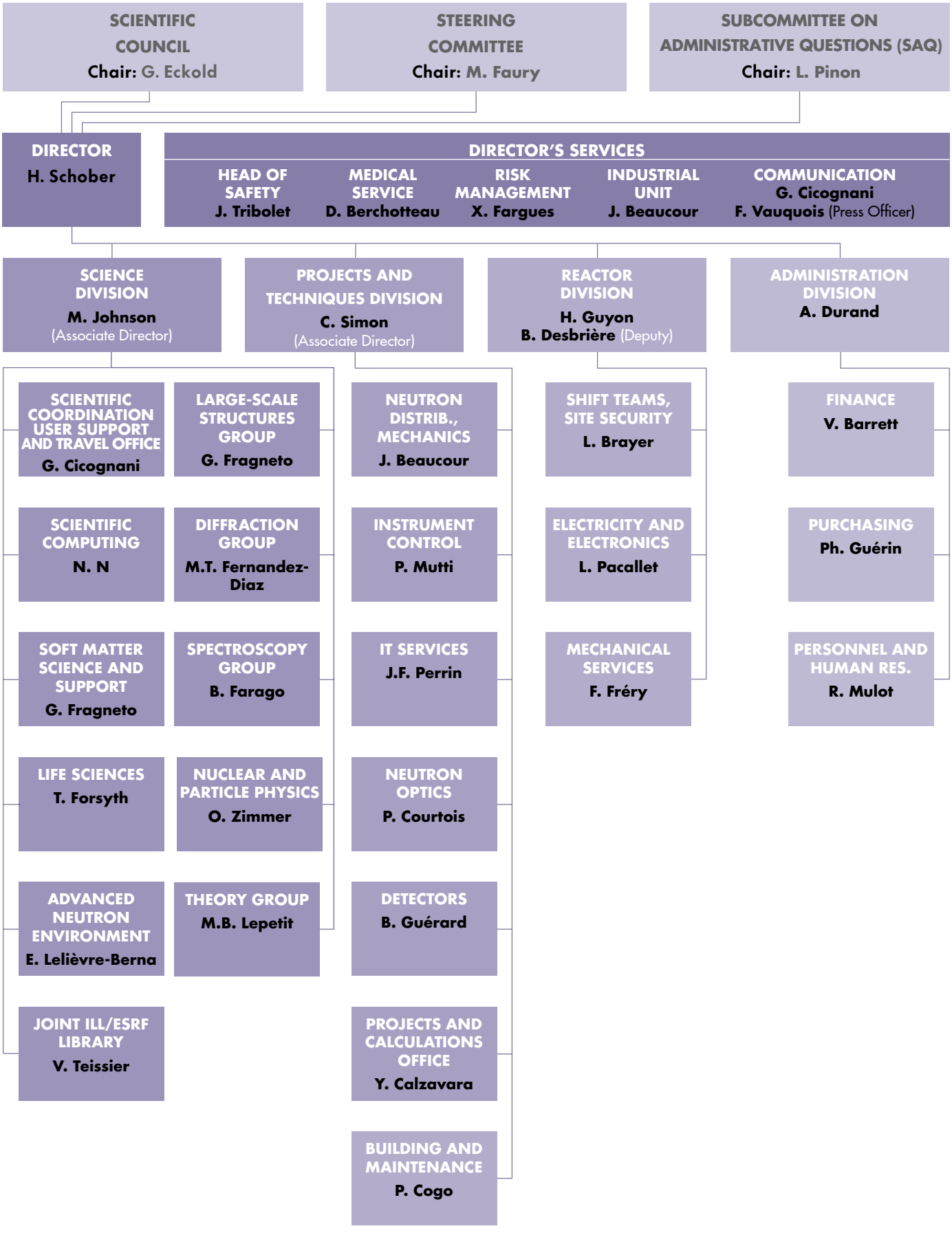
SCIENTIFIC COUNCIL
Chair: G. Eckold
STEERING COMMITTEE
Chair: M. Faury
SUBCOMMITTEE ON ADMINISTRATIVE QUESTIONS (SAQ)
Chair: L. Pinon
DIRECTOR
H. Schober
DIRECTOR'S SERVICES
HEAD OF SAFETY
J. Tribolet
MEDICAL SERVICE
D. Berchotteau
RISK MANAGEMENT
X. Fargues
INDUSTRIAL UNIT
J. Beaucour
COMMUNICATION
G. Cicognani
F. Vauquois (Press Officer)
SCIENCE DIVISION
M. Johnson
(Associate Director)
PROJECTS AND TECHNIQUES DIVISION
C. Simon
(Associate Director)
REACTOR DIVISION
H. Guyon
B. Desbrière (Deputy)
ADMINISTRATION DIVISION
A. Durand
SCIENTIFIC COORDINATION USER SUPPORT AND TRAVEL OFFICE
G. Cicognani
LARGE-SCALE STRUCTURES GROUP
G. Fragneto
NEUTRON DISTRIB., MECHANICS
J. Beaucour
SHIFT TEAMS, SITE SECURITY
L. Brayer
FINANCE
V. Barrett
SCIENTIFIC COMPUTING
N. N
DIFFRACTION GROUP
M.T. Fernandez-Diaz
INSTRUMENT CONTROL
P. Mutti
ELECTRICITY AND ELECTRONICS
L. Pacallet
PURCHASING
Ph. Guérin
SOFT MATTER SCIENCE AND SUPPORT
G. Fragneto
SPECTROSCOPY GROUP
B. Farago
IT SERVICES
J.F. Perrin
MECHANICAL SERVICES
F. Fréry
PERSONNEL AND HUMAN RES.
R. Mulot
LIFE SCIENCES
T. Forsyth
NUCLEAR AND PARTICLE PHYSICS
O. Zimmer
NEUTRON OPTICS
P. Courtois
ADVANCED NEUTRON ENVIRONMENT
E. Lelièvre-Berna
THEORY GROUP
M.B. Lepetit
DETECTORS
B. Guérard
JOINT ILL/ESRF LIBRARY
V. Teissier
PROJECTS AND CALCULATIONS OFFICE
Y. Calzavara
BUILDING AND MAINTENANCE
P. Cogo

INSTITUT LAUE-LANGEVIN
71, avenue des Martyrs
38000 Grenoble
France
www.ill.eu

FSC This report has been printed using FSC certified paper **www.fsc.org**